AN EXPERIMENTAL STUDY OF THE DEFORMATIONAL AND PERFORMANCE CHARACTERISTICS OF FOAMED BITUMEN STABILISED PAVEMENTS

A thesis

submitted in partial fulfilment

of the requirements for the Degree

of

Doctor of Philosophy

in the

University of Canterbury

by

Alvaro Gonzalez

University of Canterbury

2009

This page is intentionally left blank.

COPYRIGHT

This page is intentionally left blank.

ABSTRACT

The research presented in this thesis studies the effects of foamed bitumen on the deformational behaviour and performance of pavement materials. The research was conducted in the laboratory and the field, using specific New Zealand materials. The aggregate used is a blend of a coarse aggregate imported from the Auckland region with a crushed dust from the Canterbury region. The bitumen selected for the study is an 80/100 bitumen grade, and the active filler was a Portland Cement, both commonly used for foamed bitumen stabilization in New Zealand.

In the laboratory, samples of mixes with different foamed bitumen content were tested under various loading and stress conditions to investigate the effects of foamed bitumen on the deformational behaviour of the mix. The tests performed were: Indirect Tensile Strength (ITS), Indirect Tensile Resilient Modulus (ITM), Repeat Load Triaxial compression (RLT) and Monotonic Load Triaxial compression (MLT). Preliminary ITS and RLT tests conducted on mixes with 1% and 0% cement, at different foamed bitumen contents, indicated that mixes without cement performed poorly compared to the mixes with 1% cement. Therefore, the rest of the laboratory study was on mixes with 1% cement.

ITS tests were conducted on 150 mm specimens prepared with 0% 1%, 2%, 3% and 4% bitumen content, with a common 1% cement. Results indicated that foamed bitumen increases the ITS values of the mix, up to an estimated optimum of 2.8% bitumen content. Similar trends were obtained with ITM tests, in which a diametrical load pulse was applied on 150 mm specimens, showing an estimated resilient modulus peak near to 2.8% bitumen content.

RLT specimens were prepared at 0%, 2% and 4% bitumen content, at two compaction efforts, creating specimens at low and high bulk density. Permanent deformation RLT tests involved the application of seven stages of 50,000 load cycles each (4 Hz), with increasing deviator stress (from 75 kPa in the first stage, up to 525 kPa in the seventh stage) and at constant

confining pressure of 50 kPa. Results of RLT permanent deformation tests indicated that the increase in the foamed bitumen content resulted in an increase in the permanent deformation of the material.

MLT tests were conducted on specimens at 0%, 2% and 4% bitumen contents, at two compaction efforts, creating specimens of low and high bulk density, at confining pressures ranging from 50 kPa to 300 kPa, with a deformation rate of 2.1% per minute. Results indicated that the effect of foamed bitumen was a reduction of the peak vertical stress, or a reduction in the peak strength.

The peak stresses obtained in MLT tests were plotted in stress diagrams, and the failure was approximated as linear function of the confining stress. The fundamental shear parameters (angle of internal friction and apparent cohesion) were estimated, and results indicated that foamed bitumen has no apparent effect in cohesion but does reduce the angle of internal friction. The reduction of the angle of internal friction explains the general trends observed in the laboratory, that on one hand the compressive strength decreases with increasing bitumen content, but on the other hand, the tensile strength increases up to an optimum.

A full-scale experiment was carried out using an accelerated testing of foamed bitumen pavements at the Canterbury Accelerated Pavement Testing Indoor Facility (CAPTIF). In the full-scale experiments, the same materials that were tested in the laboratory (aggregates, bitumen, cement) were used to construct six different pavement sections, each with different contents of bitumen and cement. Three were constructed using foamed bitumen contents of 1.2%, 1.4% and 2.8% respectively, plus a common active filler content of 1.0% cement. Two more pavements were constructed adding cement only (1.0%), and foamed bitumen only (2.2%). In addition, one control section with the untreated unbound material was tested. Strains were collected using a 3D Emu soil strain system installed in each pavement section. The curing time between construction and pavement loading was approximately three months. The pavement response, such as surface deformation (rutting), surface

deflections and strains were periodically recorded during the execution of the test. The strains were collected at different depths by using an array of Emu strain gauges. Deflections were recorded using both a Falling Weight Deflectometer (FWD) and CAPTIF Beam deflectometer, which is a modified Benkelmann beam. A total number of approximately 5.6 million equivalent standard axles were applied on the pavement sections.

The rutting measured in the sections stabilised with foamed bitumen and cement was the lowest, showing that the addition of foamed bitumen significantly improved the performance of materials with 1% cement. The sections stabilised with cement only, foamed bitumen only, and the control untreated section showed large amounts of rutting and heaving by the end of the test.

Deflection measurements showed that the effect of foamed bitumen content is a reduction of pavement deflections, with the lowest deflection measured in the section stabilised with 2.8% bitumen and 1% cement. The elastic pavement strains showed that foamed bitumen reduced the tensile strains in the basecourse but did not have a significant effect on vertical compressive strains.

During the construction of pavements, material samples were taken for ITS and RLT testing. Results indicated that the highest ITS was measured in the section with 2.8% foamed bitumen content and 1% cement, and the ITS in the section without cement and foamed bitumen only was about 4-5 times lower than the ITS measured in specimens with cement. RLT specimens without cement performed poorly in comparison with the specimens with 1% cement. The specimens with 1% cement showed higher permanent deformation with increase in the foamed bitumen content, supporting the results from the previous laboratory study.

To interpret and relate the results observed in the laboratory and the field, stress path analysis was used, in which the stress ratio of the foamed bitumen layers was calculated at different depths. The analysis showed that foamed

bitumen content decreases the maximum stress ratio, hence reducing the proximity to failure and relative damage of the layer. Three-dimensional and two-dimensional finite element modelling of the CAPTIF pavements, were used to further investigate the stress and strain fields induced by the loading and to explain the pavement performance observed in the full-scale experiment.

ACKNOWLEDGMENTS

I would like to thank all the people who gave me support and encouragement over the duration of the research, especially:

Associate Professor Misko Cubrinovski, as supervisor, for his guidance, assistance, encouragement and timely comments on this thesis.

Dr. Bryan Pidwerbesky, as Co-supervisor, for his genuine enthusiasm, encouragement and support for the research.

David Alabaster, Sabine Werkmeister, Rob Douglas and Ben Hayward for their technical advice, assistance and friendship throughout the project.

Fulton Hogan, Land Transport New Zealand and Education New Zealand for their financial assistance.

Alan Fussell and Frank Adams for their assistance on the work at CAPTIF and valuable advice.

Frank Greenslade for his assistance with the electronics and laboratory work.

Thorsten Frobel and the New Zealand Stabilisation Working Group (SWG) for their support and comments on my research.

Siale Faitotonu and Mariham Tadros for their assistance in the laboratory.

Jonci Wolff, Andrea Contreras, Massoud Mogadhassi and Alejandro Amariz for sharing the PhD experience from different fields of knowledge.

And my wife Agnes, who gave up so much to allow me to complete this research.

DEDICATION

This thesis is dedicated to my parents, Octavio and Maria Teresa, for their constant support and encouragement throughout my life.

Table of Contents

List of Figures

List of Tables

Appendix Contents

Appendix List of Figures

1 Introduction

1.1 Background

A pavement is defined as the road structure above the *in situ* soil or subgrade, intended to sustain traffic loads. Flexible and rigid are two common type of pavements. Flexible pavements are constructed of bituminous and granular materials placed in layers, with better materials on top, where the intensity of stress induced by traffic is high, and inferior quality materials at the bottom, where the stress intensity is low (Figure 1.1a). Rigid pavements are constructed of Portland concrete, and are stiffer than flexible pavements (Figure 1.1b). Rigid pavements are placed either directly on the prepared subgrade or on a single layer of granular material, and are not as common as flexible pavements.

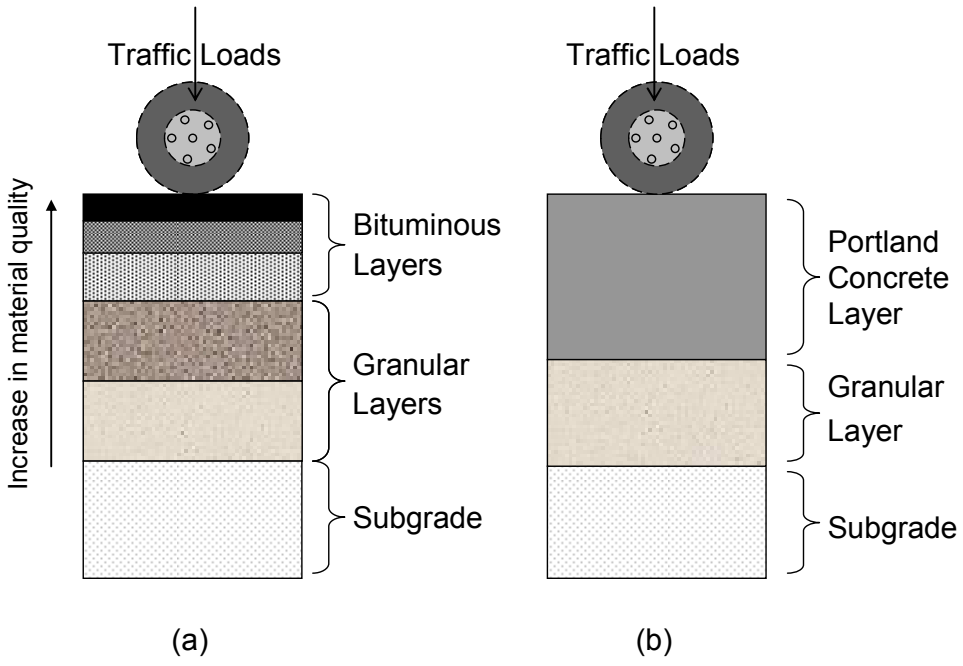

Figure 1.1 (a) Flexible pavement (b) Rigid pavement

In New Zealand, more than 95% of the roads are constructed of flexible unbound granular pavements (Hayward 2006). A typical cross section of a

New Zealand pavement is shown in Figure 1.2, which consists on three major elements:

- A thin surface (usually not exceeding 50 mm) which is most often a sprayed bituminous seal with uniform crushed stone chips, but is occasionally a bituminous mix.
- The basecourse, a layer which is constructed from unbound granular material that is usually crushed quarried rock or locally sourced aggregate.
- The subbase, which is usually one or sometimes two layers of unbound granular aggregate.

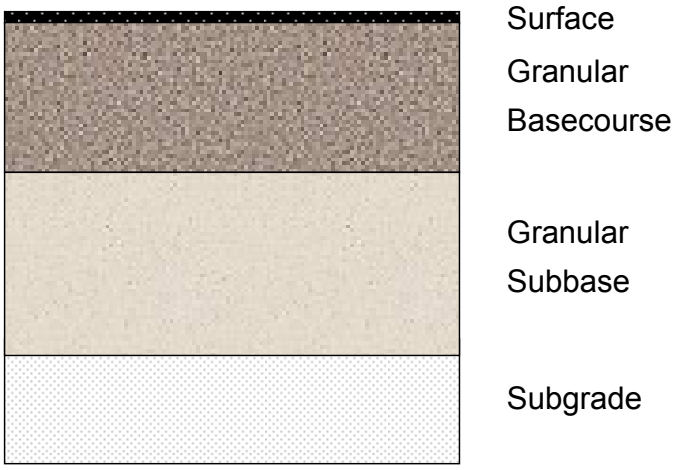

Figure 1.2 Typical cross section of a New Zealand flexible pavement

This pavement type has been adopted in New Zealand because in the past, high quality aggregate has been readily available in most regions of the country, and because in most New Zealand roads, low traffic volumes do not justify the incorporation of thick asphalt pavements, usually constructed in heavy trafficked highways.

However, in this decade, areas of New Zealand started to face a problem in the supply of aggregates that meet specifications required for the construction or rehabilitation of flexible unbound granular pavements. The area where this problem is particularly serious, because is the part of the country with the

fastest growth in infrastructure, is Auckland. This region is predicted to require 12 million tonnes of aggregate per year in 2020, a doubling of what was required in 1991 and, simultaneously, it is estimated that aggregate resources in the Auckland urban area will be exhausted between 2009 and 2012 (Compton 1998). An alternative for the aggregate supply in Auckland is the transportation of materials from other regions of the country, but it has been estimated that for every 30 km aggregates have to be transported, the cost of the aggregates doubles (AQANZ 2006). Also, new environmental restrictions in New Zealand have discouraged the development of new quarries, and therefore the aggregate supply problem Auckland is facing now is occurring in other parts of the country.

1.2 Cold-in-place recycling using foamed bitumen

Cold in place recycling of pavements is a construction technique that reclaims the existing distressed flexible pavement, simultaneously adding stabilising agents to improve the properties of the reclaimed material. The technique recycles 100% of the existing aggregates, reducing aggregate consumption and transportation of materials in the rehabilitation of roads, and although other types of recycling techniques exist (i.e. cold-in-plant), it is considered an attractive solution to reduce the aggregate supply problem in New Zealand.

The technique is conducted using a recycling machine, which is connected to tank trucks that add stabilising agents and water (Figure 1.3). Stabilising agents are added to improve the mechanical properties of the reclaimed material, and water is added to modify the moisture content to achieve higher densities during the compaction of the recycled material. The technique is called “cold” because it does not heat the existing pavement before recycling, spending less energy than other pavement recycling methods. The key part of the recycling machine is the mixing chamber, which contains the milling drum that pulverizes the distressed pavement, and the injection system, that adds the stabilising agents and water (both depicted in Figure 1.4). In the chamber, the pulverized material is mixed with the agents in one single pass of the recycling machine, producing a recycled layer ready to be compacted and shaped using rollers and graders.

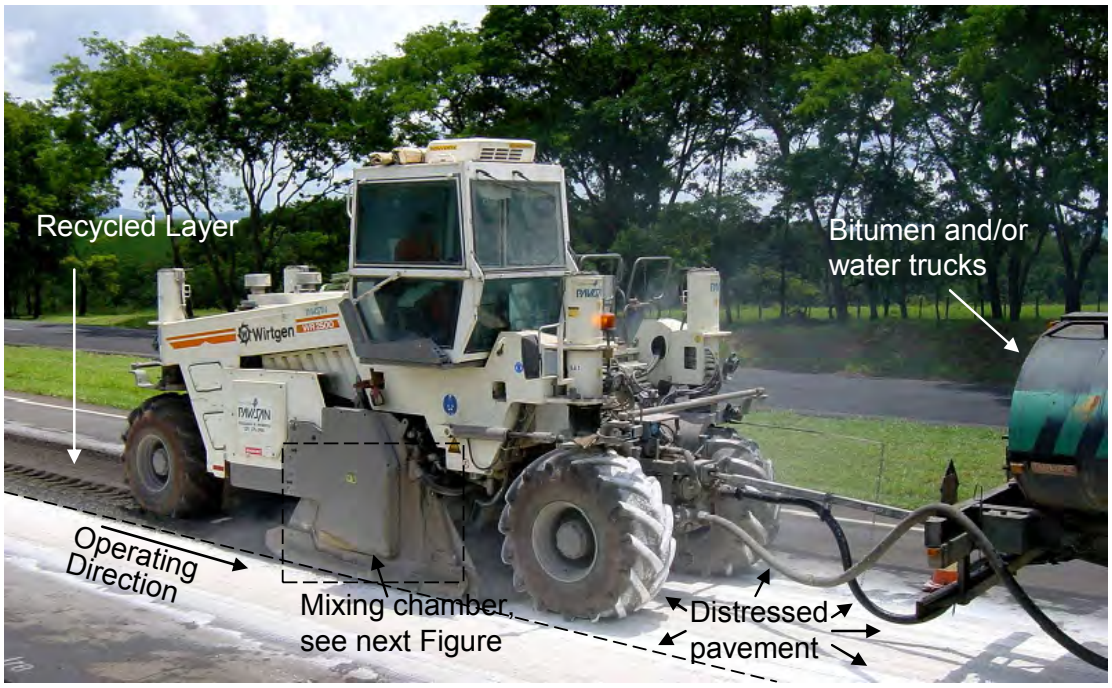

Figure 1.3 Pavement recycling machine

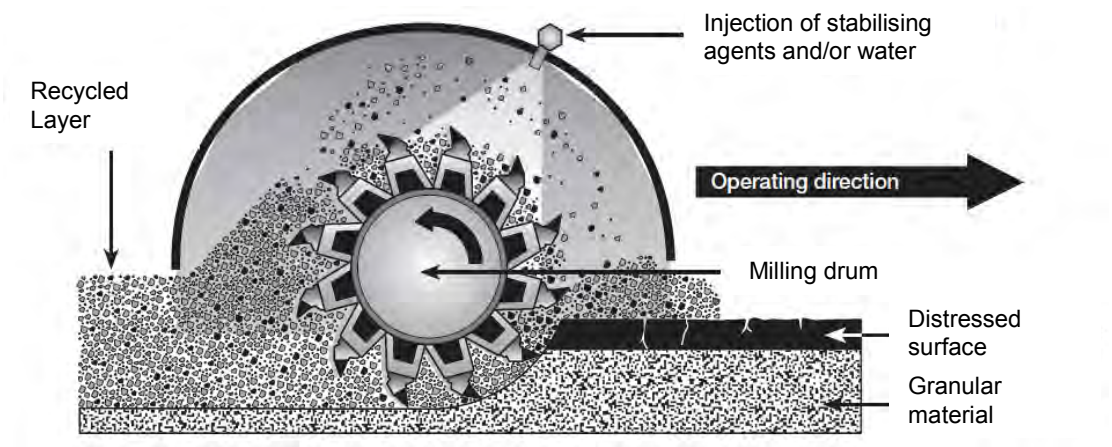

Figure 1.4 The mixing chamber and pavement recycling process (after Wirtgen 2004)

Foamed bitumen is a stabilising agent used for cold in place and in plant recycling of pavements. It consists of a hot bituminous binder that is temporarily converted from a liquid state to a foamed state, by addition of a small amount of water (1%-3%) at ambient temperature (usually between 10 °C and 30 °C). When water particles contact the hot bitumen (usually between 160 °C and 190 °C), heat energy from the bitumen is transferred to the water,

rising its temperature. When the water reaches the boiling point, it changes state from liquid to vapour and creates a thin-filmed bitumen bubble filled with steam, expanding its original volume approximately 1500 times. During this foamed state, which is a temporary state of low viscosity, bitumen can be mixed with aggregates.

Foamed bitumen has been widely used in New Zealand because it has constructive and environmental advantages over other stabilising agents, for instance:

- Once constructed and compacted, foamed bitumen pavements can immediately carry traffic, minimizing traffic delay times.
- The curing (water loss) rate of foamed bitumen is more rapid than that others bituminous agents (e.g. bitumen emulsions), and therefore the gain in strength is faster.
- The stabilization process does not involve the emission of volatiles, such as in cutback stabilization, or corrosive dust, such as when using lime or cement stabilization.

A typical New Zealand pavement that has been recycled using foamed bitumen is presented in Figure 1.5 (right), together with the original distressed flexible unbound granular pavement (left), that has been recycled up to a depth in which part of the subbase, the granular basecourse, and the distressed surface (usually referred to as Reclaimed Asphalt Pavement, RAP) have been reclaimed and treated with foamed bitumen. A thin asphalt surface course (20 to 50 mm) is normally placed on top of the foamed bitumen basecourse to provide a satisfactory skid resistant, waterproof, running surface. In New Zealand, the foamed bitumen content of a foamed bitumen layer usually ranges from 2.5% to 3.0%, and 1% cement is normally added as part of the stabilisation process to increase the strength of the recycled material.

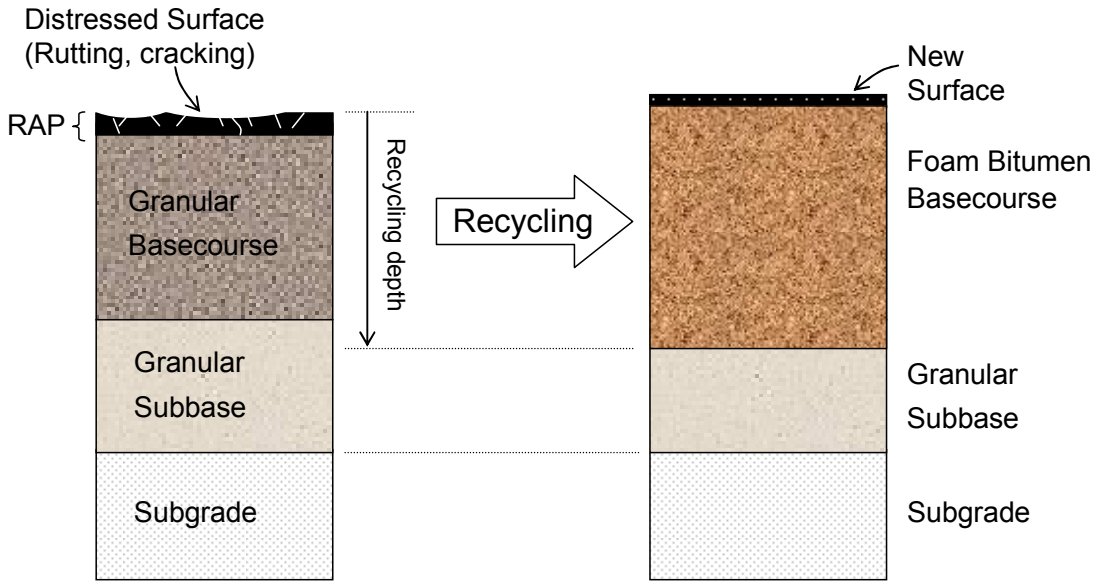

Figure 1.5 Distressed and recycled pavements

1.3 Need for the research and objectives

In the last decade, New Zealand pavement designers, contractors and road authorities have been seeking alternative pavement technologies, such as cold in place recycling using foamed bitumen, to optimize the use of the aggregate resource. However, the use of foamed bitumen mixes in road construction is constrained by a lack of data in the performance of these materials and the robustness of the pavement design methods currently available. Furthermore, there is not a clear understanding of the effects of foamed bitumen in the mechanical properties of the mix, and little effort has been made to relate laboratory with field performance. With the lack of information about the effect of foamed bitumen in the performance of pavement materials, it is difficult for pavement designers, contractors and road authorities to technically and economically justify the incorporation of foamed bitumen as a road construction material.

Therefore, the objective of this research is to understand and study the deformational characteristics and effects of foamed bitumen in the performance of pavements, involving:

- Laboratory testing, with the aim of studying the effect of foamed bitumen in the deformational characteristics of foamed bitumen mixes, tested under a wide range of stress conditions and bitumen contents.
- A full-scale experiment, where pavements were constructed at various foamed bitumen contents and tested under real accelerated traffic loads, with the objective of studying the effect of foamed bitumen in pavement response (surface deflections, elastic strains) and performance (surface deformation or rutting).
- Numerical simulations of the pavement structures, with the aim to interpret and relate laboratory and full-scale experimental results.

1.4 Thesis outline

A brief description of the motivation for this work has been given in this chapter. In order to better understand the background to the study, Chapter 2 provides a review and discussion of the current pavement design method for foamed bitumen pavements and its limitations. Common laboratory measurements conducted on foamed bitumen mixes are introduced and discussed. In addition, accelerated full-scale experiments and long-term performance of foamed bitumen pavements are included. The chapter also gives the fundamentals for the stress analysis of pavement materials and finally, an introduction to material plasticity and finite element modelling.

The bulk of the experimental study is presented in Chapters 3 and 4. Chapter 3 describes the laboratory study on foamed bitumen mixes, in which pavement materials were tested under a wide range of stress conditions and bitumen contents, using different type of tests.

Chapter 4 describes the accelerated full-scale experiment on foamed bitumen pavements, conducted in the Canterbury Accelerated Pavement Testing

Indoor Facility (CAPTIF). In this experiment, six pavement sections constructed at different foamed bitumen and cement contents were loaded applying accelerated traffic.

Chapter 5 first presents the interpretation of the experimental results, using stress diagram analysis. In the analysis, the stresses induced by the CAPTIF wheel loads were compared with the shear stress at failure obtained from monotonic triaxial static tests, using the stress ratio. A three-dimensional finite element model was used to analyze the CAPTIF pavements and a Mohr-Coulomb plastic material model was introduced to account for the effects of foamed bitumen in the angle of internal friction of the basecourse. In addition, a simpler two-dimensional (2D) finite element model of the CAPTIF pavements was conducted. The model was used to study separately the effects of the reduction of the angle of internal friction and the increase in the elastic modulus of the basecourse.

Chapter 6 summarizes the conclusions and recommendations from the previous chapters, and provides recommendations for further research.

2 Review of the literature and theory

2.1 Introduction

This chapter is a review of the literature and theory that contribute to the design and modelling of foamed bitumen pavements. The basis of the general pavement mechanistic design process is introduced, followed by a description of the current available thickness design methods for foamed bitumen pavements and their limitations. The laboratory measurements performed on foamed bitumen mixtures are summarized, and the trends found in the results of these measurements detailed, followed by a description of full-scale testing conducted overseas on foamed bitumen pavements. An introduction of the stress analysis in pavement layers was also included and finally, elasto-plastic material models and their application in finite element models for pavements are presented. Additional details from the literature about foamed bitumen mixes, for the reader not familiarized with this technology, were included in Appendix A.

2.2 Design of foamed bitumen pavements

2.2.1 Introduction to pavement design

The function of any pavement is to serve the road users safely, comfortably, and efficiently at minimum or, at least reasonable, overall cost to users and road authorities. Thus, the objective of pavement design is to provide a road surface that will remain smooth with minimal maintenance or remedial action needed during the design life of the pavement.

Pavement design has evolved from empirical methods to mechanistic pavement design methods. The general mechanistic design method for flexible pavements is an iterative process that normally involves the steps presented in Figure 2.1.

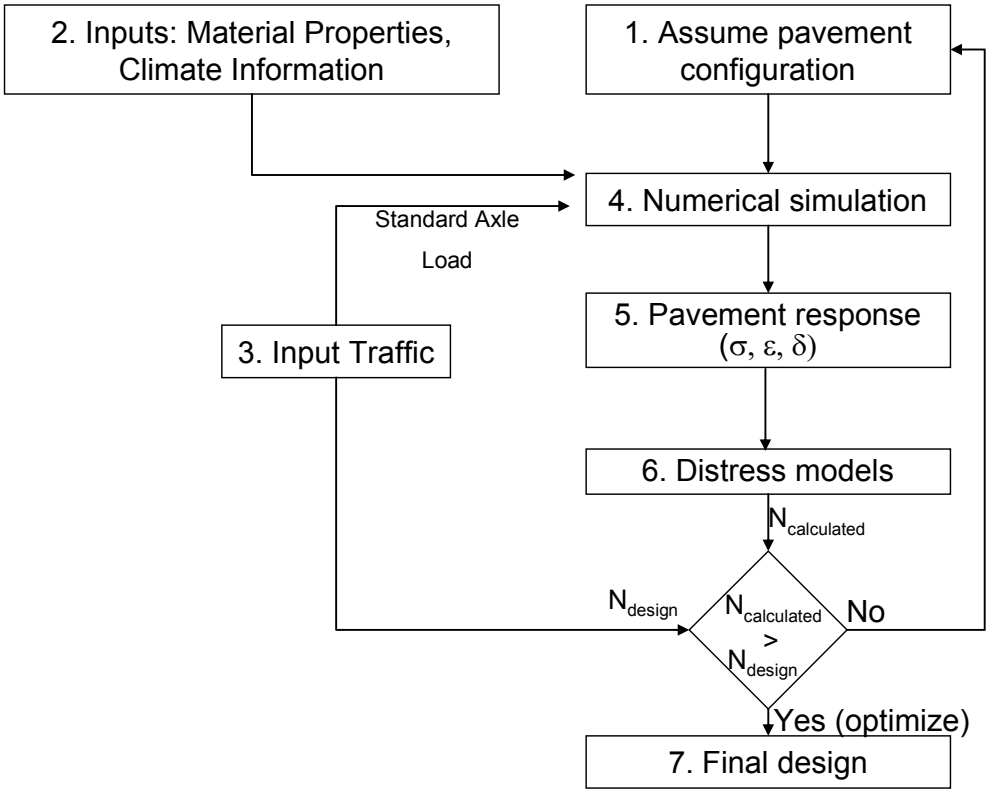

Figure 2.1 Methodology of calibrated mechanistic procedure for flexible pavement design (after Huang 2004)

In Step 1 a pavement structure is assumed, where the number of layers, the thickness of each layer, and the type of materials are defined. In Step 2 the basic elastic material properties (elastic modulus and Poisson's ratio) of each pavement layer are assumed or determined using laboratory and field data. If temperature and moisture at different times of the year vary significantly, it is important to consider this effect on the elastic modulus of the materials.

Step 3 involves the traffic estimation on the pavement structure during the design life. Because it is virtually impossible to consider all the loads that will be imposed upon the pavement structure, traffic is usually expressed in terms of the number of applications of a standard reference load called Equivalent Standard Axle (ESA), which is a single axle with dual tyres applying an axle load of 80 kN to the pavement (Figure 2.2). The real traffic is divided into a number of load groups (axle groups), each with different load magnitudes and configurations, and converted to equivalent Standard Axle repetitions. The

output of Step 3 is the load magnitude (needed for Step 4), and the number of Standard Axle repetitions (N_{design}), which is the traffic estimation on the pavement.

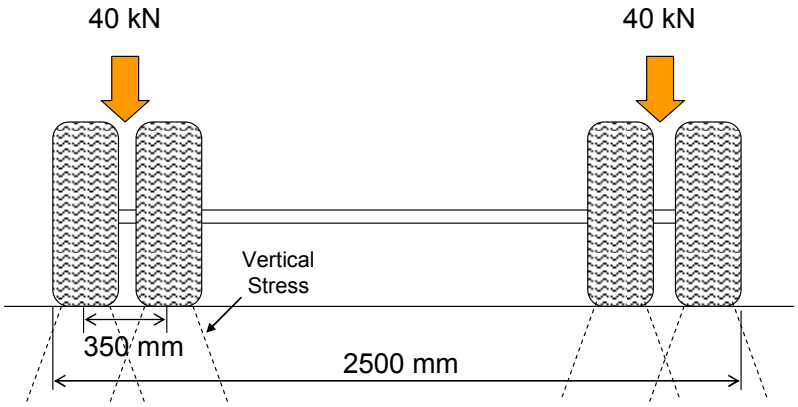

Figure 2.2 Equivalent standard axle of 80 kN

Step 4 is a numerical simulation of the pavement, either linear elastic or more complex nonlinear finite element analysis, and takes into account the geometry (numbers of layers and thickness), loads (equivalent axle load magnitude and tyre pressure) and mechanical properties of the materials adopted (resilient modulus, Poisson's ratio). Using the numerical simulation, the elastic response of the pavement is calculated (Step 5). Stresses (σ), strains (ε) and deflections (δ) are typical parameters calculated at different locations of the numerical model.

Step 6 involves the use of distress models that relate the elastic response with the number of load repetitions ($N_{calculated}$) necessary to bring the pavement to a known failure condition (e.g. area of cracks on the pavement surface, surface deformation, loss of stiffness). The distress models are available for widely used materials such as hot mix asphalt, but a limited number of models have been developed for non-conventional materials, such as foamed bitumen mixes.

Finally, if the calculated number of load repetitions from Step 6 ($N_{calculated}$) equals or exceeds the predicted traffic (N_{design}) from Step 3, the initially assumed pavement structure is adopted as the final design, otherwise, the thickness or the properties have to be modified and the design process has to

be repeated. If $N_{calculated}$ largely exceeds N_{design}, the structure is over-designed, which means that the pavement thickness should be reduced.

2.2.2 South African design method for foamed bitumen pavements

The most accepted method for the structural design of foamed bitumen pavements is published in the "Interim Technical Guidelines (TG2): The Design and use of Foamed Bitumen Treated Materials" (Asphalt Academy 2002). This method was developed using data generated from laboratory tests and accelerated pavement tests, later described in Section 2.4.

The method suggests that foamed bitumen pavements behave in two separate phases (Figure 2.3). The first phase starts after construction, when the layer is in an intact, undamaged condition and provides some fatigue resistance, and ends when, after the application of several traffic loads, the layer reaches an "equivalent granular state", with the time to reach this state defined as the "effective fatigue phase". The term equivalent granular state is used to describe the loss in elastic modulus of the material, and is comparable to granular materials only in the elastic modulus, and not in the physical composition of the materials (Asphalt Academy 2002).

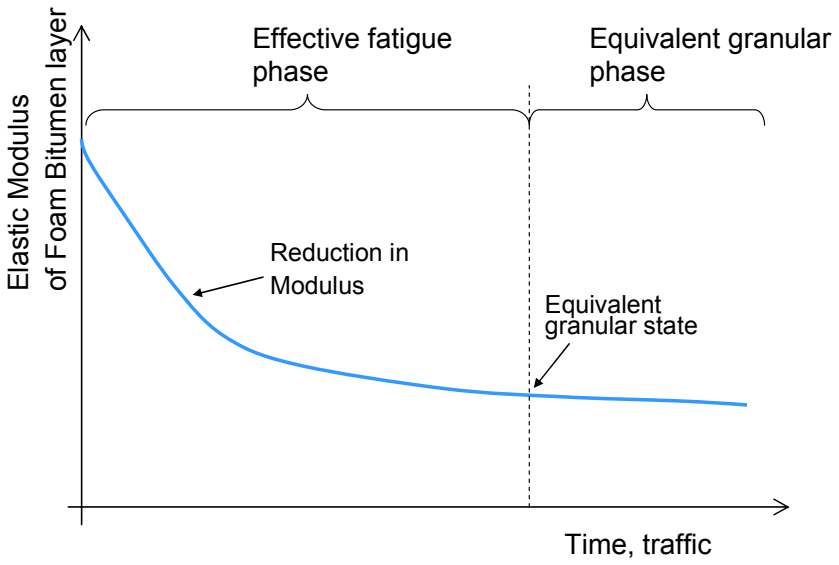

Figure 2.3 Behaviour of pavements with foamed bitumen treated materials (after Asphalt Academy 2002)

2.2.3 **Design inputs and distress models**

The material properties, pavement response and distress models (Steps 2, 5 and 6 in Figure 2.1) suggested by the method differ between the effective fatigue phase and the equivalent granular phase. In the fatigue phase, the horizontal tensile strains at the bottom of the layer, both underneath and between the tyres are calculated, using a linear-elastic numerical simulation of the pavement structure. In the equivalent granular phase, the major and minor principal stresses are determined at four locations in the pavement: one quarter below the top of the layer and one quarter above the bottom of the layer, both under and between the wheel loads (Figure 2.4).

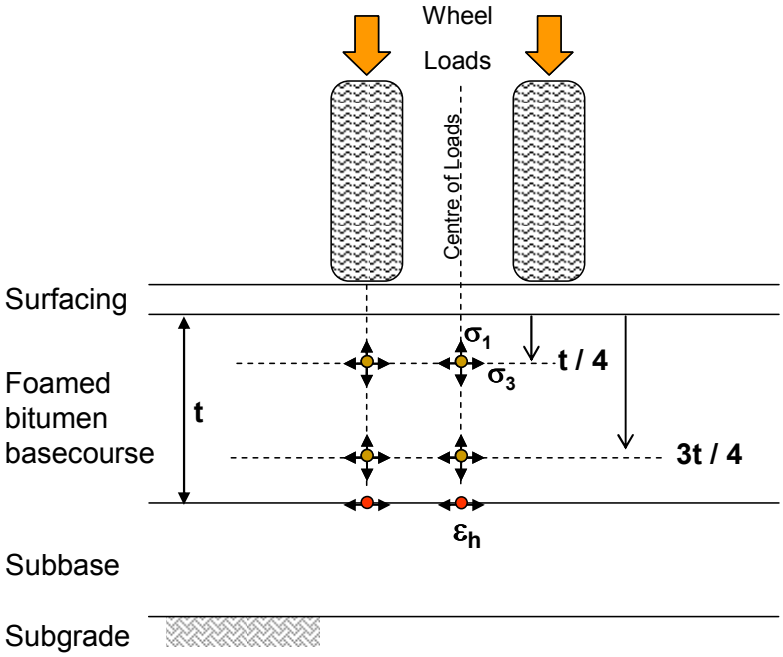

Figure 2.4 Location of the critical design parameters for the South African structural design method

The life of the layer is determined using the distress models that relate the number of load repetitions (load cycles) to attain the terminal condition of each phase. The terminal distress condition for the first phase is a loss of stiffness and a 2 mm permanent deformation of the foamed bitumen layer, while for the second phase is 18 mm of permanent deformation in the foamed bitumen layer.

The effective phase equation is similar to those of cemented materials adopted in South Africa (Theyse et al. 1996), and it has the following form:

$$N_{F,FB} = 10^{\left(A - 0.708\left[\frac{\varepsilon}{\varepsilon_b}\right]\right)} \qquad \text{(Eq. 2.1)}$$

where $N_{F,FB}$ is the number of load cycles during the effective fatigue life of the foamed bitumen layer, A is a coefficient related to the category of the road or reliability (risk) of the design, ε is the calculated horizontal tensile strain at the bottom of the layer (see ε_h in Figure 2.4) and ε_b is the strain-at-break measured in the monotonic strain-at-break beam testing. This test, developed in South Africa by Otte (1972), gives a measure of the 'flexibility' of a mix and involves monotonically loading of a four-point beam until failure, as shown in Figure 2.5. The applied load and vertical displacement are measured during the test, and are used to calculate the horizontal stress and strain through linear elastic beam theory. The strain-at-break is calculated using the peak force measured during the test (Long and Ventura 2004).

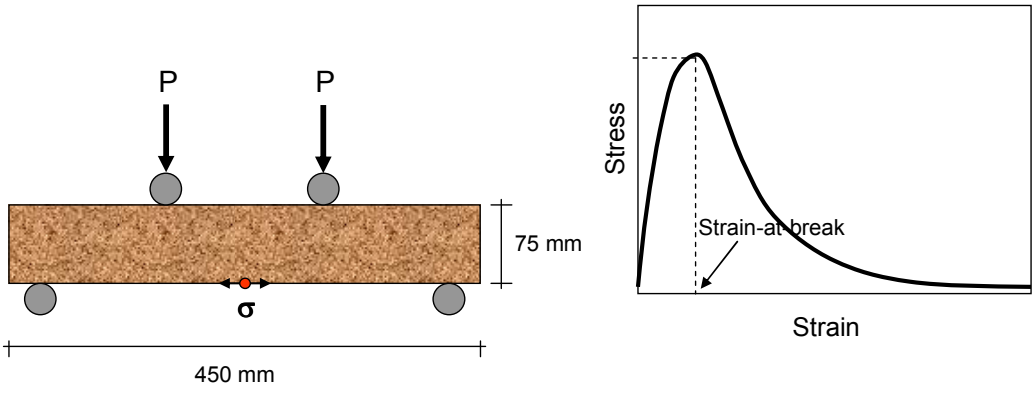

Figure 2.5 Strain-at-break test setup and typical stress-strain response from the test

The second phase equation is expressed as:

$$N_{PD,FB} = \frac{1}{30} 10^{(A + 11.938 \cdot RD + 0.0726 \cdot PS - 1.628 \cdot SR + 0.691 \cdot (cem/bit))} \qquad \text{(Eq. 2.2)}$$

Where $N_{PD,FB}$ is the number of load repetitions, A is a coefficient related to the category of the road or reliability of the design, RD is the relative density of the foamed bitumen mix, PS is the plastic strain expressed in percentage, SR is the stress ratio and (cem/bit) is the cement to bitumen ratio of the foamed bitumen mix.

The relative density (RD) is calculated using the following formula:

$$RD = \frac{DD_{mix}}{ARD_{mix} \times D_w} \times 100 \qquad \text{(Eq. 2.3)}$$

where:
DD_{mix} = dry density of the mix (kg/m^3),
D_w = density of water (kg/m^3)
and ARD_{mix}, the apparent relative density, is determined using the individual solid density (SD) values for the aggregate, cement, bitumen and water:

$$ARD_{mix} = SD_{aggregate} + SD_{bitumen} + SD_{cement} + SD_{water} \qquad \text{(Eq. 2.4)}$$

The volume of the mix is usually estimated using the dimensions of the specimens where the mix was compacted (Long and Ventura 2004). The stress ratio (SR) is calculated using the following formula:

$$SR = \frac{\sigma_1^a - \sigma_3^a}{\sigma_3^a \left[\tan^2\left(45 + \frac{\phi}{2}\right) - 1 + \left[2\,c\,\tan\left(45 + \frac{\phi}{2}\right) \right] \right]} \qquad \text{(Eq. 2.5)}$$

where σ_1^a and σ_3^a are the major and minor principal stresses, expressed in kPa, calculated from the response model (Figure 2.4), ϕ is the angle of internal friction and c is the cohesion (kPa) of the foamed bitumen material studied, determined from monotonic triaxial tests. The stress ratio equation was also adopted in the South African Mechanistic Pavement Design Method

(Theyse et al. 1996) for the permanent deformation (rutting) modelling of unbound granular materials.

The South African guidelines classify the foamed bitumen mixes into four categories (FB1, FB2, FB3 and FB4) depending on their Unconfined Compressive Strength (UCS) and Indirect Tensile Strength (ITS) values, which are laboratory tests commonly performed in foamed bitumen mixes. The guidelines provided performance models for materials FB2 and FB3 only, because only these two materials were extensively tested in the field and laboratory when the guidelines were published.

2.2.4 **Limitations**

The South African method was considered a good contribution to the state of the practice of the foamed bitumen technology and a useful tool for practitioners and it was developed to provide a required standardised methodology for the design of foamed bitumen pavements with the best available knowledge at the time. However, as the TG2 procedures became more widely implemented, limitations became apparent, some rather serious by nature.

The distress models presented in the previous section showed to be unreasonable in that a substantial reduction in the calculated number of load cycles (N_{FB}) could result due to foamed bitumen stabilisation. For example, if the base layer of a crushed aggregate material in a typical South African catalogue pavement is substituted with a layer comprised of the identical material stabilised with foamed bitumen (at the same level of density), the number of load cycles decrease (Jenkins et al. 2008).

It is also interesting to analyze the negative effect of foamed bitumen content in Equation 2.2. For a constant cement content (e.g. 1%) the increase in foamed bitumen content (e.g. from 2% to 3%) reduces the cement to bitumen ratio (cem/bit) (e.g. from 0.5 to 0.33), which causes a reduction of the number of admissible load repetitions ($N_{PD,FB}$), if the other parameters of the equation remain constant. This characteristic of Equation 2.2 is caused by the type of

laboratory data from which the equation was calibrated, later discussed in Section 2.3.4.

In addition, the design model for the second phase (Equation 2.2) was highly sensitive to the relative density of the mixture. For example, for a typical stress ratio (SR) and cement to bitumen content ratio (cem/bit), the TG2 model predicts that an increase in relative density (RD) from 0.75 to 0.85 would result in an increase in the structural capacity of the foamed bitumen stabilised layer from approximately 1 to more than 17 million ESAs (Jenkins et al. 2008).

2.2.5 **Current New Zealand design method for foamed bitumen pavements**

The current pavement design method used in New Zealand for State Highways is based on the AUSTROADS pavement design guide (Austroads 2004), which adopted a mechanistic-type methodology previously presented in Figure 2.1.

To adapt the AUSTROADS pavement design guide to New Zealand conditions, a supplement was published by Transit New Zealand (Transit NZ 2007). The supplement includes guidelines for engineering practitioners in applying AUSTROADS design procedures resulting from research results and experience gained in New Zealand.

The supplement proposes the methodology published in the South African TG2 guidelines, with some variations. During the preparation of the supplement it was suggested to model the first fatigue phase of the foamed bitumen layer using the distress model for hot mix asphalt materials included in the AUSTROADS guide (Austroads 2004), following recommendations made by Australian practitioners (Vorobieff 2005). However, it was argued that this behaviour was not observed in New Zealand foamed bitumen pavements, and there was not enough evidence to justify the use of the hot mix asphalt equation for foamed bitumen mixtures. Therefore, the New

Zealand supplement suggested that only the second (equivalent granular) phase should be accounted in the design:

While it is possible to analyse the "seating-in" (fatigue) phase using the AUSTROADS hot mix asphalt performance criterion, it is unclear how appropriate the criterion is for foamed bitumen stabilised materials. Given this uncertainty, it is generally appropriate to design the foamed bitumen stabilised layer for the steady-state condition only.

2.2.5.1 Design inputs and distress models

The New Zealand supplement suggests the following general material properties for the mechanical characterization of foamed bitumen layers:

- Elastic modulus of the order of 800 MPa;
- Poisson's ratio =0.3;
- Anisotropic layer ($E_{vertical}$=2$E_{horizonal}$);
- No sub-layering

The distress model adopted for this method is the permanent deformation in the subgrade, which is commonly referred to as "subgrade strain criterion". The distress model adopted the vertical strain at the top of the subgrade as the critical pavement response (Figure 2.6). The allowable equivalent standard axles (ESAs) are calculated using the AUSTROADS subgrade criterion:

$$N = \left[\frac{9300}{\mu\varepsilon}\right]^7 \qquad \text{(Eq. 2.6)}$$

where $\mu\varepsilon$ is the maximum vertical (compressive) strain (microstrains) at the top of the subgrade and N is the allowable number of ESAs at this strain before an unacceptable level of permanent deformation develops. The response of the pavement is usually calculated using CIRCLY (MINCAD

2004), a linear elastic, multi-layered software for numerical simulation of pavements.

2.2.5.2 Limitations

The most important limitation of this design method is that pavement life is calculated using the subgrade criterion only, ignoring the permanent deformation of the foamed bitumen layer. This contradicts the reported performance on foamed bitumen layers tested under accelerated traffic loads, where two thirds of the total pavement rutting has been measured in a foamed bitumen basecourse (Long 2001), detailed later in Section 2.4.2.

In addition, the effect of foamed bitumen is modelled only by the elastic modulus of the layer, and is not clear how the foamed bitumen content affects or improves the performance of the pavement.

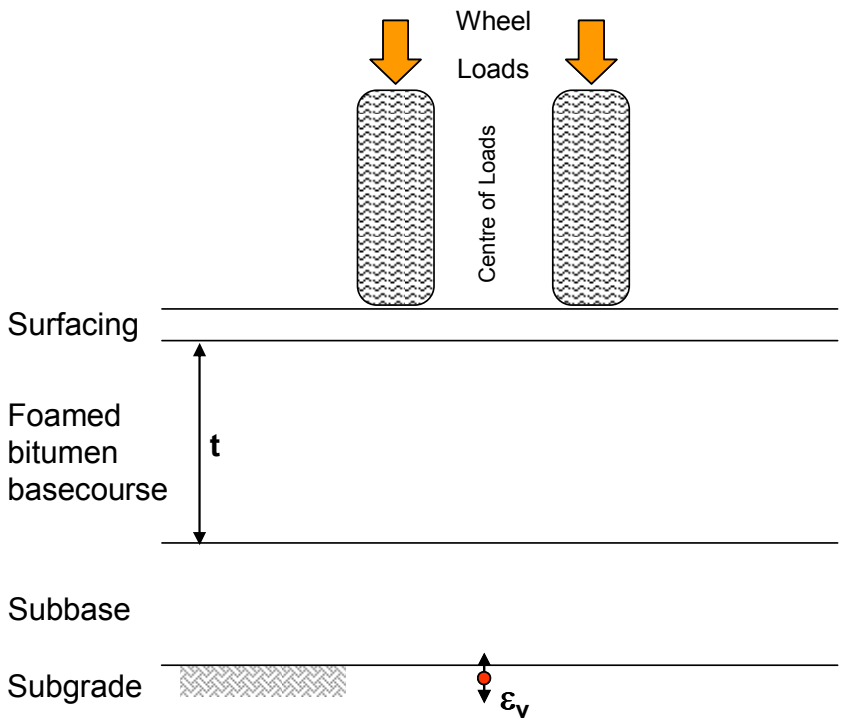

Figure 2.6 Location of the critical design parameters used in the New Zealand supplement to the AUSTROADS pavement design guide

2.2.6 **Queensland Department of Main Roads Method (Australia)**

Since 1997, pavement recycling using foamed bitumen has become an attractive alternative to traditional overlays for rehabilitation of existing pavements in the State of Queensland. The experience gained through pavement construction, laboratory testing, and monitoring of foamed bitumen pavements has contributed to the development of a design equation for foamed bitumen pavements in this State.

Although field data in Queensland was limited when the design equation was suggested, there was enough data to indicate that the primary distress mechanism of foamed bitumen stabilised pavements was fatigue failure of the stabilised layer (Jones and Ramanujam 2004). Therefore, the Queensland Department of Main Roads (QDMR) adopted the Austroads asphalt fatigue criterion used for asphalt design for a reliability of 95% to estimate the fatigue performance of foamed bitumen stabilised material.

2.2.6.1 Design inputs and distress modes

The fatigue relationship was recommended provided the assumed volumetric percentage of binder does not exceed 8% and the resilient modulus of the stabilised layer does not exceed 2,500 MPa. The design modulus (S_{mix}) is based on the soaked indirect tensile resilient modulus results at the nominated design binder content for the rehabilitation project. Therefore:

$$N = \frac{6918\left(1.08 + 0.856V_b\right)}{S_{mix}^{0.36} \times \mu\varepsilon} \qquad \text{(Eq. 2.7)}$$

where:

- N = number of load cycles to fatigue of the foamed bitumen layer
- V_b = volumetric bitumen content (normally between 6% and 8%)
- S_{mix} = Stiffness of foamed bitumen mix, measured using the Indirect Tensile Resilient Modulus (MATTA testing) on soak specimens.
- $\mu\varepsilon$ = induced horizontal tensile strain at bottom of foamed bitumen layer

2.2.7 **City of Canning (Australia)**

The City of Canning in Western Australia conducted a research project to study the modulus and fatigue performance of in situ foamed bitumen pavement materials measured in the laboratory (Leek 2009).

Samples of foamed bitumen mixes were collected at various sites in the Cities of Canning and Gosnells in Western Australia. The aim of the research was to determine if a design relationship could be developed to predict the fatigue life of in situ foamed bitumen stabilized pavements, and if the viscoelastic properties of the bitumen binder were reflected in the stiffness and fatigue performance of foamed bitumen mixes.

2.2.7.1 Design inputs and distress modes

Slabs were cut from different foamed bitumen pavement sections located in the City of Canning. The slabs were then cut into beams for flexural beam testing, in order to measure the fatigue properties of the foamed bitumen samples. The results of the testing showed that the performance of individual beams varied widely. While bitumen content and stiffness would be considered to influence fatigue life, due to the scatter of test results no significant relationships were observed between modulus and fatigue life or bitumen content and fatigue life (Leek 2009). Therefore a simplified equation was proposed, excluding specific reference to bitumen content and stiffness:

$$N = \left[\frac{1558}{\mu\varepsilon}\right]^6 \qquad \text{(Eq. 2.8)}$$

where:

- N = allowable number of load repetitions of strain level $\mu\varepsilon$
- $\mu\varepsilon$= induced horizontal tensile strain at bottom of foamed bitumen layer

2.2.8 **Transportation Research Laboratory (Great Britain)**

A design guide was developed by the Transportation Research Laboratory (TRL) in the United Kingdom for the design and use of cold recycled materials for pavements (Merrill et al. 2004). The guide presents design charts instead of design equations. The charts were developed using asphalt fatigue relationships developed in previous research reports (Nunn 2004), assuming that foamed bitumen mixes behave similar to hot asphalt mixes.

The guide covers all material types that could be considered as cold recycled materials and both in situ and ex situ (recycled in plant) construction processes. The guide defines three families of materials: fully hydraulic bound, fully visco-elastic bound and unbound material. Foamed bitumen mixes classify within the visco-elastic 'hydraulic' binders

2.2.8.1 Design inputs and distress modes

Bitumen bound materials are classified in this method according to their stiffness measured in the Indirect Tensile Resilient Modulus test. The guide classifies the mixes into one of three zones labelled B1, B2 and B3. Once the foamed bitumen mix is classified, the designer selects the appropriate thickness design chart for the foundation class; the thickness for the design traffic can be determined for the curve associated with the material zone.

Figure 2.7 shows an example of the design curves used in the TRL guideline. The designer has to first decide which material zone is representative of the foamed bitumen mixes to be used in the field, using laboratory resilient modulus measurements. Once the material zone is defined (Zone 1, 2 or 3), the designer has to use the expected traffic input data (X-axis in Figure 13, expressed in ESA x 10^6) and read the intersection of the traffic with the material zone, which gives the thickness of the foamed bitumen layer.

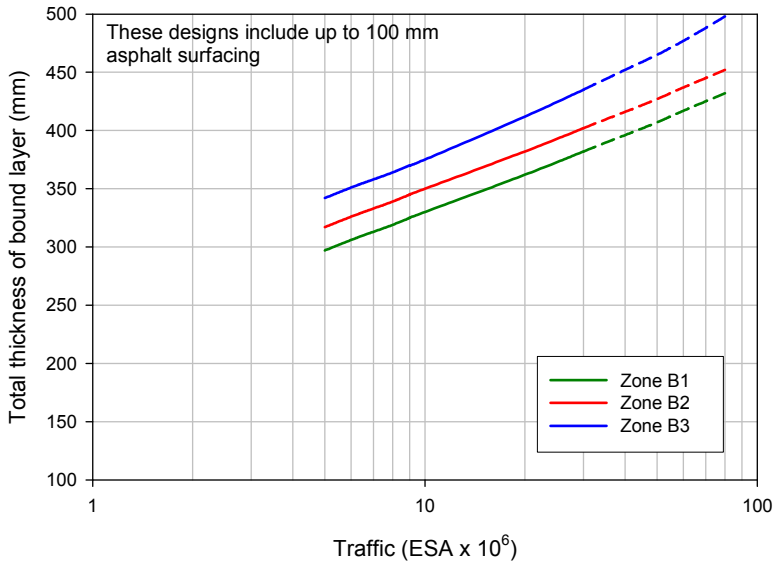

Figure 2.7 Design curves for bitumen bound cold recycled material, Foundation Class 1 (after Merrill et al. 2004)

2.3 Laboratory measurements

2.3.1 Introduction

Different types of laboratory tests have been conducted on foamed bitumen mixes, ranging from conventional to more advanced tests. Indirect Tensile Strength (ITS) and Unconfined Compressive Strength (UCS) are tests used to assess the strength or admissible maximum stress of foamed bitumen mixtures, and are considered conventional tests adopted in practice. Monotonic triaxial tests are normally used in pavement engineering to estimate the peak stress at different confining stresses, with the aim of assessing the shear strength parameters of the mix. Cyclic load are more advanced tests used to study the dynamic response of foamed bitumen mixes applying loads that are well below the maximum load at failure, and are closer in magnitude to actual loads applied in real pavement structures.

This section presents laboratory measurements commonly performed on foamed bitumen mixes. The procedures of the tests are briefly summarized, followed by a discussion of the general trends obtained when the effect of foamed bitumen content has been studied in the laboratory.

2.3.2 Indirect Tensile Strength (ITS) and Unconfined Compressive Strength tests

ITS and UCS tests (Figure 2.8) are standard tests that involve monotonic loading of the specimens up to maximum stress or failure. The dimensions of the foamed bitumen ITS specimens are normally 100 or 150 mm in diameter and 75 mm (± 5 mm) in height, while UCS specimens are normally 150 mm diameter and 125 mm (± 5 mm) height. The ITS specimens are diametrically loaded, inducing a horizontal tensile stress at the centre of the specimen caused by the shape of the specimen, which is estimated using linear elastic theory. UCS specimens are axially loaded and the compressive stress is calculated using the force-to-area quotient. The ITS and UCS values are defined as the maximum stress applied to the specimens during the tests.

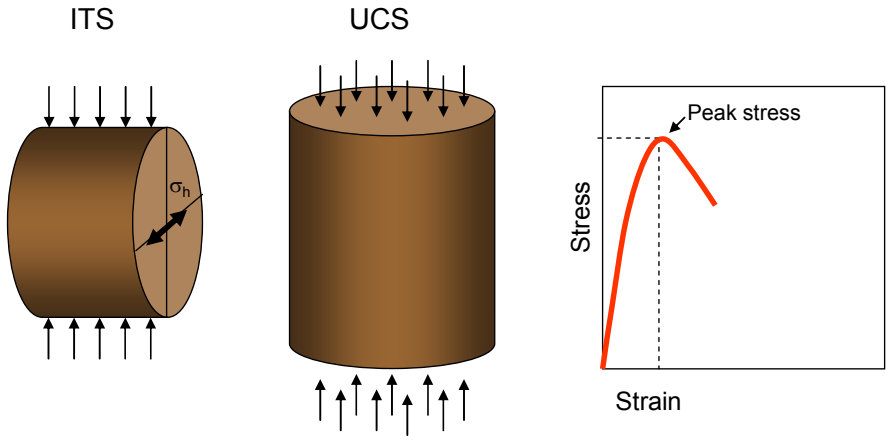

Figure 2.8 ITS and UCS specimens

ITS and UCS tests have been extensively conducted by researchers in foamed bitumen mixes. Long and Theyse (2002), studied the effect of foamed bitumen on the UCS and ITS values of one type of granular material stabilised at two foamed bitumen contents, with constant cement content (2%). The results showed that an increase in foamed bitumen (from 1.8% to 3.0%) decreases the average UCS in 36%, while ITS increases for 43%. Long and Ventura (2004) performed UCS and ITS in a different granular material stabilised at various foamed bitumen contents for a common 1% cement content, reporting a UCS and ITS increase of 4.7% and 9.3% respectively, for an increase in foamed bitumen content from 0% to 2.25%.

Halles and Thenoux (2009) performed a study to evaluate the degree of influence that active fillers have on the properties of recycled mixes with foamed bitumen. They conducted ITS tests after 24 hours of specimens soaking in water, at two foamed bitumen contents (0 and 3%), with different active fillers type (cement, CKD, Lime, Fly-Ash) and contents (0, 1, 2 and 3%). They found a general increase in the ITS values for a 3% foamed bitumen content, as shown in Figure 2.9).

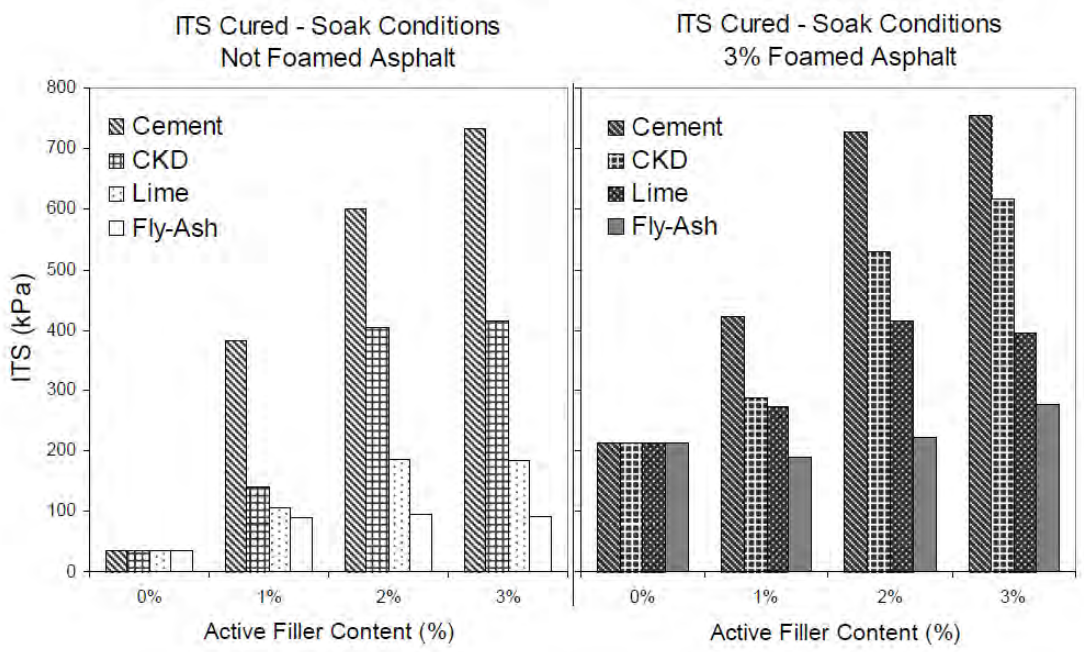

Figure 2.9 ITS values for cured specimens with and without foamed bitumen (foamed asphalt) (after Halles and Thenoux 2009)

Browne (2008) found that an increase in the foamed bitumen content increases the ITS in 5-10%, while UCS usually drops or does not show significant variation when foamed bitumen is included. These trends were measured in the laboratory study for two foamed bitumen projects conducted in New Zealand.

Frobel and Hallet (2008) also found a decrease of approximately 10% in dry ITS for every 1% increase in the foamed bitumen content in two types of mixes compacted using Marshall and Vibratory compaction. In addition, they collected ITS (dry and 24-hours soaked) and UCS data from four different

construction projects and found similar trends where, the effect of foamed bitumen on the ITS value is not always clear or too little to be conclusive, and UCS decreases when foamed bitumen content increases (Table 2.1).

Table 2.1 ITS and UCS results from four New Zealand projects (after Frobel and Hallet 2008)

Project	Bitumen (%)	Cement (%)	ITS dry (kPa)	ITS soaked (kPa)	UCS (kPa)
A	2.0	1.0	294	193	3020
A	3.0	1.0	333	263	2510
A	4.0	1.0	298	264	2170
B	2.0	1.0	349	246	3460
B	3.0	1.0	377	279	2970
B	4.0	1.0	354	266	2290
C	2.0	1.0	1140	863	4930
C	3.0	1.0	1079	889	3600
C	4.0	1.0	935	772	2660
D	3.0	1.0	467	427	3280
D	3.0	1.0	589	540	3820

2.3.3 **Monotonic triaxial tests**

Monotonic triaxial compression tests are normally conducted in foamed bitumen cylindrical specimens, applying both vertical and confining stresses. The confining stress is kept constant, with increase in vertical stress, at a slow rate, to a point where the specimen reaches its maximum vertical stress. The test is normally conducted on various specimens, at different confining stresses (Figure 2.10), with the objective of determining the shear strength parameters of the material studied (angle of internal friction, ϕ, and cohesion, c). Normally, large triaxial specimens with dimensions of 150-mm in diameter and 300-mm in height are used.

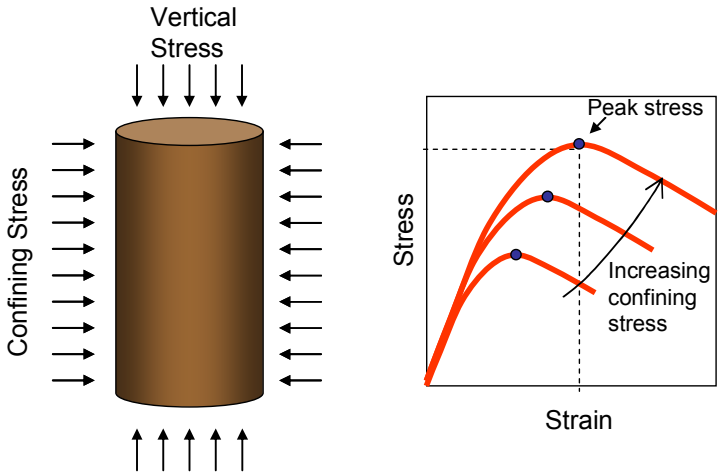

Figure 2.10 Monotonic triaxial test

Jenkins (1999) conducted monotonic triaxial tests on seven foamed bitumen mixes varying the type of granular material and the contents of bitumen and cement (Table 2.2). The tests were conducted in a displacement-controlled mode, at different confining pressures and using large (150 x 300 mm) specimens.

The general results of Jenkins' study showed that the friction angle ϕ decreases whilst the cohesion of the mix increases with the inclusion of foamed bitumen in a foamed bitumen mix. Jenkins also suggested that with the incorporation of only foamed bitumen (without cement) into a mix, the shear parameters continue to exhibit granular behaviour. However, for the tests including 1% cement or more, the foamed mix showed a marked increase in cohesion with reduction of the value of internal friction to nearly 0°. With these results, Jenkins established that stress dependant behaviour is only valid for foamed mixes without addition of active filler. Jenkins conducted a limited number of tests with the addition of cement.

Table 2.2 Details of foamed mixes for triaxial specimens (after Jenkins 1999)

Material name	Bitumen content (%)	Cement content (%)
$G1gau_2$	2.0	0.0
$G1eer_1$	1.0	0.0
$G1eer_2$	2.0	0.0
$G1eer_{2c}$	2.0	1.0
$G1eer_4$	4.0	0.0
$G2van_{1.5}$	1.5	2.0
$MGtud_2$	3.0	0.0

Long and Ventura (2004) performed a comprehensive monotonic triaxial testing program of foamed bitumen mixtures, using large specimens (150 x 300 mm). They studied the effects of density, saturation, foamed bitumen and cement content in the shear strength properties of the mixes, and concluded that the addition of cement improves cohesion, regardless of the foamed bitumen content, but reduces the friction angle. Their results also suggested that higher density values increase the friction angle and cohesion and that an increase in the moisture content reduces the cohesion. The results published by Long and Ventura are summarized in Figure 2.11 and Figure 2.12.

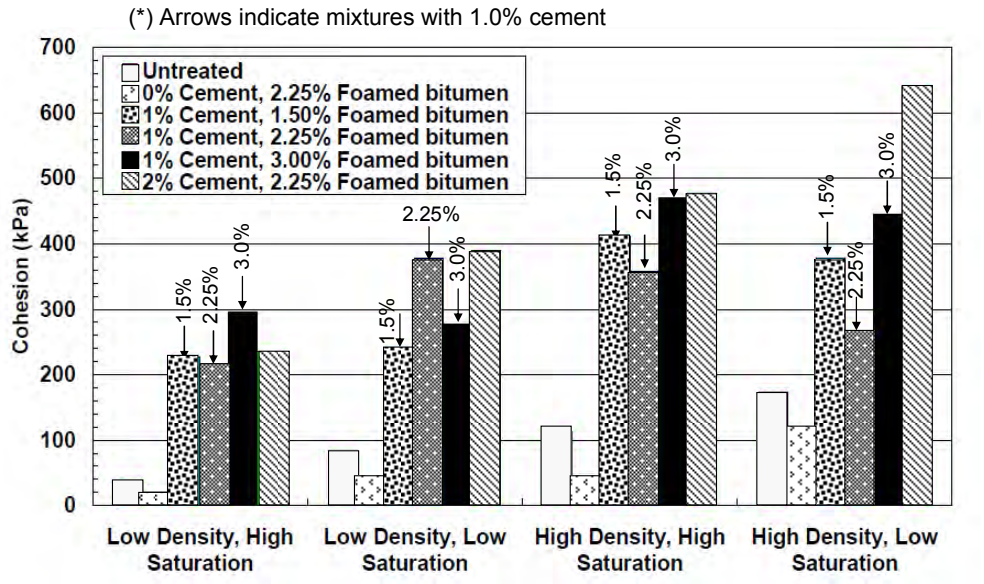

Figure 2.11 Effects of density, saturation, foamed bitumen and cement content in cohesion using monotonic triaxial test data (after Long and Ventura 2004)

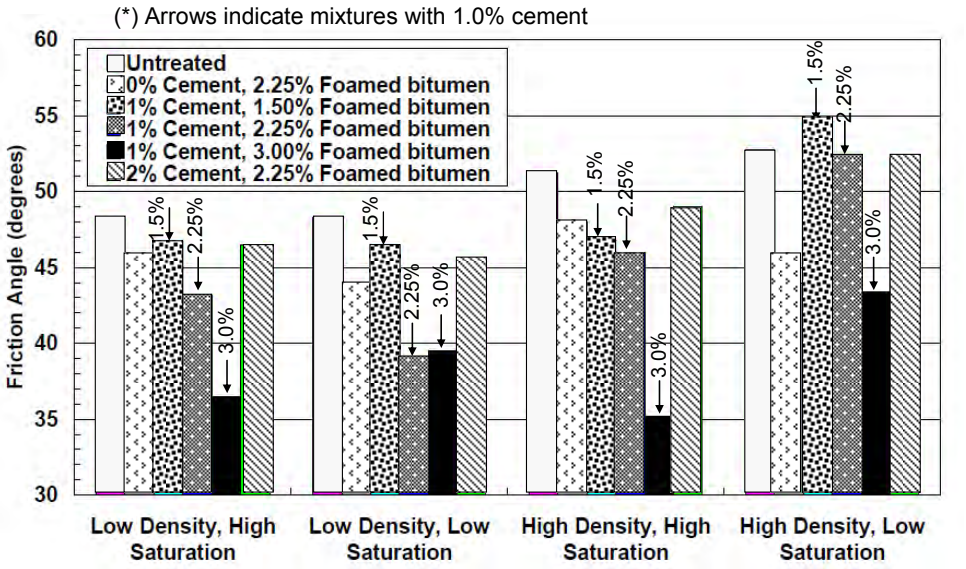

Figure 2.12 Effects of density, saturation, foamed bitumen and cement content in angle of internal friction using monotonic triaxial test data (after Long and Ventura 2004)

2.3.4 **Repeat (cyclic) load triaxial tests**

The repeat load triaxial (RLT) test is a cyclic version of the monotonic triaxial test previously described in Section 2.3.3. In RLT tests, instead of applying a load up to failure, such as in the monotonic tests, specimens are subjected to a cyclic load that is usually well below failure. A typical RLT test setup is shown in Figure 2.13, and a common cyclic load applied in these tests is depicted in Figure 2.14.

Two types of dynamic triaxial tests are normally conducted: resilient modulus and permanent strain. In the resilient modulus tests, the specimen is loaded to different combinations of confining and deviator stresses, and a limited number of cycles (e.g. 200) is applied at each stress condition. During this test, the elastic or recoverable strain (ε_r, see Figure 2.14) is measured, and the elastic or resilient modulus is calculated using the formula:

$$M_R = \frac{\sigma_d}{\varepsilon_r} \qquad \text{(Eq. 2.9)}$$

where M_R is the resilient modulus, σ_d is the deviator stress and ε_r is the recoverable vertical strain. The second common dynamic triaxial test is the permanent strain test (also known as permanent deformation test), where normally a large number of load cycles (over 10,000) are applied, and the irrecoverable or permanent strain ε_p is recorded (Figure 2.14). During the permanent strain test the resilient strains are also collected.

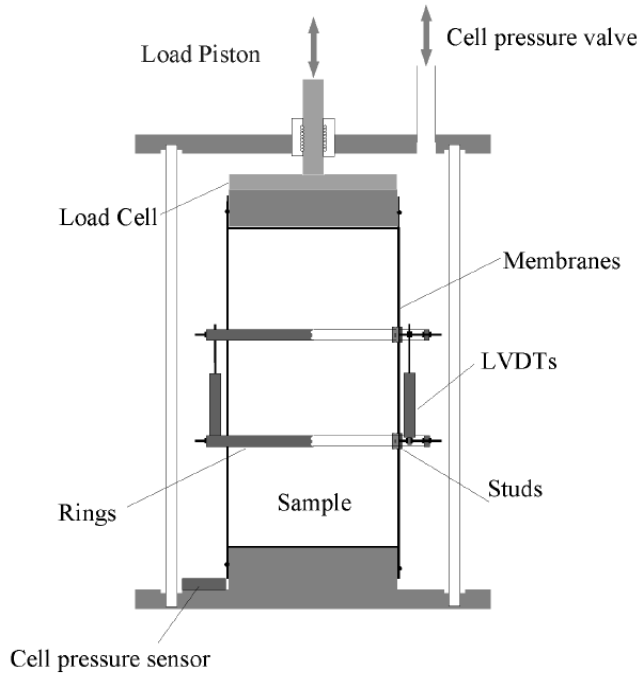

Figure 2.13 Example of triaxial cell and system for measuring axial displacement using LVDTs

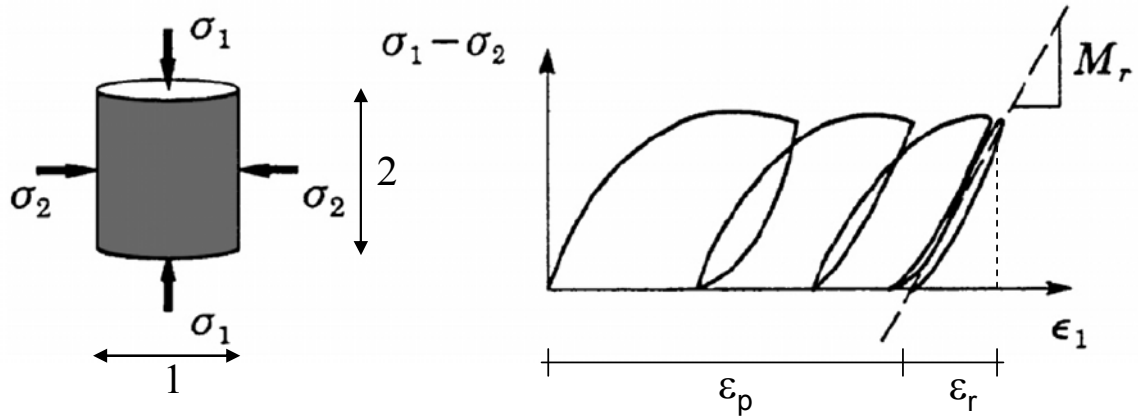

Figure 2.14 Normal behaviour of foamed bitumen mixes in triaxial cyclic test

2.3.5 **Resilient modulus tests on foamed bitumen mixes**

Jenkins (1999) performed resilient modulus tests on the same mixes mentioned in Section 2.3.3 (Table 2.2). He observed a granular-type behaviour in foam mixes without cement (i.e. M_r is highly dependant on the stress applied) and also identified three cases in which the stress-dependent behaviour of foam mixes becomes less evident or insignificant: the inclusion of cement in the foamed mix, foamed bitumen contents approaching 4% and specimens in which, before conducting the resilient modulus tests, are not pre-conditioned with cyclic pulses. Jenkins fitted the resilient modulus data collected from his triaxial tests into nonlinear models, obtaining correlation coefficients (R^2 values) between 0.69 and 0.99 and also presented some results for the characterization of Poisson's ratio, which is also a stress-dependent variable.

Long and Ventura (2004) utilized resilient measurements from permanent deformation triaxial tests to study the effects of density, saturation, bitumen and cement content model on the resilient modulus of foamed bitumen mixes. The researches found a large amount of variability in the resilient moduli results and suggested that the inclusion of foamed bitumen to the untreated mix results in a small reduction in the resilient moduli, while treatment with cement results in a significant increase in the resilient modulus (Figure 2.15). Long and Ventura tried to fit regression models to the resilient moduli data obtained, but the R^2 values obtained were low (between 0.10 and 0.52) and many of the variables studied (density, saturation, bitumen content) were statistically insignificant or the sign of the regression coefficients incorrect, and for some combinations of foamed bitumen and cement, it was not possible to fit a model. They finally concluded that the model fits should not be used to predict resilient modulus, in part because the effect of foamed bitumen was too little in comparison to the cement.

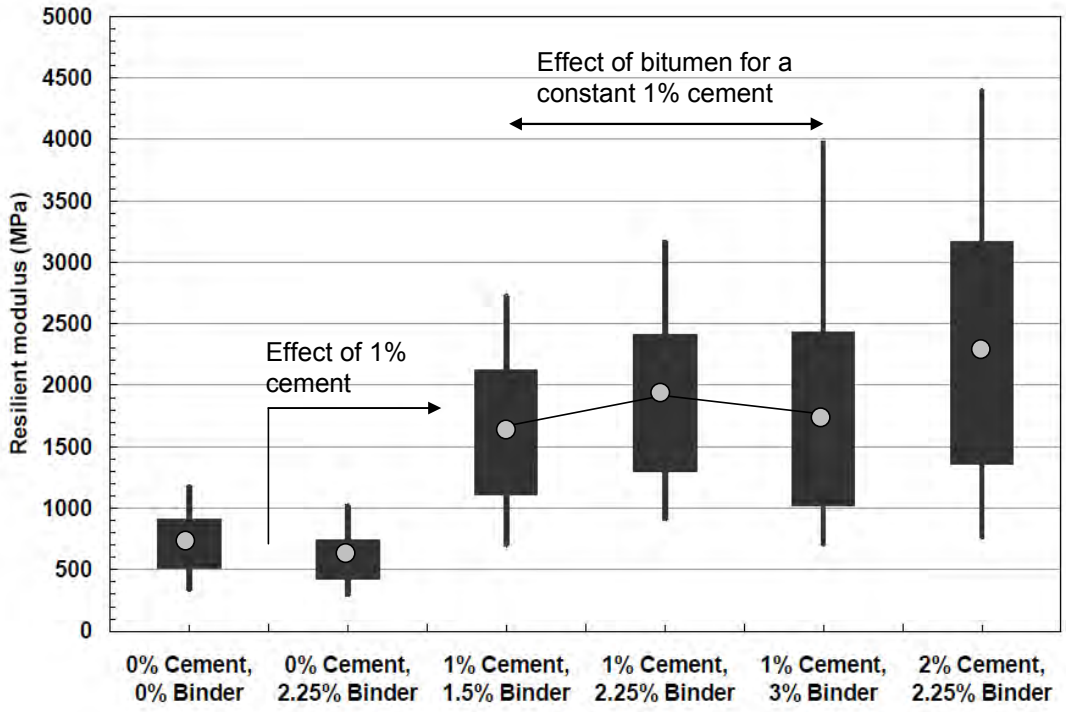

Figure 2.15 Resilient modulus measured during permanent deformation tests (after Long and Ventura 2004)

2.3.6 **Permanent strain tests on foamed bitumen mixes**

Jenkins (1999) performed two sets of permanent strain or permanent deformation tests. Tests were carried out on virgin specimens at different stresses to establish the stress dependency of the permanent deformation behaviour. The first set of tests was performed at the University of Stellenbosch (South Africa) applying a Haversine wave load signal at a frequency of 2 Hz and at one constant confining stress level of 50 kPa. Tests were monitored and readings were manually initiated and recorded at intervals necessary to obtain information on changes in deformation behaviour. The second set of tests was conducted at Delft University of Technology, where the triaxial set-up utilized a Haversine wave load signal at a frequency of 5 Hz and at one constant confining pressure value of 12 kPa. The most important conclusion of the test results is that a “critical stress ratio” defines the boundary between stable permanent deformation rate and accelerated permanent deformation rate under repeated loading. Jenkins suggested that a ratio of $\sigma_d/\sigma_{d,f}$ = 55%, where σ_d is the deviator stress applied

during the dynamic test, and $\sigma_{d,f}$ is the peak deviator stress at failure measured in monotonic tests, at the same confining stress (σ_3), defines the critical boundary for foamed bitumen treated materials with 4% or less bitumen and without cement. Jenkins' finding is summarized in Figure 2.16, where the stresses are plotted in a Mohr's stress diagram. Jenkins also found that 52% is the critical boundary for foamed treated materials with cement.

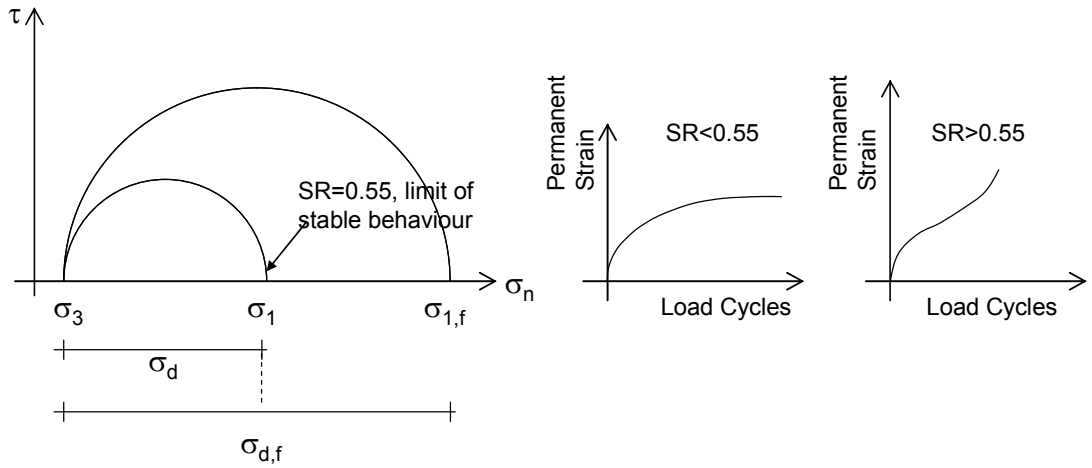

Figure 2.16 Stress limit for stable and unstable behaviour of foamed bitumen mixes with less than 4% bitumen, expressed in a Mohr's diagram

Long and Ventura (2004) studied the effect of foamed bitumen, cement, density and moisture on permanent deformation, applying 50,000 load cycles at 4 Hz to several triaxial specimens. They found that treating the granular material with foamed bitumen for a common 1% cement does not improve the resistance to permanent deformation, arguing that the quality of the untreated unbound granular material without stabilisation was too high to clearly see the effects of foamed bitumen.

Jenkins et al (2007), based on a large amount of triaxial test data collected from two South African research institutions (CSIR Transportek and Stellenbosch University) concluded that the number of cyclic loads applied in permanent deformation triaxial tests should exceed 250,000 in order to ensure that any tertiary flow behaviour is captured in the measurements. They also concluded that dominance of neither density nor saturation is apparent in the permanent deformation behaviour of foamed bitumen mixes, and the

variability of permanent deformation results make difficult to rank the performance of these mixtures.

Kim et al. (2008) applied cyclic loading to triaxial specimens prepared using material sourced from seven construction sites located in the State of Iowa, at five foamed bitumen contents and without active filler. A total of six specimens per source were prepared using foamed bitumen contents of 1.0%, 2.0% and 3.0% (2 replicates per bitumen content). The loading involved 10,000 repetitions of a 138 kPa stress applied for 0.1 second with a rest period of 0.9 seconds, which was applied at a constant temperature of 40˚C. Kim et al. defined a 'flow number', which is the number of load cycles where the permanent strain starts to increase at a high rate, depicted in Figure 2.16, and studied the effect of foamed bitumen on this value. They observed that increase in foamed bitumen content decreases the flow number, indicating less resistance to permanent deformation. They also observed that the number of specimens that failed (i.e. collapse) increased as the foamed bitumen was increased from 1.0% to 3.0%.

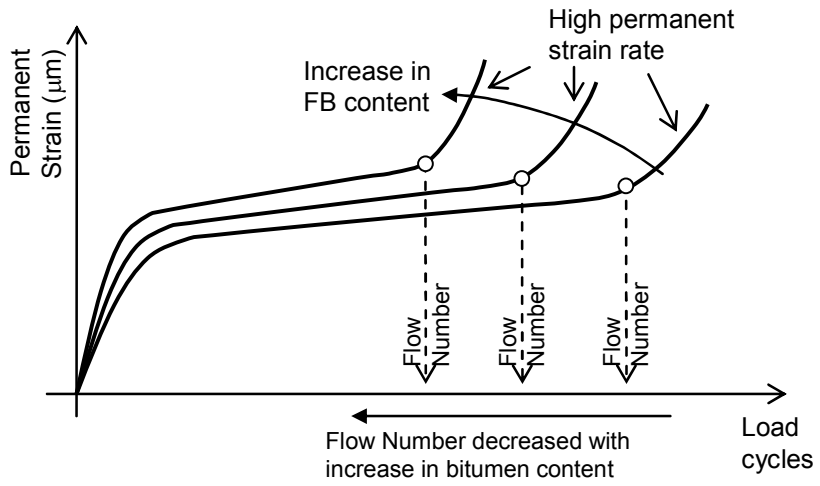

Figure 2.17 Permanent deformation behaviour observed by Kim et al. (2008)

2.3.7 **Indirect tensile resilient modulus tests**

Indirect tensile resilient modulus tests are similar to ITS tests, in that specimens are diametrically loaded, inducing a horizontal tensile stress at the centre of the specimen, but differs in that the stress applied is cyclic and

normally well below the failure of the specimen. During the tests, a small number of load cycles are applied and the horizontal resilient strain recorded using external LVDTs. The strains are used to calculate the resilient modulus of the material using linear elastic theory.

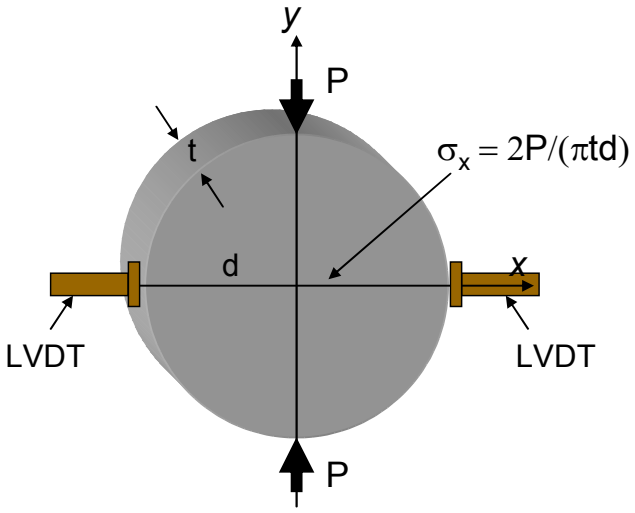

Figure 2.18 Typical configuration for indirect tensile resilient modulus test

Saleh (2004b) tested foamed bitumen materials prepared at different bitumen contents and moisture, with the objective of optimizing the indirect tensile resilient modulus. He obtained increase in resilient modulus with increase of foamed bitumen content, up to an optimum value of approximately 3% (Figure 2.19). Nataatmadja (2001) obtained similar results using the test to evaluate the effect of foamed bitumen and type of compaction. Nataatmadja found that Marshall compaction produced higher resilient modulus values compared with the gyratory compaction method, and that Marshall compaction showed an optimum bitumen content associated with the maximum density. The gyratory compactor produced specimens that were less dependent on bitumen content but had higher density values. In the study, Nataatmadja found an increase in the resilient modulus up to an optimum value, similarly to Saleh. Saleh found relatively high resilient modulus values, because he tested foamed bitumen mixes prepared with fly ash and 2% cement.

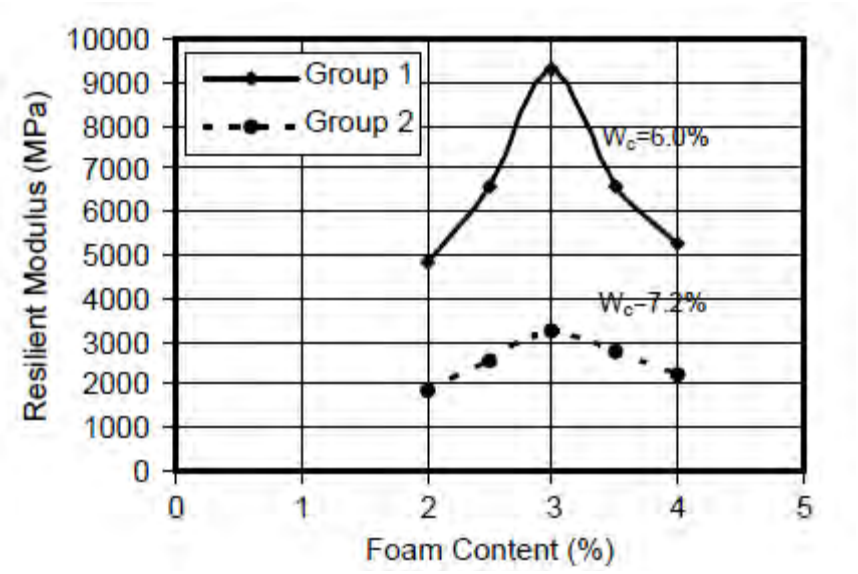

Figure 2.19 Indirect tensile resilient modulus results obtained by Saleh (2004b)

2.4 Field measurements

2.4.1 Introduction

The most realistic and reliable source of pavement response is obtained in the field. There are two sources of field data; full-scale Accelerated Pavement Test (APT) facilities and monitored in-service roads. The advantage of APT facilities over in-service roads is the rapid application of loads and data collection, which allows pavements to be tested and evaluated in a short time. The costs involved in field tests are considerably high, and therefore testing can be carried out only in a limited number of combinations of pavement materials, layer thickness, climatic and loading conditions.

Foamed bitumen pavements have been studied in both APT facilities and monitored roads. The main focus of these experiments has been the development of mechanical and empirical models for the design of foamed bitumen layers, using data from pavements stabilised at one specific bitumen content. The following section is a summary of the most relevant field testing programmes found in the literature.

2.4.2 **South African APT, P243/1 road**

Long et al (2002) developed the structural design models for the South African Interim guidelines (Section 2.2.2) using data collected from pavements loaded with a Heavy Vehicle Simulator (HVS), a linear type of full-scale accelerated testing facility showed in Figure 2.20. This is a mobile research facility, in which the trajectory of the wheels that apply the loading is a straight line.

Figure 2.20 Type of Accelerated Pavement Testing facility used in South Africa for the testing of foamed bitumen pavements

The first testing of foamed bitumen pavements using the South African HVS was conducted in the P243/1 road in 2001, and originally consisted of two foamed bitumen treated sections of 8.0 m length each, named section 409A4/B4 and section 411A4. The reclaimed material was a cement treated base with old multi-seal surfacings and an untreated cemented subbase, treated with 2.0% cement and 1.8% foamed bitumen. The pavement dimensions, shown in Figure 2.21a, were the same for the two sections, but the load magnitude and sequence applied was different for each section.

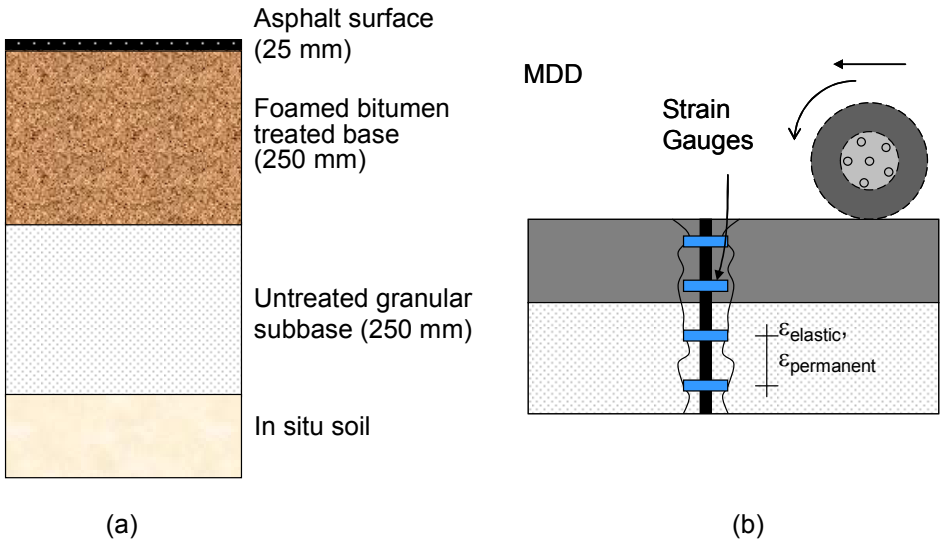

Figure 2.21 (a) Foamed bitumen pavement tested in the P243/1 road section (b) Multi depth deflectometer

The loading of the pavement consisted of two phases, detailed in Table 2.3. In Phase 1, after the application of 307,224 80 kN load repetitions in section 409A4, the HVS was moved to create a new test section (409B4). This new 8 m test section consisted of 4 m of the previous test section, and 4 m of untrafficked pavement. During the application of the loads, the pavement condition was assessed at regular time intervals including measurements of the surface elastic deflection, permanent deformation, moisture conditions and visual inspection. Water was added at the end of the test to induce additional damage in the pavement sections.

The elastic and plastic deformations of the foamed bitumen layer were measured using a Multi Depth Deflectometer (MDD), a device installed in the pavement that measures elastic and permanent vertical strains at different depths (see Figure 2.21b). The resilient moduli of the foamed bitumen treated layer were back-calculated using data from the elastic MDD measurements.

Table 2.3 Loading sequence for P243/1 HVS test

Phase	Sections	Repetitions	Load (kN)	Tyre Pressure (kPa)	Comments
1	409A4	0 - 307,224	80	800	
	409B4	307,244 - 454,830	100	850	
		454,830 - 462,524	100	850	Water added
2	411A4	0 - 958,714	40	620	
		958,714 - 1,299,597	80	800	
		1,299,597 - 1,313,645	80	800	Water added

During the initial loading of the pavements it was observed a reduction of the elastic modulus of the foamed bitumen basecourse. The back-calculated modulus for Section 411A4 is presented in Figure 2.22, where the initial modulus ranged between 1000 and 3400 MPa, to a range between 600 to 1,000 MPa for a constant traffic load of 40 kN. This reduction in elastic modulus was again observed when the load was increased to 80 kN.

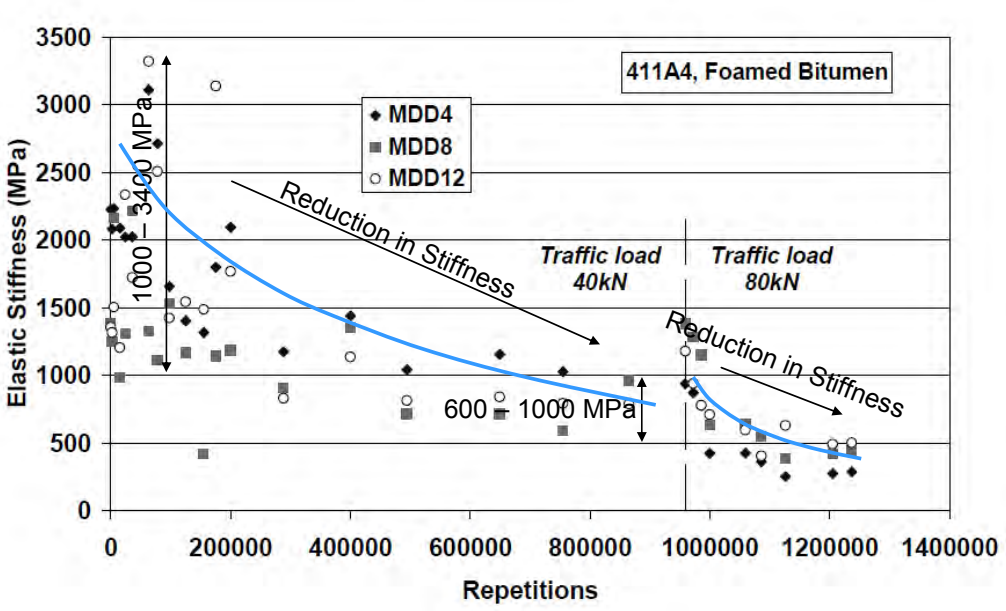

Figure 2.22 Calculated elastic modulus of foamed bitumen layers versus load repetitions for P243/1 test (Long et al. 2002).

The accumulation of in-depth permanent deformation of the foamed bitumen layer was also measured with the MDD. In section 411A4, 2 mm of deformation were measured at the end of the 40 kN load, and after the

application of the 80 kN load this value increased approximately up to 3 mm, a 66% of the total surface deformation (4.5 mm). The measured rutting was lower than the expected by the researchers, and water was introduced into the pavement through surface cuts to induce further damage. Although significant rutting was only experienced after the addition of water, there was still relatively little permanent surface deformation at the end of the test (5.5 mm in section 409A4 and 5.4 mm in section 411A4).

2.4.3 **South African APT, N7 road**

Theyse (2004) reported two sections tested using the South African HVS in the N7 road, with dimensions shown in Figure 2.23. The recycled material consisted in multiple surface seals, a crushed stone base and a crushed stone subbase. The pavement was recycled using a foamed bitumen content of 2.3% with a Portland cement content of 1%. Two sections, with the same pavement dimensions, were tested applying the loading sequence detailed in Table 2.4.

Table 2.4 Loading sequence for N7 HVS test

Sections	Repetitions	Load (kN)	Tyre Pressure (kPa)	Comments
415A5	0 – 48,628	40	620	
	48,628 – 423,374	80	800/850	
	423,374 – 498,863	100	800	
416A5	0 – 1,168,850	40	620	
	1,168,850 – 1,618,850	80	800/850	
	1,618,850 – 1,742,850	80	800	Water

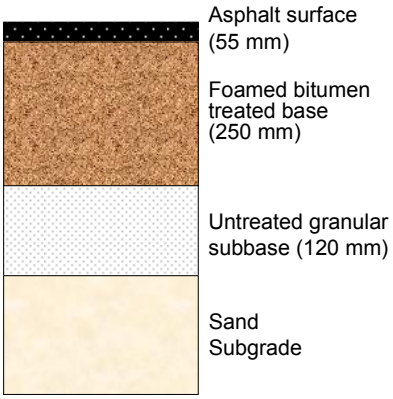

Figure 2.23 Foamed bitumen pavement tested in the N7 road section

The elastic and plastic deformations of the foamed bitumen layer were measured using Multi Depth Deflectometer (MDD), previously described in Section 2.4.2. The elastic deformations were used to estimate the resilient modulus of the foamed bitumen layers, depicted in Figure 2.24 and Figure 2.25 for sections 415A5 and 416A5 respectively. Surface deformation or rutting was also recorded throughout the test.

The resilient modulus of section 415A5 initially ranged between 900 and 1500 MPa, and that of section 516A5 between 1500 and 2600 MPa. After the initial trafficking the resilient modulus decreased to values representative of high quality unbound crushed stone materials (300 – 600 MPa), following a similar behaviour to that observed in the previous P243/1 HVS experiment.

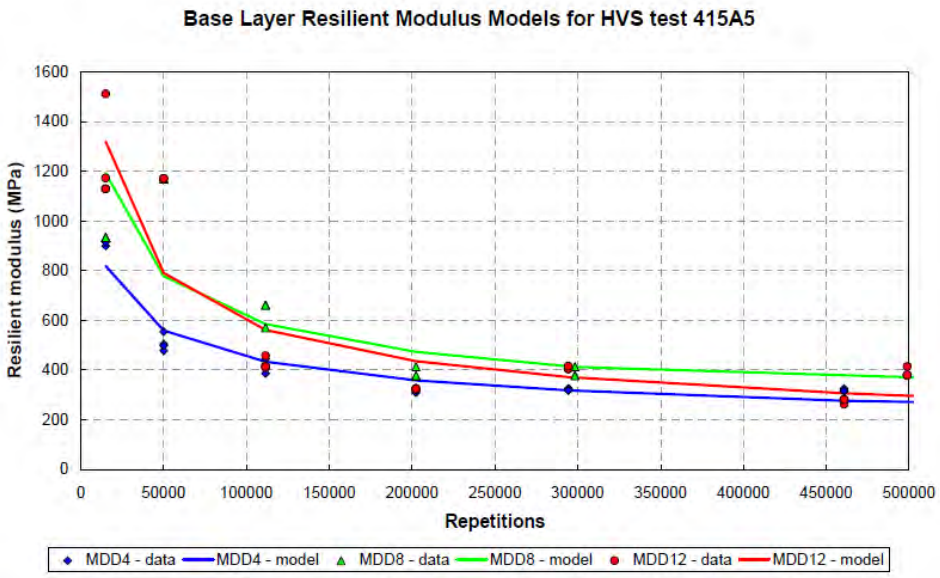

Figure 2.24 Resilient modulus measured at 415A5 pavement section (Theyse 2004)

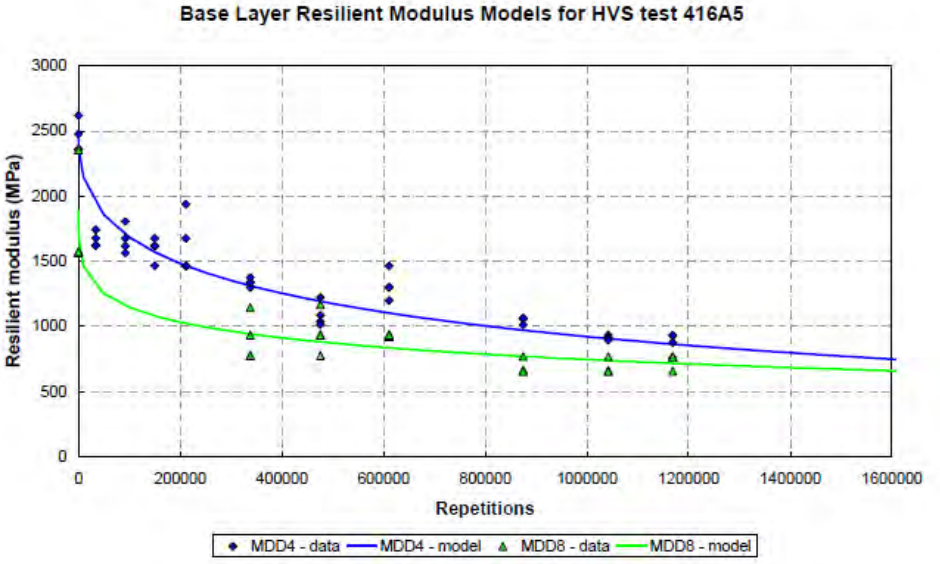

Figure 2.25 Resilient modulus measured at 416A5 pavement section (Theyse 2004)

The rutting measured in sections 415A5 and 416A5 is presented in Figure 2.26. In section 415A5 this value constantly increased with the application of the 80 kN load, while in section 416A5 a relatively constant 3 mm rutting was measured from 200,000 to 1,168,850 40 kN load repetitions. To induce additional deformation in the pavement section 416A5, the load was increased to 80 kN, inducing 3 mm of additional rutting. Finally, water was introduced

into the pavement through surface cuts, which notably increased surface rutting.

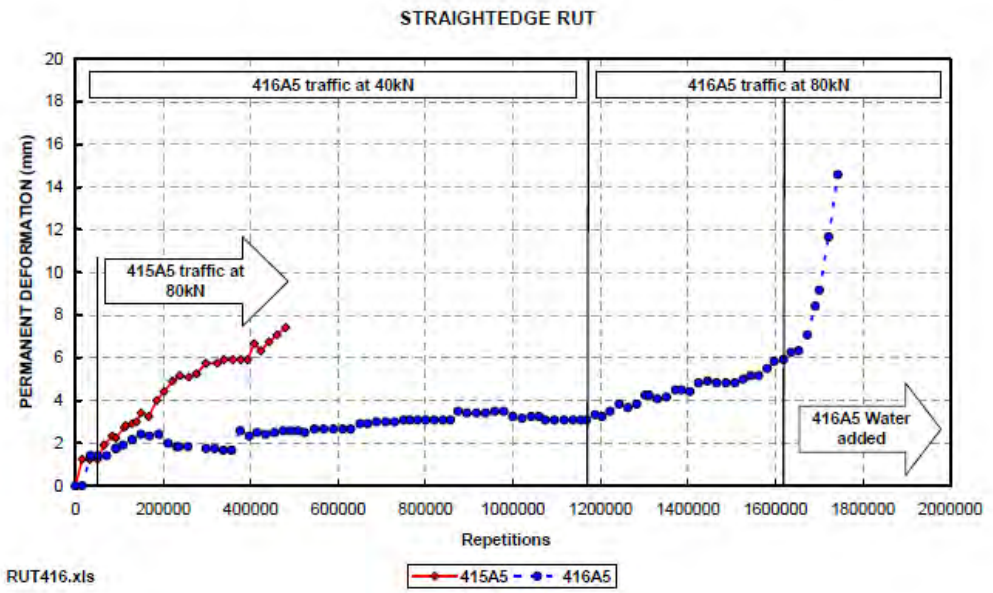

Figure 2.26 Rutting measurements in sections 415A5 and 416A5 (Theyse 2004)

2.4.4 **Kansas APT, University of Kansas**

An accelerated full-scale experiment in foamed bitumen pavements was conducted at the Civil Engineering Infrastructure Systems Laboratory of Kansas State University (United States), which is a fixed (not mobile), linear APT facility. The experiment considered three foamed bitumen pavements with different dimensions and an additional control unbound granular pavement, all of them placed on a silty clay subgrade, with a common 75 mm thick hot mix asphalt surface (Figure 2.27a). The recycled material consisted in a mixture of 50% reclaimed asphalt pavement (RAP), 37% of a Kansas unbound granular (UG) material and 12% A7-6 soil (clay), which was considered representative of a recycled pavement in Kansas State. The recycled material was stabilised with 3% foamed bitumen and 1% Portland cement contents.

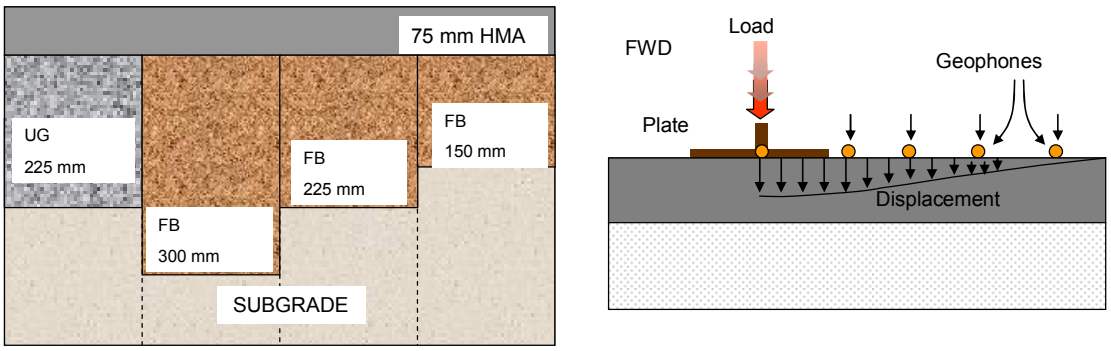

(a) (b)

Figure 2.27 (a) Pavements tested in Kansas accelerated experiment (b) Principle of the Falling Weight Deflectometer test

Several sensors were placed in the tested sections to monitor pavement response, including pressure cells and strain gauges. In addition, to complement measurements obtained from these sensors, Falling Weight Deflectometer (FWD) and Drop Weight tests were performed. The FWD simulates the load imposed on a pavement by a moving wheel load, by dropping a known mass onto the pavement surface from a selectable drop height, while geophones placed on the pavement surface measure deflection, as shown in Figure 2.27b. The Drop Weight is a test that follows the same principle of the FWD test, but with a different mass and measurement system. The FWD test will be further described in Chapter 4 (Section 4.2.3.2). The Weight Drop test consisted of dropping a weight of 27.2 Kg on a set of rubber plates that transmitted the load to a circular steel plate, 225 mm in diameter, resting on the top of the pavement. The dynamic impact load was measured with a load cell under the rubber plates and the surface deflections by several LVDTs. A typical load applied by the FWD is between 26 and 53 kN, while the load applied by the weight drop device ranges between 8.9 and 11.125 kN.

All four pavement sections were loaded with 500,000 axle load repetitions, at room temperature and under moderate moisture levels in the subgrade soil. The loads were applied using a dual-wheel single axle with a total load of 75.7 kN for the first 100,000 load cycles, followed by 400,000 load cycles of a dual-wheel tandem axle with a total load of 142.4 kN.

FWD testing was performed twice before the experiment started, and two times during accelerated loading. Because the deflection data collected were considered insufficient for determining the change in layer moduli with accelerated loading, the FWD tests were complemented by Weight Drop tests performed in the same location 12 times during the experiment. The basecourse layer moduli back-calculated from the weight drop deflections are presented in Figure 2.28. All pavements show decrease in the modulus, including the unbound granular pavement.

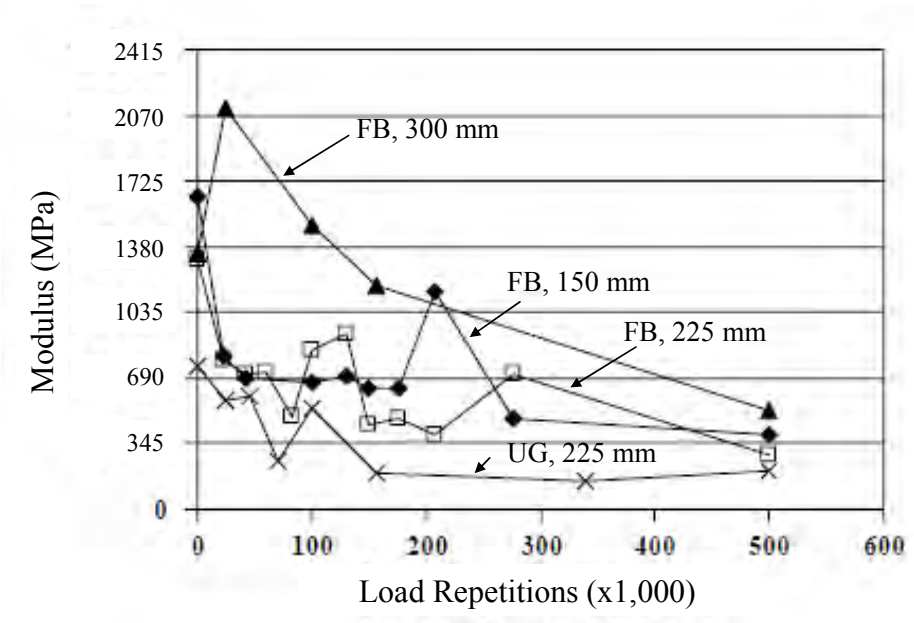

Figure 2.28 Back-calculated basecourse layer modulus from weight drop deflections (after Romanoschi and Metcalf 2001)

At the end the application of the loads, all four pavements exhibited rutting in the wheelpath (Figure 2.29). Because no cracking or other type of distress was observed during the experiment, the comparison of the performance of the four pavements was done only on the basis of the analysis of the permanent deformation and rut depth, computed from the measured transverse profiles. The foamed bitumen pavements showed rut depths between 6.4 mm and 10.2 mm, comparable with that of Kansas granular base after 100,000 passes of a 75.7-kN single axle and 400,000 passes of a 142.4-kN tandem axle. Using these deformation measurements, plus the results obtained from compressive vertical stresses at the top of the subgrade, the authors concluded that 25 mm of recycled foamed bitumen basecourse shows

performance equivalent to that of a 25 mm conventional Kansas granular base.

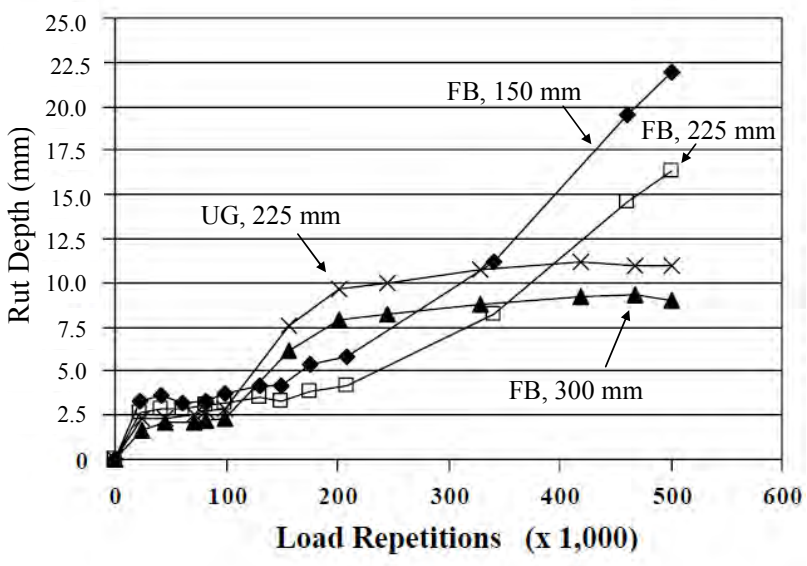

Figure 2.29 Rut depth measurements versus load repetitions (after Romanoschi and Metcalf 2001)

Based on FWD deflections, the authors also recommended an empirical structural layer coefficient used in the AASHTO guide for design of pavement structures (AASHTO 1993) of 0.18 for the foamed bitumen material. This value is higher than a common granular base (0.13) but lower than hot mix asphalt materials (between 0.33 and 0.44).

2.4.5 **Athens Highway, Greece**

A field experiment in a major Greek heavy trafficked highway was undertaken by the Laboratory of Highway Engineering of the National Technical University of Athens, with the objective of exploring the field performance of cold in place recycled pavements using foamed bitumen stabilization. The investigation focused mainly on the applicability of the falling weight deflectometer technique to study the variation in deflections of the foamed bitumen pavement with time, caused by the variation of the resilient modulus of foamed bitumen layers. The original pavement structure (Figure 2.30) consisted of distressed asphalt layers, cement bound materials (CBM) and a granular layer. The recycled layer consisted of 250 mm of foamed bitumen

mix, which was constructed recycling the old pavement layers and adding 3.2% foamed bitumen and 1% cement. In addition, 30% of sand was added to improve the particle size distribution of the recycled materials.

The elastic modulus of the hot mix asphalt and foamed bitumen treated layers were back-calculated using FWD deflections during the first 14 months after construction. The reported results of the FWD measurements indicated an increase in the foamed bitumen elastic modulus over time, an opposite trend to that obtained in the South African and Kansas full-scale APT experiments previously presented. The authors attribute this gain of strength to the curing (loss of moisture) of the foamed bitumen layer. A representative example of the measured FWD deflection is presented in Figure 2.31 (Loizos and Papavasiliou 2007).

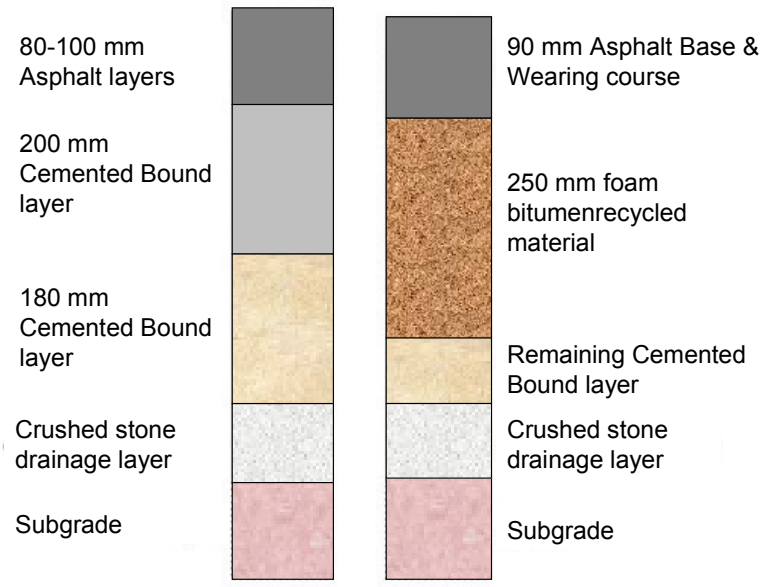

Figure 2.30 Original and rehabilitated pavement structure using foamed bitumen recycling in the Greek Highway

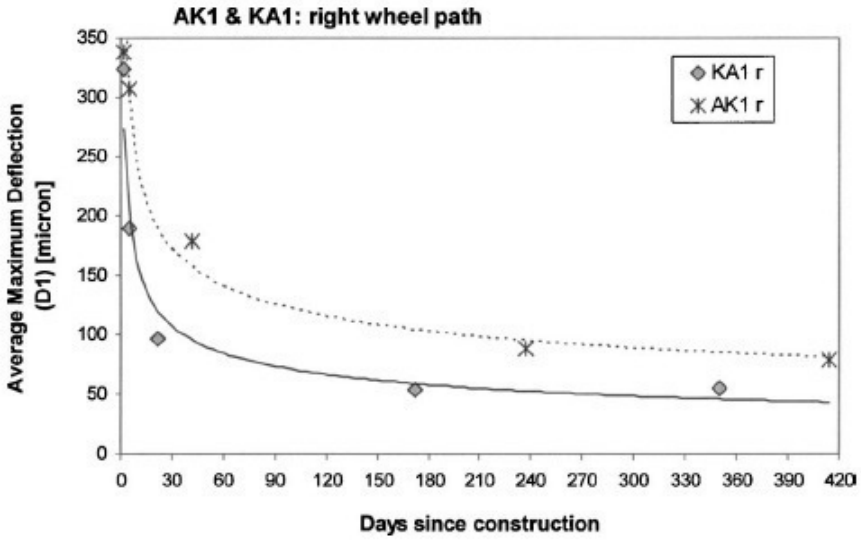

Figure 2.31 Variation of deflections measured in Greek Highway (after Loizos and Papavasiliou 2007)

2.5 Stress analysis of pavements

2.5.1 **Introduction**

Wheel loads on pavements result in a distribution and reduction of stresses throughout the pavement. As the vehicle passes over the pavement, the stress level changes from a small to a higher value (Figure 2.32). Stresses act in three-dimensions and all these stresses have an effect on how the material behaves.

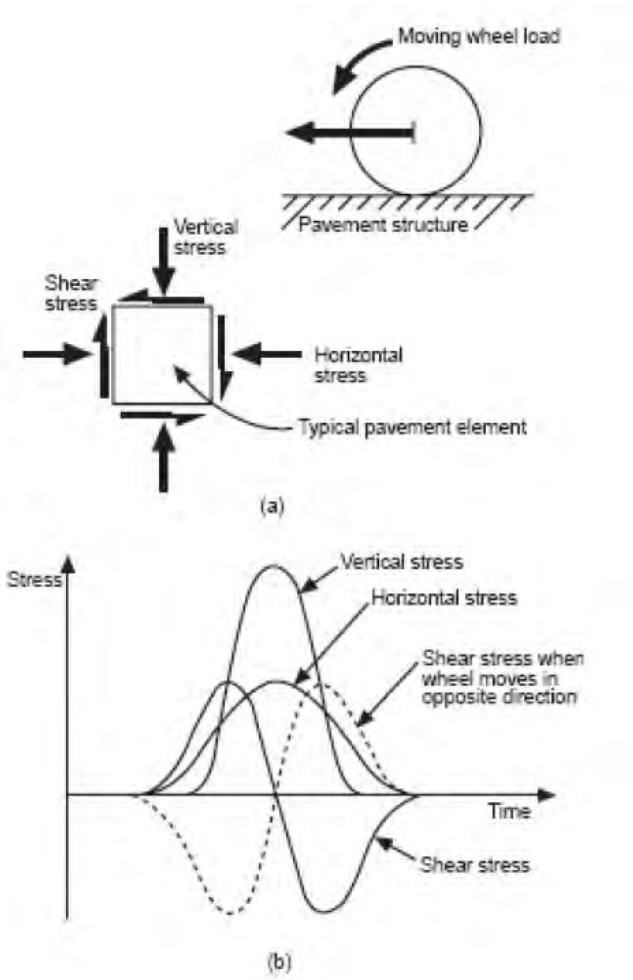

Figure 2.32 Example of stress condition under a moving wheel load: (a) stress on a pavement element; (b) variation of stresses with time

The stresses acting on a given element can be defined by its normal and shear stress components, as shown in Figure 2.33. It can be proven that for any general state of stress through any point in the body, three mutually perpendicular planes exist on which no shear stresses act. The resulting stresses on these planes are thus represented by a set of three normal stresses, called principal stresses σ_1, σ_2 and σ_3. The principal stresses are physical invariants that are independent of the adopted coordinate system.

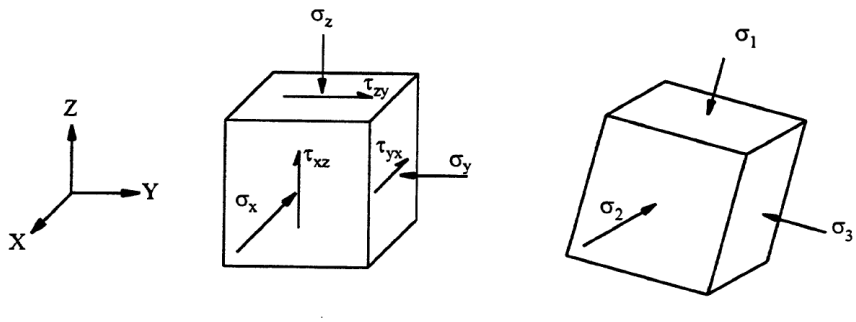

Figure 2.33 Stress acting on an element (after Lekarp et al. 1996)

The shear and normal stress components can be expressed in terms of the second-order stress tensor:

$$\sigma = \begin{pmatrix} \sigma_{11} & \sigma_{12} & \sigma_{13} \\ \sigma_{21} & \sigma_{22} & \sigma_{23} \\ \sigma_{31} & \sigma_{32} & \sigma_{33} \end{pmatrix} = \sigma_{ij} \qquad \text{(Eq. 2.10)}$$

The invariants of a stress tensor can be defined in a number of ways. The first invariant of the stress tensor (I_1) is usually expressed as a function of the three principal stresses σ_1, σ_2 and σ_3:

$$I_1 = \sigma_1 + \sigma_2 + \sigma_3 \qquad \text{(Eq. 2.11)}$$

which is three times the conventional mean stress, $p=(\sigma_1+\sigma_2+\sigma_3)/3$. The stress tensor can be decomposed into two tensors, the deviatoric stress tensor and the hydrostatic or spherical stress tensor. The deviatoric stress tensor is sometimes referred to as the stress deviator tensor. The decomposition is given by:

$$\sigma_{ij} = S_{ij} + \frac{1}{3}\sigma_{nn}\delta_{ij} \qquad \text{(Eq. 2.12)}$$

where S_{ij} is the deviator stress tensor, $\sigma_{nn}= \sigma_{11}+\sigma_{22}+\sigma_{33}$ is the hydrostatic stress, and δ_{ij} is the Kronecker delta (δ=1 when i=j and δ=0 when i≠j). The tensor S_{ij} or matrix [S] is that part of the stress state which represents the

shear or deviatoric state of stress. The tensor $1/3\sigma_{nn}\delta_{ij}$ refers strictly to the hydrostatic stress or mean normal stress acting on the body. Each diagonal component on the diagonal of the tensor $1/3\sigma_{nn}\delta_{ij}$, that is $\sigma_{nn}/3$, denotes the mean pressure p, and can be expressed as:

$$p\delta_{ij} = \begin{pmatrix} p & 0 & 0 \\ 0 & p & 0 \\ 0 & 0 & p \end{pmatrix} \qquad \text{(Eq. 2.13)}$$

The deviatoric stress tensor S_{ij} can be expressed as follows:

$$S_{ij} = \sigma_{ij} - p\delta_{ij} \qquad \text{(Eq. 2.14)}$$

where p is the mean pressure and is equal to $I_1/3$. Deviatoric stress tensor is a second-order symmetric tensor. The first invariant of this tensor is zero, and the second invariant is expressed as:

$$J_2 = \frac{1}{6}\left[(\sigma_1 - \sigma_2)^2 + (\sigma_2 - \sigma_3)^2 + (\sigma_1 - \sigma_3)^2\right] \qquad \text{(Eq. 2.15)}$$

In engineering practice, often a quantity called octahedral shear stress, τ_{oct}, is used. This shear stress is equal to the magnitude of the projection of the stress vector on an octahedral plane which makes equal angles with the three principal directions. The mean pressure, $I_1/3$, remains constant on the octahedral plane. The expression for τ_{oct} is given by:

$$\tau_{oct}{}^2 = \frac{1}{9}\left[(\sigma_{11} - \sigma_{22})^2 + (\sigma_{22} - \sigma_{33})^2 + (\sigma_{11} - \sigma_{33})^2\right] + \frac{2}{3}\left[(\sigma_{12})^2 + (\sigma_{23})^2 + (\sigma_{13})^2\right] \qquad \text{(Eq. 2.16)}$$

The second invariant of the deviatoric stress tensor, J_2, is directly proportional to τ_{oct}, and given by:

$$J_2 = \frac{3}{2}\tau_{oct}{}^2 \qquad \text{(Eq. 2.17)}$$

The stress invariants will be used in this research to compare the stress paths applied by moving wheel loads and stress paths applied in laboratory tests.

2.5.2 **Stress paths**

One of the ways to describe stress paths is to represent stress history on the deviatoric stress-mean stress space. For example, the second invariant of the deviatoric stress tensor S_{ij} (J_2), and the first invariant of the stress tensor σ_{ij} (I_1) can be used.

To illustrate the use of stress diagrams, the loading history of a cylindrical triaxial specimen is presented in Figure 2.34. The figure also shows the I_1-$J_2^{1/2}$ stress diagram and a graph where the confining stress (σ_c) and deviator stress (σ_d) history is plotted. The specimen has been initially loaded with a uniform confining stress $\sigma_{c,1}$. At this initial condition, no deviator stress is applied, therefore $\sigma_1=\sigma_2=\sigma_3=\sigma_{c,1}$, and the stress invariants take the following values:

$$I_1 = \sigma_1 + \sigma_2 + \sigma_3 = 3\sigma_{c,1} \qquad \text{(Eq. 2.18)}$$

$$J_2 = 1/6\ [\ (\sigma_{c,1}- \sigma_{c,1})^2 + (\sigma_{c,1}- \sigma_{c,1})^2 + (\sigma_{c,1}- \sigma_{c,1})^2\ ] \qquad \text{(Eq. 2.19)}$$

If the deviator stress ($\sigma_d=\sigma_1-\sigma_3$) is increased from the initial zero condition to an arbitrary value σ_d, keeping the initial confining stress constant ($\sigma_{c,1}$) both I_1 and $J_2^{1/2}$ stress invariants increase to:

$$I_1 = (\sigma_d + \sigma_{c,1}) + \sigma_{c,1} + \sigma_{c,1} = \sigma_d + 3\sigma_{c,1} \qquad \text{(Eq. 2.20)}$$

$$J_2 = \frac{1}{6}\left[(\sigma_d)^2 + (\sigma_d)^2 + (0)^2\right] = \frac{\sigma_d^{\,2}}{3} \qquad \text{(Eq. 2.21)}$$

and the stress path follows a line towards the upper right part of the stress diagram (stress path 1, in Figure 2.34

Figure 2.34). If the specimen is unloaded by reducing the deviatoric stress to zero and keeping the same confining stress constant, the stress condition will return to its original value (stress path 2). If the confining stress is increased from $\sigma_{c,1}$ to $\sigma_{c,2}$ then $I_1=3\sigma_{c,2}$, keeping $J_2=0$ (stress path 3) and if a deviator stress σ_d is applied again, the final stress condition (stress path 4) is:

$$I_1 = (\sigma_d + \sigma_{c,2}) + \sigma_{c,2} + \sigma_{c,2} = \sigma_d + 3\sigma_{c,2} \qquad \text{(Eq. 2.22)}$$

$$J_2 = \frac{1}{6}\left[(\sigma_d)^2 + (\sigma_d)^2 + (0)^2\right] = \frac{{\sigma_d}^2}{3} \qquad \text{(Eq. 2.23)}$$

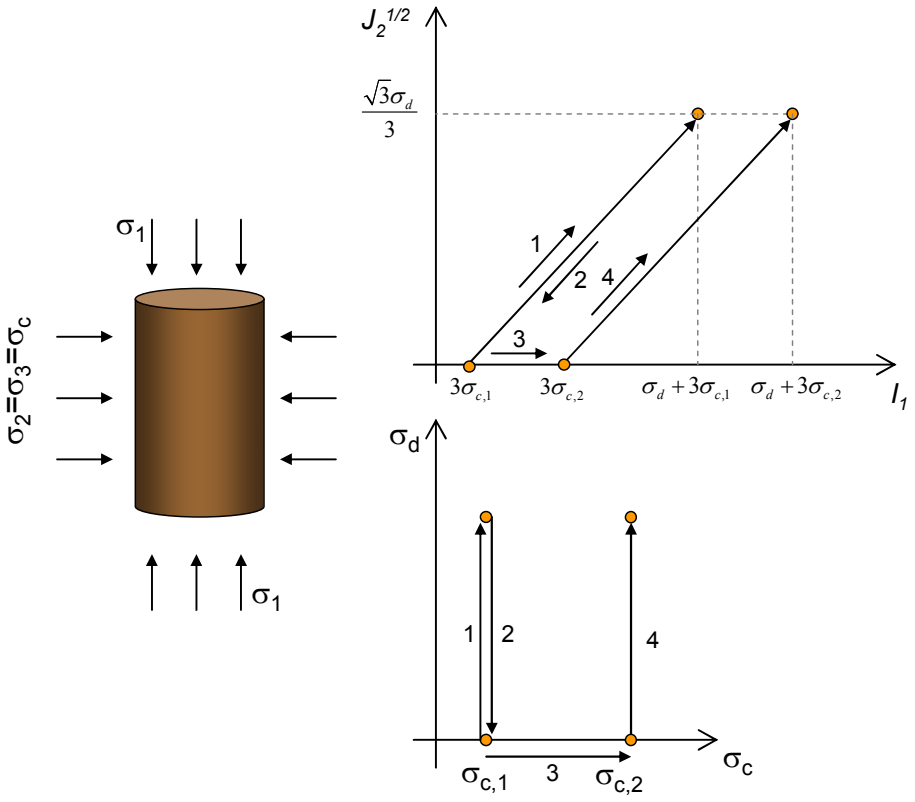

Figure 2.34 Stress paths for a compression triaxial test with uniform confining stress

2.6 Elasto-plasticity material models and finite elements modelling

2.6.1 **Introduction**

Foamed bitumen materials can carry tensile stress and can undergo plastic or irrecoverable deformation under traffic loading. A common way of simulating such material behaviour is through the use of elasto-plasticity. If the stress is always less than the yield level, the material behaviour is assumed to be elastic. Otherwise, the material develops inelastic deformation. In the conventional plasticity theory this is also known as plastic flow. In such case, the material is considered to be an elastic-perfectly plastic material. Stress levels above the yield level are not possible, and deformations will continue to take place until the stress is reduced below the yield stress through either the load being redistributed to other parts in the structure/pavement or reversed.

Hardening can also be added to conventional elasto-plastic models to model more complex stress-strain behaviour. Hardening involves either change in size or position (or both) of the yield surface leading to the development of plastic strains or a change in stiffness, or available complex hardening rules can be used to accommodate realistically actual behaviour of materials.

Mohr-Coulomb and Drucker-Prager criteria are commonly used for modelling failure of materials of frictional nature, in which hydrostatic pressure has an important effect on strength (Desai 1984). Jenkins et al (2007) have reported the effect of foamed bitumen and cement in the fundamental shear parameters (Mohr-Coulomb) of foamed bitumen mixes.

2.6.2 **Mohr-Coulomb**

According to the Mohr-Coulomb criterion, the shear strength increases with increasing normal stress on the failure plane:

$$\tau_f = c + \sigma_n \cdot \tan\phi \qquad \text{(Eq. 2.24)}$$

here, τ_f is the shear stress on the failure plane, c is the cohesion of the material, σ_n is the normal effective stress on the failure surface, and ϕ is the angle of internal friction. The concept of Mohr circle can be used to express the criterion in terms of principal stresses.

According to the Mohr-Coulomb criterion, the yield strength in terms of conventional triaxial compression is higher than that in conventional triaxial extension; this shows the dependence of the behaviour on the mean stress (p). At the same time, the Mohr-Coulomb criterion is expressed in terms of maximum and minimum principal stresses, and hence does not incorporate the effects of intermediate principal stresses.

The two parameters associated with the Mohr-Coulomb failure criterion, i.e. the angle of internal friction ϕ and cohesion c, can be determined from laboratory tests. The Mohr-Coulomb failure line is the envelope of Mohr circles at failure, and the values of ϕ and c could be determined as shown in Figure 2.35. Conventional triaxial compression tests on cylindrical specimens (Section 2.3.3) are commonly used to determine the cohesion and angle of internal friction. Typically three tests are required to determine c and ϕ.

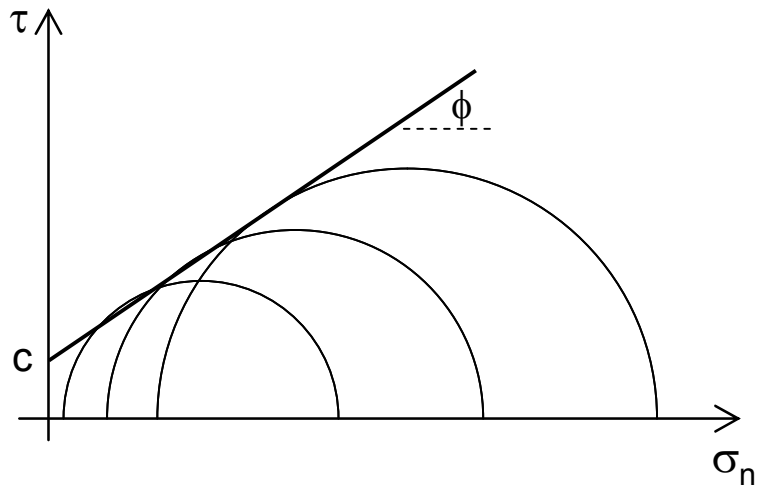

Figure 2.35 Mohr circles at failure and determination of shear strength parameters

2.6.3 **Drucker-Prager**

A generalization allowing to account for the effects of all principal stresses was suggested by Drucker and Prager (1952) by using the invariants of the stress tensor. The generalized criterion can be written as:

$$F_s = \sqrt{J_2} - \alpha \cdot I_1 - k \qquad \text{(Eq. 2.25)}$$

where α and *k* are positive material parameters, I_1 is the first invariant of the stress tensor, and J_2 is the second invariant of the deviatoric stress tensor. The equation represents a straight line in an I_1 versus J_2 plot. In the three-dimensional stress space, the criterion plots as a right circular cone, and the projection on the Π-plane, which is the plane that forms equal angles with the principal stresses axes, is a circle, as shown in Figure 2.36. When the state of stress reaches the failure surface, the material undergoes plastic deformation.

The two material parameters α and k for the Drucker-Prager model can be determined from the slope and intercept of the failure envelope plotted on the I_1-$J_2^{(1/2)}$ space. In order to establish the failure envelope for a given material, it is necessary to perform laboratory tests up to failure. The values of α and k can also be expressed in terms of the angle of internal friction ϕ and cohesion c, by matching the common intersection points at the vertices of the hexagonal failure envelope (Figure 2.36).

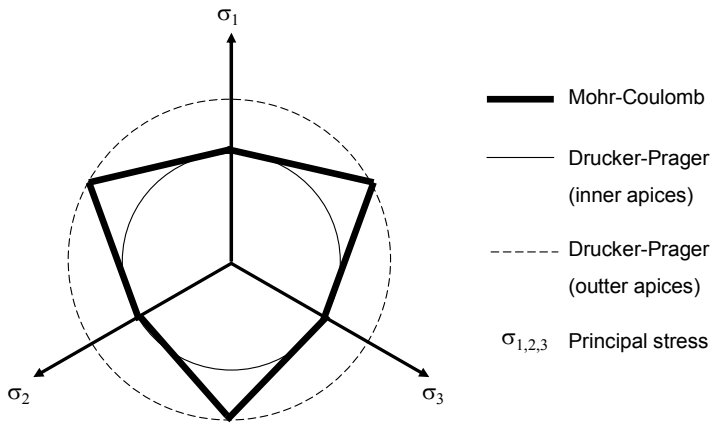

Figure 2.36 Projections of Mohr Coulomb and Drucker-Prager criteria on the Π plane

One weakness of the Drucker-Prager yield criterion is that the maximum strength in compression is the same as the maximum strength in extension (i.e. for the cases when $\sigma_1>\sigma_2=\sigma_3$ and when $\sigma_1=\sigma_2>\sigma_3$) because its yield surface is circular on the plane, contradicting the characteristics of granular materials. On the contrary, Mohr-Coulomb does show a difference between them by a hexagonal cross section, as demonstrated in Figure 2.36. Thus, the Drucker-Prager criterion could overestimate the strength in extension of a granular material.

The advantage of the Drucker-Prager material model over Mohr-Coulomb is that Drucker-Prager can be incorporated into 2D finite element analyses thanks to the simple shape of the conical envelope. 2D finite element analyses are significantly less time-consuming than 3D analyses.

2.6.4 **Finite elements**

Current linear elastic programmes used in foamed bitumen mechanistic design procedures (Section 2.2.1) ignore the elastoplastic behaviour of pavement materials. Hence, finite element modelling (FEM) is required to incorporate the non-linear stress-strain relationships of these materials.

Many researchers have customised general finite element packages to develop finite element programs specific to pavements. Some of these programs include DEFPAV (Snaith 1980) developed at Queens University Belfast, FENLAP (Finite Element Non-Linear Analysis for Pavements) (Brunton 1992) developed at Nottingham, and ILLI-PAVE (Thompson 2002) from the University of Illinois. Other finite element programs like ANSYS and ABAQUS are general commercial finite element packages. Commercial finite element packages are more time consuming as they require the user to develop the geometry and choose (if available in the material library) or program a suitable material model. Further, commercial finite element packages cannot easily accommodate trial changes in pavement thickness as a new geometry needs to be created each time. However, conventional

packages have the advantage of being readily available, and allow for analysis of complex geometries (Arnold et al. 2003).

Currently, most of the modelling research in pavements is undertaking using three dimensional (3D) instead of two dimensional (2D) finite element models, because their ability of representing more realistic field conditions, and because the increase in computer power that has reduced the time spent in the analyses. However, most of these analyses correspond to the modelling of one single load repetition of a static wheel load.

Saleh et al (2003) developed a three-dimensional finite element model in ABAQUS, as part of a study of the effect of increasing axle load and tyre pressure on pavement deterioration. For the study, they simulated the conditions at the Canterbury Accelerated Pavement Testing Indoor Facility (CAPTIF) located in Christchurch, New Zealand, and compared the results of the finite element modelling with the actual pavement measurements. In the finite element model, both the unbound granular base and the subgrade materials were modelled as elastic-plastic materials using the Drucker-Prager material model (Section 2.6.3). The wheels were simulated with two static loads on the model surface. The effect of cyclic or repetitive loading was not considered in this model, and deformation was calculated with the application of one monotonic load pulse. The researchers calculated the surface deformation (rutting) by numerically integrating the calculated vertical permanent strain values with depth. Integration of the permanent strains for the case of a dual load of 50 kN and a tyre inflation pressure of 750 kPa yielded a total permanent deformation of 0.43 mm, with 0.16 mm of rutting occurring in the base layer and 0.27 mm of rutting in the subgrade layer. The real pavement rutting was measured excavating three trenches in the CAPTIF pavements. The average permanent deformation showed that basecourse and the subgrade were 3.4 and 3.0 mm respectively. The model was not accurate to determine the magnitude of the permanent surface deformation, but could correctly predict the trends observed in the CAPTIF, in which 46.9% of the surface deformation occurred in the basecourse, versus the 37.2% predicted by the finite element model (Table 2.5).

Table 2.5 Surface deformation results predicted in ABAQUS and measured in CAPTIF by Saleh et al. (2003)

			% of total deformation	
Layer	ABAQUS (mm)	CAPTIF (mm)	Measured by CAPTIF	Predicted in ABAQUS
Basecourse	0.16	3.0	46.9%	37.2%
Subgrade	0.27	3.4	53.1%	62.8%
Total	0.43	6.4	-	-

Arnold (2004) analyzed four pavements tested in the CAPTIF using ABAQUS. The researcher modelled the elastic behaviour of the material using a porous elasticity material model, which is available in the ABAQUS material library, and the plastic behaviour, using the linear Drucker-Prager material model. Using laboratory data from triaxial testing, he defined three plastic zones of the granular materials studied (Ranges A, B and C in Figure 2.37).

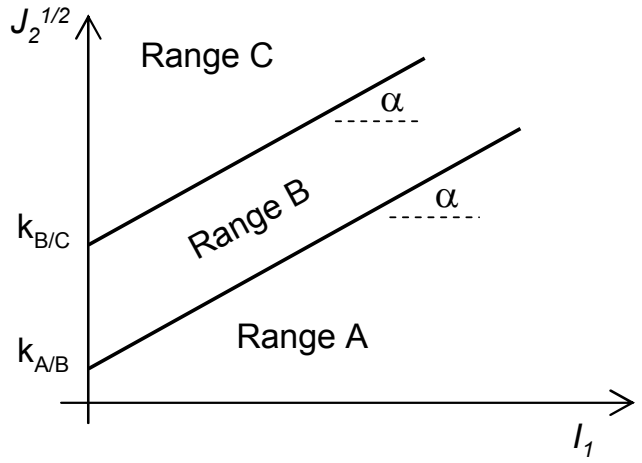

Figure 2.37 Plastic limits defined for the surface deformations of granular pavements

Arnold calculated the plastic deformations using both failure lines (A/B and B/C), using an axisymmetric finite element model. The wheel load was approximated as a circular load of 40 kN with a uniform contact stress of 750 kPa. He obtained surface deformations 0.20 to 0.97 mm for the A/B failure line, and between 0.08 and 0.20 for the B/C failure line, lower than the real rut depths measured in the actual CAPTIF pavements tests (approximately 6

mm). Arnold argued that the calculated permanent deformation from the finite element model should not be considered a predicted rut depth, because the analysis is static, and its purpose is to asses whether or not stresses within the pavement exceeded the range boundaries defined in Figure 2.37.

2.7 Summary

The Chapter presented a summary of the literature and theory that contribute to the design and modelling of foamed bitumen pavements. Some key points from the literature review relevant to the thesis are summarized below:

- The South African mechanistic design method, which was developed using accelerated pavement tests and laboratory experiments, suggests that foamed bitumen pavements behave in two separate phases. The first is an effective fatigue phase, in which the foamed bitumen layer provides fatigue resistance. The second is the equivalent granular phase, in which the material behaviour is comparable to granular materials. The distress models suggested by the South African method, which are equations that relate the number of admissible load repetitions with design imputs (such as stress ratio, density, bitumen and cement contents), yield a reduction in the number of admissible load repetitions when the foamed bitumen content increases in a foamed bitumen mix (e.g. from 2% to 3%).

- The New Zealand design method for foamed bitumen pavements ignores the effective fatigue phase, since this material behaviour has not been observed in New Zealand foamed bitumen pavements. The New Zealand design method only considers the deformation of the subgrade layer as the design criterion (AUSTROADS subgrade criterion), ignoring the permanent deformation of the foamed bitumen layer.

- Indirect tensile strength (ITS) and Unconfined Compressive Strength (UCS) tests reported in the literature provide non-conclusive trends. The ITS value normally increases with increase in foamed bitumen content, up to an optimum, but in other cases an optimum is not clearly observed. Conversely, the UCS value normally decreases with increase in bitumen content.

- Monotonic load triaxial tests show decrease in peak axial stress with increase in the foamed bitumen content, for a constant content of active filler (normally 1% cement). The fundamental shear strength properties (angle of internal friction and cohesion) of foamed bitumen mixes is calculated using monotonic load triaxial tests, showing decrease in the angle of internal friction with increase in foamed bitumen content. The addition of cement has a significant effect on cohesion, while the foamed bitumen content does not seem to show important effect on this value.

- Repeat (cyclic) load triaxial tests conducted on foamed bitumen mixes suggest that a stress ratio (applied-stress/peak-stress) of 55% is defined as the boundary between a stable permanent deformation rate and an accelerated permanent deformation rate, under repeated loading.

- Resilient modulus measured in repeat load triaxial tests show an important increase in resilient modulus when 1% cement is added to the mix, while a comparatively less important effect, or even decrease, is measured when foamed bitumen is added.

- Accelerated pavement testing conducted in South Africa and Kansas (United States) on foamed bitumen pavements show that the elastic moduli of foamed bitumen pavements decrease with increasing number of load applications. However, deflection measurements collected from a monitored heavy trafficked highway in Greece suggest that after 14

months of service the elastic modulus of the foamed bitumen layer increases with time. In the South African full-scale experiments, damaged was observed only when water was introduced in the pavements.

- Stress diagrams, based on the first invariants of the stress tensor (I_1) and the second invariant of the deviator stress tensor (J_2), are used to describe the stress history applied on an element.

- Mohr-Coulomb and Drucker-Prager are two material models used for the modelling of granular-type materials. The parameters that define the failure line for these models (angle of internal friction and cohesion) are normally determined using conventional monotonic triaxial test data. These models are incorporated to finite element programs for the modelling of the plastic deformation of pavements.

This page is intentionally left blank.

3 Laboratory Experimental Work

3.1 Introduction

This chapter presents the laboratory evaluation of the materials adopted in the full-scale accelerated pavement experiment. The main objective of the laboratory experimental work was to study the response of the foamed bitumen mixes under a wide range of stresses or loading conditions, using different types of tests to characterize the performance of these mixes.

The laboratory work included the physical characterization of the materials selected (aggregates and bitumen) as well as preliminary studies to define some specific parameters for this research project (e.g. curing conditions, stress level and load sequence applied in repeat load triaxial tests). The tests done were:

- Indirect tensile strength
- Indirect tensile resilient modulus
- Repeat Load Triaxial permanent strain
- Repeat Load Triaxial resilient modulus
- Static (monotonic) triaxial

The study started eight months before the construction of the full-scale experiment, and it was conducted at the Transportation Engineering Laboratory at the University of Canterbury. Particular attention was given to study the effects of foamed bitumen on materials in which active filler (1.0% cement) has been incorporated, because the mixes without active filler showed a poor behaviour.

The effects of foamed bitumen on the laboratory tests was interpreted using stress analysis, by comparing the failure stress state of the mixes, obtained

from Monotonic Triaxial Tests, with the stress paths applied in the other laboratory tests.

3.2 Materials and preparation of specimens

3.2.1 **Aggregate**

3.2.1.1 Source selection criterion

As was presented in Chapter 1, the main objective of this research project was to study the effects of foamed bitumen stabilisation on the performance of a representative granular material used in New Zealand. Therefore, the granular material had to satisfy the following requirements:

- To have a grading in compliance with the current TNZ M/4 specification for basecourse aggregate (TNZ 2006) (i.e. to be a representative aggregate used in New Zealand for road construction).
- The aggregate source should be located in a region of New Zealand where high-quality aggregates are not readily available for road construction.
- The quality of the aggregate should be moderate to poor according to the experience of road engineering practitioners. In such case, the effects of stabilisation should be more relevant than in a good quality aggregate.

The source of the granular material was recommended by Transit New Zealand in consultation with the University of Canterbury and the New Zealand Stabilisation Group. The aggregate was sourced from a quarry located in the Auckland region.

3.2.1.2 Characteristics

The geological origin of the aggregate source is a Greywacke rock, which is a collective term covering argillite, siltstone and sandstone. Greywacke is not considered an inherently weak rock by geologists (Black 2004) because the coarser grained siltstones and sandstones have the potential to provide good quality aggregates. The Greywacke rock is considered the most readily

available source of aggregates for Auckland and improving its properties could partially solve the aggregate supply problems in the region (Section 1.1).

The crushed aggregate was named “H40” and its maximum size is 40 mm. It has a dark colour and poorly-sorted angular grains. The specific gravity of the aggregate is 2.69 t/m^3, the maximum dry density is 2.22 t/m^3, and the optimum basecourse moisture content is 4.0%.

The construction of the stabilised pavement for the full-scale project had been scheduled for January 2007, about nine months after the commencement of the laboratory study, and therefore the aggregate particle size distribution could have varied due to the natural variability inherent in the quarry production. In other words, it was impossible to predict the aggregate size distribution to be supplied by the quarry at the time of construction of the full-scale experiment. To minimize the risk of aggregate variability, the production from the quarry was analyzed using six months of data available at that time. Later, the average particle size distribution of the quarry was calculated and this particle size distribution was reconstituted and used in the laboratory study. Details of the aggregate production are included in Appendix B.

The particle size distribution of the H40 aggregate is presented in Figure 3.1, which also includes: 1) variability in quarry production (represented by bars showing the standard deviation); 2) TNZ M/4 grading envelope and 3) the recommended envelope for foamed bitumen stabilisation (Ruckel et al. 1983). The figure shows that H40 complies with the TNZ M/4 specification. Also, small variability was found in the fine part of the aggregate (below 2 mm), which was considered as a positive factor as this is the main fraction where foamed bitumen disperses or interacts with the aggregate (Jenkins 1999).

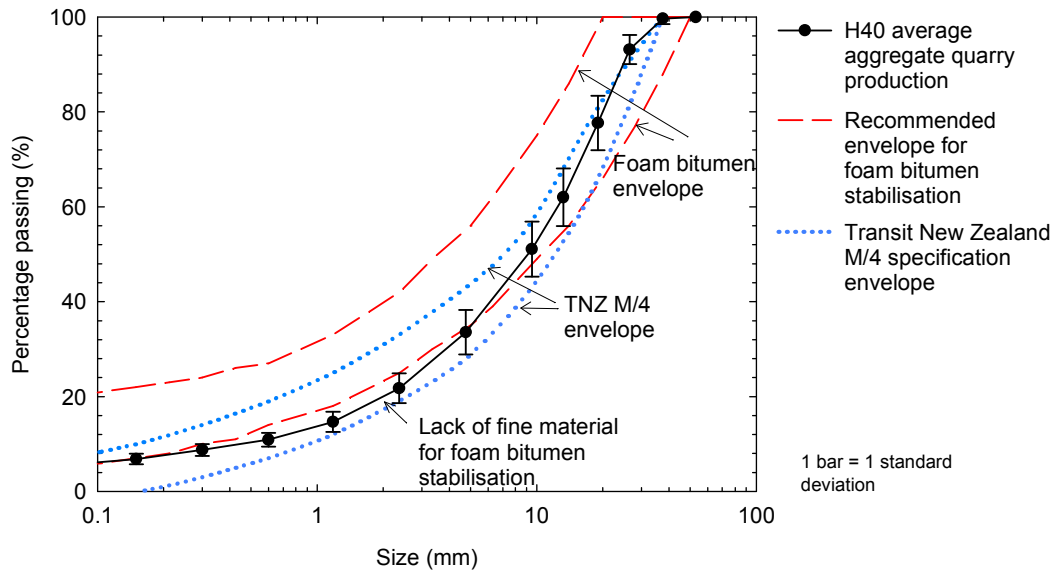

Figure 3.1 Particle size distribution variability in H40 quarry and envelopes for foamed bitumen stabilisation and New Zealand aggregates

As shown in Figure 3.1, The particle size distribution of the H40 aggregate was not directly suitable for foamed bitumen stabilisation because it was too coarse according to the recommended grading envelopes found in the literature (Asphalt Academy 2002). Therefore, H40 particle size distribution was adjusted using a crusher dust ("AP5") material, which is an aggregate commonly used in the production of Hot Mix Asphalt, to bring it into the recommended grading zone. The AP5 was obtained from a different Greywacke source located in Christchurch and a final mix of 85/15 (aggregate/dust), by mass, was found suitable to satisfy the grading requirements for foamed bitumen stabilisation. The maximum dry density of the AP5 is 1.82 t/m^3, the optimum moisture content is 9.0%, the specific gravity 2.7 t/m^3 and the maximum particle size is 5 mm. No plastic fines were found in the H40/AP5 aggregate mix following the ASTM D4318-05 standard (ASTM 2005). The particle size distribution of the AP5 material and the final H40/AP5 blend are depicted in Figure 3.2. The figure shows that the final blend complies with the recommended foamed bitumen grading but is still a relatively coarse material for foamed bitumen stabilisation. A picture of the H40 coarse fraction and the AP5 is shown in Figure 3.3.

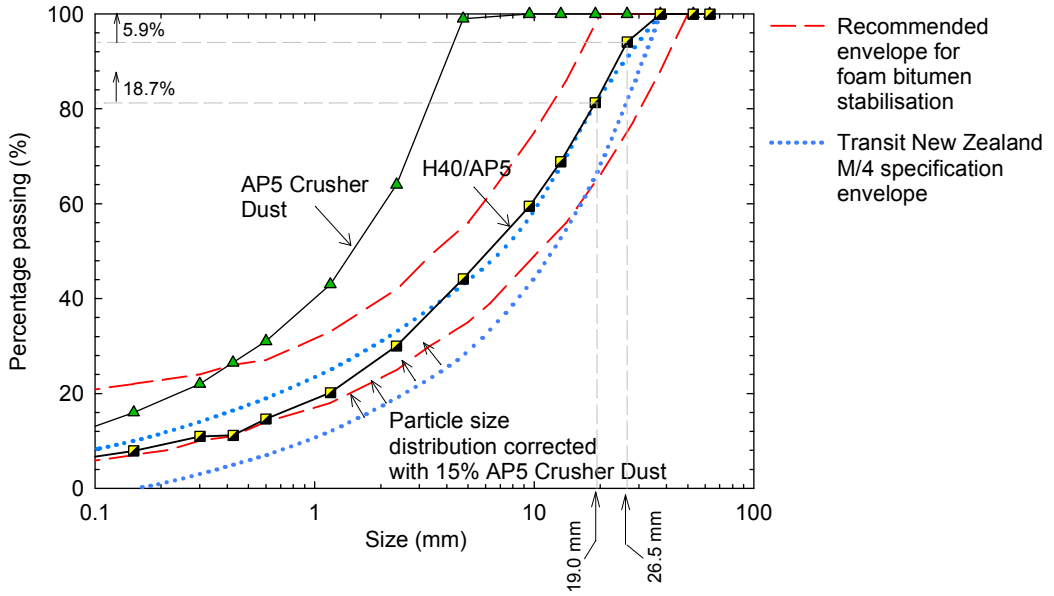

Figure 3.2 Particle size distribution of H40, AP5 and final H40/AP5 mix for foamed bitumen stabilisation

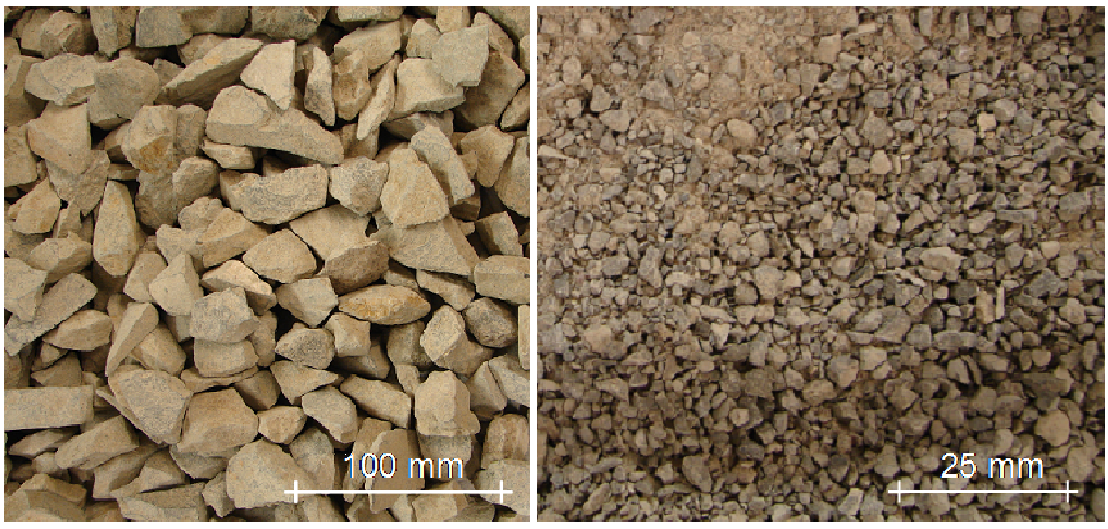

Figure 3.3 Pictures of H40 (coarse fraction) and AP5 aggregates used for the experimental study

Although the two aggregate sources adopted are different, this type of blending could represent the actual construction method in the field, in which a granular pavement is recycled after several years of service. If the existing pavement material is too coarse, a readily available finer material (e.g. the AP5 crusher dust), from a different source, could be used to improve the particle size distribution of the reclaimed pavement. The transportation of the

fine aggregate material to the field will increase construction costs, but the cold in place recycling using foamed bitumen is likely to remain attractive over traditional construction techniques, in which the existing deteriorated pavement has to be demolished and dumped, while a 100% of the new material needs to be imported to the field. Therefore, if the amount of imported aggregate is low, the cold in place recycling rehabilitation alternative is likely to remain costly effective and attractive from a technical, economical and environmental perspective (Section 1.2). The most important rehabilitation project using foamed bitumen found in the literature, in which 30% of the aggregate was imported to improve the particle size distribution of the existing pavement, is the highway that links Athens and Korinthos in Greece (Loizos and Papavasiliou 2007), a heavily traffic road that is part of the Trans European Network (Section 2.4.5).

3.2.1.3 Optimum moisture content

Vibratory compaction was used to determine the optimum moisture content of the aggregate. This compaction method was selected because it has been successfully used in other foamed bitumen research (Jenkins et al. 2008; Long and Ventura 2004); is suitable to prepare large triaxial specimens (Arnold et al. 2003; Werkmeister et al. 2004) described later in this Chapter; and is the New Zealand Standard for unbound material. Five H40/AP5 material samples of 5,500 g were mixed at target water contents of 4.0%, 5.0%, 6.0%, 7.0% and 8.0%. The compaction and material sample size was conducted following the New Zealand Vibrating Hammer Compaction test NZS 4402.4.1.3:1986 (NZS 1986). The samples were compacted in two layers of 20 mm each, applying a vibratory load for 180 seconds. Figure 3.4 shows the relationship moisture-dry density for the vibratory compaction. The figure shows that the optimum moisture content for the H40/AP5 aggregate mix is near to 6.0%. This optimum moisture content is consistent with individual optimum moisture contents obtained from the H40 and AP5 aggregates (4.0% and 9.0%, respectively).

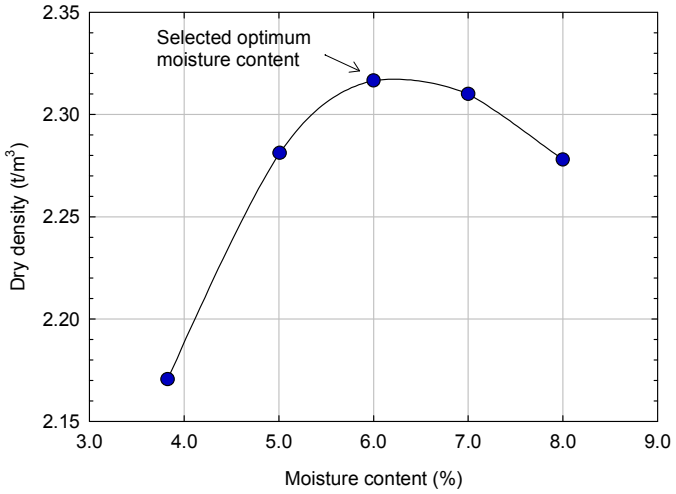

Figure 3.4 Relationship moisture-dry density obtained using vibratory compaction for the H40/AP5 aggregate

3.2.2 **Bitumen**

3.2.2.1 Physical and engineering properties

A commonly imported bitumen used for foamed bitumen stabilisation in New Zealand was adopted for this project. The bitumen was sampled from a local source in Christchurch. The physical properties of the bitumen are summarized in Table 3.1. The bitumen grade was classified as 80/100 using the current classification system used in New Zealand. The penetration, softening point and viscosity were determined in accordance with ASTM D5, ASTM D36 and ASTM D4402 respectively.

Table 3.1 Physical properties of the 80/100 bitumen grade

Penetration at 25 °C	87
Viscosity at 60 °C (mPa.s)	50129
Viscosity at 135 °C (mPa.s)	485
Softening point (°C)	48

3.2.2.2 Foaming characteristics

The physical properties provided in the previous section do not fully determine the quality of the bitumen to be used in a foamed bitumen mix. The foaming

properties or foamability of each bitumen type needs to be tested. Two characteristics form the basis of bitumen's suitability for use: the Expansion Ratio (ER) and Half-Life (HL). The expansion ratio is a measure of the viscosity of the foam and will determine how well the binder will disperse in the mix, and it is calculated as the ratio of the maximum volume of foam relative to the original volume of the bitumen. The half-life is a measure of the stability of the foam and provides an indication of the rate of collapse of the foam during mixing. It is calculated as the time taken in seconds for the foam to collapse to half of its maximum volume (see Appendix A, Section A.2).

Jenkins (1999) argued that characterisation of foamed bitumen by determining the expansion ratio and half-life time of the foam does not provide a complete understanding of the foaming potential and the characteristics of the foamed bitumen. He found the main problem of the normal method for measuring half-life time and expansion ratio in the laboratory is that the process of spraying foam into the receiving vessel takes a considerable time (5 seconds) compared to the half-life itself. As a result, he introduced a Foam Index (FI) based on the observed decay on various foams to characterise the foaming quality. The calculation of this index involves a correction factor ("c") to account for the foam collapse during the 5 seconds spray. The FI is calculated using the following equation:

$$FI = -\frac{\tau_{1/2}}{\ln 2} \times \left(4 - ER_m - 4 \times \ln\left(\frac{4}{ER_m} \right) \right) + \left(\frac{1+c}{2 \times c} \right) \times ER_m \times t_s \qquad \text{(Eq. 3.1)}$$

where:

c = ER_m/ER_a

t_s = Time of spraying to discharge all foam (seconds)

$\tau_{1/2}$ = Half-life (seconds)

ER_a = Actual expansion ratio

ER_m = Measured expansion ratio

The characteristics of the foam were investigated using the foamed bitumen laboratory model WLB10 available at the Transportation Laboratory at

University of Canterbury. The objective of the investigation was to determine the combination of foaming water and temperature that yields the foam with the best properties (i.e. the maximum Foam Index). To produce the foam, the testing method proposed by the TG2 South African guidelines was used (Asphalt Academy 2002; Jenkins 1999). During the bitumen foaming, the water pressure was set at 6 Bar in the WLB10 laboratory while the air pressure was fixed at 5 Bar. The air was simultaneously injected with the water into the bitumen. The full experimental design matrix presented in Table 3.2 was tested.

Figure 3.5 summarizes the foamability results for the bitumen 80/100 studied, expressed in terms of Foam Index. Detailed expansion ratio and half-life values were included in Table 3.3. The Figure also includes the recommendations provided by the Interim South African Guidelines (Asphalt Academy 2002) that classify the foam as ranging “unsuitable” to “very good” according to the Foam Index value. This classification is made assuming that the temperature of the aggregate during mixing is 25 °C.

Table 3.2 Full experimental design matrix for the optimization of the bitumen foaming properties

		Foaming water content (%)				
		1.5	2.0	2.5	3.0	3.5
Temp (°C)	160	●●	●●	●●	●●	●●
	170	●●	●●	●●	●●	●●
	180	●●	●●	●●	●●	●●

Note: (●) is one replicate of the experiment

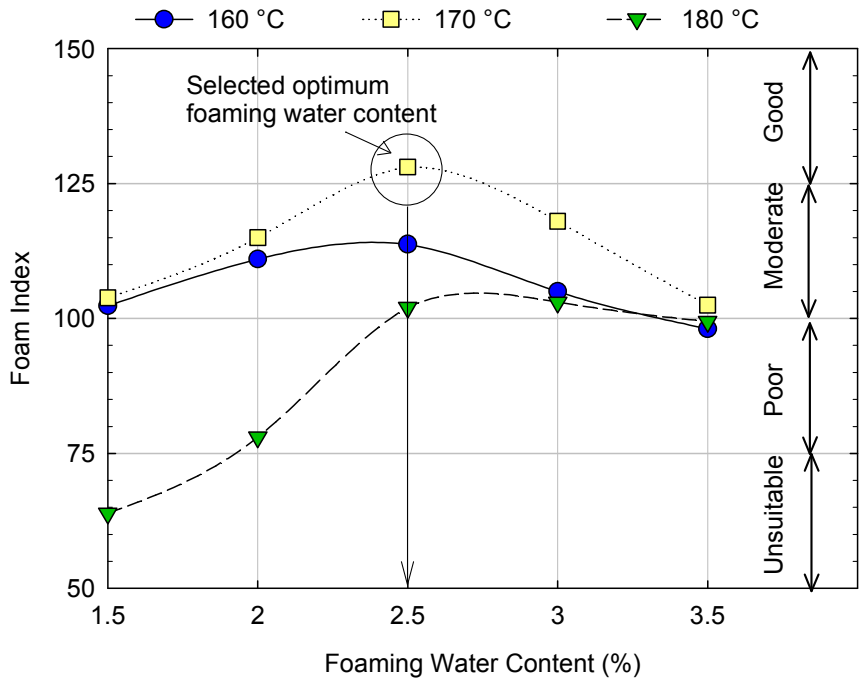

Figure 3.5 Effect of foaming water content and temperature on the foam index for the bitumen studied

The results show that at 2.5% foaming water in combination with a bitumen temperature of 170 °C yields a Foam Index of 128, which is classified as "Good" by the South African Guidelines. For other foaming water contents and at temperature of 160 °C, the foam quality was classified as "Moderate" and at 180 °C and at low foaming water contents the foam quality decreased to "Poor". Therefore, special care was taken during the subsequent production of mixes to keep the temperature in a range of 170 ± 2 °C.

The foam index results were consistent with results previously published by Saleh (2004a) who reported similar FI values for New Zealand bitumen with a penetration grade of 80/100 from different sources.

Table 3.3 Foaming parameters

		Replicate 1		Replicate 2		Average			
T (°C)	Wc (%)	ER	HL	ER	HL	ER	HL	c	FI
160	1.5	11	10	11	10	11	10	0.78	102
	2.0	11	10	11.5	9.5	11	10	0.77	111
	2.5	12	9.5	12	9	12	9	0.77	114
	2.0	11	10	11	10	11	10	0.78	105
	3.5	11	9	11	9	11	9	0.78	98
170	1.5	9	18	10	18	10	18	0.80	104
	2.0	11	15	11.5	15	11	15	0.78	115
	2.5	12	12	12	12	12	12	0.77	128
	2.0	13	9	11	8	12	8.5	0.77	118
	3.5	14	6	11	6	13	6	0.77	102
180	1.5	1.5	9	5.5	9	5.5	9	0.75	64
	2.0	2.0	10	8	10	9	10	0.80	82
	2.5	2.5	12	7	12	7	12	0.77	102
	2.0	3.0	12	7	12	6	12	0.77	99
	3.5	3.5	12	6	12	7	12	0.77	99

3.2.3 **Preparation, mixing and compaction of materials**

3.2.3.1 Specimen and maximum aggregate size

The diameter of the cylindrical specimens is 150 mm; this large diameter permits the incorporation of a higher proportion of the total H40/AP5 mix. Aggregate sizes larger than 26.5 mm were not used in the preparation of samples to ensure that the maximum aggregate size did not exceed ¼ of the 150 mm diameter specimens. The fraction over 26.5 mm represents only 5.9% of the total H40/AP5 mix (see Figure 3.2). If small specimens (100 mm diameter) were used for the experiments, the maximum aggregate particle size allowed was 19.0 mm (approximately ¼ of the diameter), which requires almost a fifth (18.7%) of the total aggregate to be discarded (see Figure 3.2). The importance of using a large proportion of the actual aggregate in laboratory testing was studied by Sweere (1993) and Lekarp and Isacsson (2001). They conducted a series of repeat load triaxial tests on large scale equipment and found that aggregates should be tested at their natural

maximum size, with the implicit requirement that large specimens are required.

3.2.3.2 Aggregate preparation

The H40 aggregate was separated into five fractions: 19 mm, 13.2 mm, 9.5 mm, 4.75 mm and passing 4.75 mm. The aggregates retained in each sieve were kept in large trays or buckets and later remixed for the reconstitution of the H40 material. The mass required from each sieve are presented in Table 3.4, where the AP5 crusher dust was also included.

Table 3.4 Weighs used for aggregate reconstitution

Sieve Size (mm)	Source	Mass (gr)
26.5	H40	Discarded
19.0	H40	1960.5 (*)
13.2	H40	2145.9
9.5	H40	1007.1
4.75	H40	1726.6
Under 4.75	H40	3175.4
Under 4.75	AP5	1944.9
Total		11960.5

(*) Not included in the foamed bitumen mixing bowl

The aggregate was kept in the oven at 25 °C for at least two hours before mixing with foamed bitumen, because temperature has been reported as an important aspect affecting the mechanical properties of foamed bitumen mixes (Gaudefroy et al. 2007; Lee and Kim 2006; Van De Ven et al. 2007). 25 °C was selected being representative of the aggregate temperature during the scheduled construction of the full-scale experiment during January - February, based on average soil temperatures reported for Christchurch (NZ Weather Station 2006). The selected temperature also agrees with the classification of the foam quality described previously in 3.2.2.

3.2.3.3 Mixing with foamed bitumen

Before mixing, the WLB10 laboratory foaming was set at 170 °C, the foaming water flow was adjusted to 2.5% (see Figure 3.5) and the discharge time was

adjusted to add the target bitumen content. The foam production was verified measuring the Half Life and Expansion Ratio at least two times before the mixing with the aggregates, to ensure that the quality of the foam was suitable for mixing.

The mixer available at the Transportation Laboratory is a Hobart® mixer, and can produce batches of about 10 kg of material for each bitumen discharge. However, the H40/AP5 aggregate was too coarse for this mixer and the particles larger than 19.0 mm were discarded for the mixing with foamed bitumen. This coarse fraction was kept separate, and later moisturized and manually incorporated to the foamed bitumen mix. Although this mixing does not represent the field conditions, in which all the reclaimed aggregate is mixed together with the foamed bitumen, it is known that at normal temperatures (20 °C) of the aggregate, foamed bitumen disperses mainly in the aggregate fraction below 1-2 mm (Asphalt Academy 2002) and therefore not including the largest particles of the aggregate should not significantly affect the quality of the mix. A comparison of the Indirect Tensile Strength of foamed bitumen mixtures measured in the laboratory and the field, which showed consistent values between field and laboratory mixes, is later presented in Chapter 4 (Figure 4.21). The comparison showed that Indirect Tensile Strength values measured in laboratory-mixed specimens and field-mixed specimens are similar, which suggests that the mixing processes are equivalent. This laboratory procedure, in which the coarse fraction is separate and later incorporated to the mix has also been adopted by other researchers in foamed bitumen mixes (Long and Ventura 2004).

The mixing moisture content was equated to 85% of the optimum moisture content determined in Section 3.2.1.3 (6.0%). Only the mixes for the preliminary permanent deformation study (Section 3.3.4.2) were prepared using a mixing moisture content of 70% of the optimum moisture content. To add the water, the H40/AP5 blend was placed in the bowl of the Hobart® mixer and mixed for five minutes to ensure that moisture was uniformly added to the aggregate. The same water content (610 g) was added to all the mixes studied to avoid the introduction of another variable into the study (moisture).

Active filler (1% cement) was incorporated during this initial mixing. A few seconds before the mixing of the aggregates with foamed bitumen, a final foam check was conducted to verify that the WLB10 was working properly. The bowl and the mixer were placed under the foaming nozzle of the WLB10. The Hobart® mixer was set at fast mixing speed, to ensure a high mixing energy, representative of field conditions. Once the mixer was set working, the foam was discharged and mixed with the aggregate for 30 seconds (Wirtgen 2004). Immediately after completing mixing, the foam mix was placed on a large tray and the additional coarse material retained in the 19.0 mm sieve was added and manually blended with a small shovel and scoop. Once a consistent and uniform mix was achieved, the tray with the material was covered with plastic bags to avoid excessive moisture loss and maintain the temperature of the mix relatively constant.

For materials with cement only (without the incorporation of foamed bitumen) the mixing was conducted manually in the large tray mentioned before.

3.2.3.4 Compaction

For the Indirect Tensile Strength tests the specimens were compacted using a CBR-type mould (150 mm diameter) in two layers to produce a sample approximately 75 (± 5) mm height. Once the compaction was finished the sample was extruded manually or using a jack.

The large triaxial specimens were compacted in six layers of approximately 48 mm to 50 mm each, yielding a total of approximately 288 mm (± 3) mm height and 150 mm diameter. Specimens were created using two compactive efforts for the triaxial permanent deformation tests, as well as the monotonic triaxial tests, to study the effect of compaction energy, as will be explained in Section 3.3.4 of this chapter. A split mould was used for the triaxial specimen compaction with a membrane placed on the split mould. Between 1,800 and 2,000 g of mix were used for each lift depending on the compaction effort applied to the sample. After the sixth lift, an additional 100 g of fine material (< 4.75 mm) were placed on the sample surface and compacted for 10 seconds to ensure a uniform, flat surface.

Once the compaction was finished the specimens were left for curing at a room temperature of 20 °C, in double sealed plastic bags.

3.2.3.5 Determination of the curing period

Most researchers (Jenkins 1999; Kekwick 2005; Muthen 1999) as well as the available guidelines (Academy 2002; Wirtgen 2004) adopted 72 hours in the oven at 40 °C as a representative period of curing, equivalent to an approximately 6 months curing period in the field. Nevertheless, these curing conditions were developed for different materials and different environmental conditions. It was necessary, therefore, to define a curing period for the particular mixes used in this study to let the specimens gain strength gradually with time.

The oven curing at a relatively high temperature (40 °C) is usually used to represent the long-term curing in the field by accelerating water loss. Oven curing could not be totally suitable in the case of cement modified mixes, because it will stop cement hydration and this will affect the resulting strength of the mix (Saleh 2003). Because cement was considered to be an active filler for this research, curing in the oven was avoided to allow cement to fully develop its strength properties.

To determine a suitable curing time for the foamed bitumen mixes, a triaxial specimen with 2.0% foamed bitumen and 1.0% cement was produced. The Resilient Modulus of the specimen was monitored for two weeks to study the potential variation in the material response. The sample was prepared and compacted following the procedure presented in Section 3.2.3. Immediately after the compaction, the specimen was placed in the triaxial apparatus and enclosed with two membranes to avoid moisture loss. The resilient modulus was measured at different stress conditions, as per the stress sequence proposed by the European Standard for Unbound Materials (Standarization 2003). A description of the triaxial machine and the European Resilient Modulus test is included in Section 3.3.4 of this chapter. Resilient Modulus measurements were taken 1, 3, 4, 5, 7, 9, 11 and 14 days after the

preparation of the sample. The average Resilient Modulus, which is the average of all the Resilient Moduli measured during the test at different combinations of confining and deviator stress, is plotted against time in Figure 3.6, which shows that most of the gain in strength is achieved during the initial week (7 days) of curing. The curing occurred even though there was little moisture loss (approximately a reduction from 5.1% to 4.8%), because the specimens were double sealed. Therefore, this gain in strength could be attributed to active filler (1.0% cement) reaction.

Based on these results, a curing period of 14 days was found suitable for the mixes tested. It was decided to keep the specimens in sealed plastic bags to retain relatively high moisture contents in the specimens during the testing. A high moisture content could be more representative of sub-optimal pavement conditions often encountered in New Zealand.

A similar curing procedure was adopted by Saleh (2004a), who stated that after 100 hours (4.1 days) of curing, about 80% of the gain in resilient modulus is achieved and established that 7 days at room temperature was a suitable curing period for foamed bitumen mixes. However, these tests were conducted in small 100 mm diameter specimens and the resilient modulus was measured applying the Indirect Tensile resilient modulus test, later detailed in this chapter. Long and Ventura (2004) adopted a 28 days curing period for triaxial specimens with foamed bitumen and cement or foamed bitumen only.

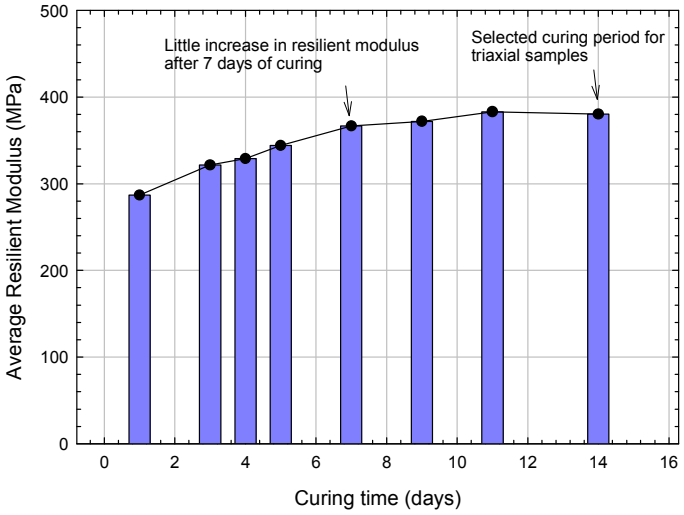

Figure 3.6 Relationship between resilient modulus and curing time for specimen containing 2.0% foamed bitumen and 1.0% cement

3.3 Laboratory tests

3.3.1 **Indirect tensile strength test (ITS)**

3.3.1.1 Testing method

The Indirect Tensile Strength (ITS) was determined using the Humboldt Master Loader HM-3000 (Figure 3.7a), in accordance with the New Zealand Standard NZS 3112: Part 2:1986. The loading speed applied during the test corresponds to 50.8 mm/min.

The specimens were placed in the loading frame and aligned to ensure that the axis of symmetry and direction of loading act through the centroid of the specimens. Once the specimens were placed in the loading frame the HM-3000 was switched on and the specimens were loaded. The load was measured using a load cell with a capacity of 10 kN. The ITS values of the specimens were obtained using the following equation that relates the maximum horizontal stress in the specimen with the applied load applied by the loader:

$$ITS = \sigma_{x-\max} = \frac{2 \times P_{\max}}{\pi \times d \times t} \times 1000 \qquad \text{(Eq. 3.2)}$$

where:

ITS	= Indirect tensile strength (kPa)
$\sigma_{x\text{-}max}$	= Maximum tensile stress in horizontal (x) direction (kPa)
P_{max}	= Maximum applied force (N)
d	= diameter of specimen (mm)
t	= specimen height (mm)

The stress distribution in the specimen is shown in Figure 3.8.

Some of the samples prepared for ITS testing were soaked for 24 hours at a 25 °C bath to determine the moisture sensitivity of the mixes.

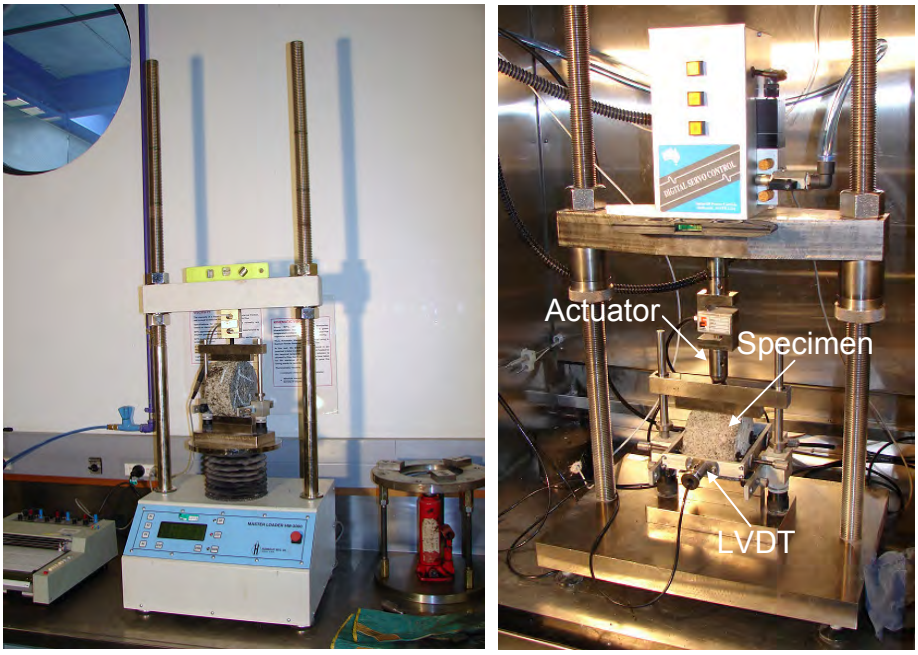

Figure 3.7 (a) Humboldt Master Loader HM-3000 (b) Material Testing Apparatus and foamed bitumen specimen

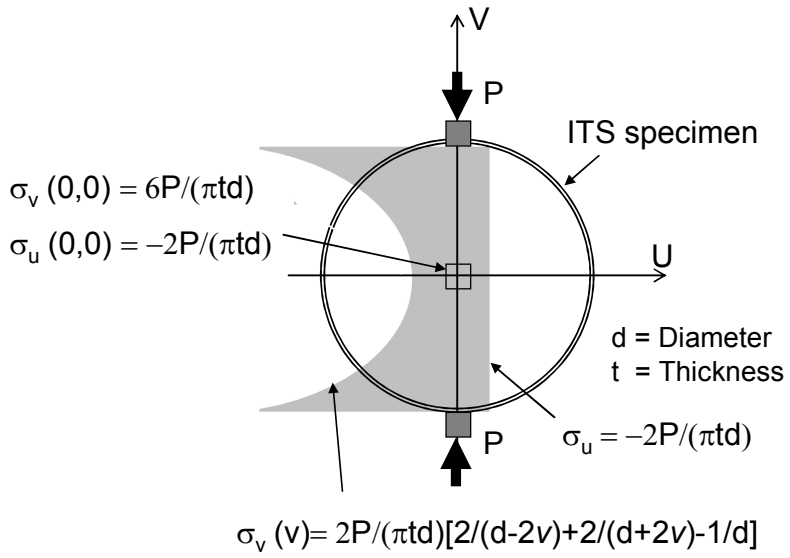

Figure 3.8 Stress distribution in a specimen during indirect tensile tests (Claesson and Bohloli, 2002)

3.3.1.2 Experimental design

The Indirect Tensile Strength was determined for mixes containing 1.0% cement and foamed bitumen contents of 0.0%, 1.0%, 2.0%, 3.0% and 4.0%. Specimens without cement were also prepared, but were severely damage with the 24 hours soaking, and were not tested.

3.3.2 **Results**

The results of the ITS tests are presented in Figure 3.9. The results indicate that ITS increases as the bitumen content increases, up to about 3.0%. At 4.0%, the ITS value decreases, showing that a large volume of bitumen negatively influences the tensile strength of the mix for the materials studied. This is presumably because there are not enough fines to be mixed with the bitumen and therefore the superficial, un-binded bitumen acts as a lubricant thereby reducing the strength of the material.

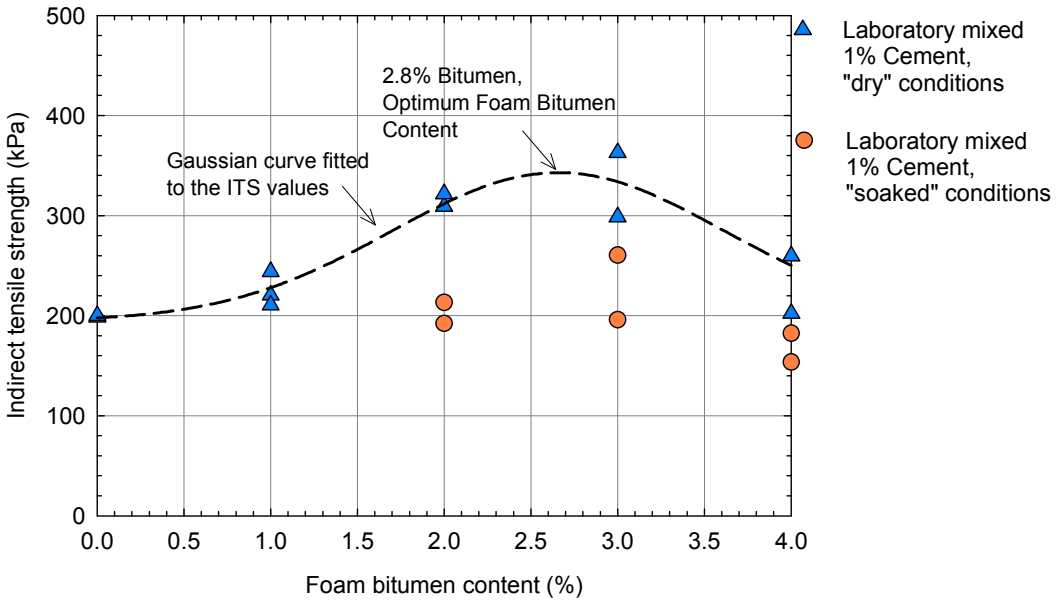

Figure 3.9 Indirect tensile strength results

A Gaussian-type curve was fitted to the ITS results to estimate the bitumen content that yields the maximum strength of the mix. The calculated value was approximately 2.8% bitumen content, which was selected as the optimum foamed bitumen content for the aggregate, at 1.0% cement.

The soaked ITS were determined for foamed bitumen contents of 2.0%, 3.0% and 4.0% only; tensile strength retained (TSR) was calculated for these specimens and yielded values of 64%, 68% and 61% respectively. This range of TSR values is recommended for moderate wet climate zones using South African (Asphalt Academy 2002) recommendations.

3.3.3 **Indirect tensile resilient modulus tests**

3.3.3.1 Testing method

Application of elastic theory indicates that when a cylindrical specimen is loaded diametrically there is a very uniform distribution of tensile stress perpendicular to the direction of the applied load. This tensile stress distribution is used to simulate the tensile stresses that occur at the underside of pavement layers when a pavement is subjected to axle loads.

The indirect tensile resilient modulus was measured using a procedure similar to the Australian Standard AS2891.13.1:1995 for the determination of the resilient modulus of asphalt (Standards Australia 1995). The difference between AS2891.13.1:1995 and the procedure used is that specimens were prepared using vibratory compaction instead of gyratory compaction (Australian Standard AS2891.2.2). Vibratory compaction was preferred to keep one type of compaction throughout the research, and avoid the introduction of another variable into the laboratory study. To measure the indirect tensile resilient modulus, the Material Testing Apparatus (MATTA) was used (Figure 3.7b). MATTA is a pneumatic testing machine manufactured by IPC Australia. The pneumatic system had a maximum load capacity of 5 kN. The indirect tensile resilient modulus equipment comprises a testing frameand platens with loading strips that are contoured to the radius of the specimen. The load is applied across the vertical diameter and the specimen deflections are measured across both the vertical and horizontal diameters.

MATTA is capable of applying an approximately triangular shaped Haversine load pulse, with a rise time in the range of 0.025 s to 0.1 s. The rise time is defined as the time required for the load pulse to rise from 10% to 90% of the peak force. The machine is provided with a temperature controlled cabinet which maintains the temperature within ± 0.5 °C of the target temperature in the test.

The machine applies a vertical load on a cylindrical specimen that induces horizontal deformation. This deformation is measured by two external LVDTs lined up with the specimen diameter (see Figure 3.7b). Five pulses were applied as preconditioning. Once these pulses have been applied, the external LVDTs are adjusted and 5 additional pulses are applied and used to evaluate the resilient modulus.

In summary, the test specification requires that the testing machine apply a repeated load pulse with a rise time of 0.04 s and a pulse repetition period of 3.0 s. The test is carried out under strain controlled conditions with a specified recovered horizontal strain of 50 $\mu\varepsilon$.

The modulus is calculated using the following formula (Standard Australia 1995):

$$M_r = \frac{\sigma_{x-\max}}{\varepsilon_{x-\max} \times (1+3\nu) \times 1000} \quad \text{(Eq. 3.3)}$$

where:

$\sigma_{x\text{-max}}$ = Maximum tensile stress in horizontal (U) direction in Figure 3.8 (kPa)

$\varepsilon_{x\text{-max}}$ = Maximum tensile strain in horizontal (U) direction in Figure 3.8 ($\mu\varepsilon$)

ν = Poisson's ratio

This formula assumes a linear elastic behaviour of the mixes, and the theoretical stress distribution within the specimens is depicted in Figure 3.8.

3.3.3.2 Experimental design

The Indirect Tensile Resilient Modulus was determined for mixes at 1.0% cement at foamed bitumen contents of 0.0%, 1.0%, 2.0%, 3.0% and 4.0%.

3.3.3.3 Results

The results from the indirect tensile resilient modulus tests are summarized in Figure 3.10. The trend obtained is similar to those of the ITS tests, where the resilient modulus increased as the foamed bitumen content increased up to about 3.0%. At 4.0%, the ITS value decreases, showing that a large volume of bitumen negatively influences the indirect tensile resilient modulus of the mix, in a similar fashion to that of the ITS tests.

These results show that foamed bitumen improves the tensile behaviour of the stabilised material when the bitumen contents are within certain limits (up to 3% bitumen content for the materials tested in this study). The Resilient Moduli obtained are within the expected values reported in the literature. For instance, Nataatmadja (2001; 2002) found optimum resilient modulus values

of 12,000 MPa and 14,000 MPa for specimens compacted using Marshall compaction at foamed bitumen contents of 2.5%, plus 2% of lime. In New Zealand, Saleh (2004b) reported resilient modulus of 7,500 MPa for specimens at 3.0% foamed bitumen content and 2% cement, similar to the results presented in this research. These values are considerably higher than modulus proposed by the current New Zealand structural design method for foamed bitumen pavements (NZ 2007), which suggests an elastic modulus for the foamed bitumen layer of 800 MPa (see Section 2.2.5.1), and also higher than values reported from full-scale pavement tests (between 500 to 3,000 MPa), described in Section 2.4. However, the test configuration plays an important role in the measurements, i.e. the stress and deformational conditions applied in one particular test yield a range of resilient modulus values, while the conditions applied using other type of tests or a different test configuration could give different results.

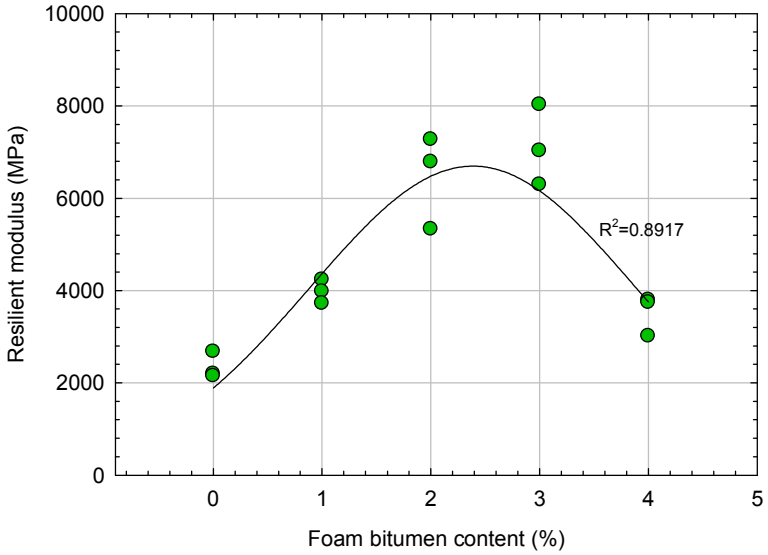

Figure 3.10 Indirect tensile resilient moduli results

3.3.4 **Repeat (cyclic) load triaxial tests**

3.3.4.1 Testing method

Resilient modulus and Permanent Deformation tests were performed on the materials studied using the triaxial apparatus. The Repeat Load Triaxial (RLT) test is a cyclic version of the monotonic triaxial test, widely used in geomechanics, to determine stress-strain behaviour of granular materials. The available RLT system, presented in Figure 3.11, applies the load using a

pneumatic servo-controlled loading ram of 10 kN capacity. The load measuring system uses an internal load cell while the axial displacement is measured using two externally mounted LVDTs (5 mm range). The system applies a constant confining pressure using air or water. The data is collected using a Control and Data Acquisition System (CDAS) linked to a computer. The triaxial apparatus available can test specimens with a maximum diameter of 150 mm and a height of 300 mm. The applied load was measured with an internal Wykeham Farrance 10 kN load cell.

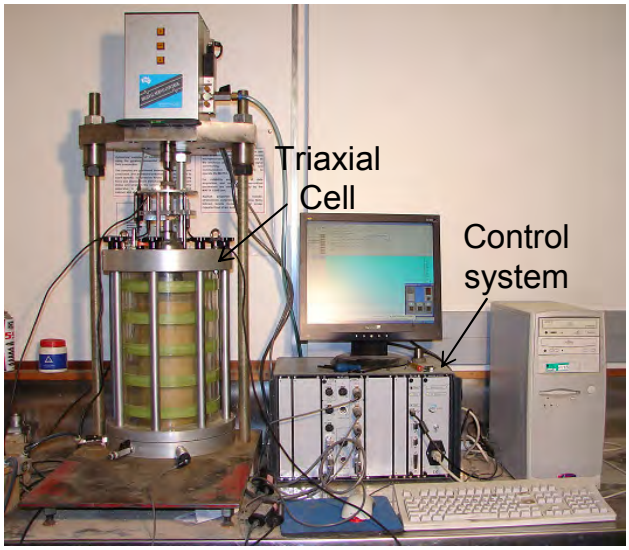

Figure 3.11 Repeat load triaxial system used for testing

Triaxial testing for evaluating the permanent deformation of granular-type materials is widely accepted in pavement engineering in New Zealand (Transit 2007) and Australia (Vuong 2004). Therefore, triaxial permanent deformation tests were given due attention in this research project.

Permanent deformation tests are usually time-consuming since they require application of a very large number of load cycles. To minimise the number of permanent deformation tests required, a multi stage approach was adopted in this study. In the multi stage approach, a sequence of stresses is applied on the same specimen. At each stage (stress level) a large number of load cycles (usually from 10,000 to 50,000) are applied, keeping the stress amplitude constant. If the sample does not fail under the cyclic load application, then the

load is increased and a new set of load cycles is applied until the sample fails or the specified number of cycles is completed. The multi stage method has been adopted and validated by a number of researchers in granular materials (Arnold et al. 2003; Chazallon et al. 2006; Lekarp and Dawson 1998; Lekarp and Isacsson 2001; Werkmeister et al. 2004).

In the present laboratory study, two sets of permanent deformation tests were conducted. The first set corresponds to a preliminary study to evaluate the general performance of the mixes under RLT conditions with the following specific objectives:

- To assess the general effects of foamed bitumen and cement on the H40/AP5 unbound granular material under repeated loading conditions, in particular effects on permanent deformation and resilient modulus.
- To establish a suitable regime or sequence of stress amplitude levels.

The preliminary testing was conducted at two different confining pressures (50 kPa and 100 kPa) and at different total vertical loads (σ_v), which was sequentially increased at each stage by increasing the stress ratio (σ_v/σ_c) as summarized in Table 3.5. Drainage was not allowed during the test by closing the valves at the pedestal of the triaxial cell, to keep the moisture constant. Details of the compaction of these specimens are presented in Appendix C, Section C.1.

Table 3.5 Stress sequence followed during the preliminary testing of materials

Stress Level	σ_c	σ_v	σ_c	σ_v	Ratio (σ_v /σ_c)
1	50	100	100	200	2
2	50	150	100	300	3
3	50	200	100	400	4
4	50	250	100		5
5	50	300			6

σ_c : Confining stress; σ_v : Vertical stress

3.3.4.2 Results of preliminary repeat load triaxial tests

The results for the preliminary tests are presented from Figure 3.12 to Figure 3.14. Figure 3.12 presents the results of the triaxial tests at a confining pressure of 50 kPa for different deviator stresses and for the specimens without cement (0% cement). The results show that foamed bitumen does not have a significant improvement effect on the performance of the untreated aggregate. While the untreated material survived the fourth stress stage, where a deviator stress of 250 kPa was applied, the specimens at 2.0% and 4.0% foamed bitumen failed under this loading magnitude.

Figure 3.13 (left) shows the resilient modulus values collected during the permanent deformation tests, for the specimens with 0% cement. Although there is a slight increase in modulus with foamed bitumen content (approximately 5-10%), the enhancement is not conclusive to make the incorporation of foamed bitumen justifiable.

Figure 3.14 presents the results for the specimens at 1.0% cement. Specimens survived the five stress stages showing small amounts of vertical deformation (below 4.0×10^3 μm), in comparison with the tests conducted without cement. Little difference was measured for the specimens with 2% and 4% foamed bitumen content (3.8×10^3 μm and 3.6×10^3 μm, respectively) and therefore the effect of foamed bitumen was not conclusive, although the specimen with 0% foamed bitumen showed the smallest deformation (2.5×10^3 μm). Resilient modulus measurements recorded during the permanent deformation tests show approximately a 20% increase in resilient modulus when 2-4% foamed bitumen is added, as presented in Figure 3.13 (right). The figure also shows the comparatively greater effect of 1.0% cement in the mean resilient modulus (M_r) value (dotted horizontal lines). At 0.0% cement this value is about 210 MPa, while at 1.0% cement, M_r attains 372 MPa for the stress conditions followed during the test (77% increase).

Similar results were found for the specimens tested with 100 kPa confining pressure, presented in Appendix D, in which samples without cement failed after the first stage and the effect of foamed bitumen was not totally clear for specimens with 1% cement.

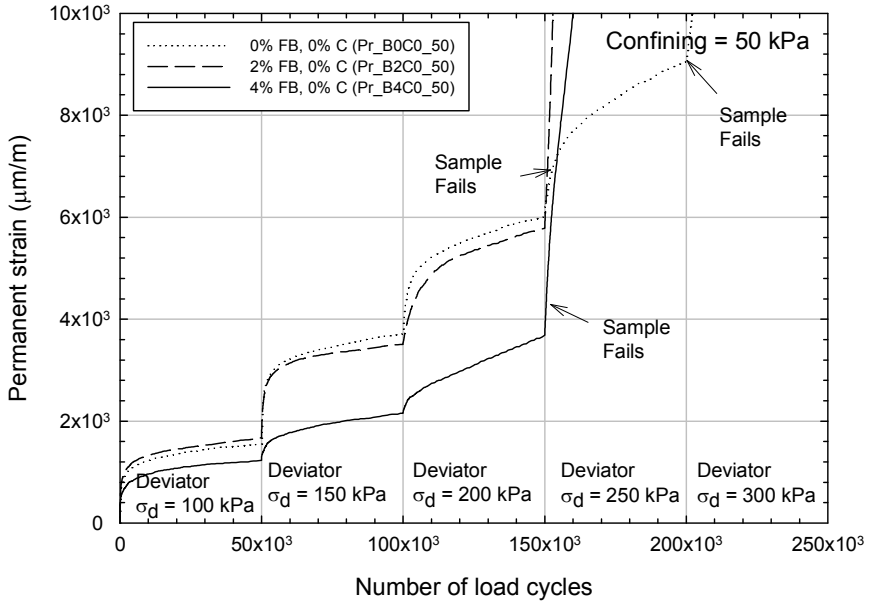

Figure 3.12 Results of preliminary permanent deformation study on mixes at 0% foamed bitumen (50 kPa confining pressure)

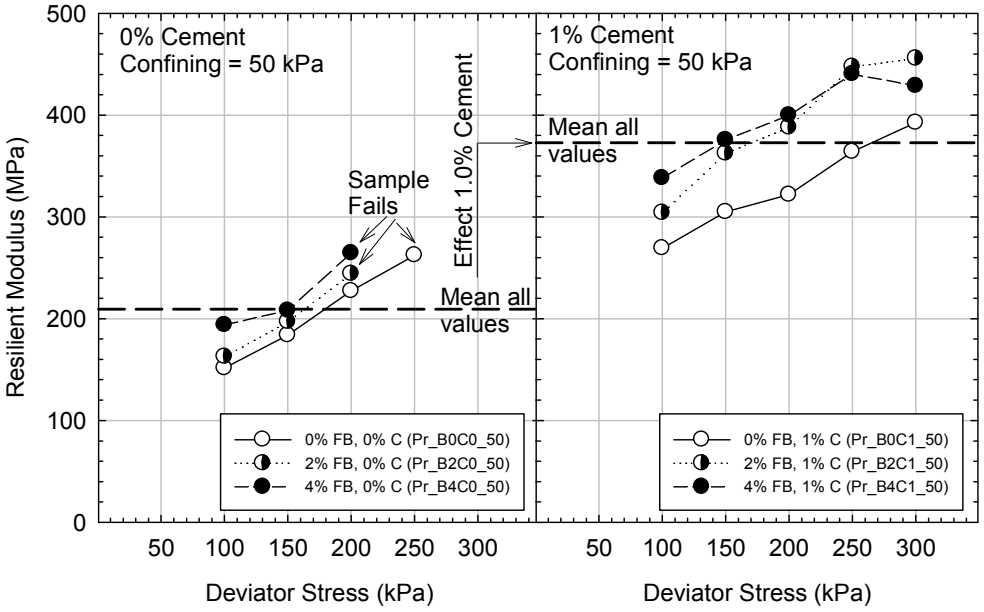

Figure 3.13 Resilient modulus measured during the preliminary RLT study for mixes with 0 and 1% cement (50 kPa confining pressure)

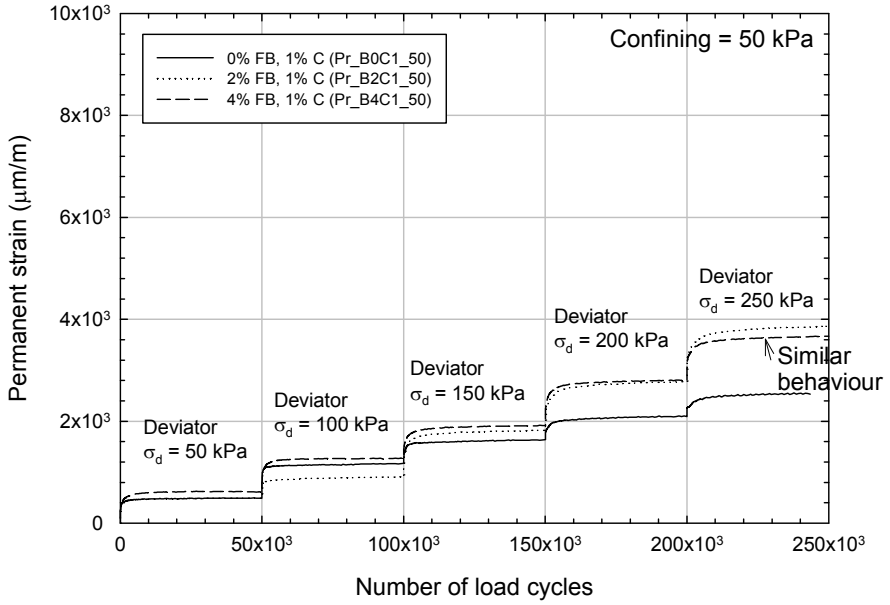

Figure 3.14 Results of preliminary permanent deformation study on mixes at 1% cement (50 kPa confining pressure)

Based on the results provided by the preliminary RLT tests:

- The focus of the RLT study would be on mixes with 1.0% cement, because the performance of the mixes with no active filler was unsatisfactory. This was also supported by the soaking of the ITS specimens.

- Because little difference was observed among the 1% cement specimens under the stress conditions applied, a new and more severe stress sequence was required. This new stress sequence would ideally use the maximum capacity of the available RLT machine, loading the specimen from a low stress condition up to the highest applicable stress. Also, for practical reasons, the experiment should last about 24 hours to test one sample per day. This would also allow to apply a large amount of load cycles (beyond 250,000) as recommended by Jenkins et al (2007). In addition, a low confining pressure was required to produce a high deviator stress, and therefore 50 kPa was chosen as a common confining stress. The stress sequence presented in Figure

3.15 was adopted for the permanent deformation study, in which seven stress stages of 50,000 load cycles are applied, and deviator stresses of 75 kPa, 150 kPa, 225 kPa, 300 kPa, 375 kPa, 450 kPa and 525 kPa.

3.3.4.3 Results of detailed repeat load triaxial tests

For the second set of tests, specimens prepared with a common 1% cement at bitumen contents of 0, 2 and 4% were tested. The compaction effort was introduced as another factor into the study of the permanent deformation of bitumen mixes. This factor was incorporated because:

- It was intended to replicate as close as possible field conditions, including density of mixes. Since the RLT study was conducted prior to the construction of the accelerated full-scale experiment, the actual density of the materials in the field was yet unknown.

- Inconsistencies or non-conclusive results have been reported in the literature when the effect of density has been studied on permanent deformation of foamed bitumen mixes (Long and Ventura 2004). These inconsistencies were attributed to the large variability of the testing. Therefore, tests were replicated 3 or 4 times to obtain reliable results.

The stress sequence applied was presented in Figure 3.15. Specimens were tested under undrained conditions to keep the moisture content of the materials constant during the application of the cyclic loads. Details of the compaction of these specimens are presented in Appendix C, Section C.2 (low compaction effort) and C.3 (high compaction effort). A summary of the bulk densities attained for low and high compaction specimens is presented in Figure 3.16. The bulk densities for the monotonic triaxial specimens, later presented in this chapter, were also detailed in this figure.

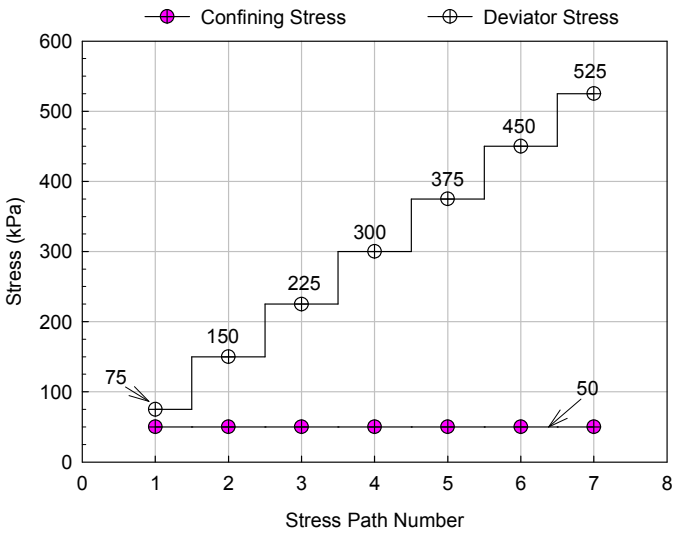

Figure 3.15 Loading stress sequence adopted during the second set of permanent deformation RLT tests

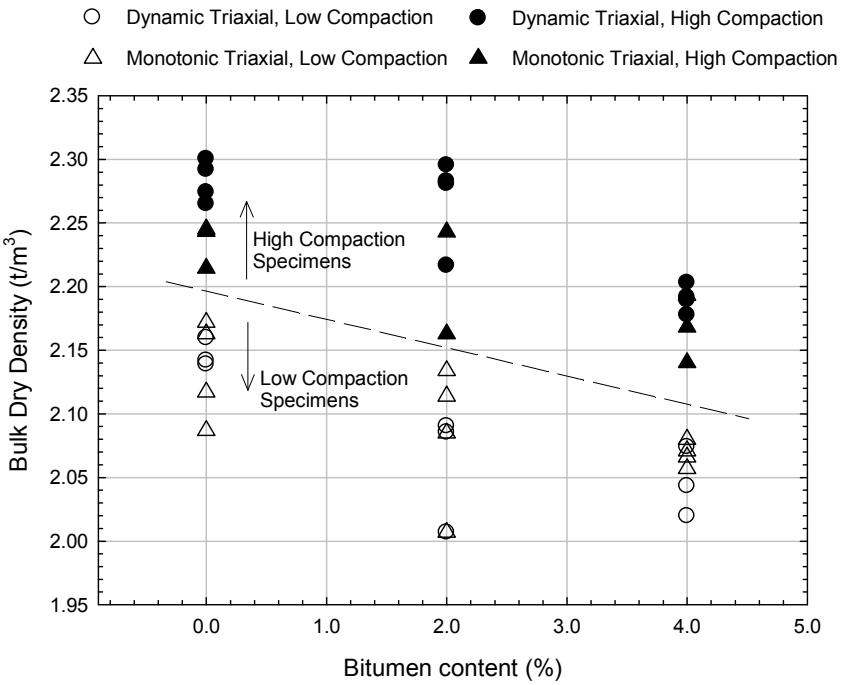

Figure 3.16 Summary of bulk densities measured in triaxial specimens

It is important to notice that the low compaction effort was achieved by reducing the compaction time of the virating hammer (Section 3.2.3.4). This time was reduced to approximately 15 seconds (instead of the 180 seconds applied following the vibrating hammer standard).

3.3.4.4 Detailed tests results: effect of bitumen

The results for the permanent deformation RLT tests are presented in Figure 3.17 and Figure 3.18 for low and high compaction level, respectively, and show the permanent deformation for the seven stages, where 50,000 load cycles were applied. The final permanent deformation at each stage was added to the subsequent permanent deformation of the next stage.

Each specimen tested was named using characters and numbers that describe the type of test, the bitumen and cement contents, the compaction effort applied and the replicate number. For instance, D_B2C1_LC_1 stands for a Detailed test (D), with a Bitumen and Cement content of 2% and 1% respectively (B2C1), compacted applying Low Compaction effort (LC). The last digit (1) stands for the replicate number (e.g. D_B2C1_LC_1 and D_B2C1_LC_2 are two different, but nominally identical specimens).

At higher bitumen contents, the measured permanent deformation is higher, showing that foamed bitumen is increasing the deformability of the material. As depicted in Figure 3.18, part of the data from specimen D_B4C1_LC_2 is missing because the measured vertical deformation exceeded the range of the external LVDTs sensors installed in the RLT machine.

The higher permanent deformation at higher bitumen contents was, to some extent, reported by Long and Ventura (2004), who conducted permanent deformation tests on RLT specimens keeping the cement at 1.0% with foamed bitumen contents of 1.5%, 2.25% and 3.0%, but instead of applying the same stress level to all mixes, they applied different stresses following a stress ratio approach. The stress ratio is defined in Long and Ventura's research as the ratio of the applied vertical stress (σ_1^a) during the permanent deformation test to the maximum allowable or peak stress (σ_1^m) obtained during a monotonic triaxial test, when a confining stress σ_3 is applied. The stress ratio is given by:

$$SR = \frac{\sigma_1^a - \sigma_3}{\sigma_1^m - \sigma_3} \qquad \text{(Eq. 3.4)}$$

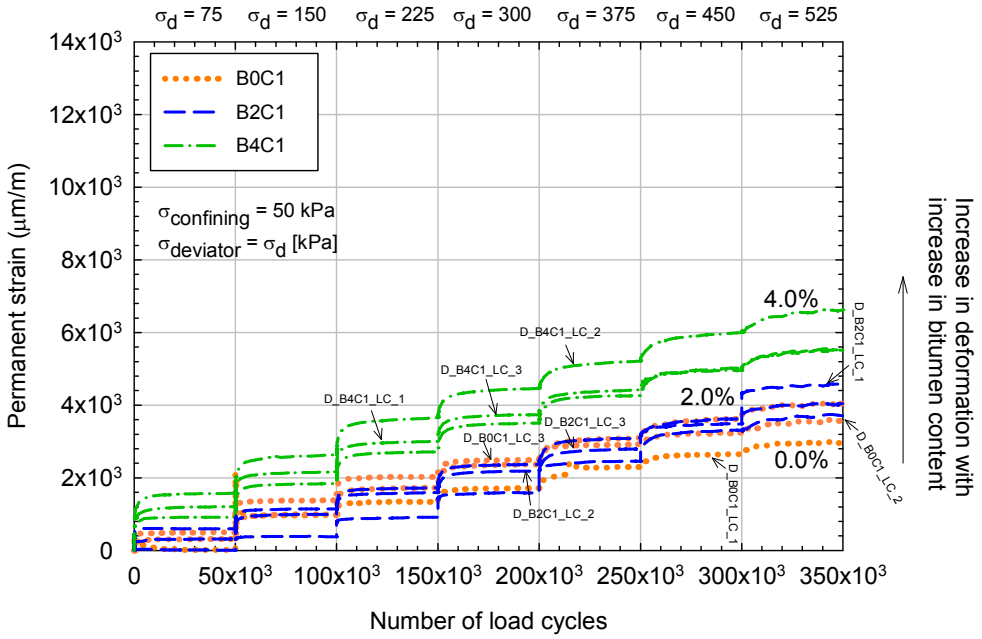

Figure 3.17 Average results of RLT permanent deformation tests at low compaction level

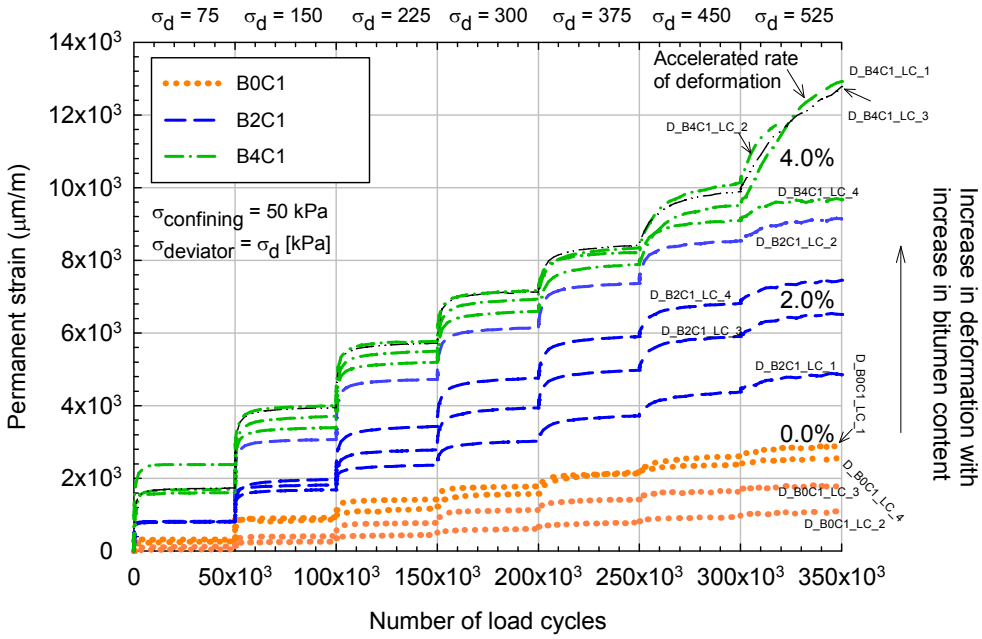

Figure 3.18 Average results of RLT permanent deformation tests for high compaction level

In Long and Ventura's study, the triaxial specimens were tested at stress ratios of 0.25, 0.5, 0.75 and 1.0, approximately. However, the peak or

maximum stress (σ_1^m) obtained during the monotonic tests was different for different bitumen contents. As depicted in Figure 3.19, the peak stress applied to specimens with 1.0% cement is reduced for specimens with foamed bitumen. In other words, a stress ratio of, for instance, 0.50 is more severe for a triaxial specimen without foamed bitumen than a specimen with foamed bitumen, and the absolute stress conditions applied to specimens at different bitumen contents were not comparable.

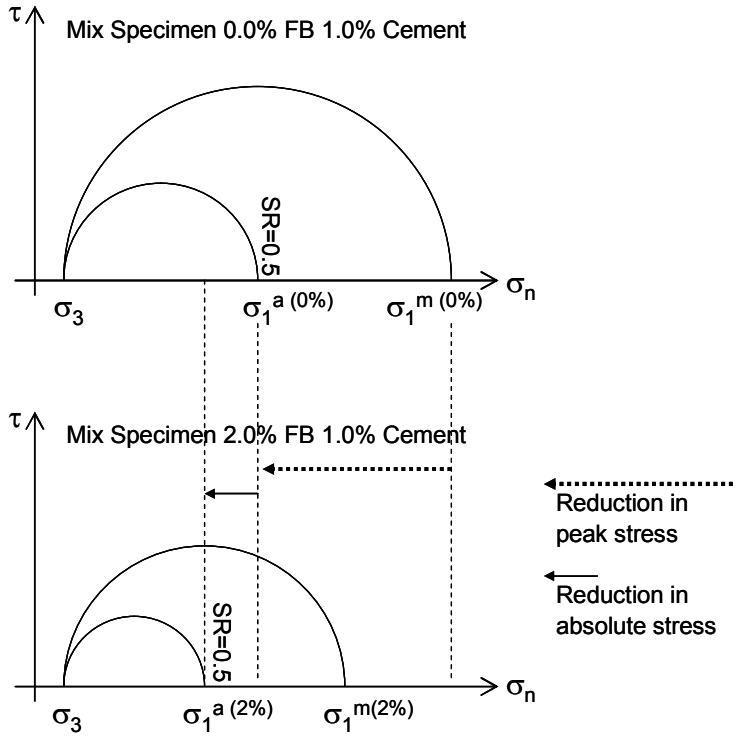

Figure 3.19 Stress ratio applied to mixes with and without foamed bitumen plotted using Mohr's circles

Long and Ventura summarized the overall results fitting a linear model to the data. The model incorporated different parameters that were studied in their research: stress ratio (SR), relative density (RD), saturation level (SAT), plastic strain (PS), and the foamed bitumen (BIN) and cement (CEM) contents. Their empirical model is summarized in the following equation:

$$\text{Log } N = c_1 + SR^3 \times (c_2 + c_3\, CEM + c_4\, BIN^2) + c_5 \times RD + c_6 \times SAT + c_7 \times PS + c_8 \times CEM \quad \text{(Eq. 3.5)}$$

where N is the number of load cycles needed to reach a defined plastic strain at a stress level defined by SR. The cement content, foamed bitumen content, relative density, saturation and plastic strain are expressed in percentage, while the stress ratio as a ratio from 0 to 1. The model coefficients ($c_{1...8}$) were determined by the researchers and are summarized in Table 3.6. The coefficient that multiplies the foamed bitumen content is c_4 with a value of -0.093. The negative value of this coefficient indicates that when the foamed bitumen content is increased, the number of load cycles needed to reach a specific plastic strain decreases. To illustrate this, the effect of foamed bitumen in this equation was plotted against the number of load cycles for two stress ratios in Figure 3.20, which shows a decrease in the required number of load cycles to achieve a given deformation at a higher bitumen content. The trend presented could be even less favourable to foamed bitumen if instead of the stress ratio the actual stress levels were used, as discussed above.

Table 3.6 Model coefficient for combined model (after Long and Ventura 2004)

Variable	Coefficient	P-value
c_1	4.882	0.0000
c_2	-1.004	0.0000
c_3	-0.953	0.0000
c_4	-0.093	0.0000
c_5	0.022	0.0000
c_6	-0.003	0.0003
c_7	0.071	0.0000
c_8	0.178	0.0000
R^2	0.72	
Standard error of estimate	0.601	

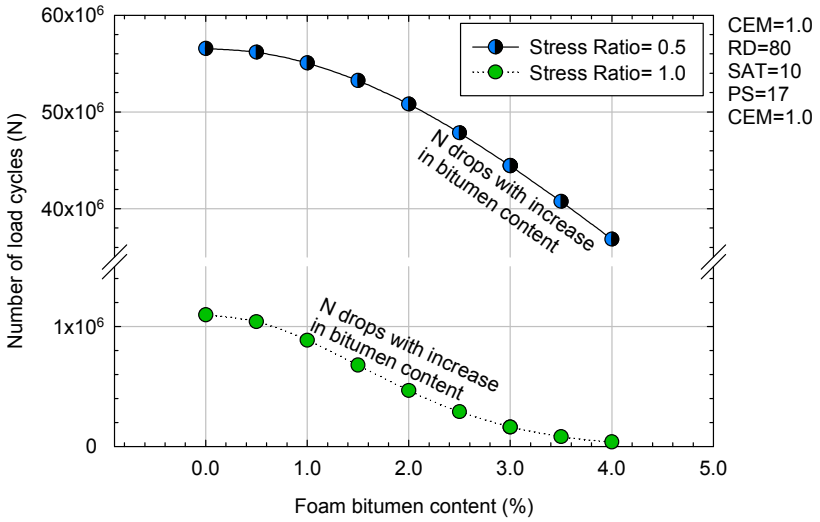

Figure 3.20 Results obtained using the Long and Ventura's model for permanent deformation in RLT tests, at different foamed bitumen contents

3.3.4.5 Detailed test results: effect of compaction effort or bulk density

The second important observation made from the detailed test is that specimens compacted at a low energy level showed lower permanent deformation than high compaction specimens, which is an opposite trend from the commonly observed for the unbound granular materials. The final or total permanent deformation measured after 350,000 load cycles is shown in Figure 3.21 for all tests. It was expected that samples at lower density would exhibit higher permanent deformation; this trend was observed only in specimens with 1.0% cement and no foamed bitumen.

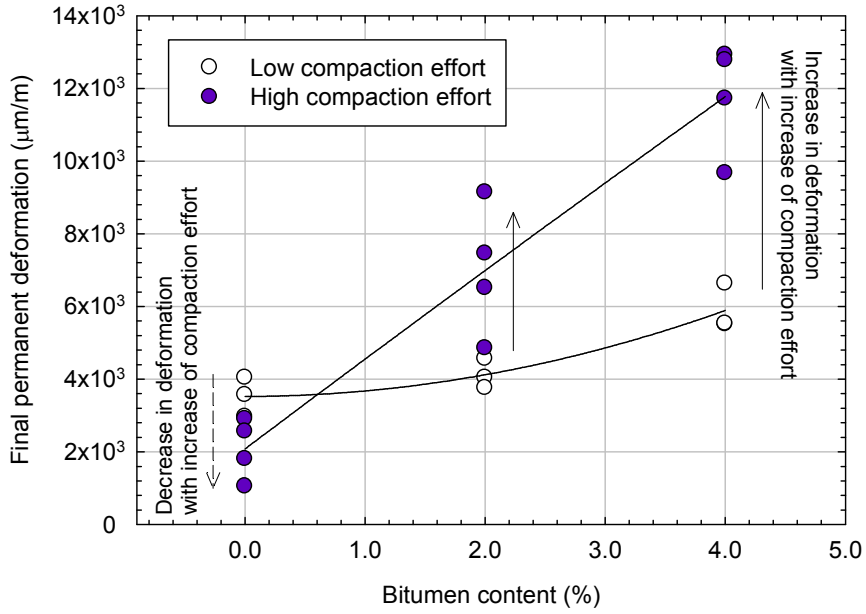

Figure 3.21 Effect of compaction effort at different foamed bitumen contents

The effect of bulk density was also studied by Long and Ventura (2004). They prepared several specimens at different foamed bitumen and cement contents for permanent deformation tests, applying the same compaction effort but varying the moisture content. To summarize the results, they fitted a cubic model to the data for each combination of bitumen and cement. The model incorporated different variables in a similar fashion as the previously presented equation, in which the effect of bitumen was discussed. They incorporated in the equation the stress ratio (SR), relative density (RD), saturation level (SAT), plastic strain (PS). The foamed bitumen (BIN) and cement (CEM) content are not included because in this case the equations were developed for each specific material combination. The model is expressed as follows:

$$\text{Log } N = c_1 + c_2 \times SR^3 + c_3 \times RD + c_4 \times SAT + c_5 \times PS \qquad \text{(Eq. 3.6)}$$

The model coefficients ($c_{1...5}$) were calculated for the different combinations of bitumen and cement contents studied, presented in Table 3.7. The values back-calculated from the experimental results for the relative density coefficient (c_3) were found unreasonable for three out of the four mixes with

foamed bitumen and cement, and Long and Ventura argued that c_4 had an incorrect sign. In other words, they found that at higher densities the permanent deformation was higher.

Table 3.7 Model coefficients for individual model

	HNN	HNS	HSB	HSS	HSA	HAS
Bitumen (%)	0	0	1	1	1	2
Cement (%)	0	2.25	1.5	2.25	3.0	2.25
c_1 (constant)	3.318 (p=0.000)	-0.651 (p=0.475)	7.099 (p=0.000)	6.829 (p=0.000)	5.397 (p=0.000)	6.944 (p=0.000)
c_2 (stress ratio)	-1.657 (p=0.000)	-1.396 (p=0.000)	-2.339 (p=0.000)	-1.474 (p=0.000)	-2.953 (p=0.000)	-3.628 (p=0.000)
c_3 (relative density)	**0.046 (p=0.002)**	**0.093 (p=0.000)**	**Note 1,2**	**Note 2**	**0.020 (p=0.025)**	**Note 2**
c_4 (saturation)	-0.017 (p=0.000)	-0.018 (p=0.000)	-0.004 (p=0.065)	Note 2	-0.002 (p=0.195)	Note 1
c_5 (plastic strain)	0.078 (p=0.000)	0.090 (p=0.000)	0.065 (p=0.000)	0.070 (p=0.000)	0.066 (p=0.000)	0.063 (p=0.000)
R^2	0.66	0.65	0.73	0.64	0.81	0.86
Standard error	0.535	0.625	0.569	0.443	0.621	0.445
Data points	371	469	371	364	433	427
Note 1) Variable statistically insignificant Note 2) Coefficient has incorrect sign						

Note: The value in parentheses represents the P-value

3.3.4.6 Verification of the deformation with random stress sequence

The results obtained during the permanent deformation tests were intuitively unexpected, though previous laboratory work was suggesting such outcome. The author anticipated a reduction in permanent deformation with the addition of foamed bitumen and an increased compaction effort. One of the factors that could have affected the results was the loading stress sequence chosen for the tests. Other permanent deformation tests, such as the current standard for the study of unbound granular pavements in New Zealand, apply different combinations of confining and deviator stresses that could be more representative of the actual loading history of a pavement layer (Transit 2007).

To study the effect of the stress sequence, one sample with 2.0% foamed bitumen and 1.0% cement was prepared with low compaction effort (see compaction table in Appendix C, Section C.5). The same stress paths for the detailed study were chosen, but the order of application of these stress levels was randomized. Instead of sequentially applying deviator stresses with an increasing amplitude from σ_d=75 kPa to σ_d = 525 kPa in a stepwise manner, a random sequence of amplitudes was applied in order of σ_d = 375 kPa, 150 kPa, 300 kPa, 450 kPa, 225 kPa, 75 kPa and 525 kPa.

The results of the random-loading test are presented in Figure 3.22, where results from the regular stress-sequence tests, for the specimens with 2% foamed bitumen and 1% cement, are also shown. For the random stress sequence sample, an important amount of permanent deformation ($2.2x10^3$ μm) was observed after the application of the first stress path (σ_d= 375 kPa). Little deformation (less than $0.1x10^3$ μm) was measured with the next two stress stages but when the load was increased again to σ_d = 450 kPa and previous maximum stress level was exceeded, additional deformation of about $0.8x10^3$ μm was observed. When the stress applied was released to a less severe condition during the following two stages, a slight rebound ($0.2x10^3$ μm/m) in permanent deformation was observed. An increase in deformation of about $1.2x10^3$ μm occurred when the last and most severe stress stage was applied (σ_d = 525), leading to a final permanent deformation of $4.226x10^3$ μm/m.

The final permanent deformation in the three specimens loaded, after the incremental regular stress sequence, was $4.562x10^3$ μm/m, $4.041x10^3$ μm/m and $3.704x10^3$ μm/m respectively (average=$4.102x10^3$ μm, Standard Deviation=$0.432x10^3$ μm) for the three replicates at 2% foamed bitumen and 1% cement and low compaction level. In the irregular-loading test similar level of permanent deformation of 4.226 $x10^3$ μm/m was achieved. Thus, the final permanent deformation of the randomized stress sequence is within the range of the incremental stress sequence, indicating that, with the limited amount of

data available, the observed effect of foamed bitumen could not be explained with the particular features of the incremental stress sequence applied.

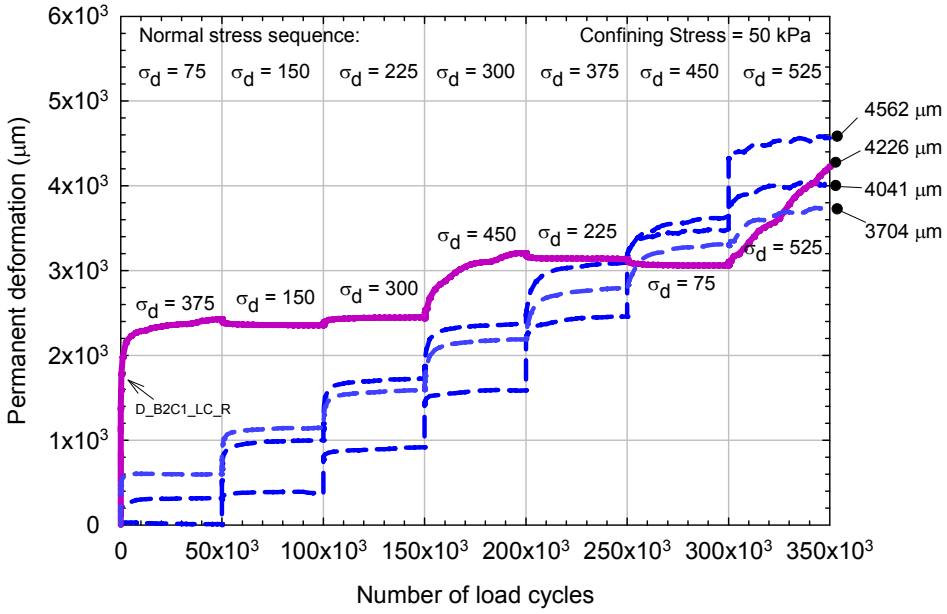

Figure 3.22 Permanent deformation test on a sample at 2.0% foamed bitumen and 1.0% cement where the stress sequence was randomized

3.3.5 **Resilient modulus tests and experimental design**

Resilient modulus tests were conducted applying the European Standard cyclic load triaxial test for unbound mixtures (Standarization 2003). The standard supplies a high and low stress sequence, and the tester has to decide which is more appropriate and representative of field conditions. The high stress sequence is associated with materials located in the part of the pavement structure near the surface and near the vehicle tyres while the low stress sequence is associated with materials located in the lower levels of the pavement structures. Because in New Zealand the granular bases and foamed bitumen layers are usually placed near the pavement surface, the high stress sequence was adopted. Also, in the full scale experiment, the pavement consisted of a thin asphalt surface plus a stabilised basecourse, as explained in Chapter 4.

The European Standard applies 30 stress stages of 200 load cycles each, at different combinations of confining and deviator stresses (Figure 3.23). The

first stage is a pre-conditioning stage where 1,000 load cycles are applied at a combination of high confining and deviator stress.

Triaxial resilient modulus tests were conducted on 12 specimens, at 3 bitumen contents (0.0%, 2.0% and 4.0%), at 2 compactions levels and 1% cement.

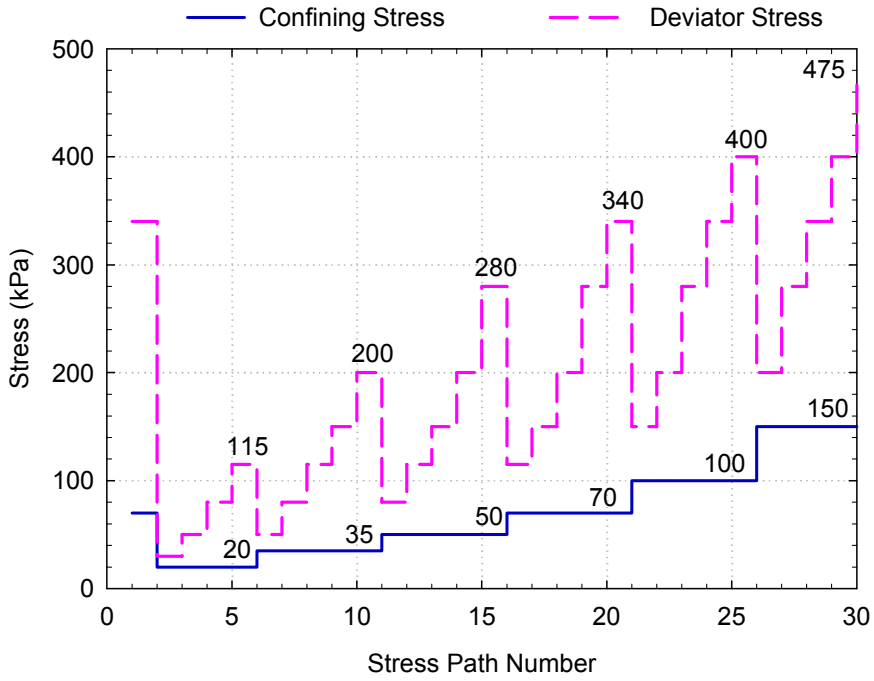

Figure 3.23 Loading stress sequence adopted for RLT resilient modulus tests

3.3.6 **Results Resilient modulus triaxial tests**

The results for the resilient modulus tests are presented in Figure 3.24 and Figure 3.25 for both low and high compaction level specimens, which includes two replicates for such test condition presented in these Figures.

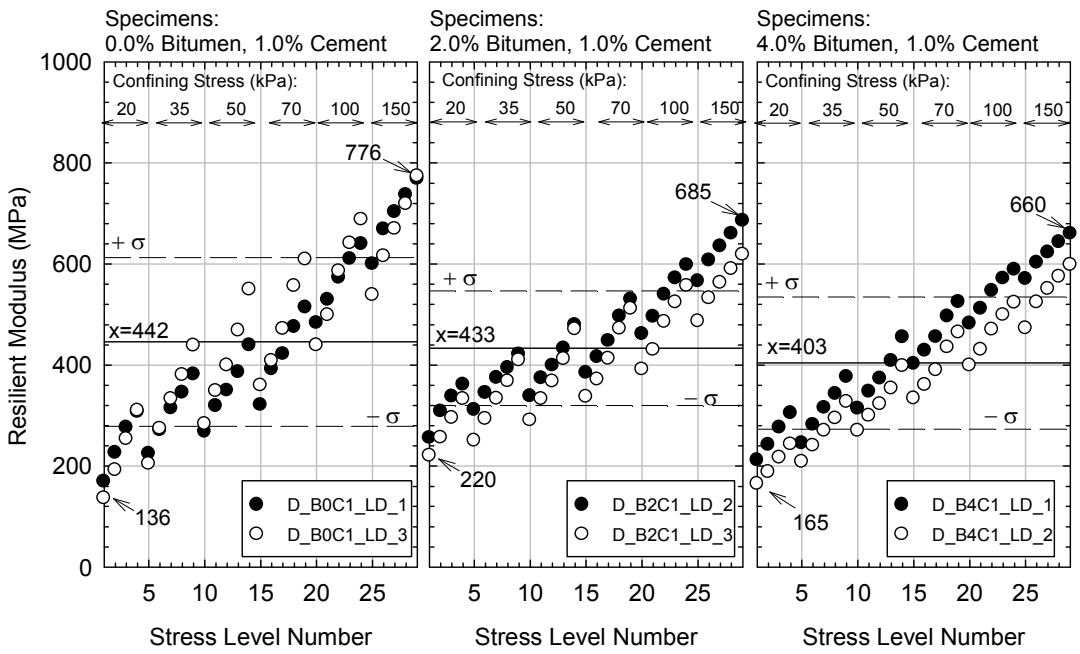

Figure 3.24 Resilient modulus measured on specimens prepared by low compaction

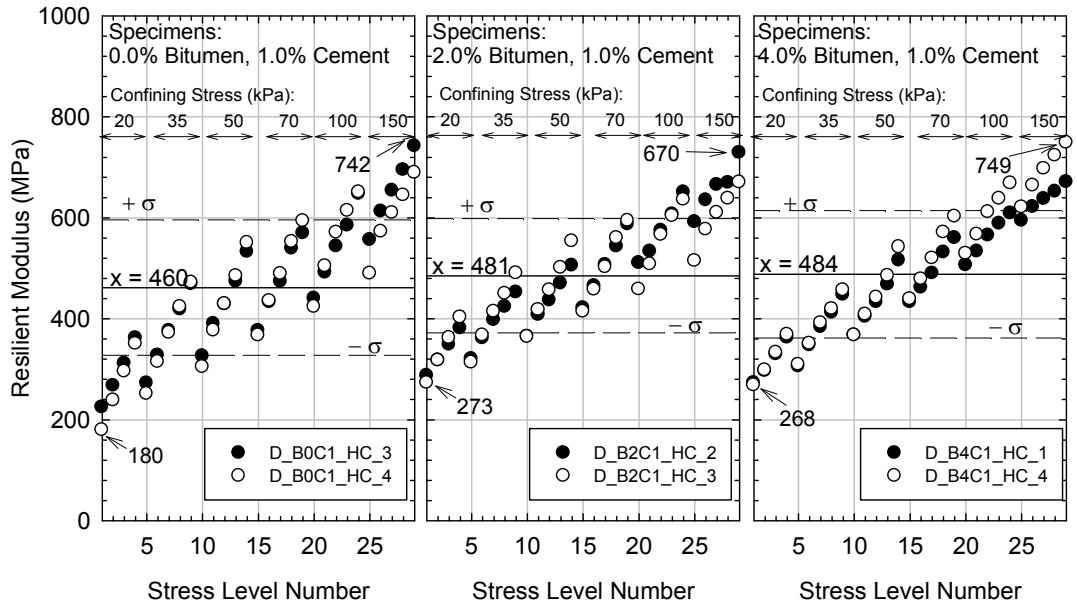

Figure 3.25 Resilient modulus measured on specimens prepared by high compaction

Results show the stress dependency and densification effects on the resilient modulus of the mixes tested. Both confining pressure and deviator stress cause a hardening effect, following the typical behaviour of unbound granular materials (Werkmeister 2004), in which for a relatively low level of stress, the

elastic modulus of the material increases with rising magnitudes of load, or strain hardening (Figure 3.26).

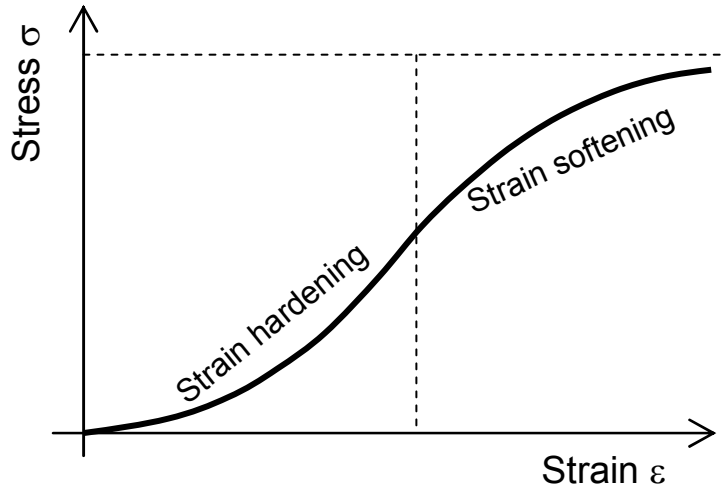

Figure 3.26 Stress – strain behaviour of unbound granular materials (after Werkmeister 2004)

The average resilient modulus from all stress levels measured on both specimens is shown in the figure with a solid horizontal line. The average values indicate that the resilient modulus is not significantly affected by the 2% foamed bitumen content in mixes with 1.0% cement (variation of +5.2% and -8.8% for low and high compaction effort, respectively). The average values slightly increase (approximately average of 12%) with the compaction level. The resilient modulus fluctuated from 136 MPa to 776 MPa for the low-compaction effort specimens, and from 180 to 749 MPa for the high-compaction effort specimens. The specimens with 1% cement only showed lower modulus at low stress conditions and higher modulus at high stress condition. The spread of the data is represented in Figure 3.24 and Figure 3.25 using dashed horizontal lines for upper and lower standard deviation from the two tests. A wider spread was found for the specimens with cement only (0% foamed bitumen), indicating that specimens with foamed bitumen in comparison show reduced dependency on the confining stres.

The stress dependent behaviour is commonly encountered for granular-type materials such as foamed bitumen mixes. Several models have been

proposed to account for this effect; one of the most widely used models was proposed by Witzack and Uzan (1988):

$$M_R = k_1 \left[\frac{\theta}{P_a}\right]^{k_2} \left[\frac{\tau}{P_a}\right]^{k_3} \quad \text{(Eq. 3.7)}$$

where:

θ = Bulk stress ($\sigma_1 + \sigma_2 + \sigma_3$)

τ = Octahedral stress ($\sigma_d^{1/2}/3$)

k_1, k_2, k_3 = regression coefficients

This model has proved to provide satisfactory predictions of the elastic behaviour of granular materials in the field (Gonzalez et al. 2007). Also, it has been recently used by other researchers in foamed bitumen (Fu and Harvey 2007) to characterise the stress dependant behaviour and temperature sensitivity of these mixes.

The data collected during the resilient modulus tests were fitted to the Witzack-Uzan model and are presented in Table 3.8.

Table 3.8 Witczack-Uzan model fitting results for triaxial specimens

Bitumen	Compaction	k_1	k_2	k_3	R^2
0.0	Low	2.870	0.347	0.278	97.3
2.0	Low	3.347	0.214	0.186	93.1
4.0	Low	2.109	0.481	0.050	93.7
0.0	High	4.188	0.113	0.357	98.6
2.0	High	4.007	0.168	0.198	97.9
4.0	High	3.139	0.338	0.083	98.4

The fitting of the data to the Witzack-Uzan equation yields R^2 values between 93.7% and 98.6%, indicating that the proposed model describes the stress dependency of the materials reasonably well under the triaxial stress

conditions applied in these tests. The overall measured versus predicted data for the N=348 measurements are compared in Figure 3.27.

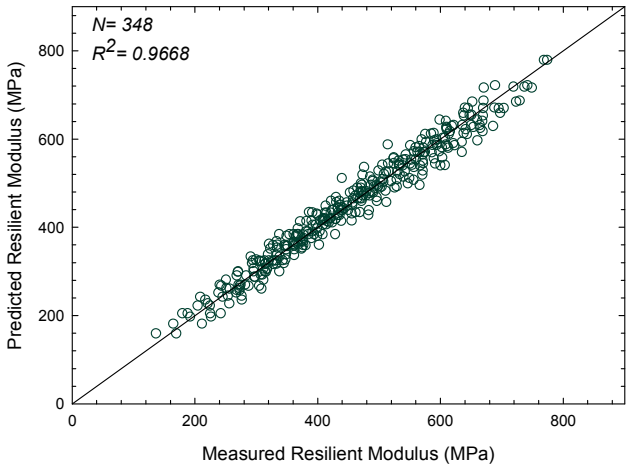

Figure 3.27 Measured versus predicted resilient moduli by the Witczack-Uzan model

3.3.7 **Monotonic triaxial tests**

3.3.7.1 Objectives and test method

Monotonic shear failure tests were conducted on the materials studied, for comparison with the RLT permanent deformation tests and to determine the fundamental shear properties (i.e. angle of internal friction, ϕ; and cohesion, C) of the mixes studied. Only materials at 1.0% cement were considered because of the poor performance observed in specimens without active filler. Details of the compaction of these specimens are shown in Appendix C (Section C.4).

The RLT system described above was also used for monotonic shear failure tests. However, the load capacity of the RLT system was not sufficient to produce the failure of the triaxial specimens and therefore the triaxial cell was mounted in the Humboldt Master Loader HM-3000 (Figure 3.7).

The original 10 kN load cell was replaced by a 50 kN load cell to record the stress applied during the test. The deformation of the sample was measured using an external LVDT, while the load was measured by a chart recorder.

The strain rate was set at 2.0%/min, the rate used by other researchers in foamed bitumen (Jenkins et al. 2007; Long et al. 2002; Long and Ventura 2004) which was selected so results could be compared with measurements available in the literature.

3.3.7.2 Experimental design

The specimens were tested at a range of confining stresses. At each bitumen content, at least one specimen was tested at low confining pressure (50 kPa) and at high confining pressure (300 kPa); this range of confining pressures was applied to ensure any difference in the measured peak stresses was clearly shown, as this leads to a better and more reliable calculation of the shear parameters ϕ and C.

3.3.7.3 Results: peak axial stress

The peak axial stresses measured in the monotonic tests are detailed in Table 3.9, and plotted using contour plots in Figure 3.28, indicating that foamed bitumen reduces the maximum or peak axial stress of the specimens at 1% cement, while an increase in confining stress increases the peak axial stress. This trend is consistent with the observed results from the permanent deformation triaxial tests presented before, in which higher permanent deformation was measured at higher bitumen contents.

The monotonic results also indicate that at high compaction level, the strength of the material is higher. This trend partially contradicts the observations made from the permanent deformation tests previously presented.

Table 3.9 Summary of the measured peak vertical stresses measured in triaxial specimens

Sample ID	Bitumen (%)	Cement (%)	Compaction Effort	Bulk Density (kg/m^3)	Confining (kPa)	Peak Vertical (kPa)
M_B0C1_LC_4	0.0	1.0	Low	2172	50	2172
M_B0C1_LC_3	0.0	1.0	Low	2163	50	2214
M_B0C1_LC_2	0.0	1.0	Low	2087	300	3741
M_B0C1_LC_1	0.0	1.0	Low	2117	300	3637
M_B2C1_LC_3	2.0	1.0	Low	2134	50	1550
M_B2C1_LC_1	2.0	1.0	Low	2007	175	1895
M_B2C1_LC_2	2.0	1.0	Low	2085	175	1856
M_B2C1_LC_4	2.0	1.0	Low	2114	300	2306
M_B4C1_LC_3	4.0	1.0	Low	2066	50	1345
M_B4C1_LC_4	4.0	1.0	Low	2080	50	1100
M_B4C1_LC_2	4.0	1.0	Low	2071	300	1629
M_B4C1_LC_1	4.0	1.0	Low	2057	300	1437
M_B0C1_HC_1	0.0	1.0	High	2243	50	2305
M_B0C1_HC_2	0.0	1.0	High	2245	50	2710
M_B0C1_HC_3	0.0	1.0	High	2214	300	4003
M_B2C1_HC_3	2.0	1.0	High	2243	50	1958
M_B2C1_HC_2	2.0	1.0	High	2251	175	2413
M_B2C1_HC_1	2.0	1.0	High	2247	175	2183
M_B4C1_HC_3	4.0	1.0	High	2168	50	1298
M_B4C1_HC_2	4.0	1.0	High	2193	300	1720
M_B4C1_HC_1	4.0	1.0	High	2140	300	2025

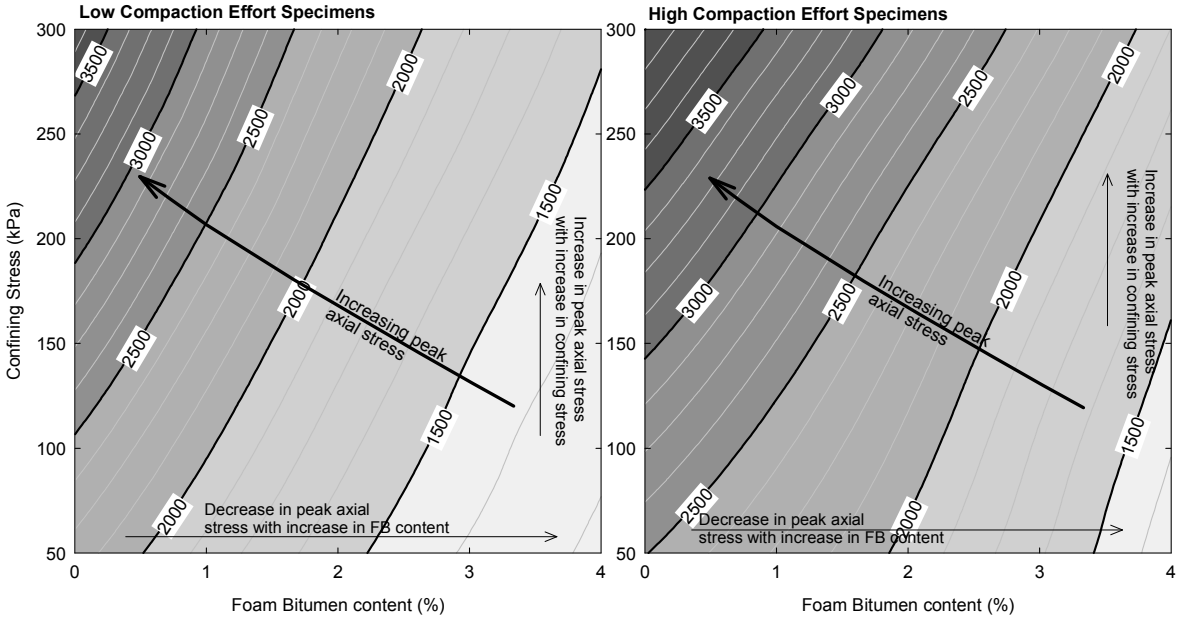

Figure 3.28 Contour plots of peak axial stress (in kPa) measured at different confining stresses and bitumen contents in monotonic load triaxial test

3.3.7.4 Results: calculation of shear strength parameters

The peak stresses measured during the monotonic triaxial tests were used to calculate the fundamental shear parameters of the mixes. The peak stresses measured at different confining pressures define the failure conditions of the material and can be used as a benchmark to analyse relative damage that will result from repeated load applications at lower stresses such as those applied during permanent deformation tests (Jenkins et al. 2007). The shear parameters have been incorporated into structural design methods (Theyse et al. 1996) to calculate maximum deviator stress that a granular material can sustain, and some researchers have proposed the utilization of shear parameters for the structural characterization of hot mix asphalt too (Fwa and Tan 2005).

The shear strength parameters, angle of internal friction (ϕ) and cohesion (c), were calculated for both low and high compaction specimens using the triaxial data. The peak stress values were plotted in a conventional shear stress – normal stress diagram and a linear failure envelope was fitted to the data. The

failure envelope was modelled as linear, even though generally is recognised as non-linear and therefore not entirely accurate in representing the shear properties of the material. This approximation, in which the cohesion is estimated by using the intercept of the failure line with the shear stress axis, is uncertain, owing to the curvature of failure envelopes observed in most materials (Mitchell 1993). Therefore, the cohesion is only an apparent value estimated from the available monotonic triaxial results. Nevertheless, provided that the stress applied to a material is not very low, the Mohr–Coulomb approximation of the strength remains sufficiently accurate for material modelling purposes (Jenkins et al. 2007). The fitted failure envelopes as well as the peak stresses are plotted in Figure 3.29 and Figure 3.30 for both compaction levels.

The shear parameters were expressed in terms of Mohr-Coulomb failure criterion, presented in Table 3.10, which show a reduction in the angle of internal friction when foamed bitumen is added, while the effect on cohesion is not clear. The reduction of internal friction was also observed by Jenkins et al. (2007), who also stated that cohesion is to a large extent controlled by the active filler content when the foamed bitumen content is fixed and the active filler content is increased.

When density is increased, both angle of internal friction and cohesion overall values increased. The R^2 values obtained from linear regression were relatively good for the specimens at 0.0% and 2.0% foamed bitumen. The R^2 values for the low compaction level specimens at 4.0% were considerably lower because the measured peak stresses did not show significant variation with confining stresses.

Table 3.10 Calculated Mohr-Coulomb parameters

Compaction Level	Bitumen (%)	Cement (%)	Friction angle Φ (°)	Cohesion c (kPa)	R^2
Low	0.0	1.0	46	386	99.4%
Low	2.0	1.0	30	391	99.5%
Low	4.0	1.0	13	436	25.9%
High	0.0	1.0	46	434	99.0%
High	2.0	1.0	33	469	83.3%
High	4.0	1.0	27	343	81.5%

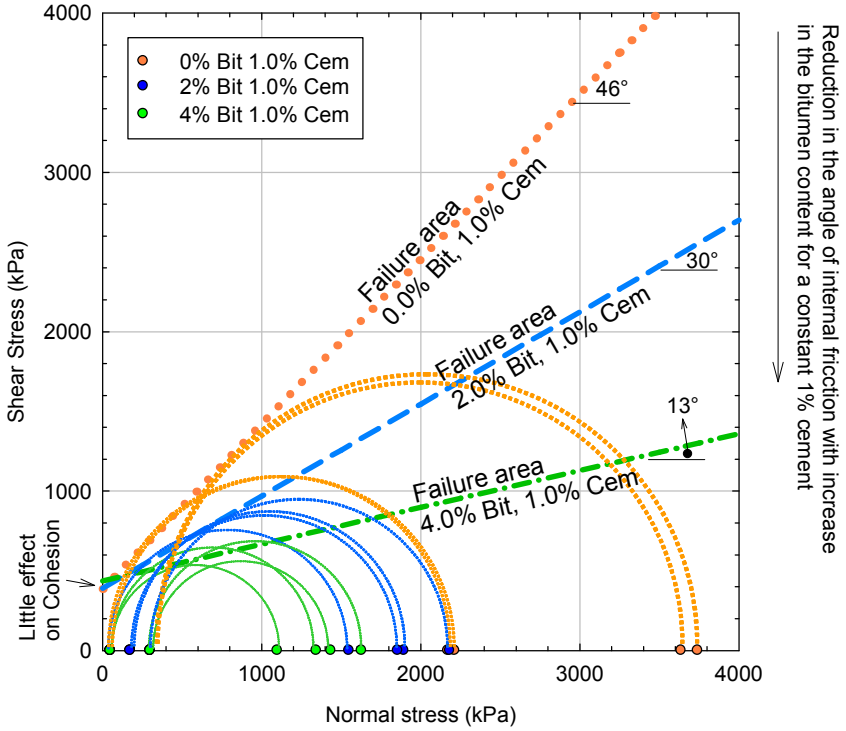

Figure 3.29 Mohr's circles and failure envelopes for low compaction level samples

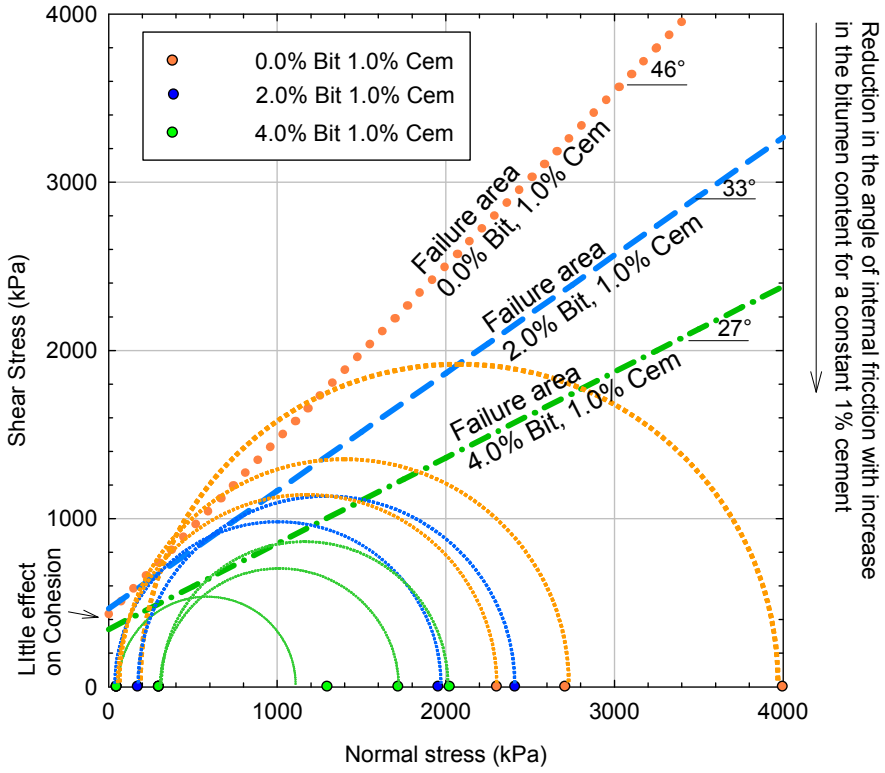

Figure 3.30 Mohr's circles and failure envelopes for high compaction level samples

3.4 Interpretation and discussion of results

3.4.1 Scope of observations

The preliminary study on foamed bitumen mixes indicated that the addition of 1% cement has a major contribution to the strength of the mixes and therefore the focus of the laboratory study was the effect of adding foamed bitumen to mixes with 1% cement. Based on these results, the following tests were conducted on materials with 1% cement and different foamed bitumen contents:

- Indirect tensile resilient modulus tests
- Indirect tensile strength tests
- Permanent deformation repeat load triaxial tests
- Resilient modulus repeat load triaxial tests
- Static (monotonic) triaxial tests

Both indirect tensile resilient modulus and indirect tensile strength tests showed similar results: there is an optimum foamed bitumen content (estimated in 2.8%) that maximizes the indirect tensile property. Conversely, the cyclic triaxial results show an opposite trend to those of the indirect tensile tests. The triaxial permanent deformation measurements indicated that at higher bitumen contents, permanent deformation increases. The same trend was found in the monotonic or static triaxial tests where a reduction of the shear strength of the materials was observed at higher bitumen contents. When the resilient modulus was measured under repeat load triaxial conditions, the effect of bitumen was found to be negligible.

In summary:

- Foamed bitumen increases the strength of the material when measured under indirect tensile conditions (e.g. ITS increase from 200 kPa to 320 kPa when foamed bitumen content increases from 0% to 2%, or an increase of 60%).
- Foamed bitumen decreases the strength of the material when measured under compressive triaxial conditions (e.g. monotonic peak stress decreases from $\sigma_{v[average]}$= 2709 kPa to $\sigma_{v[average]}$= 1550 kPa when foamed bitumen content increases from 0% to 2% for low compaction effort, at 50 kPa confining stress, or a 43% reduction).
- Foamed bitumen increases the permanent deformation under repeated loading in triaxial compression for both low and high compaction specimens.
- Foamed bitumen does not have a significant effect on the average resilient modulus when measured under triaxial conditions (i.e. the average resilient modulus fluctuates from 403 MPa to 442 MPa for low compaction specimens, and from 460 MPa to 484 MPa for high compaction specimens, or a variation of approximately 5 to 10%)

- Foamed bitumen increases the resilient modulus when measured under indirect tensile conditions (e.g. from 2100 MPa to 6200 MPa when foamed bitumen content increases from 0% to 2%).
- High compaction effort increases the permanent deformation of triaxial specimens with foamed bitumen (e.g. increase of final deformation from an average of $4x10^3$ μm to $6x10^3$ μm for specimens at 2% bitumen, when the compaction effort is increased).

The first five observations do not show a conclusive effect of foamed bitumen: while the effect in triaxial compression is a reduction in strength, this trend reverses in indirect tensile tests, showing that the type of loading and deformation mode is critically important for the response of the material. To better analyze and interpret the behaviour of the material studied, the stresses applied to the specimens in the various types of tests were scrutinized, as described in the following Section.

3.4.2 **Interpretation of results using stress analysis**

3.4.2.1 Laboratory stress paths expressed in I_1- $J_2^{(1/2)}$ stress diagram

The laboratory tests applied in foamed bitumen materials follow different loading conditions. The load applied in triaxial tests consists of a uniform confining stress ($\sigma_2=\sigma_3$) plus an axial vertical (dynamic or static) stress (σ_1). Conversely, the stress conditions applied in the indirect tensile tests are not uniform throughout the specimen. The horizontal (tensile) stress in the centre of the specimen is induced by a compressive vertical load and one of the horizontal stresses (perpendicular to the diametric plane of the specimen) is zero. To graphically represent the stress paths applied in laboratory tests, an I_1-$J_2^{(1/2)}$ stress diagram was selected for the data interpretation. The advantage of using this diagram is that non-uniform stress conditions (such as the indirect tensile test) can be represented graphically and compared with conventional triaxial stress paths because the stress invariants I_1 and J_2 take into account the three dimensional stress state of the material studied (2.5.2).

The stress paths applied in laboratory tests were plotted in Figure 3.31 for triaxial and indirect tensile stress conditions. The load applied in the triaxial tests (both monotonic and repeat load triaxial tests) consists of a constant lateral (confining) stress ($\sigma_2=\sigma_3=\sigma_{conf}$) plus a deviator (static or dynamic) stress ($\sigma_d=\sigma_1-\sigma_{conf}$), which expressed in terms of the stress invariants yields:

$$I_1 = \sigma_d + 3\sigma_{conf} \quad \text{(Eq. 3.8)}$$

$$J_2 = \frac{\sigma_d^{\,2}}{3} \quad \text{(Eq. 3.9)}$$

The horizontal position of the triaxial stress paths depends on the confining stress (the intersection of the line with the X axis is three times the confining pressure). The slope of the lines is the same for all triaxial tests because the confining pressure remained constant (0.5773). The seven permanent deformation repeat load triaxial stress states, with a confining stress of 50 kPa, were plotted with bold circles in Figure 3.31. The stress state with no deviator stress ($J_2=0$) is represented by a “0” on the X-axis, therefore, the stress path applied on each stress stage is the line that links the point 0 with the respective number of the stress stage in the figure (e.g. line 0-5 is the stress path applied in the fifth stress stage).

The stress condition of the material in the ITS test is not uniform as depicted in Figure 3.8, where the vertical (V-axis in the plot) stresses (σ_v) vary within the specimen, while the horizontal stress (σ_u) remains constant except near the edges of the specimen. The horizontal (tensile) stress at the centre of the specimen with diameter ‘d’ and thickness ‘t’, which is the height of the specimen measured at the out-of plane axis perpendicular to the U-V plane of the specimen, is induced by the applied compressing vertical load (P), on the cylindrical specimen, while the out-of plane horizontal stresses is zero. The equations describing the stress condition at the centre of the specimen, assuming linear elastic behaviour of materials, are shown in Figure 3.8. The stress path describing the stress condition at the centre of the specimen (U=0, V=0) was chosen for the stress analysis, because is the location with the

highest principal-tensile to principal-compressive stress ratio of the specimen (Claesson and Bohloli 2002), or in other words, the most critical location. The stress invariants calculated at the centre of the specimen are:

$$I_1 = \frac{4P}{\pi td} \qquad \text{(Eq. 3.10)}$$

$$J_2 = \frac{52}{3}\left[\frac{P}{\pi td}\right] \qquad \text{(Eq. 3.11)}$$

with P, t and d defined as above. The stress path for the ITS is plotted in Figure 3.31, which results in a rise at a gradient of 1.04 in the I_1- J_2 $^{(1/2)}$ stress diagram. This stress path is steeper than the others (slope = 1.0408) because the horizontal stress is proportional to the vertical stress increase.

For convenience and further data interpretation, the Unconfined Compressive Strength (UCS) stress path was also included in the figure.

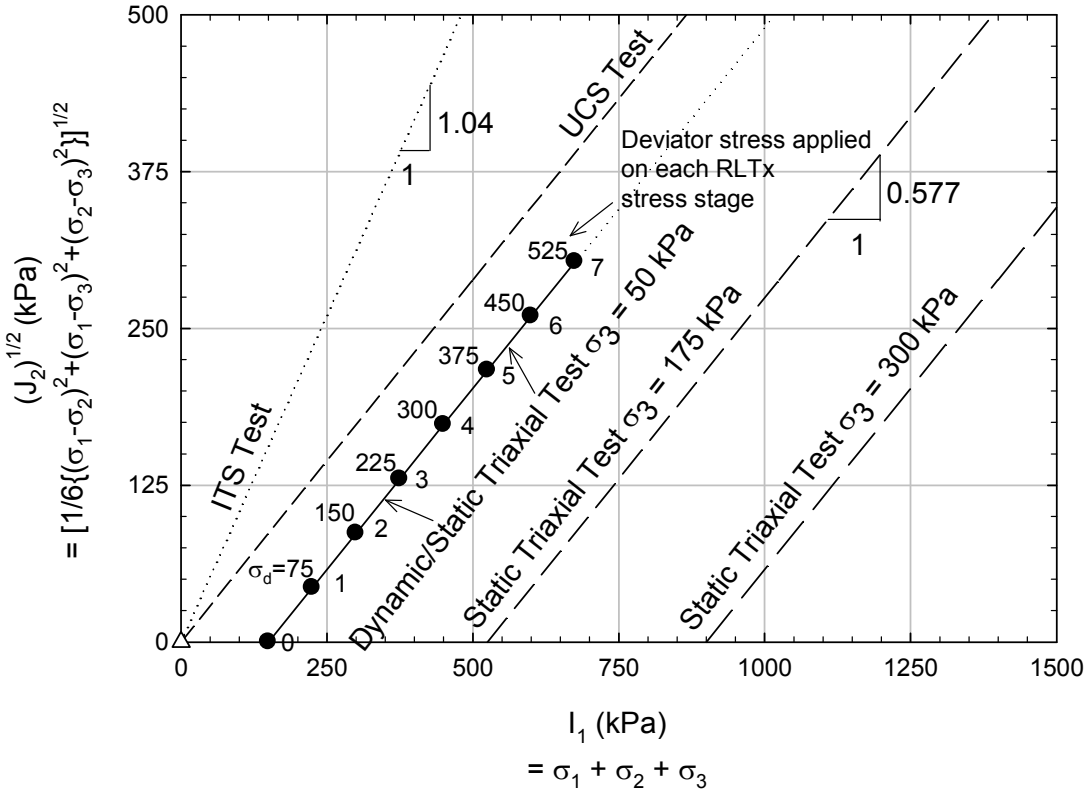

Figure 3.31 Stress paths of the laboratory tests expressed in I_1-J_2 diagram

3.4.2.2 Stress ratio analysis and discussion

The stress ratio has been commonly used as a measure of the relative damage for granular materials because it indicates the proximity to failure. This concept has been also applied in pavements (Jenkins et al. 2007; Theyse et al. 1996), by comparing the shear failure of the material with the current, cyclic stress applied. If the stress ratio is low, the material will develop some limited plastic deformation for a finite number of load repetitions, but the response will remain essentially elastic after the initial loading (e.g. the first stress stages in Figure 3.17 and Figure 3.18). At higher stress ratios, the plastic irrecoverable deformation increases, up to a certain stress level at which the permanent strain will accumulate rapidly with failure occurring in a relatively low number of load cycles (e.g. the last stress stage in Figure 3.17 and Figure 3.18 for the mix with 4% foamed bitumen and 1% cement). Although the stress ratio approach isa relatively simple and widely adopted concept, it ignores the influence of the load rate when comparing static and cyclic (dynamic) results. The cyclic load in triaxial tests was stress-controlled with a constant frequency of 4 Hz (pulse = 250 ms) and therefore the load rate was higher at higher stress levels (higher stress magnitude was applied for the same pulse length). In the monotonic triaxial tests the deformation rate was controlled (2%/min) and therefore the load rates are not totally comparable between tests. However, the purpose of the analysis was to determine the approximate stress ratio of the mixes at different stress conditions, and therefore it was considered accurate for the discussion of results.

The stress ratio was calculated by comparing the stress path at a stress state of shear failure (peak stress) obtained in monotonic load triaxial tests, with the stress path applied in permanent strain repeat load triaxial tests, using the I_1-$J_2^{(1/2)}$ stress diagram. The peak stresses from the static triaxial tests (Table 3.9), and the estimated failure envelopes were not plotted in the previously presented Figure 3.31. Instead, these were plotted in a separate chart (Figure 3.32) using a different scale, because the magnitudes of the peak axial

stresses applied in monotonic load triaxial tests are between 2 to 4 times higher than the stresses applied in the repeat load triaxial tests. The small, hatched rectangle at the bottom left part of the figure represents the stress range covered in Figure 3.31.

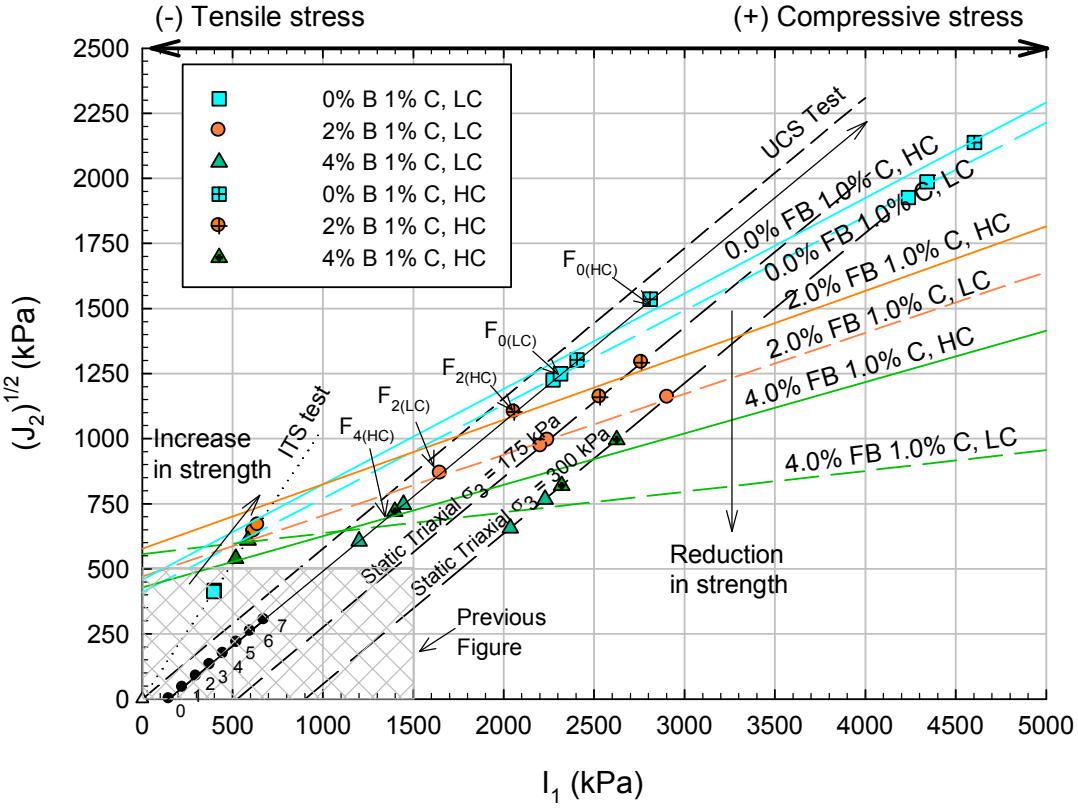

Figure 3.32 Peak stresses from triaxial tests plotted in I_1-$J_2^{(1/2)}$ diagram

In Figure 3.32 the failure envelopes estimated from the monotonic load triaxial tests are shown together with the relevant test data (large symbols). The failure envelopes were again approximated as linear, and the effects of curvature on the failure envelopes at low stresses omitted. The estimated failure lines show reduction of the slope with increase in the foamed bitumen content, which is consistent with the failure lines plotted in the Mohr-Coulomb stress diagram.

The peak stresses attained in the ITS test at 0%, 2%, and 4% foamed bitumen are also included in Figure 3.32, but these were not used in the

calculation of the failure lines. It is worth noting that ITS results showed somewhat a different trend from the monotonic load triaxial tests, in which an increase of foamed bitumen, up to 3.0%, leading to an increase in the strength of the foamed bitumen mixes. This trend is explained by the reduction of the angle of internal friction when foamed bitumen is added into the mix, in combination with the effects of foamed bitumen content on the cohesion and curvature of the failure envelope. The effects of the reduction in ϕ are more prominent at high normal stresses and hence are exhibited in the conventional triaxial compression tests, whereas for the ITS test the normal stresses are low and hence the cohesion and curvature of the failure envelope have dominant effects on the strength and deformation of foamed bitumen mixes.

The stress ratios applied in the permanent deformation repeat load triaxial tests were calculated by comparing the size or length of the stress path, applied in each of the stress stages of the repeat load triaxial tests, with the length of the stress path at failure measured in the monotonic load triaxial tests, for the confining pressure of 50 kPa. The endpoint of the stress paths at failure, for each foamed bitumen content of 0, 2 and 4%, are indicated in Figure 3.32 with the symbols F_0, F_2, and F_4 respectively, for low and high compaction specimens (e.g. $F_{4(HD)}$ is the endpoint of the estimated peak stress path applied in the specimen with 4% foamed bitumen prepared with high compaction energy). Therefore, the stress ratio for each mix is the quotient between the size of the stress path applied in the repeat load triaxial test, and the size of the stress path at failure. For instance, the stress ratio for the mix with 4% foamed bitumen, prepared with high compaction energy, at the stress stage 7, is the quotient of the length 0-7 with respect to the length of 0-$F_{4(HC)}$, as shown in Figure 3.32.

The stress ratios calculated at deviator stresses of 75 (Stage 1), 300 (Stage 4) and 525 kPa (Stage 7), for 0, 2 and 4% foamed bitumen contents, for the high compaction energy specimens, are presented in Figure 3.33. The figure shows that the applied stress ratios were much higher for specimens at higher foamed bitumen content, and therefore, the damage or permanent strain was

higher, for a given deviator stress level. The most severe stress condition of the repeat load triaxial tests (stress path number 7, σ_d=525 kPa) is a stress ratio of approximately 40% of the failure stress for specimens at 4.0% foamed bitumen and 1.0% cement. The maximum stress ratio was 27% for specimens at 2% foamed bitumen, and 21% for specimens without foamed bitumen. In other words, the stress applied to the mixes with 4% foamed bitumen was twice higher (in relative terms) than that for the 0% foamed bitumen mixes, and therefore a higher irrecoverable deformation is expected.

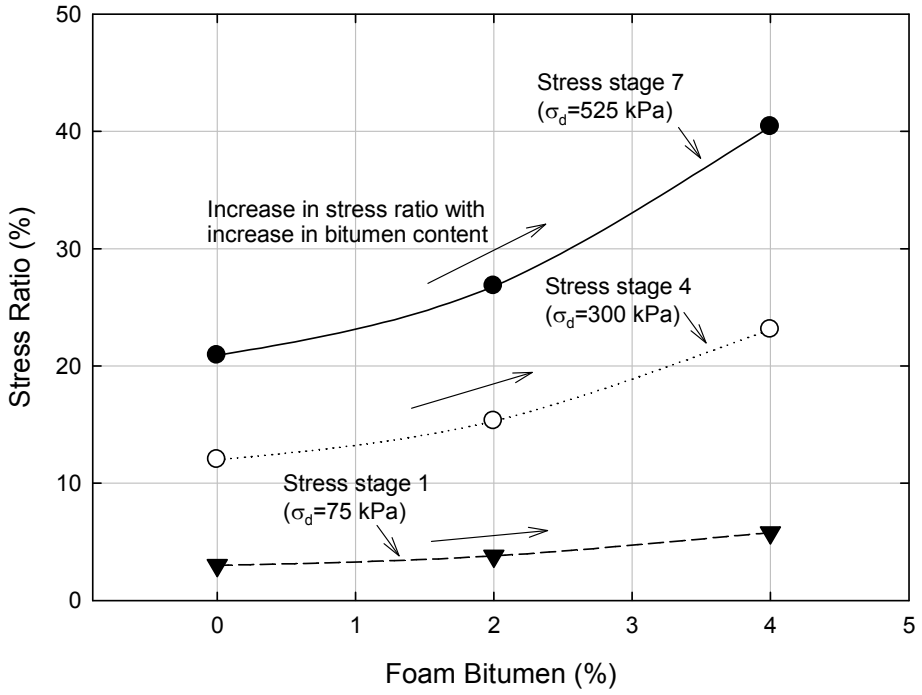

Figure 3.33 Stress ratios at different foamed bitumen contents

3.4.3 **Effect of the compaction effort in the dynamic permanent deformation tests**

3.4.3.1 Discussion on the volumetric properties of the mixes

Permanent deformation repeat load triaxial results were presented in Figure 3.17 and Figure 3.18, showing that permanent deformation is higher at high compaction energy than low compaction energy for the specimens at 2.0% and 4.0% bitumen. This trend indicates that the plastic deformability of the material increases when a higher compaction effort is applied on the preparation of the specimen. This was considered an unexpected behaviour because it is known that granular materials compacted at higher energy levels

exhibit lower permanent deformation in triaxial tests (Barksdale 1972; Dodds 1999; Holubec 1969; Thom 1988). The trend was not observed in specimens without foamed bitumen and 1.0% cement, which essentially showed lower permanent deformation with an increase in the compaction effort. Conversely, the trend described above was not observed in monotonic tests (in monotonic tests the peak stress augmented at high compaction levels for specimens with and without foamed bitumen). That is, the negative effect of compaction was only observed in triaxial specimens with foamed bitumen and cement when a large number of cyclic loads were applied during the permanent deformation tests. As discussed in Section 3.3.4.5, this result was also obtained in other studies (Long and Ventura 2004) but authors argued that the behaviour was associated with testing variability and the low effect of density on repeat load triaxial tests.

The observed behaviour of foamed bitumen mixes in triaxial tests could be explained by an approximate analysis of the volumetric composition of the specimens tested. Foamed bitumen materials are more complex than hot mix asphalt and soil materials because the former contain an aggregate skeleton with an active filler (aggregate and cement), a viscoelastic material (bitumen), water and voids. The voids are partially filled with bitumen and water.

The mixes tested in the repeat load triaxial study were produced using the same water content during the mixing process (5.1% over the dry weight of the aggregate) to keep the moisture content constant and isolate the effect of foamed bitumen (Section 3.2.3). However, the saturation level (percentage of water over the voids) was not the same among the different mixes.

The average estimated volumetric properties of the specimens are presented in Figure 3.34. These properties were estimated using the bulk volume of the specimens, calculated during compaction, rather than the real volume, and therefore are not totally accurate. The figure shows the volume, in percentage, of the different components of the specimens for the three foamed bitumen contents tested (0.0%, 2.0% and 4.0%) and at the two compaction efforts applied during compaction. The common 1.0% cement content was

considered part of the aggregate skeleton and therefore is not shown in the figure.

The calculated voids in the mineral aggregate (VMA), air voids (VA) and voids filled with bitumen (VFB) for each case are presented in Table 3.11. The specimens without foamed bitumen (0.0% FB, 1.0% C) showed VMA values of 20.6% and 15.5% for specimens compacted at low and high effort, respectively. This indicates that the governing mechanism against permanent deformation in the absence of foamed bitumen is the density of the aggregate skeleton. The VMA values found in the mixes with foamed bitumen were higher than values found by other researchers. Saleh (2004a) found VMA close to 15% measured in 100 mm diameter specimens at 3.0% foamed bitumen content. However, in Saleh's research the particle size distribution of the untreated material was an AP20 (an aggregate finer than the H40/AP5), the maximum aggregate size was 13.2 and the compaction type applied was gyratory compaction, commonly used to simulate compaction conditions of hot mix asphalt materials in the field, and therefore the VMA results are not totally comparable.

When bitumen foam is incorporated, the intergranular stresses are transmitted through the aggregate as well as the bitumen 'soft spots' that weaken the material when loaded in compression. Also, the bitumen fills part of the voids of the mineral aggregate, reducing the available air voids volume and increasing the saturation of the specimens. In other words, the increase in compaction effort enhances the strength of the aggregate skeleton, however, the effect of adding foamed bitumen counteracts this effect because it creates a weaker material (in compression) and also increases the saturation level of the mix, which is likely to increase the build-up of pore pressure during the triaxial testing.

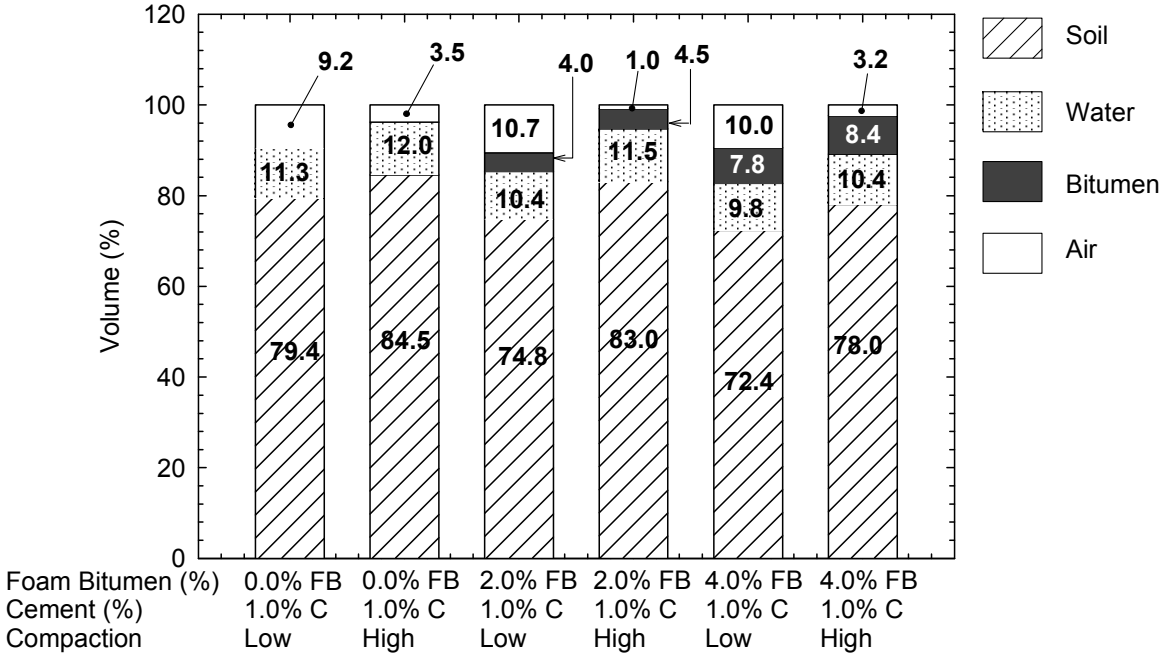

Figure 3.34 Estimated volumetric relationships for different compaction efforts and bitumen content

Table 3.11 Estimated volumetric properties of triaxial specimens

Mix	VMA (%)	VA* (%)	VFB (%)	VFW (%)	VFW* (%)	VA (%)
H40AP5 0.0% LC	20.6	20.5	0.0	54.8	54.8	9.2
H40AP5 0.0% HC	15.5	15.4	0.0	77.4	77.4	3.5
H40AP5 2.0% LC	25.2	21.1	15.8	41.3	49.3	10.7
H40AP5 2.0% HC	17.0	12.5	26.5	67.7	92.0	1.0
H40AP5 4.0% LC	27.6	19.8	28.2	35.5	49.5	10.0
H40AP5 4.0% HC	22.0	13.6	38.2	47.2	76.4	3.2
M20FA (3.0% FB)	15.0	8.4	44.2	-	-	-
M20FA2C (3.0% FB)	15.8	9.2	41.7	-	-	-

The basic relationship between effective stress (σ'), total stress (σ) and pore pressure (u) is given by:

$$\sigma = \sigma' + u \qquad \text{(Eq. 3.12)}$$

for a completely saturated soil. Bishop (1960) proposed the following equation for the effective stress on a partially saturated soil:

$$\sigma' = \sigma - u_a + \chi(u_a - u_w) \qquad \text{(Eq. 3.13)}$$

where u_a is the air pressure, u_w is the water pressure and the term (u_a-u_w) represents the soil water suction and adds to the effective stress (σ') since u_w is negative. χ is a parameter that for a dry soil is 0 and for a saturated soil is 1.0. The Bishop equation assumes that negative pore pressures increase strength. When a saturated soil is subjected to repeated cycles of loading, the granular structure begins to break down and a part of the confining stress is transferred to the pore water with a concurrent reduction of effective stress and strength (Bishop 1960). This, in turn, leads to an increase in shear strain under constant stress cyclic loading.

3.4.3.2 Preparation of specimens for pore pressure measurements

To determine the importance of the pore pressure and saturation level of the specimens mentioned above, two rounds of additional experiments were conducted on four specimens prepared with 4.0% bitumen and 1.0% cement. In each round, two triaxial specimens were prepared applying high compaction energy and the other two applying low compaction energy. For the first round of tests (specimens 90 and 91), conducted in September 2008, the original supply of H40 aggregate (Section 3.2.1.1) was used in the preparation of the mixes. For the second round of tests (specimens 92 and 93), carried out in January 2009, the original supply of H40 was not available. Hence, approximately 60 kg of additional H40 material were delivered to the Transportation Laboratory. The preparation, compaction, curing and testing was identical to that of the detailed repeat load triaxial tests presented before in Section 3.2.3. The only additional measurement collected in the permanent strain tests was the pore pressure, using an external transducer connected to the pedestal of the triaxial cell and to an external data acquisition system. The dry bulk specimens for each specimen are shown in Table 3.12. Details of the compaction of specimens were included in Appendix C, Section C.7.

Table 3.12 Properties of triaxial specimen for pore pressure tests

ID	Bitumen (%)	Cement (%)	Compaction energy	Dry Density (t/m^3)	Comments
PP_4BC1_LC_1	4.0	1%	Low	2.016	Over-consolidated
PP_4BC1_HC_1	4.0	1%	High	2.215	Over-consolidated
PP_4BC1_LC_2	4.0	1%	Low	2.009	Different H40 supply
PP_4BC1_HC_2	4.0	1%	High	2.116	Different H40 supply

3.4.3.3 Determination of the B-Value

Before the repeat load triaxial testing of the specimens, the B-value of the specimens was determined. The B-value is a no dimensional value defined as:

$$B = \frac{\Delta u}{\Delta \sigma} \qquad \text{(Eq. 3.14)}$$

where $\Delta\sigma$ is the amount of isotropic stress increment and Δu is the amount of pore pressure increment, both expressed in the same stress units (e.g. kPa). The B-value is a measurement of the relative saturation of the specimen. When the specimen is 100% saturated, the pore pressure measured in the specimen should equal the confining stress (B=1.0), and when the specimen is completely dry the value should be zero.

The determination of the B-value was carried out by placing the specimens with 4% foamed bitumen and 1% cement in the triaxial cell, and applying increments of isotropic stress. The B-value for the first round of specimens (90 and 91) was measured increasing the confining stress from 0 to 138 kPa, in

one load step, resulting in an increase in pore pressure of 11.5 kPa for the low compaction specimen and of 40.5 kPa for the high compaction specimen, yielding B-values of 0.083 and 0.29 respectively. However, the relatively high confining pressure (138 kPa) applied during the tests could have affected the specimen by reducing the air voids of the mixes. Therefore, for the second set of tests (specimens 92 and 93), instead of a large increment of isotropic stress, 10-kPa increments, from 0 to 50 kPa, were applied. After each stress increment of 5 kPa, the pore pressure was recorded for each specimen, as shown in Figure 3.35. The results show that, for the high compaction specimen, an increase in 1kPa of confining stress yields an almost equal increase of 0.97 kPa of pore pressure, indicating that the specimen is practically fully saturated. Conversely, the low compaction specimen showed little increase in the measured pore pressure with increase in the confining stress (0.06 kPa for every 1 kPa of confining stress) indicating that this specimen is not saturated.

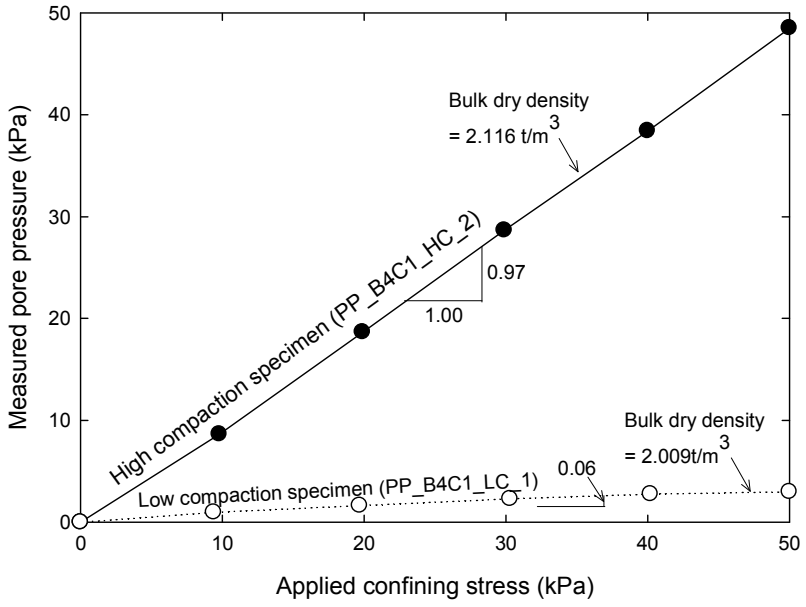

Figure 3.35 Determination of the B-value for triaxial specimens with 4% foamed bitumen and 1% cement, prepared with low and high compaction efforts

3.4.3.4 Permanent deformation and pore pressure results

A multi-stage permanent deformation test was conducted on each of the four specimens described in Section 3.4.3.2. The confining pressure applied

during the test was 50 kPa, following the same multi-stage stress sequence previously presented in Figure 3.15 for the detailed permanent strain tests. During the application of the cyclic loads, permanent deformation and pore pressure were simultaneously recorded.

The results for the first round of tests are shown in Figure 3.36. In the figure, the permanent strain (μm/m) was plotted together with the measured pore pressure. The permanent strain trends remained similar to those of the previous repeat load triaxial tests, in which the irrecoverable final deformation is higher in the specimens compacted with higher energy ($5.9x10^3$ μm/m) compared to specimens compacted with low energy ($4.7x10^3$ μm/m). The average pore pressure for the high compaction specimens ranged from approximately 20 kPa, in the first stage, to 23 kPa in the last stage, while for the low compaction specimen these values ranged from 6 to 9 kPa approximately. Therefore, the pore pressure measured during the dynamic loading of the triaxial specimens was about three times greater for samples compacted at high energy compared with those at low energy.

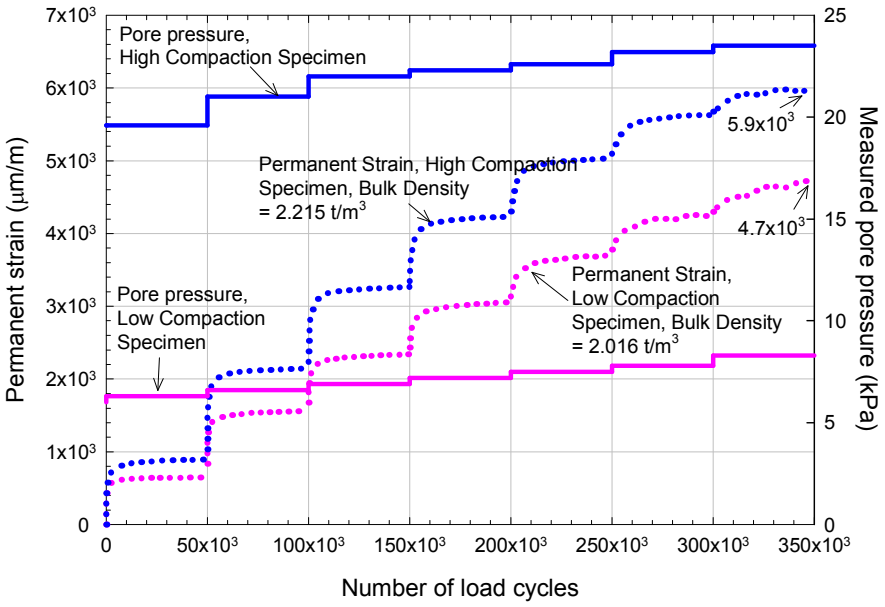

Figure 3.36 Pore pressure experiment for specimens at 4.0% bitumen and 1.0% cement (first set of pore pressure tests)

The results for the second round of tests are shown in Figure 3.37. In the figure, the permanent strain (μm/m) was plotted together with the measured pore pressure. The permanent strain trends remained similar (higher deformation in high compaction specimens), but in both tests the final permanent strain was lower than that in the first set of tests ($4.7x10^3$ μm/m versus $5.9x10^3$ μm/m for high compaction tests, and $4.0x10^3$ μm/m versus $4.7x10^3$ μm/m for low compaction test). This could be originated by the inherent variability of the triaxial tests, or by the different aggregate supply from which the second round of specimens were prepared. The average pore pressure for the high compaction specimen ranged from approximately 9.2 to 10.2 kPa during the test, while the pore pressure for the low compaction specimens an approximately constant pore pressure of 2.7 kPa was measured throughout the experiment. Even though the results from the first set of test differ from those of the second set of test, the results show similar trends in both permanent strain and pore pressure measurements.

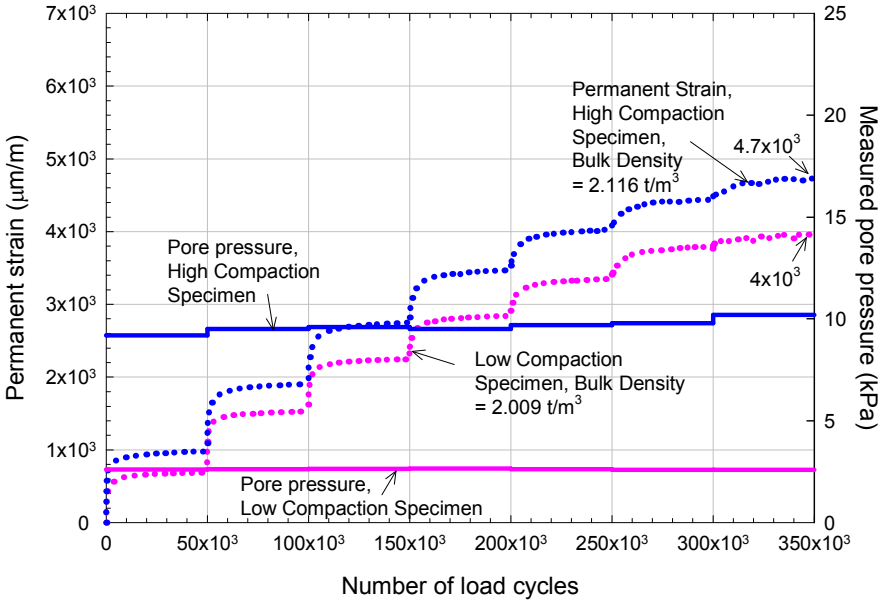

Figure 3.37 Pore pressure experiment for specimens at 4.0% bitumen and 1.0% cement (second round of pore pressure tests)

The pore pressure measurements could explain the higher permanent deformation observed in foamed bitumen specimens prepared applying high compaction energy, by examining the Bishop's (1960) equation:

$$\sigma' = \sigma - u_a + \chi(u_a - u_w) \quad \text{(Eq. 3.13)}$$

The χ parameter remains unknown, but the B-value suggests that χ is close to 1.0 for high compaction specimens, and is much lower for low compaction specimens, which leads to a higher effective (σ') stress in the high compaction specimens, assuming that the air (u_a) pressure will remain similar for high and low compaction specimens. In other words, the length of the stress paths applied during the permanent deformation triaxial tests (Figure 3.32) was greater for the high compaction specimens, and this could have contributed to increase the deformability of the material. Overall, these results illustrate the importance of the degree of saturation of foamed bitumen mixes, which could offset the effect of a higher density. Therefore, actions should be taken during the construction of foamed bitumen mixes to minimize the water content after construction, either by using a lower amount of compaction water (and higher compaction energy) or delaying the surfacing of the foamed bitumen layer to allow the evaporation of the water (curing).

3.5 Summary and concluding remarks

The Chapter presented laboratory tests on the materials adopted for this research which were also used in the accelerated full-scale testing of pavements presented in the following Chapter. Different loading conditions on the foamed bitumen mixes were applied using dynamic repeat load triaxial tests, static or monotonic triaxial tests, indirect tensile strength tests and indirect tensile resilient modulus tests.

Based on the results, the following conclusions are made:

- The aggregate mix H40/AP5 selected for the study is a suitable material for foamed bitumen stabilisation and complies with New Zealand aggregate specifications.

- The 80/100 bitumen selected for the study is suitable for foamed bitumen stabilisation according to the available foamed bitumen guidelines.

- Fourteen days was found to be the minimum curing time for the mixes studied based on the resilient modulus variation measured using repeat load triaxial tests.

- The addition of foamed bitumen to the material at 1.0% cement increases the ITS value with an optimum bitumen content of approximately 2.8%. This value was adopted as the optimum for the full- scale testing of pavements.

- The addition of foamed bitumen to mixes with 1.0% cement increases the resilient modulus measured under indirect tensile stress conditions. The measurements show a peak at 3.0% foamed bitumen content.

- The addition of foamed bitumen to the mixes with 1.0% cement increases the permanent deformation measured under RLT conditions. This indicates that the deformability of the material measured under RLT conditions increases when foamed bitumen is added.

- The addition of foamed bitumen in RLT samples at 1.0% cement does not significantly improve the resilient modulus values (only 5%-10%). The addition of 1% cement improved the performance of the RLT specimens. A reduction in the stress dependency of the materials was observed when foamed bitumen is added.

- In the triaxial static tests, the incorporation of foamed bitumen to mixes with 1.0% cement reduced the maximum allowable peak stress, indicating that triaxial compressive strength of the material decreases when foamed bitumen is added, similar to dynamic RLT results.

- With the triaxial static test data, the fundamental shear parameters (angle of internal friction and cohesion) of the mixes studied were calculated. Results indicate that the addition of foamed bitumen to mixes with 1.0% cement reduces the angle of internal friction, but conclusive effects on cohesion were not observed. Also, at higher compaction effort the shear strength parameters increase. The decrease in the angle of internal friction also indicates that the material is less stress dependant when foamed bitumen is added.

- The results of the laboratory tests (both in compression and tension) were interpreted using stress analysis. The stresses applied in the laboratory tests were plotted in I_1-$J_2^{1/2}$ stress diagram, together with the attained peak stresses for the mixes and estimated shear failure envelopes. These plots showed that the effect of adding foamed bitumen is a reduction of the compressive strength of the mixes, and a simultaneous increase of the tensile strength, which explains the apparently “contradictory” effects of foamed bitumen reported in the literature depending on the type of test used.

- The stress paths applied in Repeat Load Triaxial tests were compared with the failure stresses using the stress ratio between the current applied stress and the stress at failure, which was considered a measure of the relative size of the load. The results showed that an increase in the foamed bitumen content effectively increase the stress ratio or relative size of the load for a constant deviator stress, as a result of the reduction of the compressive strength of the mix

- The high compaction effort applied to specimens with foamed bitumen increases the degree of saturation of the materials. The higher saturation caused a higher pore pressure when specimens are subjected to cyclic loading, which negatively affects the performance of the specimens by increasing permanent deformation, which explains the trends observed in the literature.

This page is intentionally left blank

4 Full-Scale Accelerated Testing of Pavements

4.1 Introduction

This chapter presents the field experimental study on foamed bitumen pavements, conducted at the Canterbury Accelerated Pavement Testing Indoor Facility (CAPTIF), a pavement research facility owned and operated by Transit New Zealand. In the study, six pavement sections were constructed using different contents of foamed bitumen and cement, and tested applying full-scale accelerated loading.

The general features of the pavement testing facility, and different types of measurements collected during the execution of the test are detailed in the first part of this chapter. The following sections provide details about the design and construction of the pavement sections, and the laboratory testing of pavement materials collected during construction.

The bulk of the chapter is the presentation of results collected from the six pavement sections tested, in which a total number of approximately 5,710,000 equivalent standard axles (ESAs) were applied. During the application of the loads, various measurements were collected to estimate the effect of foamed bitumen stabilisation and cement on the performance of the pavements. Surface deformation was measured using a transverse profilometer, surface deflections using both a Falling Weight Deflectometer (FWD) and beam deflectometer, and strains were recorded at different depths of the pavement using an array of Emu strain gauges.

The chapter follows with a post-mortem analysis of the pavement tested, in which transverse profiles were inspected at trenches excavated in each pavement section. Also, in this last part of the experiment, material samples were collected for bitumen extraction and moisture contents. The last part of

the chapter is a discussion and interpretation of the experimental results, where the field pavement tests and laboratory tests results are also compared.

4.2 Canterbury Accelerated Pavement Testing Indoor Facility (CAPTIF)

4.2.1 General features

CAPTIF is located in Christchurch, South Island of New Zealand. It consists of a 58 m long (on the centreline) circular track, contained within a 1.5 m deep by 4.0 m wide concrete tank, so that the moisture content of the pavement materials can be controlled and the boundary conditions are known (Figure 4.1). CAPTIF is enclosed by a hexagon-shaped building that is 26-m wide and 6-m high. A centre platform carries the machinery and electronics needed to drive the system. Mounted on this platform is a sliding frame that can move horizontally by 1 m. This radial movement enables the wheel paths to be varied laterally and can be used to have the two "vehicles" operating in independent wheel paths. At the ends of this frame, two radial arms connect to the Simulated Loading and Vehicle Emulator (SLAVE) units. These arms are hinged in the vertical plane so that the SLAVE units can be removed from the track during pavement construction, profile measurement, etc, and in the horizontal plane to allow vertical movement of the SLAVE units (Steven 2005).

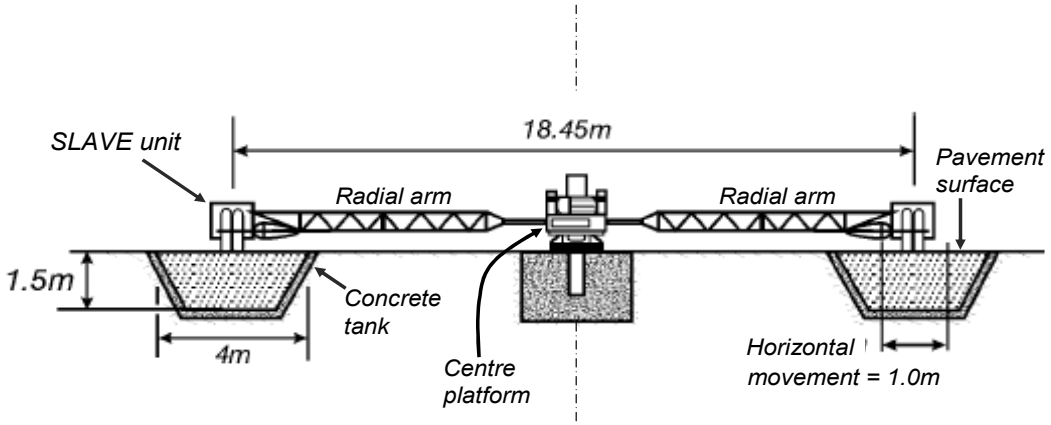

Figure 4.1 SLAVE and cross-section of the test track

The response of the pavement during CAPTIF tests is monitored using strain coil instrumentation installed in the pavement (fabricated at CAPTIF). The

relay boards, triggering systems, and software were developed at the University of Canterbury. All the strain coil pairs are calibrated and tested before their installation.

4.2.2 **Simulated loading and vehicle emulator (SLAVE)**

The main feature of CAPTIF is the Simulated Loading and Vehicle Emulator (SLAVE). The SLAVE unit (Figure 4.2) consists of an assembly of the axle, hydraulic motor, suspension, a frame, instrumentation, and standard truck wheel hubs and tyres. The standard vehicles are equipped with half-axle assemblies that can carry either single- or dual- tyred wheels. The vehicles can be loaded to between 21 kN and 60 kN, equating to axle loads of 42 kN - 120 kN, by adding steel plates in increments of 2.75 kN. The standard axle suspension incorporated to the SLAVE units produce realistic dynamic wheel responses to the changing roughness of the pavement surfaces. The operational limits of the SLAVE are shown in Table 4.1 (Pidwerbesky 1996).

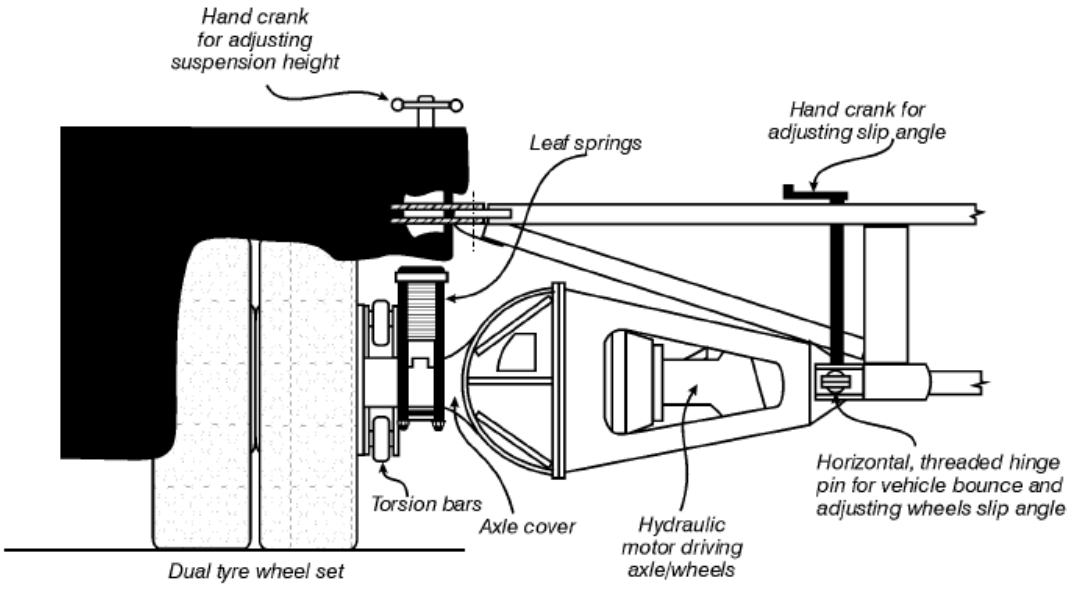

Figure 4.2 Cross-section of one SLAVE Vehicle with Dual Tyres and Multi-leaf Suspension

The SLAVE units are fixed to the outer ends of two diametrically opposed radial arms, attached by hinges to the outer ends of the sliding frame mounted on the central platform (Figure 4.1). The position of the horizontal hydraulic

rams that move the sliding frame, shifting the position of the SLAVE units laterally, is specified to the nearest 1 cm. The wheels of the SLAVE unit are self-driven and simulate tractive forces. The hydraulic output from the main pump, which is located in the centre platform, powers the hydraulic motors driving the wheels. Consequently, travelling speed is regulated by the control of this pump output. The SLAVE control system was designed so that the unit could operate continuously without operator intervention, and if a sensor reported a level outside a preset limit, the control system would bring the SLAVE to a stop. The base elevation of the central pedestal can be altered by up to 150 mm, to maintain the dynamic balance of the machinery located in the centre platform, the sliding frame, and the radial arms when the pavement surface level changes.

Table 4.1 Characteristics of the Simulated Loading and Vehicle Emulator (SLAVE)

Item	Characteristic
Test wheels	Dual- or single-tyres; standard or wide-base; bias or radial ply; tube or tubeless; maximum overall tyre diameter of 1.06 m
Mass of each vehicle	21 kN to 60 kN, in 2.75 kN increments
Suspension	Air bag; multi-leaf steel spring; single or double parabolic
Power drive to wheel	Controlled variable hydraulic power to axle; bi-directional
Transverse movement of wheels	1.0 m centre-to-centre; programmable for any distribution of wheel paths
Speed	0-50 km/h, programmable, accurate to 1 km/h
Radius of travel	9.2 m

4.2.3 **Instrumentation and data-acquisition**

4.2.3.1 CAPTIF beam deflectometer

The CAPTIF beam deflectometer (Figure 4.3) measures the surface deflection bowl of a pavement under the influence of a wheel load in much the same way as a Benkelman Beam, except that the former uses an electro-magnetic gap measuring sensor at the end of the beam to measure the vertical distance between the sensor and a target disc placed on the pavement surface. The

Deflectometer probe is positioned between the tyres of the dual-tyred wheel of the SLAVE unit and, as the wheel is moved away, the rebound of the pavement is measured, to the nearest 0.01 mm, every 50 mm of horizontal movement. A separate, associated device measures the horizontal movement of the wheel.

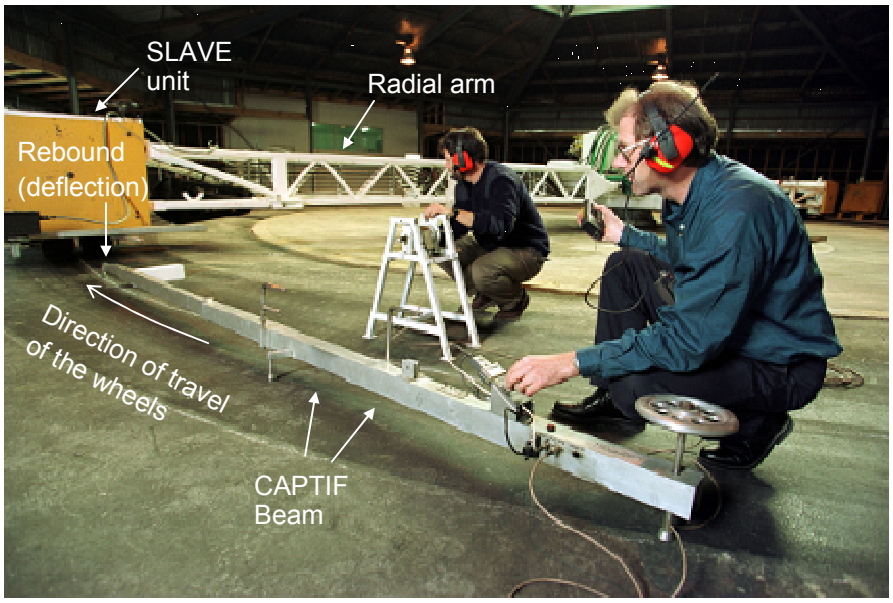

Figure 4.3 CAPTIF beam deflectometer

4.2.3.2 Falling weight deflectometer

The Falling Weight Deflectometer (FWD) simulates the load imposed on a pavement by a moving wheel load by dropping a known mass onto the pavement surface from a selectable drop height. The Dynatest® FWD is a computer-controlled, hydraulically-operated deflectometer towed behind a vehicle. In CAPTIF, the FWD is normally towed by one SLAVE unit during the measurements of surface deflections, see Figure 4.4).

Deflections are recorded using a data acquisition and computing system. The mass drop height is adjustable. The FWD measured the deflection of the pavement directly under and at specific distances from the centre of the dropped load, using a row of geophones affixed to the FWD trailer. During the testing, the geophones were lowered to just rest on the pavement surface.

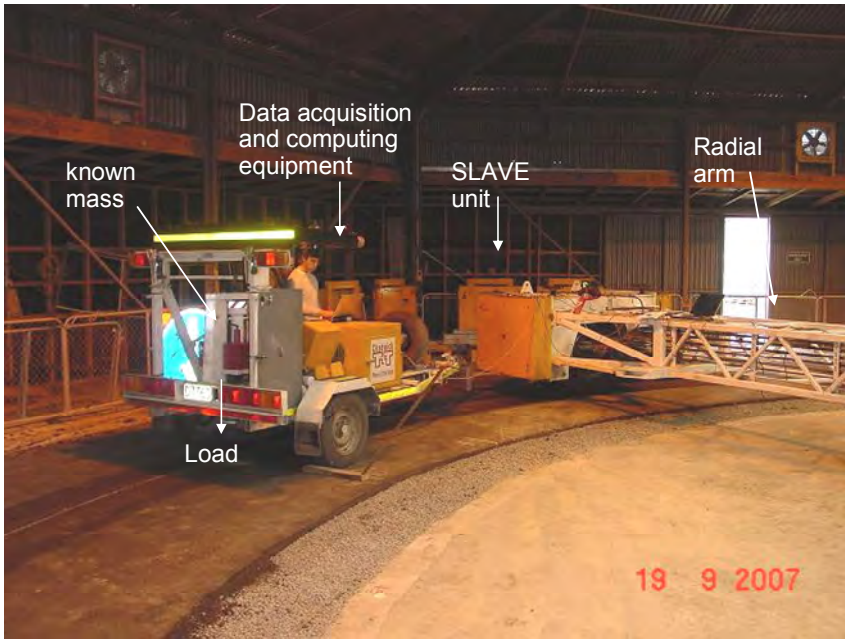

Figure 4.4 FWD deflectometer measurements in CAPTIF pavement

4.2.3.3 PRIMA deflectometer

PRIMA light falling weight deflectometer follows the same principle of the FWD; a mass is dropped over the pavement surface and the deflection is recorded. The main difference with the FWD is that PRIMA is a light, portable device that is normally used to verify the quality of the pavement granular layers in pavement construction. PRIMA can be loaded from 10 to 20 kg drop weight setups, and load plates ranging from 100-mm to 300-mm in diameter can be installed, yielding a dynamic force range from 1 kN to 15 kN applied on the pavement surface. The drop mass is manually lifted by the operator to a maximum drop height of 850 mm. The total weight of the standard equipment is approximately 17 kg. Deflection is measured by a geophone at the centre of the load plate, additional geophones can be located outside the loading plate on the surface of the pavement tested.

4.2.3.4 Scala penetrometer

The Scala Penetrometer or hand cone penetrometer is a portable device used to determine the penetration resistance of a soil. The cone is driven by a 9 kg

mass that falls free from the top of the apparatus. The penetration depth of the cone is read after each blow to the nearest 1 mm. The Scala Penetrometer used in CAPTIF is manufactured in accordance with NZS 4402 Test 6.5.2: 1988, and is a simple and useful tool for profiling soil strength at depth. The penetration provides an empirical relationship with the CBR value, which is included in Appendix E.

4.2.3.5 Surface profiles

Transverse surface profiles are measured using the CAPTIF Profilometer (Figure 4.5). The Profilometer consists of a braced aluminium beam, 4.4 m long, supported at each end by adjustable feet. An aluminium carriage is driven along the beam by an electric motor and drive chain. The carriage holds a Linear Variable Differential Transducer (LVDT) with a jockey wheel riding along the pavement surface. Vertical displacement is recorded every 25 mm of horizontal travel of the carriage. The analog output signals from the position sensor and LVDT are converted to a digital signal by electronics contained within the device, and a Psion hand-held computer captures the digital data (Steven 2005).

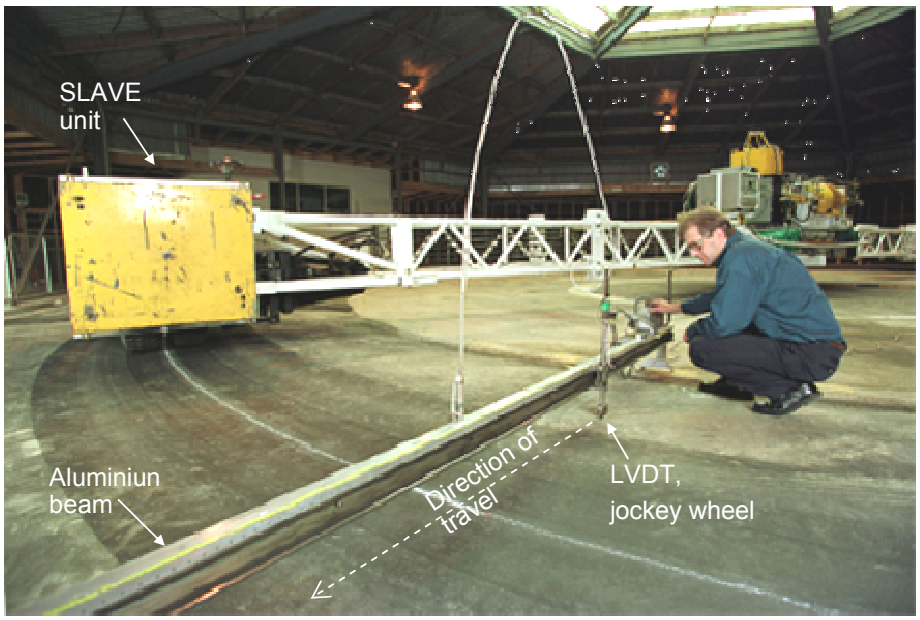

Figure 4.5 CAPTIF profilometer

4.2.3.6 Dynamic pavement strain system

Dynamic pavement strains in both vertical and horizontal directions were measured using the Emu soil strain system (Dawson 1994). The soil strain measuring system determines minute strains (less than 100 μm/m) with good resolution (±50 μm/m) using Bison Coil type strain sensors. The sensors use the principle of inductance coupling between two free-floating, flat, circular wirewound induction coils coated in epoxy, with a diameter of 50 mm. One of the two discs acts as the transmitter coil, creating an electro-magnetic field, which induces a signal in the receiving coil. The magnitude of the induced signal is inversely proportional to the spacing between the two coils. The Emu system determines the change in the induced signal as the coils move relative to each other, and the variation of the signal relative to the initial at-rest signal is available for measuring as a voltage. The initial or "at-rest" voltage is also available for measuring. The operation of the system is shown schematically in Figure 4.6. The gauge length or separation distance between each paired coil is a function of the initial voltage and the change or delta in the gauge length is a function of the varying voltage. Each coil pair is calibrated individually prior to installation and the coil pairs can be either orientated coaxially or co-planar. The coaxial arrangement gives a stronger signal than the co-planar arrangement. The discs are installed during the formation of the subgrade and the overlying layers, to minimise the disturbance to the materials (Steven 2005). More details of the Emu strain system are presented in Appendix F.

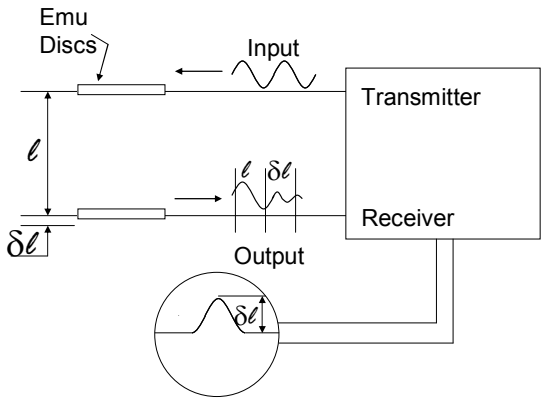

Figure 4.6 Schematic diagram of the Emu system (after Brown 1981)

4.3 Design of the foamed bitumen experiment

4.3.1 **Mix design and materials used**

The Indirect Tensile Strength test (ITS) was used to define the maximum foamed bitumen content for the full scale experiment. The ITS has been used by other researchers to optimize the bitumen content of foamed bitumen mixes in the laboratory (Kim et al. 2007), but ITS results at different bitumen contents have not been compared with field performance. The maximum foamed bitumen content used in the pavement test was 2.8%, which corresponds to the estimated maximum Indirect Tensile Strength value (Section 3.3.1) measured in specimens with 1% cement.

The aggregate used for the construction of the stabilised basecourse layers is a blend of 85% H40 and 15% AP5, by mass, previously described in Section 3.2. The bitumen used in the stabilisation of the pavements is an 80-100 grade bitumen, collected from the same source to that described in Section 3.2. An ordinary Portland cement was also used in the stabilisation of the basecourse.

4.3.2 **Structural design of pavements**

The CAPTIF pavements should satisfy the following requirements:

- The pavement should show 15-20 mm of rutting after approximately $1x10^6$ Equivalent Standard Axles (ESAs, Section 2.1), which is the normal number of load repetitions applied in CAPTIF projects.
- The minimum thickness of the basecourse should be at least 200-mm, for the installation of at least one pair of vertical Emu strain sensors in the basecourse.

Two pavement properties that can be easily modified in CAPTIF experiments, the basecourse thickness and the elastic modulus of the subgrade, were adjusted in the design of pavements, so that the requirements mentioned above are satisfied. In CAPTIF, the pavement thickness is modified by

changing the subgrade level and laying a different basecourse thickness, and the elastic modulus of the subgrade by changing the moisture content and density during construction.

The published pavement design methods for foamed bitumen pavements are the Interim Technical Guidelines for the Design and Use of Foamed Bitumen Treated Materials (Asphalt Academy 2002) and the New Zealand supplement to the AUSTROADS pavement design guidelines (NZ 2007). Limitations have been found in these methods, previously described in Sections 2.2.4 and 2.2.5.2, and therefore the results of the pavement design were taken as an approximation only, instead of an accurate forecast of the pavement performance. Details of the structural design are included in Appendix G.

The pavement structure adopted for the CAPTIF experiment (Figure 4.7) consisted of a 20-mm thin asphalt layer, a 200-mm basecourse placed on a 1300-mm subgrade with an elastic modulus between 60 to 80 MPa. The pavement was designed assuming a 2.8% foamed bitumen and 1.0% cement content. The same thickness and subgrade properties were adopted for all pavement sections. The difference amongst different sections was the foamed bitumen and cement contents used in the construction of the basecourse layer.

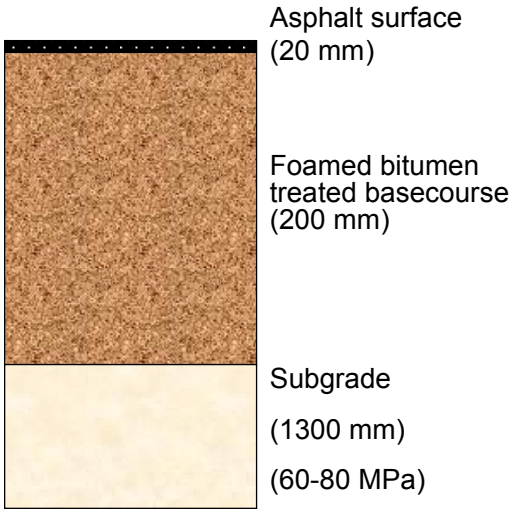

Figure 4.7 Pavement structure adopted in the CAPTIF foamed bitumen experiment

4.3.3 **Layout design**

CAPTIF enables up to six pavement sections of about 10-m length each to be tested (Figure 4.8). Four sections were stabilised using 1% cement at different foamed bitumen contents (0.0%, 1.2%, 1.4% and 2.8%). One section was retained as a control or reference section with the H40 unbound granular material only, and another section had foamed bitumen only (2.2%), to separate the effects of the foamed bitumen mixes with and without cement. At CAPTIF, sections are normally named using alphabet characters (A, B, C), but for clarity in this thesis the sections were named B12C10, B14C10, B28C10, B00C10, B00C00 and B22C00, where the first two digits (after B) indicate the bitumen content and the last two digits (after C) indicate the cement content. For instance, section B14C10 was built adding 1.4% of foamed bitumen and 1.0% cement. Two short transition zones (shaded area in Figure 4.8) were incorporated in order to achieve a better contrast between the sections stabilised with foamed bitumen plus cement and the other three sections. In Figure 4.8, DD and MC indicate the Dry Density and Moisture Content measured in each pavement section using a nuclear gauge, later given in Section 4.4.3. The figure also shows the 58 measurement stations (from 00 to 57) and the location of the Emu soil strain transducers. Details of the pavement sections are also detailed in Table 4.2.

Table 4.2 Detail of the CAPTIF pavement sections

Measurement Stations	ID	Bitumen (%)	Cement (%)	Dry Density (t/m^3)	Moisture Content (%)
57 to 08	B12C10	1.2	1.0	2.021	3.6
08 to 18	B14C10	1.4	1.0	2.012	4.8
18 to 27	B28C10	2.8	1.0	1.976	4.2
27 to 28	Transition	-	-	-	-
28 to 37	B00C10	0.0	1.0	1.971	5.0
37 to 47	B00C00	0.0	0.0	2.060	2.8
47 to 56	B22C00	2.2	0.0	2.016	2.0
56 to 57	Transition	-	-	-	-

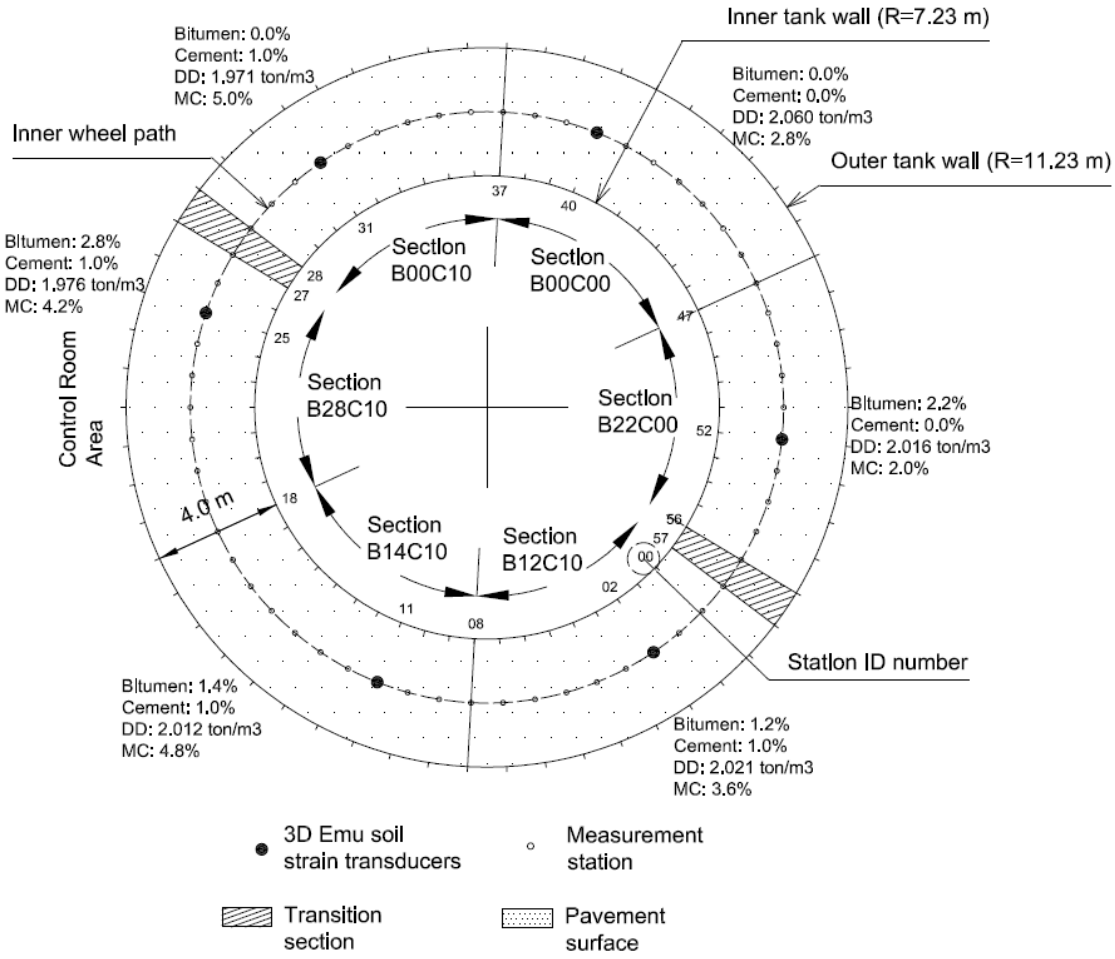

Figure 4.8 Top view of foamed bitumen stabilisation experiment at CAPTIF

4.4 Pavement construction

4.4.1 **Subgrade**

Approximately 775 mm of an existing silty clay subgrade ("Waikari" subgrade) used in previous CAPTIF projects was left undisturbed in the concrete tank wall (Figure 4.9). The CBR of this layer is approximately 20%, estimated using Scala Penetrometer readings (Section 4.2.3.4). The top 525 mm of the subgrade was clay, locally named "Tod" clay, extended in lifts of 225 (Lift 1), 150 (Lift 2) and 150 (Lift 3) mm and compacted using a roller available at CAPTIF. The density and moisture contents of the subgrade were adjusted during construction to achieve a 6% to 8% CBR value, which is equivalent to

an elastic modulus of 60 to 80 MPa, using the following formula (Croney and Croney 1998):

$$E = 10(CBR) \quad \text{(Eq. 4.1)}$$

where E is the elastic modulus of the subgrade, in MPa, and CBR is expressed in percentage. Although this relationship is not particularly reliable, similar relationships for this type of material have been published in pavement design guides (Austroads 2004). The range 60-80 MPa was defined as the target elastic modulus of the subgrade in the structural design of the pavement (Section 4.3.2). The density and moisture contents were verified for each of the three subgrade layers, using a nuclear gauge. The average moisture content and measured dry density was approximately 22% and 1540 kg/m^3. The moisture contents taken by the nuclear gauge were corrected using oven dry samples, extracted from the same location where the nuclear readings were taken.

Once preparation of the three layers was completed, Scala Penetrometer and FWD tests were conducted to evaluate subgrade homogeneity. Scala Penetrometer measurements (Section 4.2.3.4) were taken up to a depth of approximately 500 mm from the subgrade surface, and the penetration rate (penetration depth per blow) was correlated with CBR values using the empirical correlation shown in Appendix E. The Scala penetrometer measurements were taken approximately every two CAPTIF measurement stations (e.g. measurement station 00, 02, 04, 06, etc).

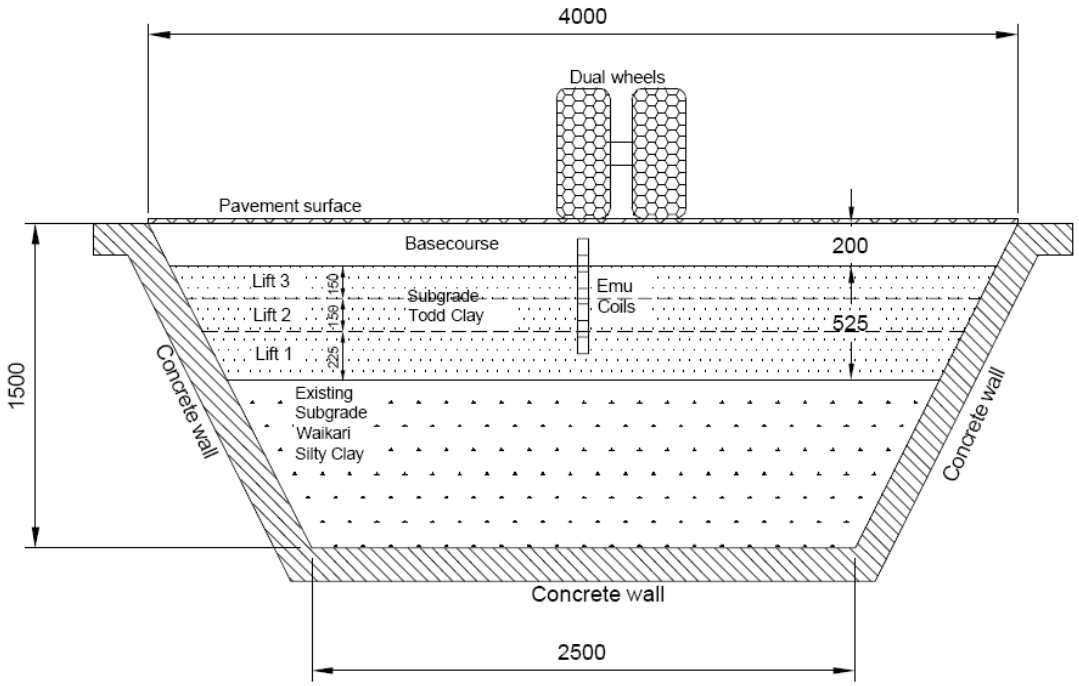

Figure 4.9 Final transverse profile in CAPTIF foamed bitumen experiment

Scala Penetrometer results are summarized in Figure 4.10, in which the average correlated CBRs collected from all the measurement stations are plotted against depth, measured from the subgrade surface. A moving average curve was included in the figure to see the trends more clearly, averaging five consecutive CBR measurements (N=5). The figure shows that the clay subgrade layers are stiffer at the upper level of each lift (i.e. the correlated CBR values at the top of the layer double those at the bottom). A higher density at the top of the layers is commonly observed in pavements, caused by the higher compaction energy applied on the surface of the layer, which decreases with increase in depth. The average correlated CBR value of the subgrade layer was 7.5%, with a standard deviation of 2.1% (Coefficient of Variation = 28.2%).

FWD deflections were taken on the subgrade surface to estimate the elastic modulus homogeneity of the subgrade. A 33-kN load was applied, equivalent to a pressure of 470 kPa on the 150-mm diameter FWD plate. The deflections, plotted versus CAPTIF measurement stations in Figure 4.11, showed an average deflection of 1.510 mm with a standard deviation of 0.177 mm (Coefficient of Variation = 11.7%), which is considered fairly homogenous

for this type of subgrade material. A simple back-calculation analysis yields a subgrade stiffness of 60 MPa approximately, which is in agreement with the target elastic modulus from the structural design of pavements. A moving average curve (average of three measurements, N=3) was included in Figure 4.11 to see the trends better.

4.4.2 **Aggregates**

Two hundred tonnes of H40 aggregates were transported by truck from the North Island of New Zealand, to Christchurch in the South Island. The material was delivered in two loads during the days before construction. The particle size distribution of each load is presented in Figure 4.12. The maximum difference in particle size distribution between the two loads was 4%, at 4.75 mm sieve, with an average difference of 0.83%.

About 30 tonnes of AP5 crusher dust material were imported from a local source in Christchurch. The particle size distribution of the AP5 material is also included in Figure 4.12.

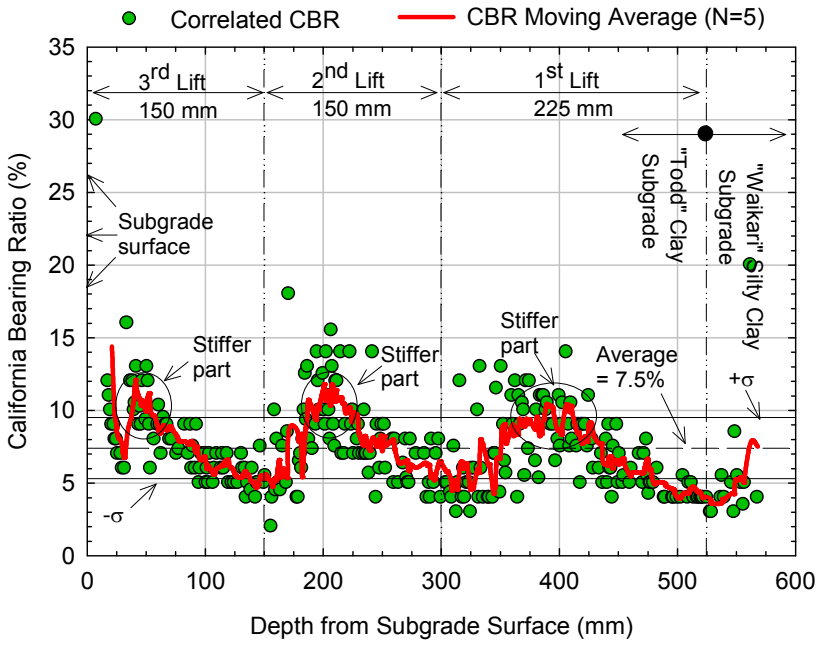

Figure 4.10 Correlated CBR values versus depth from the subgrade surface using Dynamic Cone Penetrometer

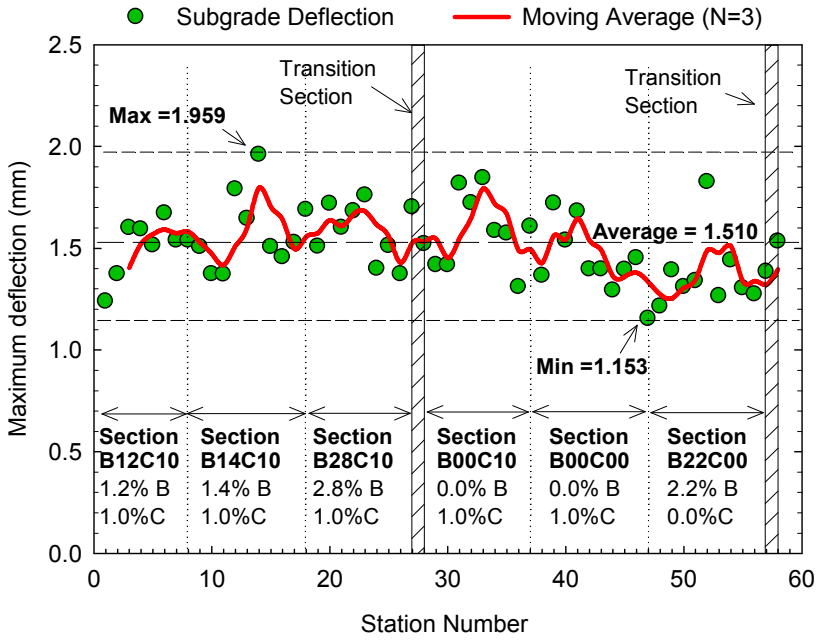

Figure 4.11 Measured Falling Weight Deflectometer deflections applying a pressure of 470 kPa on the surface of the subgrade layer

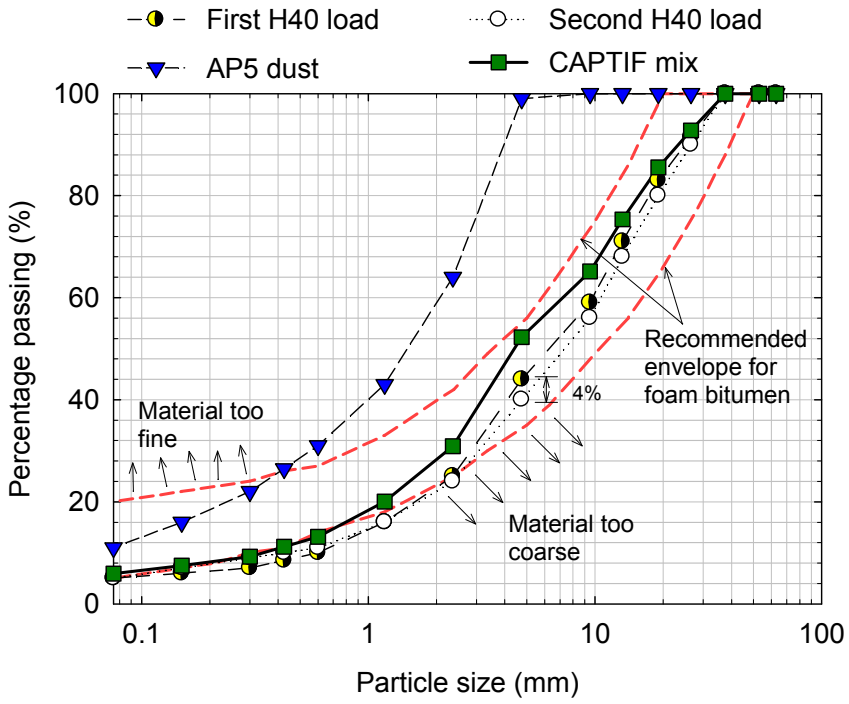

Figure 4.12 Aggregate size of materials used for basecourse construction in CAPTIF

4.4.3 Stabilisation process

The CAPTIF building is relatively small for large road construction machinery and therefore it was not feasible to directly stabilise the materials in place.

Hence, the aggregate was mixed with bitumen and/or cement outside the CAPTIF building using a Wirtgen 2500 SR recycling machine and standard construction equipment (bitumen and water tankers, excavators, loaders and pavers).

For the stabilisation process, 440 mm-deep trenches, approximately 23-m long, were excavated outside the CAPTIF building. The bottom of each trench was levelled using 100 mm of a standard granular material (Figure 4.13a). A 340-mm layer of H40 material was laid in two lifts and compacted to 95% of maximum dry density (2110 kg/m^3), at its optimum moisture content (4.0%). Later, a 70-mm thick layer of AP5 crusher dust was placed on top of the H40 layer, and compacted to 95% maximum dry density (1820 kg/m^3) at optimum moisture content (9.0%). The thickness ratio 70/340 yields approximately the target mass ratio of 15/85 obtained in the laboratory mix design (Section 4.3.1). Once the untreated material was ready, the trenches were stabilised at 410-mm depth with the recycling machine, keeping a constant speed and adding the stabilising agents. It was decided to mix the material twice (two passes of the recycler) to assure a good mixing of the materials.

The first and last 5-m of stabilised material in each trench was discarded to avoid the variability caused by the normal irregular bitumen flow observed when the recycling machine starts the stabilisation process (Figure 4.13b). The stabilised material was transported into the CAPTIF building (located about 50 m from the trenches) by loaders. During this process, material samples were taken for laboratory testing described later in this chapter. A paver was used to place the basecourse material in two layers of 100 mm each, and a steel roller was used for compaction. As the CAPTIF steel roller is lighter than a roller used in normal field construction, the basecourse was compacted in two lifts to account for the lower compaction energy applied. Nevertheless, the same compaction effort was applied to all stabilised pavements. The time between stabilisation and final compaction of the basecourse for one pavement section was between 2 to 3 hours. At the end of the construction of each pavement section, the approximate water content was estimated using a nuclear gauge.

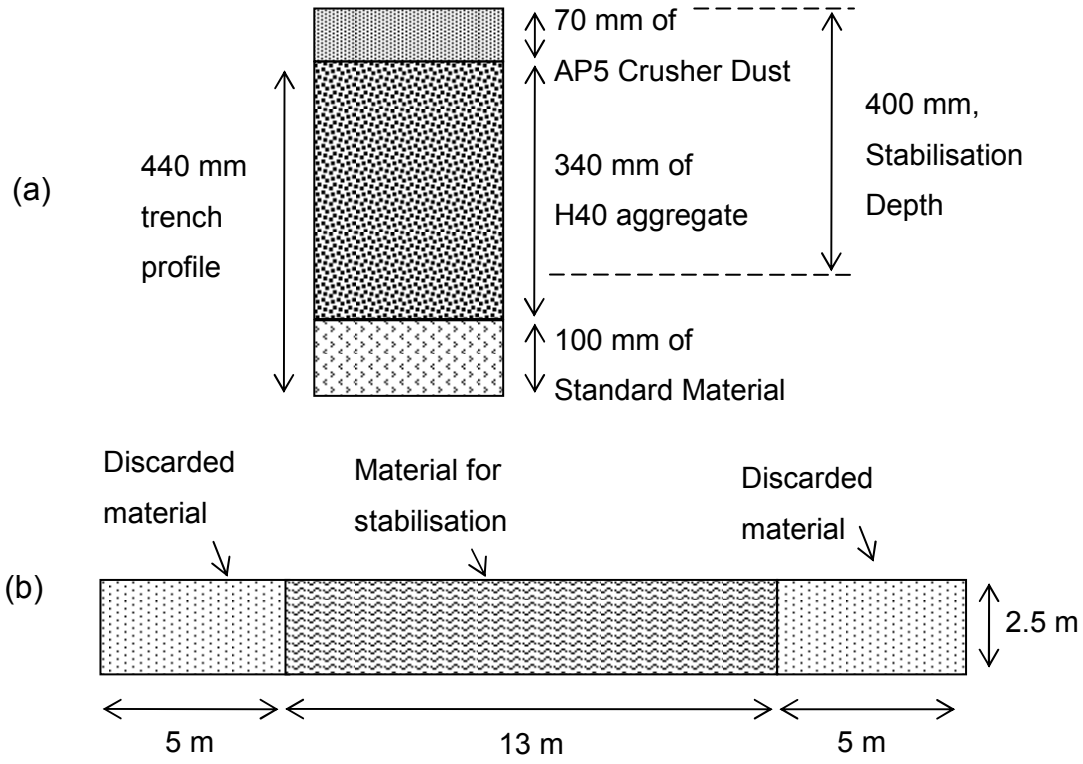

Figure 4.13 (a) Transverse profile of the trench (b) Top view of the trench excavated for stabilization.

The construction of the control unbound granular section (B00C00) was slightly different. Instead of using a mix of aggregate and crusher dust, only the unmodified H40 material was used and laid in a single layer of 200 mm. Hence, the particle size distribution in this section was not exactly the same as the other sections, but the incorporation of the AP5 crusher dust was part of the stabilisation process. A set of pictures of CAPTIF construction is included in Appendix H.

Before laying the final surface layer, the sections were cured at ambient temperature for 30 days. The average temperature measured in the basecourse layer during this period, using temperature sensors installed in sections B00C10 and B22C00, was 17.8 °C (Standard Deviation = 1.69 °C) with a minimum and maximum of 11 °C and 22.2 °C respectively, similar to that used in the laboratory study (20 °C, Sections 3.2.3.5 and 4.5). During this 30 days period, PRIMA light falling weight deflectometer readings (Section

4.2.3.3) were collected to estimate the normal reduction in deflections caused by moisture loss. Three PRIMA drops of 10 Kg were applied on each pavement station at 2, 6, 8, 13, 20 and 30 days after construction. The average results are presented in Figure 4.15. Results showed an approximately 50% reduction of deflections during the first week after construction, followed by a plateau after two weeks after construction, where almost no variation was observed. These trends suggest that decrease in deflections was mainly caused by moisture loss of the basecourse layer, instead of the reaction of 1% cement added to the mixes, because the reduction in deflections was also observed in the sections without cement. The highest reduction was measured in section B00C00 (initial and final deflections of 0.46 and 0.14 mm) and section B22C00 (initial and final deflections of 0.36 and 0.09 mm).

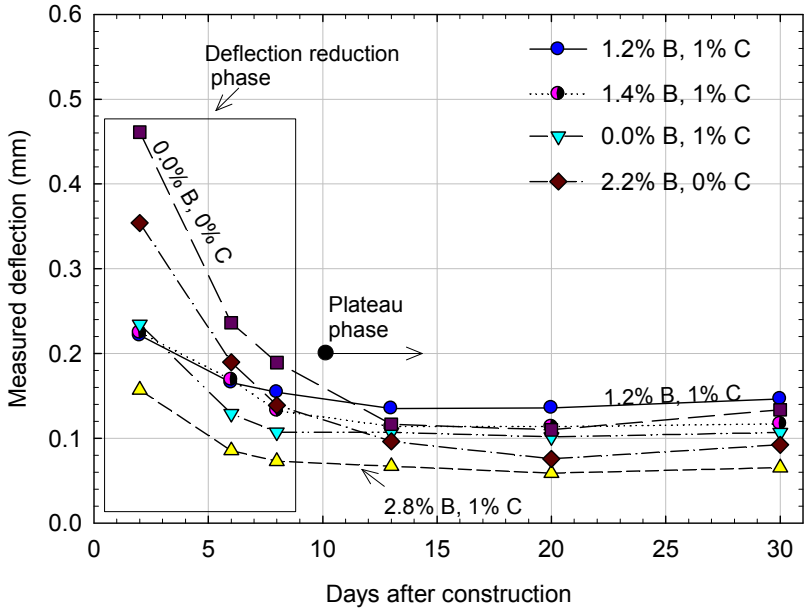

Figure 4.14 Average deflections using PRIMA light falling weight deflectometer after pavement construction.

Before placing the asphalt surface on the basecourse, moisture contents and dry densities of the basecourse were estimated using a nuclear gauge (Figure 4.15 and Figure 4.16, respectively). The first observation of the moisture content measurements is that the moisture content of each section before sealing was lower than the moisture content during construction, confirming a moisture loss during the curing period. The second observation is that

moisture loss was approximately constant for all sections with 1% cement (between 2% to 2.5%) but slightly higher for sections B00C00 and B22C00 (approximately 3%), which explains the higher reduction in deflections observed in these two sections (Figure 4.14). The figure also shows that the absolute moisture contents measured in sections B00C00 and B22C00 were 2% lower than sections with cement, because these sections were prepared with lower water content during construction.

The estimated dry densities from the nuclear gauge measurements are presented in Figure 4.16. It is important to notice that nuclear gauge measurements for moisture contents are not totally realiable, since the nuclear gauge could pick the moisture of the subgrade layer. The dry density of the stabilised sections varied from 1970 kg/m^3 (section B00C10) to 2020 kg/m^3 (section B22C00). The highest dry density was measured in the untreated section B00C00 (2060 kg/m^3), indicating that the stabilisation process reduced the dry density of the material. Similar density trends have been reported by Long and Ventura (2004) in laboratory specimens for Unconfined Compressive Strength and Indirect Tensile Strength tests. Nevertheless, the densities of the stabilised layer were fairly similar, with a variation of 50 kg/m^3 between B22C00 and B00C10 (2.5%).

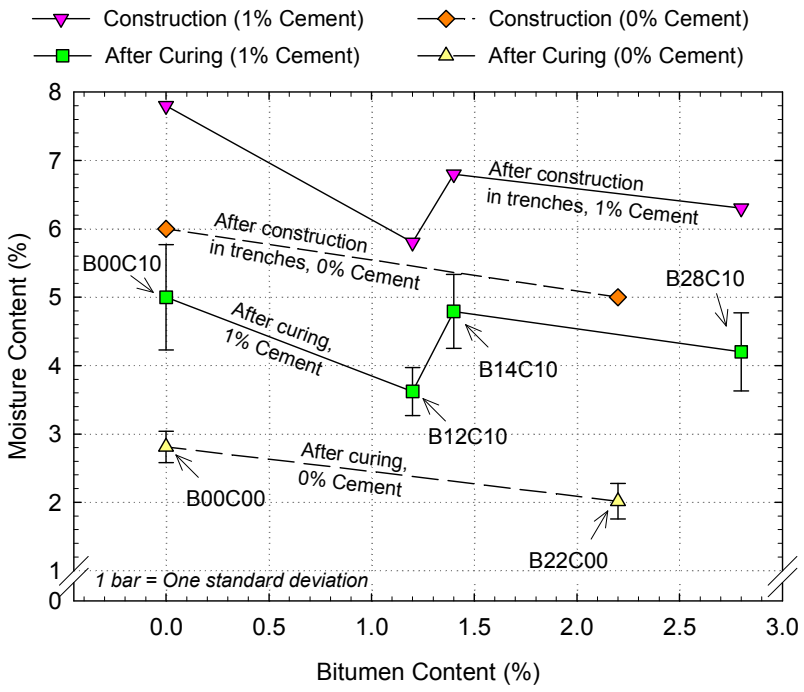

Figure 4.15 Moisture contents after construction and curing

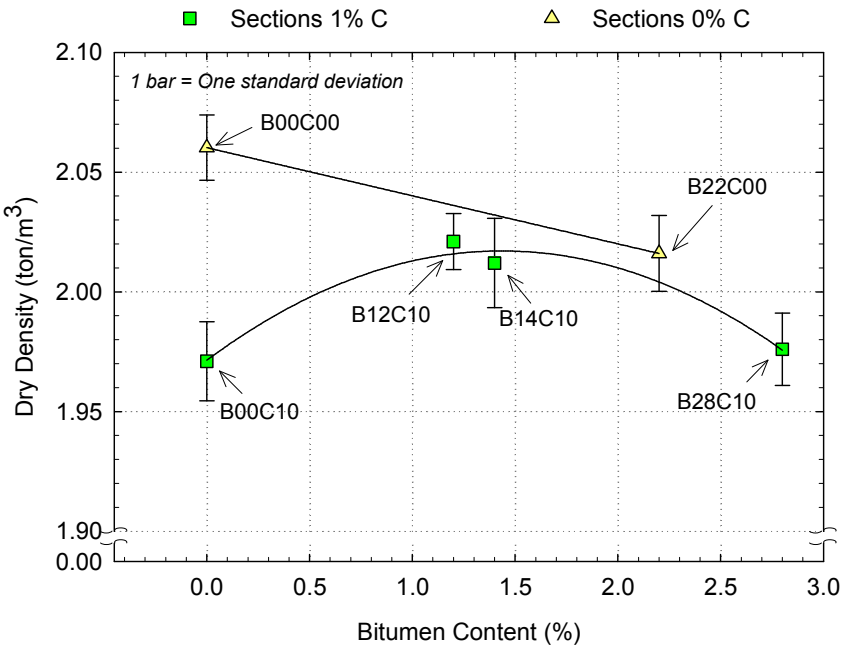

Figure 4.16 Dry densities measured after curing

The curing time between the construction of the basecourse and the commencement of trafficking was approximately three months.

4.4.4 **Surface layers**

The surfacing was constructed 30 days after construction of the basecourse layers. All sections were sealed with a single coat chipseal. After a week to allow the chipseal to set up, all sections were surfaced with a skim coat of AC10 Asphalt Concrete hot mix covering the top of the chipseal. The approximate thickness of this surface was 20 mm.

During the execution of the experiment and after the application of 200,000 load cycles, the original thin surface started to show wearing. A thin Hot Mix Asphalt (HMA) layer of 30 mm was laid over the original surface, equating to a total surface thickness of approximately 50 mm for the rest of the experiment. The curing time between the construction of the overlay and trafficking was 6 days.

A transverse profile of the final pavement structure, the placement of the wheels, the location of the coil instrumentation and the concrete tank are shown in Figure 4.9.

4.4.5 **Strain instrumentation**

The Emu strain coils were installed in each pavement section in 3D stacks, which is an arrangement of 18 coils that measures strains in vertical, longitudinal and transverse directions. The strain coils were located coaxially at a spacing of 75 mm, directly under the inner wheel. The reported depth of the vertical strains corresponds to the midpoint between two coils, while the reported depth of the longitudinal and transverse strains corresponds to the coil depth. The 3D Emu stacks were located at stations 2, 11, 25, 31, 40 and 52 (Figure 4.8). Details of the instrumentation are presented in Figure 4.17.

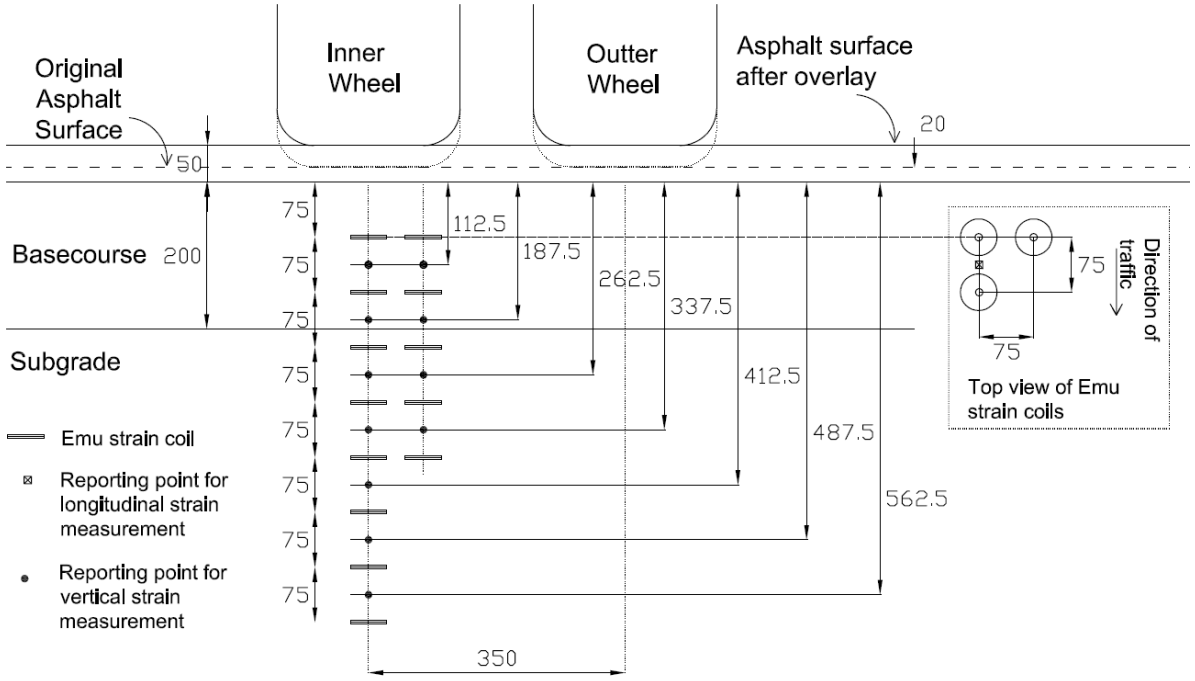

Figure 4.17 Emu strain coil instrumentation in CAPTIF foamed bitumen experiment

4.5 Laboratory testing of CAPTIF materials

4.5.1 **Sampling and specimen preparation**

4.5.1.1 Basecourse materials

During the construction of the basecourse layers, material samples were taken for indirect tensile strength tests (ITS) and repeated load triaxial tests (RLT). The samples, of approximately 80 kg each, were collected immediately

after stabilisation, from at least three different locations of the construction trenches, and placed in sealed, labelled plastic bags. The samples were delivered to the laboratory about 1 hour after construction for the preparation of RLT and ITS specimens.

The temperature of the stabilised materials with foamed bitumen after construction was approximately 30°C, measured in the construction trenches with an infrared thermometer available in CAPTIF. To reproduce field conditions during laboratory compaction, the sealed bags with the mix samples were kept in the oven of the laboratory at 30°C before compaction. The material sample from section B00C10 was kept at room temperature (20° C) before compaction, and the aggregates from the unbound granular section (B00C00) were collected from one of the H40 stockpiles in CAPTIF.

Before compaction, the aggregate particles larger than 26.5 mm were discarded from the samples to assure that the largest particles did not exceed one quarter of the mould diameter (150 mm) and to be consistent with the previous laboratory work presented in Chapter 3. The laboratory compaction of the stabilised materials was finished during the same day of collection of the sample.

The ITS specimens with dimensions of 150-mm diameter and 100-mm height were prepared using vibratory compaction, described in Section 3.2.3. The samples were cured for two weeks at a room temperature (20° C). This curing period was determined using the results presented in Section 3.2.3.5. Only samples with foamed bitumen were prepared for ITS testing (i.e. from sections B12C10, B14C10, B28C10 and B22C00). The large triaxial specimens (150-mm in diameter and approximately 300-mm in height) were also prepared using vibratory compaction. The samples were cured for 28 days at room temperature (20° C) in double sealed plastic bags. Details of the compaction of these specimens are shown in Appendix C (Section C.8).

4.5.1.2 Subgrade

The resilient modulus of the clay subgrade was measured in the laboratory. A subgrade sample was collected for RLT resilient modulus test, from one of the subgrade stockpiles located at CAPTIF, used in the preparation of the top 525 mm subgrade layer. The large triaxial specimen (150 mm x 300 mm) was prepared applying vibratory compaction in six layers of approximately 48-50 mm each, following the compaction procedure presented in Section 3.2.3 for triaxial specimens. The compaction time and moisture content were adjusted to achieve density and moisture conditions similar to those of the reported during subgrade construction. The moisture content of the subgrade triaxial specimen was 15% with a dry density of 1491 kg/m^3, while the average moisture content and dry density measured in the subgrade was approximately 22% and 1538 kg/m^3 (Section 4.4.1).

4.5.2 **Specimen properties**

4.5.2.1 Dry densities

The dry density of the laboratory specimens (both ITS and RLT) was calculated as the ratio between the total dry mass and the volume, estimated using the specimen height and compaction mould diameter (150 mm). This means that the volume has been overestimated and the dry density underestimated. The dry densities of the laboratory specimens are presented in Figure 4.18.

The field dry densities, obtained after pavement curing and previously presented in Figure 4.16, are also included for comparison. The figure indicates that laboratory dry densities measured in triaxial specimens follow the trend obtained from field measurements, depicted by similar curves. The Figure also shows that the dry density of triaxial specimens was higher than field densities for most of the specimens, suggesting that the vibratory compaction effort applied in the laboratory was higher than that the applied by the steel roller in CAPTIF.

The dry densities measured in ITS specimens were approximately 150 kg/m^3 (10%) higher than those of triaxial samples, even though the same vibratory compaction method was applied in both cases. This is explained by the higher energy compaction applied on ITS specimens, which were compacted in two layers of approximately 38-40 mm thickness (Section 3.2.3), which are thinner than the six 48-50 mm thick layers of the triaxial specimens. In other words, in ITS specimens, the same compaction effort was applied to a smaller mass of material, yielding an approximately 15% higher compaction energy per mass unit.

The dry densities obtained in ITS specimens during the laboratory study (Chapter 3) were also included in the figure for comparison, showing that dry densities obtained from laboratory mixed materials follow the same trend to that of CAPTIF mixed materials.

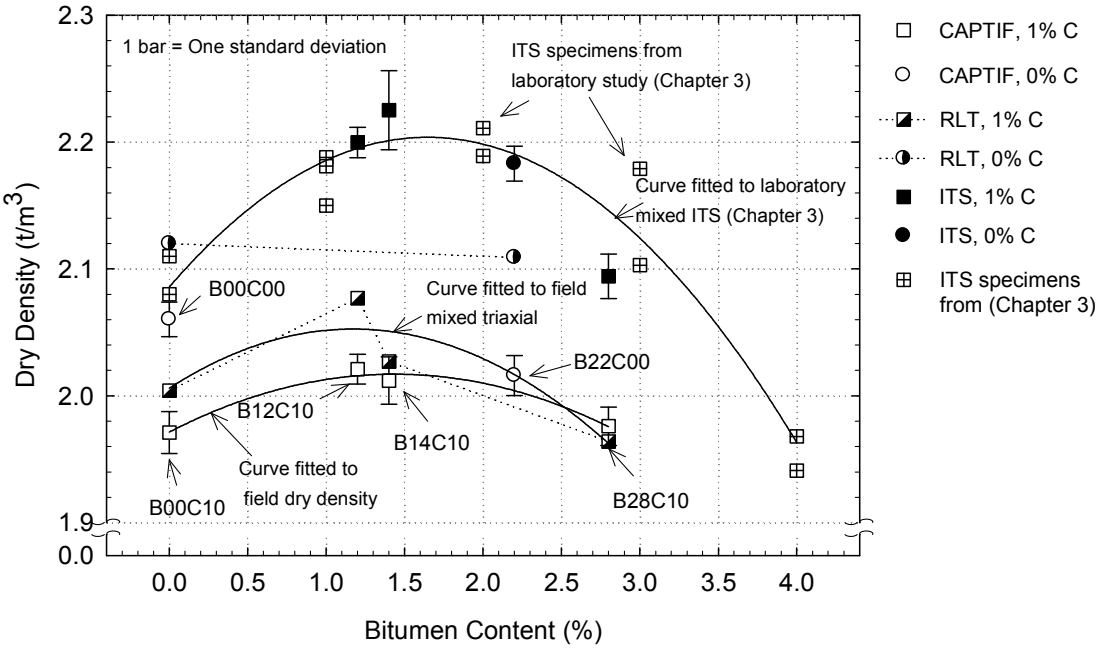

Figure 4.18 Dry densities measured in laboratory specimens and the field

4.5.3 **Test methods**

The ITS specimens were tested in a constant displacement loading machine at a rate of 50.8 mm/min as described in Section 3.3.1.

Permanent deformation tests (Section 3.3.4) were conducted on triaxial specimens. Details of the triaxial equipment were provided in Chapter 3. The stress sequence and testing procedure applied in the test follows the New Zealand standard for triaxial testing (Transit 2007), which is a test recently developed by Transit New Zealand for triaxial testing of basecourse materials. The test was conducted under drained conditions, which is a different condition to that of Chapter 3, and the loading was applied in six stress stages, where the first is a pre-conditioning stress stage. Each stress stage consists of 50,000 Haversine load cycles of 250 mSec. Figure 4.19 depicts the confining and deviator stresses applied at each stress stage. Only one specimen per pavement section was prepared and tested at room temperature (20 °C).

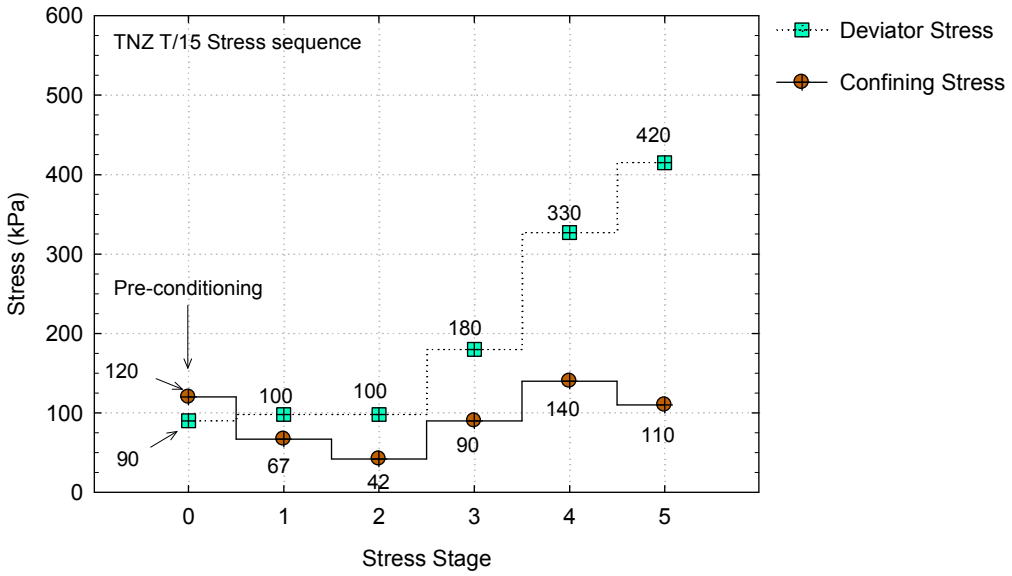

Figure 4.19 Load stress sequence followed by the TNZ T/15 standard for the triaxial testing of granular materials

The resilient modulus test conducted on the subgrade specimen followed the SHRP (Strategic Highway Research Program) protocol for determination of the resilient modulus of basecourse and subgrade soils (SHRP 1992). The SHRP protocol was preferred over the European Standard (Standarization 2003), previously described in Section 3.3.5, because SHRP contains a stress sequence specifically developed for testing of subgrade materials. The stress sequence provided by SHRP protocol consists of a preconditioning stage (500

to 1,000 cycles), followed by a stress sequence of 15 stages of 100 load cycles each. The loading stress sequence for this test is shown in Table 4.3. One load cycle consists of a 0.1 second load followed by a 0.9 second rest period.

Table 4.3 Stress sequence followed by SHRP resilient modulus test

Stage N°	σ_c (kPa)	σ_d (kPa)	Stage N°	σ_c (kPa)	σ_d (kPa)	Stage N°	σ_c (kPa)	σ_d (kPa)
1	41.4	14.9	6	27.6	14.9	11	13.8	14.9
2	41.4	28.1	7	27.6	28.1	12	13.8	28.1
3	41.4	41.7	8	27.6	41.7	13	13.8	41.7
4	41.4	55.1	9	27.6	55.1	14	13.8	55.1
5	41.4	68.7	10	27.6	68.7	15	13.8	68.7

4.5.4 **Results**

4.5.4.1 Indirect tensile strength tests

The laboratory ITS results (Figure 4.20) show an increase in strength with increase in bitumen content (approximately 96 kPa for each 1% of foamed bitumen added) for the materials constructed with foamed bitumen and 1% cement. The material from section B28C10 has almost double the strength of sections B12C10 and B14C10, indicating that the basecourse material placed in section B28C10 was stronger than the other two sections. The ITS values from section B22C00 were about one third of the ITS values measured in samples with 1% cement, indicating that 1% cement significantly increases the indirect tensile strength of the material. The variability of the results was measured using the coefficient of variation value included in Figure 4.20. Usually a maximum coefficient of variation of 25-30% is allowed in ITS testing of foamed bitumen mixes (Asphalt Academy 2002), but this value was comparatively low for the CAPTIF specimens with foamed bitumen and cement (maximum of 11.6%), indicating that field mixing, sampling and laboratory compaction were consistently conducted.

The results from the field mixed specimens were compared with the results from the preliminary laboratory mix design presented in Section 3.3.1, plotted together in Figure 4.21. The Figure indicates that ITS values obtained from reconstituted specimens in the laboratory had similar strength to those prepared using field mixes. The moisture contents of the field specimens were also included in Figure 4.21. The field moisure contents were slightly lower than the laboratory prepared specimens (moisture content=4.8% approximately).

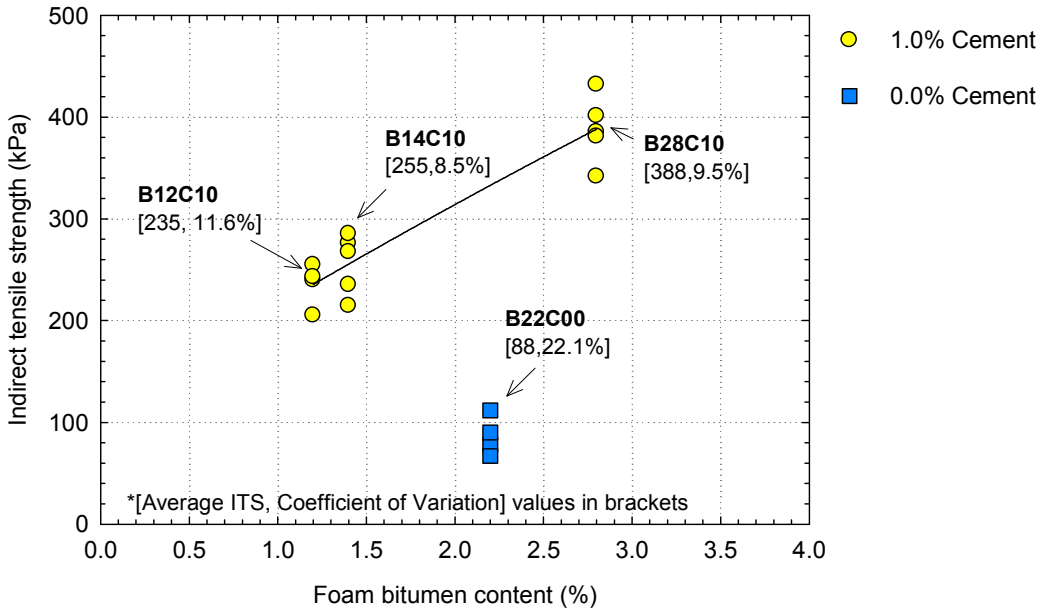

Figure 4.20 Results of the Indirect Tensile Strength (ITS) tests on field mixed materials

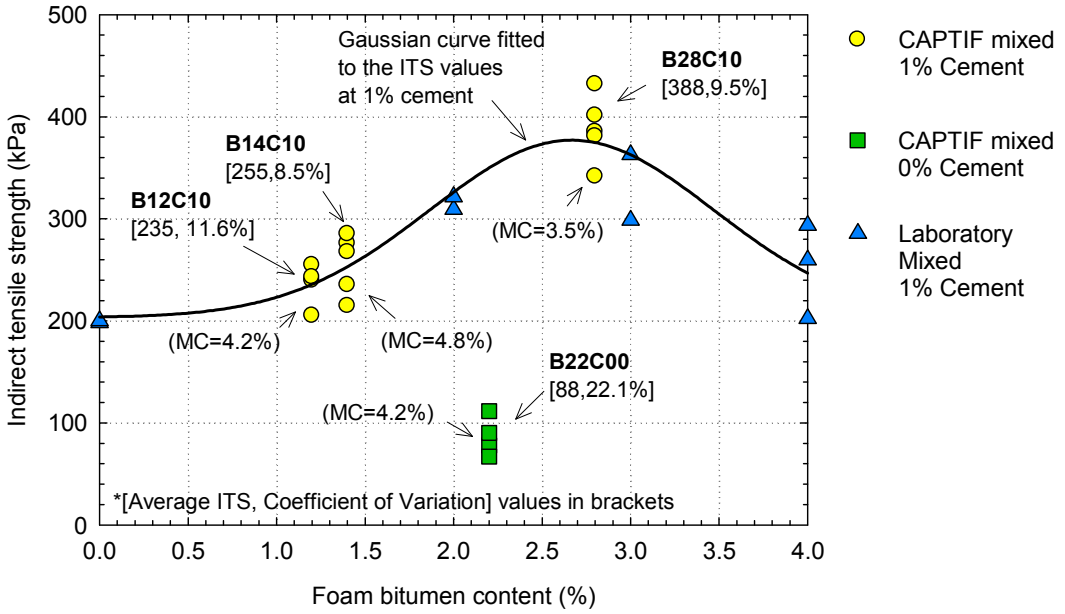

Figure 4.21 Comparison between (CAPTIF) field mixed and laboratory mixed ITS values for foamed bitumen mixes with 1% cement

4.5.4.2 Permanent deformation triaxial tests on basecourse materials

The permanent deformation measured on field-mixed materials versus the number of load cycles from each stress stage, is presented in Figure 4.22. The shape of the curves follows the common behaviour of cyclic triaxial tests, with an accelerated deformation rate phase during the initial loading, due to accumulation of irrecoverable deformation, followed by a plateau phase, in which predominantly elastic deformation is measured.

The specimens from sections B00C00 and B2200 failed in Stage 3 and 5 respectively, while all the samples at 1% cement performed well, throughout all the stages. Of the specimens at 1% cement, the measured total permanent strain increases from approximately 1.5×10^3 μm to 2.4×10^3 μm with increasing foamed bitumen content (from 0% to 2.8%) indicating that, under triaxial cyclic load conditions, the introduction of foamed bitumen reduces the permanent strain resistance of the mix (Figure 4.22), which is identical with the trend observed in tests on laboratory mixes presented in Chapter 3.

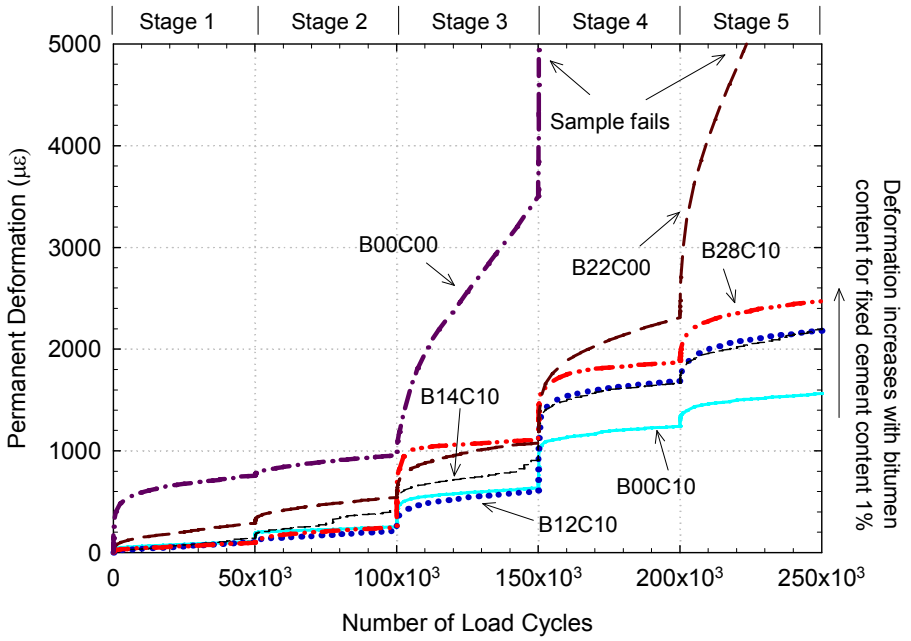

Figure 4.22 Detailed results of the permanent deformation Repeat Load Triaxial (RLT) tests on field mixed materials

The average resilient modulus from all the stress stages (1, 2, 3, 4 and 5 for specimens at 1% cement; and 1, 2, 3 and 4 for specimens without cement) is plotted against the foamed bitumen content in Figure 4.23. The average resilient moduli for mixes with 1% cement were approximately double of those for mixes without cement (432 MPa versus 197 MPa, see Figure 4.23). Comparatively, foamed bitumen has a less significant effect on the resilient modulus than cement, with minimum and maximum values measured at foamed bitumen contents of 0% (368 MPa) and 1.4% (508 MPa). The results are consistent with those from the cyclic permanent strain triaxial tests (Section 3.3.4), presented in the laboratory study, in which the average resilient modulus for mixes without cement was 205 MPa, while the modulus measured in mixes with 1% cement and 0, 2 and 4% foamed bitumen was approximately 320, 380 and 385 MPa, respectively.

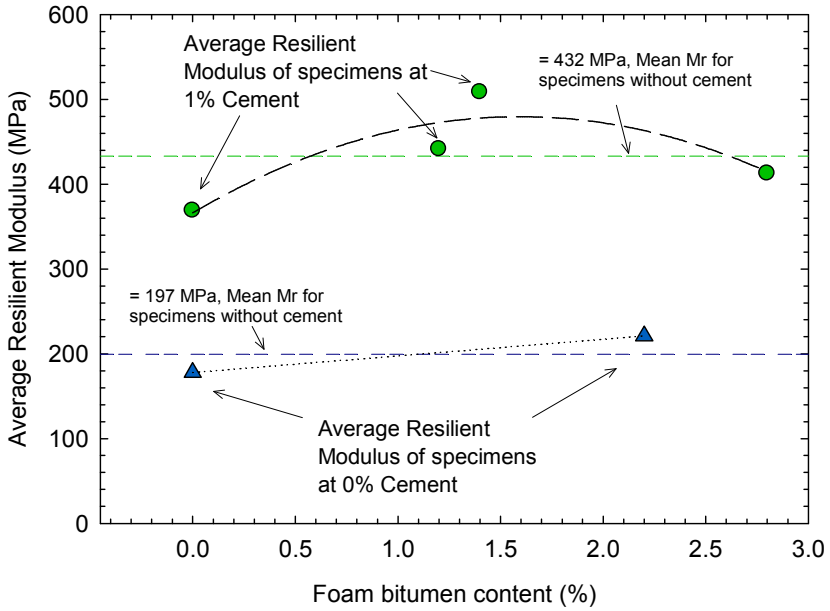

Figure 4.23 Resilient modulus measured in RLT tests

The average compressive vertical strains collected during the RLT tests are plotted against the bitumen content in Figure 4.24. This figure is similar to the resilient moduli measurements presented in Figure 4.23, because the resilient modulus is the ratio between the applied deviator stress (σ_d) and the recoverable axial strain (ε_r), as previously presented in Chapter 2:

$$M_R = \frac{\sigma_d}{\varepsilon_r} \qquad \text{(Eq. 2.9)}$$

The resilient strain measurements will be later discussed in Section 4.8.

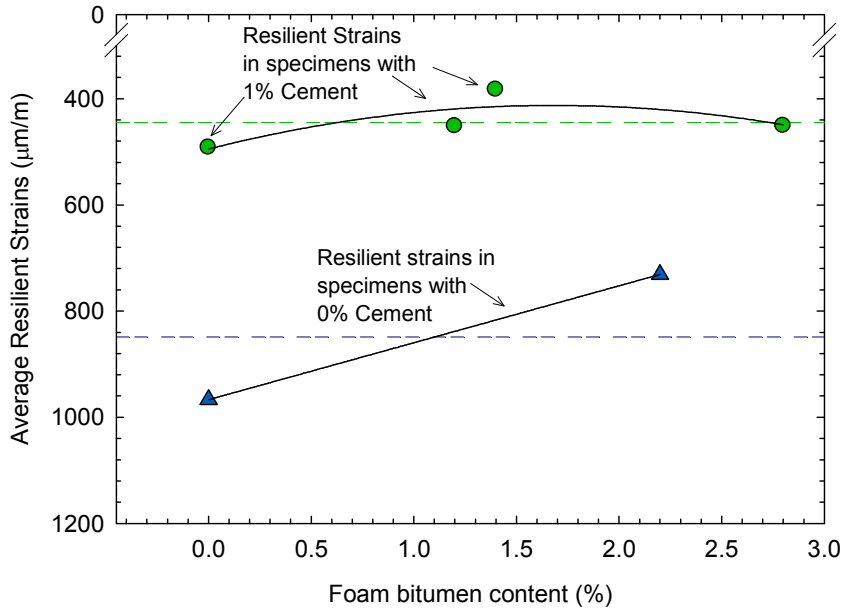

Figure 4.24 Resilient strains measured in RLT tests

4.5.4.3 Resilient modulus triaxial test on subgrade

The resilient moduli measured in the subgrade specimen are presented in Figure 4.25. The results show that the effect of deviator stress dominates the resilient modulus of the subgrade. For instance, a change in confining stress from 13.8 kPa to 41.4 kPa (Δ=27.6 kPa) yields a resilient modulus increase of approximately 20%, while the same variation in deviator stress (from 13.8 to 41.4 kPa, Δ=27.6 kPa) yields a resilient modulus reduction of approximately 100%. This is the typical behaviour of a clay material, where the increase in deviator stress decreases resilient modulus (Huang 2004). The minimum resilient moduli fluctuated between 29 and 33 MPa (for a deviator stress σ_d = 68.7 kPa), and the maximum between 80 and 93 MPa (for a deviator stress σ_d = 14.9 kPa).

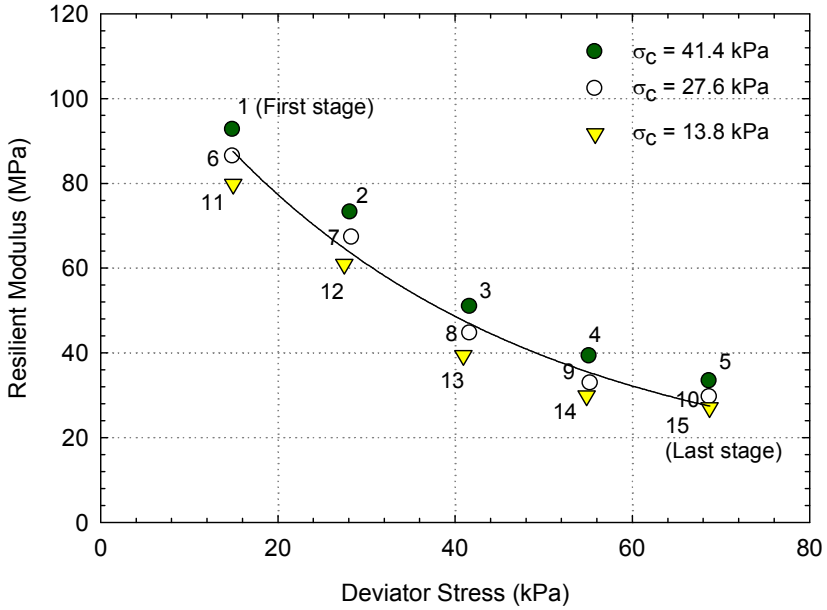

Figure 4.25 Subgrade resilient modulus versus deviator stress measured at different confining pressure

4.6 Pavement tests

4.6.1 **Loading sequence and speed**

The load was a dual truck tyre with a separation of 350 mm between the centres of the tyres inflated to 700 kPa. The original loading sequence intended that a constant loading of 40 kN, which is equivalent to 1 ESA, would be applied 1,000,000 times. It was expected to see approximately 15-20 mm of rutting after the application of 1,000,000 load repetitions, according to the predicted performance of pavements calculated in Section 4.3.2. However, a rutting depth of less than 2 mm was measured in the stabilised pavements at the early stage of the experiment (50,000 load cycles), which remained constant up to 150,000 load cycles. Since more pavement deterioration was expected throughout the project, the load was increased to 50 kN at 150,000 load cycles and to 60 kN at 502,000 load cycles (Figure 4.26).

The speed of the vehicles remained initially constant at 40 kph, but when the SLAVE units were loaded with 60 kN the speed was reduced to 30 kph to

avoid an excessive bouncing of the vehicles. The load was applied on one wheel path with a lateral wandering of 100 mm.

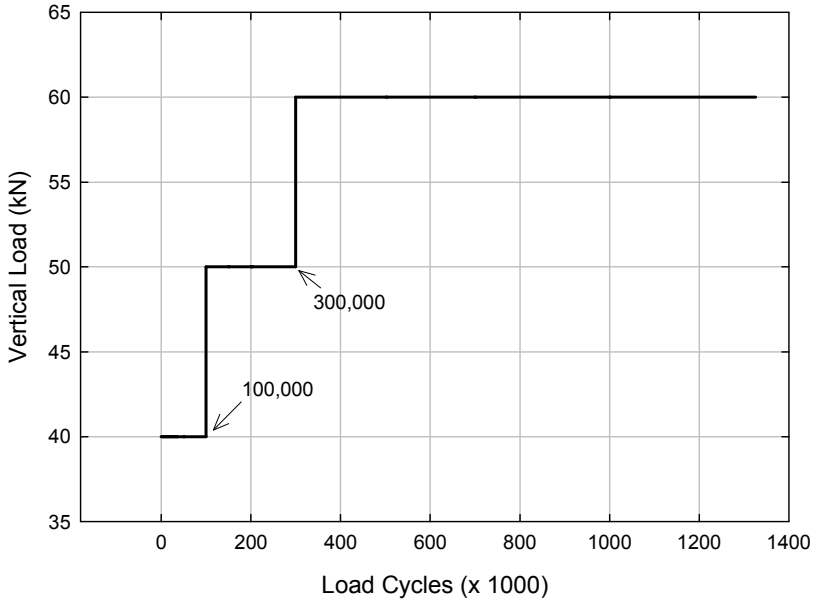

Figure 4.26 Load sequence followed during pavement testing

4.6.2 **Surface transverse profiles and rutting**

4.6.2.1 Data collection

The vertical surface deformations were taken at each of the 58 test-track measurement stations using the CAPTIF profilometer (Section 4.2.3.5), at several stages of the project. The rutting is calculated as the maximum vertical difference between the current (trafficked) level and the initial reference level of the pavement (Figure 4.27). The rutting value reported for each pavement section is the average of the individual rut depths measured in each measurement station, discarding the measurement stations located in the interface of the sections (8, 18, 37 and 47) and the transition sections (stations 27 to 28 and 56 to 57). For instance, the reported rutting for section B28C10 is the average of the eight rut depths measured from station 19 to 26 (see Figure 4.8).

A new, flat 30-mm Hot Mix Asphalt (HMA) pavement surface was placed after 200,000 load cycles, on the original, deteriorated 20-mm thick asphalt surface,

modifying the levels of the pavement (Section 4.4.4). The additional layer also decreased the pavement strains (about 30% in the basecourse and 20% at the top of the subgrade). For the accumulated rutting calculations, the rutting measured after the construction of the HMA surface (after 202,000 load cycles) was added to the previous rutting measurement at 200,000 load cycles.

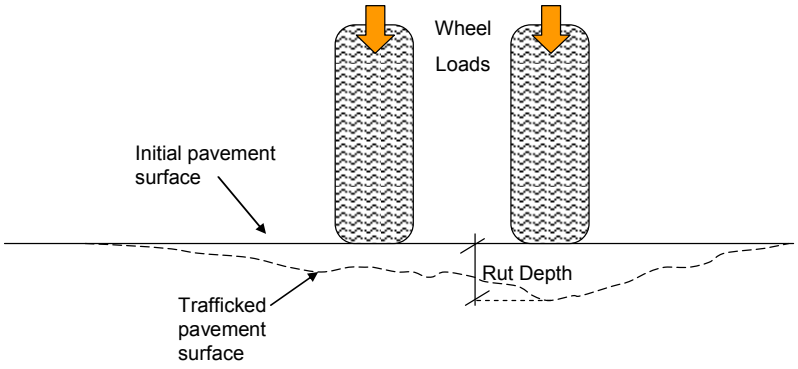

Figure 4.27 Calculation of the rut depth

4.6.2.2 Surface transverse profiles

Figure 4.28 depicts the surface deformation transverse profile for section B28C10, measured using CAPTIF Profilometer (Section 4.2.3.5). The surface profiles of the other stabilised sections with foamed bitumen and cement (B12C10 and B14C10) were similar to that of B28C10, and were included in Appendix I. The figure shows that after 200,000 load cycles the surface deformation was approximately 2 mm in both wheel paths. At 200,000 load cycles the Hot Mix Asphalt overlay was placed on the original surface, adding approximately 30 mm to the surface level. At 1,000,000 load cycles, the surface showed additional rutting increase with higher vertical deformation at the outer wheel path (3 mm versus 2 mm measured under the inner wheel load). The final surface profile in section B28C10, after 1,326,000 load cycles, showed 3 mm of heaving near the outer wheel path, with higher vertical deformation under the outer wheel path (6 mm) than the inner wheel path (3 mm).

Figure 4.29 shows the transverse surface profile for section B00C10, which started to show higher deformations than section B28C10 at 200,000 load cycles (3 mm, versus 2 mm, under the outer wheel path). After the HMA overlay, at 1,000,000 load cycles, B00C10 pavement showed approximately 3 mm of heaving in the area near the outer wheel path. In the last surface profile measurement (1,326,000 load cycles), a large amount of heaving (18 mm) and vertical surface deformation (11 mm) was observed under the outer wheel path, depicted in Figure 4.29, while the surface close to the inner wheel path was performing relatively well (4 mm of deformation). Sections B00C00 and B22C00 showed similar behaviour to that of section B00C10. A summary of the measured surface deformations and heaving is presented in Table 4.4. The transverse surface profiles from sections B12C10, B14C10, B00C00 and B22C00 are given in Appendix I.

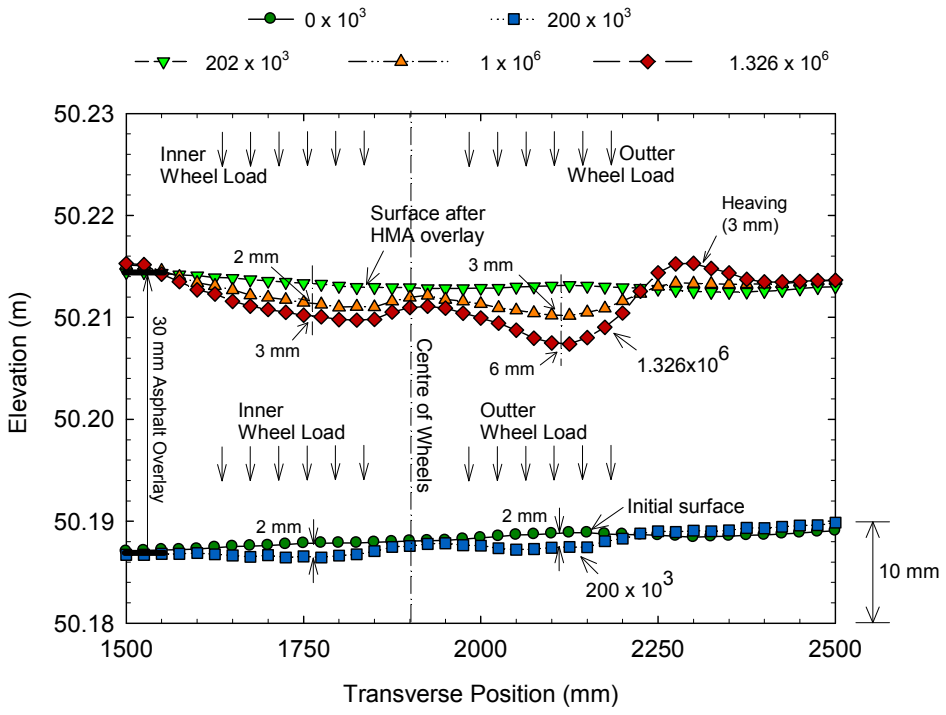

Figure 4.28 Surface deformation measured at Section B28C10

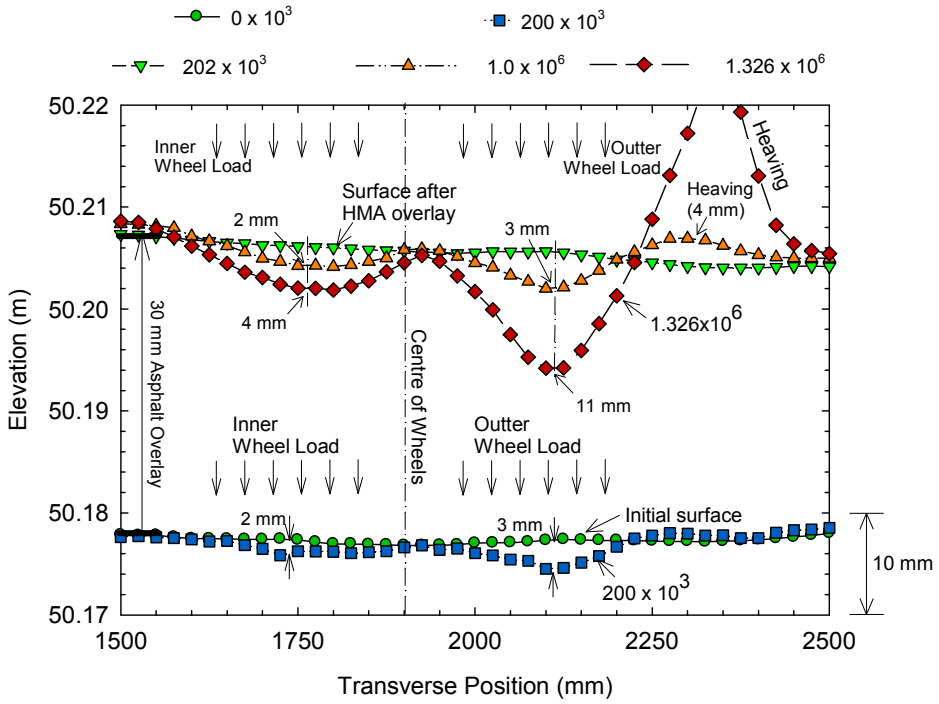

Figure 4.29 Surface deformation measured at Section B00C10

Table 4.4 Summary of surface deformation and heaving

			Surface deformation under outer wheel (in mm) path/heaving at Nc cycles:		
Section	Bitumen (%)	Cement (%)	200 x 10^3	1 x 10^6	1.326 x 10^6
B00C10	0.0	1.0	3/0	6/4	14/18
B12C10	1.2	1.0	2/0	6/0	7/3
B14C10	1.4	1.0	2/0	6/0	7/3
B28C10	2.8	1.0	2/0	6/0	8/3
B00C00	0.0	0.0	6/0	10/2	15/17
B22C00	2.2	0.0	4/0	9/2	17/14

4.6.2.3 Accumulated rutting

The rutting measurements for each pavement section versus the number of load cycles are presented in Figure 4.30. As a reference, the number of load cycles has been converted to Equivalent Standard Axles (ESAs) in the second X-axis of the figure, assuming a fourth power law:

$$ESA = \left[\frac{SLAVE\_Load}{40\_kN} \right]^4 \qquad \text{(Eq. 4.2)}$$

where SLAVE_Load is the real load applied by one SLAVE unit, and 40_kN is the reference 40-kN load. In this equation, a reference load of 80 kN instead of 40 kN is normally used, which corresponds to the full equivalent standard axle (two dual wheels of 40 kN load each, see Figure 2.2). However, it is known that in the damage induced by the vertical stresses applied by the two wheel pairs is independent, because the separation between wheel pairs (2500 mm) is too large to cause a superposition effect.

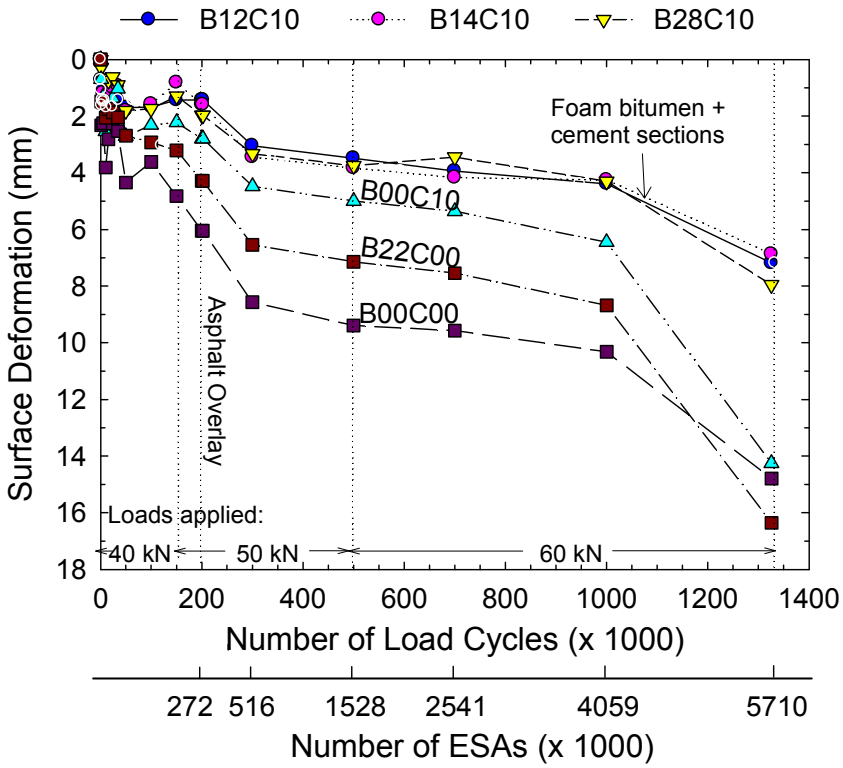

Figure 4.30 Measured surface deformation in CAPTIF foamed bitumen experiment

The curves presented in Figure 4.30 show the typical behaviour of pavements with a bedding-in phase during the initial vehicle loading with 40 kN, followed by a plateau phase after approximately 50,000 load cycles. When the load was increased to 50 kN, another increase in the rutting rate was observed. At 200,000 load cycles the 30-mm hot mix asphalt layer was placed and a

significant increase in surface deformation (about 2 mm) was observed in all sections, caused by the densification of the new surface layer. After 300,000 load cycles, the rutting increased approximately linearly up to 1,000,000 load cycles for all sections. It was expected a change in the slope of the surface deformation curves when the load was increased from 50 kN to 60 kN, after 500,000 load cycles, following the previous measurements when the load was increased from 40 to 50 kN. This result suggests that at the end of the 50-kN loading, at 500,000 load cycles, the pavements were consolidated and little change in permanent deformation occurred, even though the load was increased to 60 kN. After 1,000,000 load cycles a sudden increase in deformation for all sections was observed. This increase was caused by the evidence of heaving in all sections, which displaced the pavement located under the outer tyre, and because deformation observed in sections B00C10, B00C00 and B22C00, as will be later discussed in Section 4.7.

The rutting trends between test sections remained similar throughout the experiment, in which the sections with foamed bitumen and cement (B12C10, B14C10 and B28C10) showed lower rutting than the other three sections, followed by section B00C10, B22C00 and B00C00. From 0 to 200,000 load cycles, approximately 2 mm of rutting were measured in the sections with foamed bitumen and cement, with rutting increasing in sections B00C10, B22C00 and B00C00. After 1,326,000 load cycles, sections B00C10, B00C00 and B22C00 started to show large heaving (18 mm, 7 mm and 14 mm respectively), and rutting (14 mm, 15 mm, and 17 mm respectively), while sections B12C10, B14C10 and B28C10 performed well with lower rutting (7 mm, 7mm and 8 mm respectively) and lower heaving (3 mm for all sections). In sections B00C10, B00C00 and B22C00, cracking was observed near the outer wheel path of the asphalt surface, caused by the large displacements observed in the surface.

4.6.2.4 Additional wet testing

By the end of the pavement test (after 1,326,000 load cycles) only ±1 mm difference was found in the rutting measurements of sections stabilised with

foamed bitumen and cement (sections B12C10, B14C10 and B28C10). To accelerate the surface deformation in these sections, it was decided to cut part of the pavement sections down from the HMA surface to the top of the basecourse (approximately 50mm-deep cuts). A similar procedure had been followed in South African full-scale testing of foamed bitumen pavements (Sections 2.4.2 and 2.4.3) to accelerate the failure of foamed bitumen pavements. The 3-m long cuts were 200-mm apart, and the surface was sawed from stations 3 to 6 in section B12C10, 14 to 17 in section B14C10 and 20 to 23 in section B28C10. Once the cutting job was finished, water was uniformly applied over the surface using sprinklers available at CAPTIF. With a constant water flow, an additional load of 42,000 cycles with 60 kN was applied.

Before the application of the load during the wet testing, the dual-tyre of one of the SLAVE units was replaced for a wide-based super single tyre, but keeping the same 60 kN load. The tyre was replaced as part of another study conducted by Transit New Zealand in CAPTIF. The loading was slightly different in this part of the experiment, but the objective of the wet testing was to study the effect of the bitumen content on the moisture sensitivity of pavements. A slight change in the loading configuration did not affect this objective, because the same load (1 dual tyre with 60 kN and 1 super single tyre with 60 kN) was evenly applied on all the pavement sections.

The water introduced into the pavements, together with the accelerated loading, induced additional damage. After the application of the additional 42,000 load cycles section B12C10 started to show extensive cracking and additional surface deformation in comparison with the other two sections, with evidence of some fine loss. Conversely, no cracking was observed in sections B14C10 and B28C10.

When the wet testing was completed, pictures of the pavement surface were taken at each of the 58 measurement stations. The pictures were taken placing a digital camera at a constant height above the pavement surface, and placing a frame of dimensions 800 mm x 1000 mm directly on the pavement

surface. Pictures of stations 03 (section B12C10) and 25 (section B28C10) are presented in Figure 4.31. The pictures show the cracked surface observed in section B12C10 and the surface with no cracking in section B28C10. Additional pictures are presented in Appendix J.

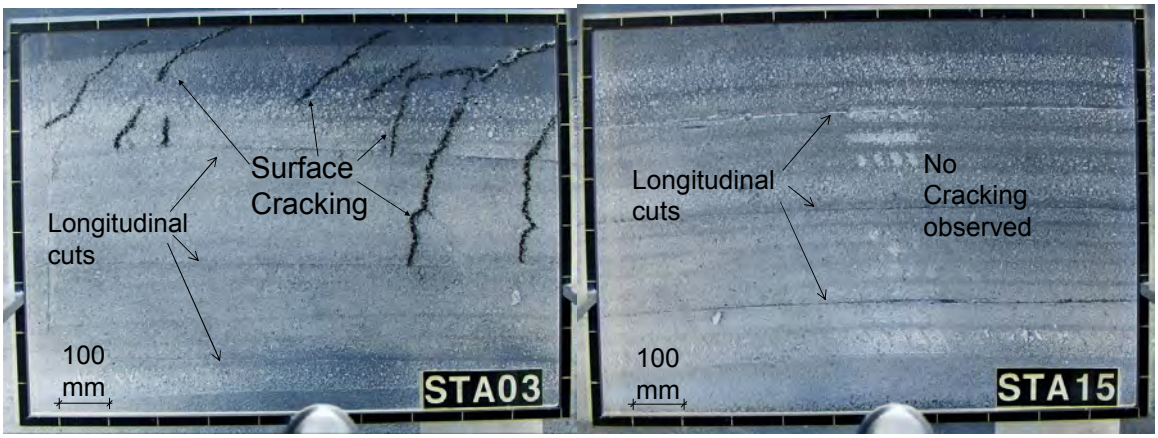

Figure 4.31 Pictures of the pavement surface after wet testing on station 03 (section B12C10) and station 25 (section B28C10)

Rutting was not calculated after the wet testing, because water penetrated into the clay subgrade, causing swelling and raising the final levels of the pavement structure, as explained later in this chapter.

4.6.3 **CAPTIF Beam deflection measurements**

CAPTIF beam deflections were taken at three locations within each pavement section, at a speed of 6 kph. The beam was located at the centre of the wheel path, and one measurement was taken at each pavement location. Deflections were not taken in the interface sections nor transition sections.

The measured CAPTIF beam deflections at 0 load cycles and 40 kN load are plotted against the bitumen content in Figure 4.32. A quadratic curve was fitted to the results to see the deflection trends better. Results show that, for pavements with 1% cement, the effect of foamed bitumen is a reduction in deflections. The average deflection measured in the section with cement only (B00C10) was approximately 0.76 mm, in section B12C10 (1.2% foamed bitumen) 0.72 mm and in section B14C10 (1.4% foamed bitumen) 0.68 mm. The lowest deflection was measured in section B28C10 (0.48 mm), indicating that the elastic modulus of the B28C10 basecourse was higher than that of

the other sections. The highest deflections were measured at the untreated section B00C00 (1.0 mm, doubling deflections of section B28C10). The deflections measured at section B2200 follows the trend of the sections stabilized with 1.0% cement, indicating that adding foamed bitumen without 1% cement also decreases deflections.

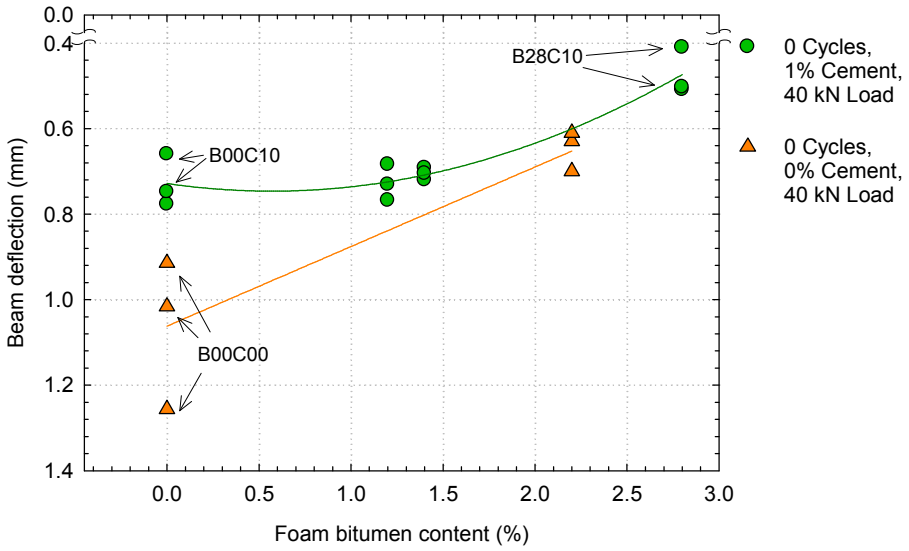

Figure 4.32 Detailed CAPTIF beam deflections versus bitumen content measured at 0 load cycles (40 kN)

4.6.4 **Falling weight deflectometer (FWD)**

4.6.4.1 Effect of bitumen content

The FWD testing was conducted applying a 40 kN load after the completion of the pavement construction 0 load cycles. The measurements were taken at each measurement station (between eight to nine measurements per section) with two FWD drops per measurement point (i.e. two replicates). The deflections close to the interface between sections (stations 8, 18, 27, 47) and deflections near to the transition sections (see Figure 4.8) were collected, but discarded for the data analysis.

The FWD results at 0 load cycles (Figure 4.33) follow a similar trend to those of the Beam measurements presented in the previous Section. At 0 load cycles, the lowest deflection was measured at section B28C10 (0.41 mm) and the highest at section B00C00 (0.90 mm). The deflections at section B22C00

also follow the trend of the cemented sections, indicating that at higher bitumen contents, deflections decrease.

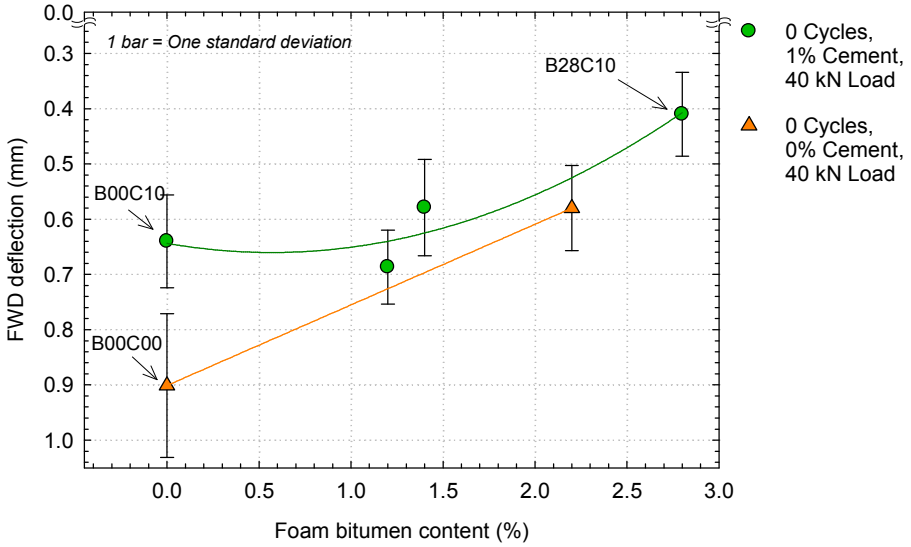

Figure 4.33 Detailed CAPTIF FWD deflections versus bitumen content measured at 0 load cycles (40 kN)

4.6.4.2 Effect of different FWD loads

At 1,000,000 load cycles, the pavement sensitivity to different FWD loads was measured. The FWD was placed at measurement stations 2, 11, 25, 31, 40 and 52) and loads of 40, 50, 60 and 70 kN were applied at each location. The maximum deflection at the centre of the loading plate was recorded under the various FWD loads.

The results of the FWD test at different load magnitudes, presented in Figure 4.34, show that surface deflection under the centre of the loading plate varied linearly with the load magnitude. The least square regression parameters for the best linear approximation for each dataset are included in this figure. The square regression coefficients (R^2) are high, with a minimum of 0.9939 in section B12C10 and a maximum of 0.9996 in section B22C00. The highest slope of the lines fitted to the data (**a** coefficient in $y = \mathbf{a}x + b$) was calculated for section B00C00 (a = 14.6), indicating that pavement deflections in this section are the most sensitive to FWD load magnitudes. The next most sensitive section is B22C00 (a=11.31), which is the most sensitive pavement

to FWD load among the stabilised pavements studied. The least sensitive pavement to FWD load is B28C10 (a = 8.03).

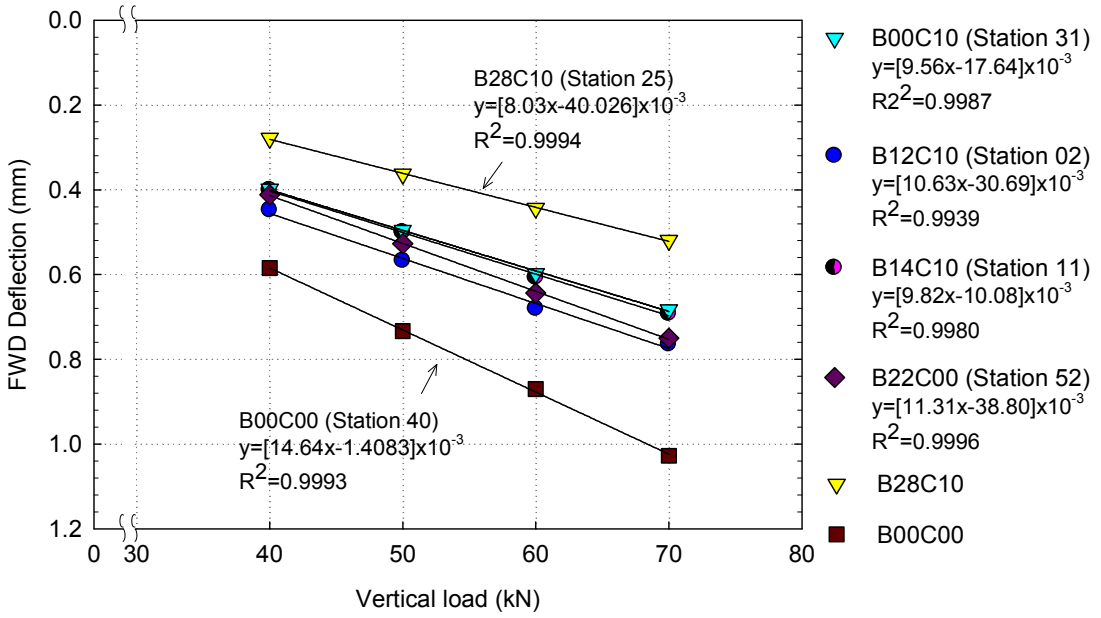

Figure 4.34 Maximum deflections measured in the FWD experiment at different loads at 1x106 load cycles

4.6.5 **Strain measurements**

4.6.5.1 Vertical strain profiles at different depths

Vertical strains taken at 1,000; 200,000; 502,000 and 1,326,000 load cycles are plotted at different depths at each measurement station for stations 11 (Section B14C10) and 40 (Section B00C00), in Figure 4.35 and Figure 4.36, respectively. The location of the Emu strain coils is also included in the figures. The coil pair installed in the interface between the basecourse and the subgrade measures a combination of vertical strains taken from the bottom of the basecourse and the top of the subgrade. The vertical strains presented were taken at wheel speed of 10 kph. During the strain measurements, the lateral movements of the wheels were restrained to ensure that the wheels rolled over the strain instrumentation as previously shown in Figure 4.17.

The measurements taken from the stabilised sections showed that vertical strains in the basecourse layer were 5 to 10 times lower than those taken from the top of the subgrade. For example, the vertical strains in B14C10 basecourse (Figure 4.35) were approximately 150 μm/m, while at the top of

the subgrade (262.5 mm) the vertical strains ranged from 1300 to 1750 μm/m. Similar trends were observed in the other stabilised sections, as summarized in Appendix K. These measurements indicate that most of the vertical elastic deformation takes place in the subgrade layer.

The vertical strain profile from station 40 (Figure 4.36) shows that vertical strains in the basecourse layer were only 3 to 4 times lower than those collected from the subgrade. The basecourse vertical strains ranged between 850 to 1,100 μm/m, while the vertical strains measured at the top of the subgrade ranged between 2850 to 4250 μm/m.

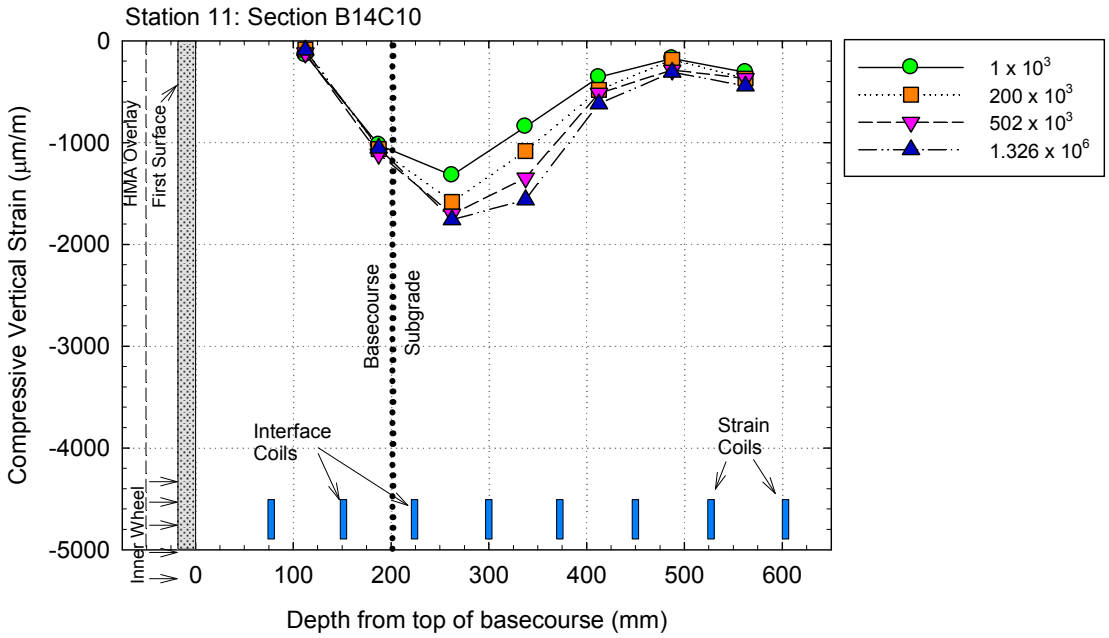

Figure 4.35 Vertical strain profiles for station 11 (section B14C10) at different stages of the project, 10 kph

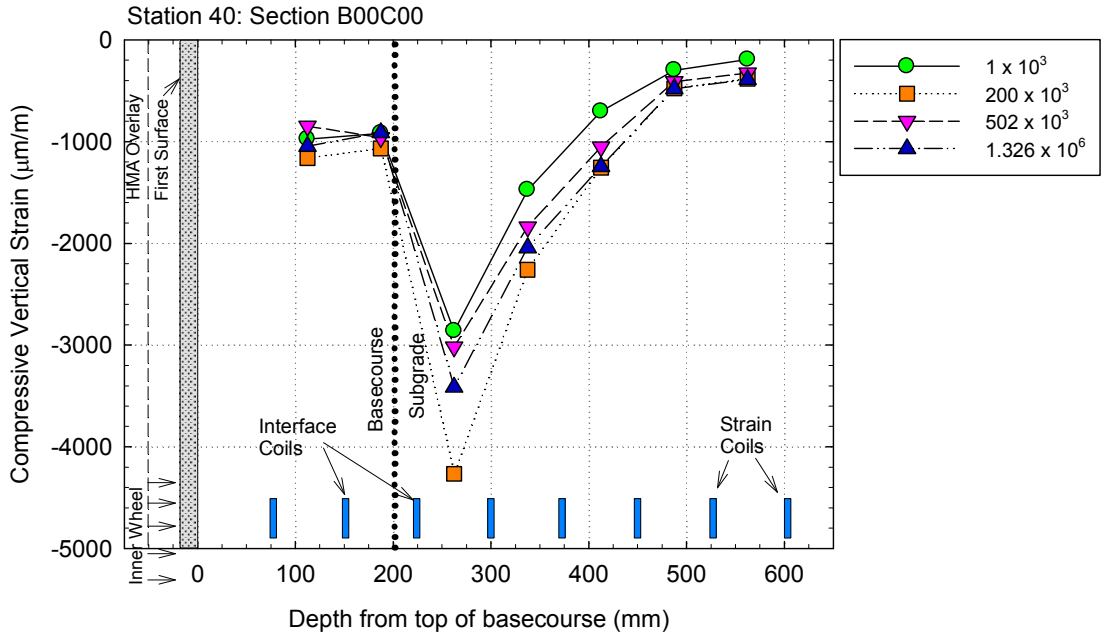

Figure 4.36 Vertical strain profiles for station 40 (section B00C00) at different stages of the project, 10 kph

4.6.5.2 History of vertical strains in the basecourse layer and top of the subgrade

Figure 4.37 presents the history of vertical strains in the basecourse for all pavement sections, measured at a vehicle speed of 10 kph. For clarity, the initial vertical strain measurements at 40 kN (from 0 to 100,000 load cycles) are plotted in a separate chart (Figure 4.38).

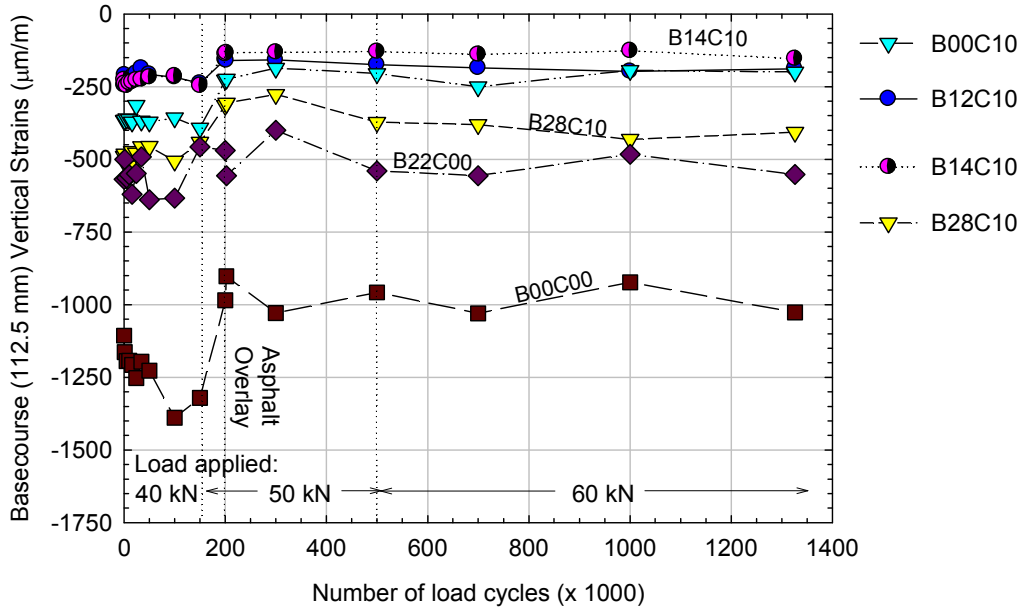

Figure 4.37 History of vertical strains measurements at the basecourse layer (112.5 mm depth), average of three coil pairs, 10 kph

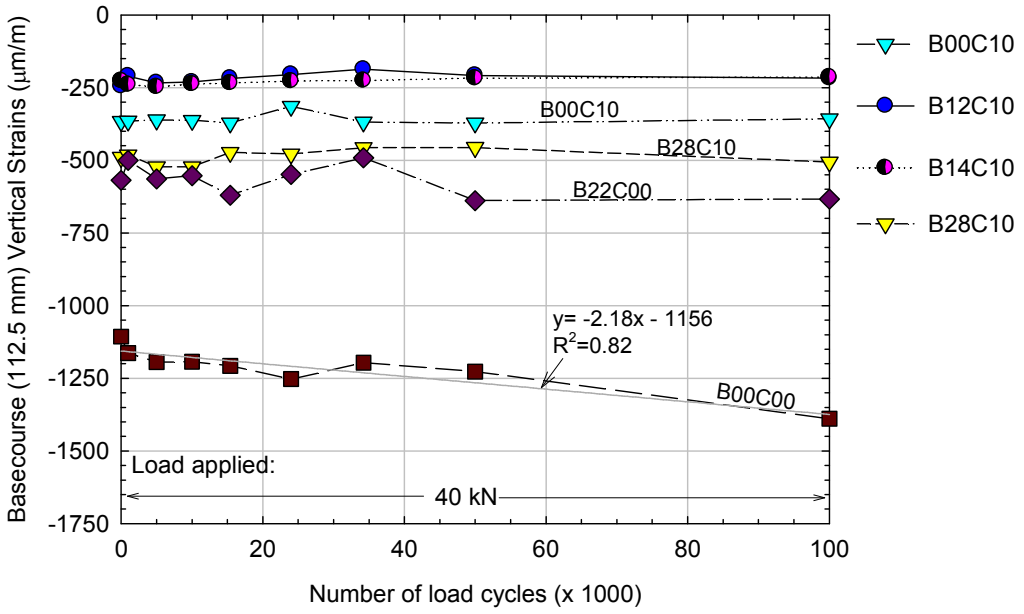

Figure 4.38 History of vertical strain measurements at the basecourse layer (112.5 mm depth), average of three coil pairs, 10 kph, between 0 and 100,000 load cycles

The vertical strains of the stabilised sections remained fairly constant during the first 100,000 load cycles. An absolute increase of about 300 μm/m was observed only at the unbound granular section (B00C00). A line was fitted to B00C00 vertical strain data, included in Figure 4.38.

A general reduction in the strains was observed in all sections when the 30-mm hot mix asphalt overlay was placed on the pavement surface, caused by: 1) the thicker surface, which spreads the applied load over a larger area, reduces the vertical stress applied in the basecourse and therefore reduces the vertical strains in the subgrade layers 2) the relative position of the strain coils to the pavement surface was shifted from 95 mm (75 mm basecourse + 20 mm surface) to 125 mm (75 mm basecourse + 50 mm surface), therefore the strains are measured at a relative deeper location (see Figure 4.17, in which the strain coil system, the original asphalt surface, and the asphalt surface after overlay are shown).

The vertical strain measured in the basecourse remained fairly constant after sections B00C10, B00C00 and B22C00 started to show large amounts of

heaving and rutting. This contradicts the normal behaviour of granular pavements, in which increase in permanent deformations yields increase in vertical strain rate (Arnold et al. 2002; Werkmeister 2006). The constant vertical strain measurement in the basecourse could be explained by the transverse position of the strain coils (see Figure 4.17), located directly under the inner wheel. The accumulated surface deformation after 1.326×10^6 load cycles, below the inner wheel load for sections B00C10, B00C00 and B22C00 was 6 mm, 8 mm and 6 mm, while below the outer wheel load was 14 mm, 15 mm and 17 mm, respectively (see surface profile for section B00C10 in Figure 4.29). In other words, the performance of the pavement below the inner wheel load remained reasonably good, with rutting depths between 6 and 8 mm. The only case, in which increase in vertical strains was observed between 0 and 100,000 load cycles, was the previously mentioned section B00C00 (Figure 4.38). This increase could be attributed to the rapid 4 mm increase in rutting under the inner wheel load in comparison with the other pavements. A summary of the rut depths at the inner and outer wheel is presented in Table 4.5.

Table 4.5 Summary of surface deformation at outer and inner wheel (in mm)

			Surface deformation outer/inner wheel at given wheel repetitions:		
Section	Bitumen (%)	Cement (%)	200×10^3	1.000×10^6	1.326×10^6
B00C10	0.0	1.0	3/2	6/4	14/6
B12C10	1.2	1.0	2/2	6/4	7/6
B14C10	1.4	1.0	2/2	6/4	7/5
B28C10	2.8	1.0	2/2	6/4	8/6
B00C00	0.0	0.0	6/4	10/7	15/8
B22C00	2.2	0.0	4/2	9/4	17/6

4.6.5.3 Effect of foamed bitumen and cement

The effect of stabilisation on the compressive vertical strains in the basecourse (depth=112.5 mm), the vertical strain at the top of the subgrade (depth=262.5 mm), and the tensile longitudinal strains measured at the

bottom of the basecourse layer (depth=150 mm) was studied. The strains collected for the analysis were taken at 502,000 and 1,326,000 load cycles, with a load of 60 kN, and vehicle speed of 10 kph.

The compressive vertical strains measured in the basecourse are presented in Figure 4.39. The highest vertical strains were measured at the untreated section B00C00 (1050 μm), followed by section B22C00 (625 μm). The vertical strains measured in the sections stabilised with a common 1% cement were lower than the sections without cement. The vertical strains measured in section B00C10 were about 200 μm, in sections B12C10 and B14C10 between 130-220 μm, and increased in section B28C10 up to 400 μm.

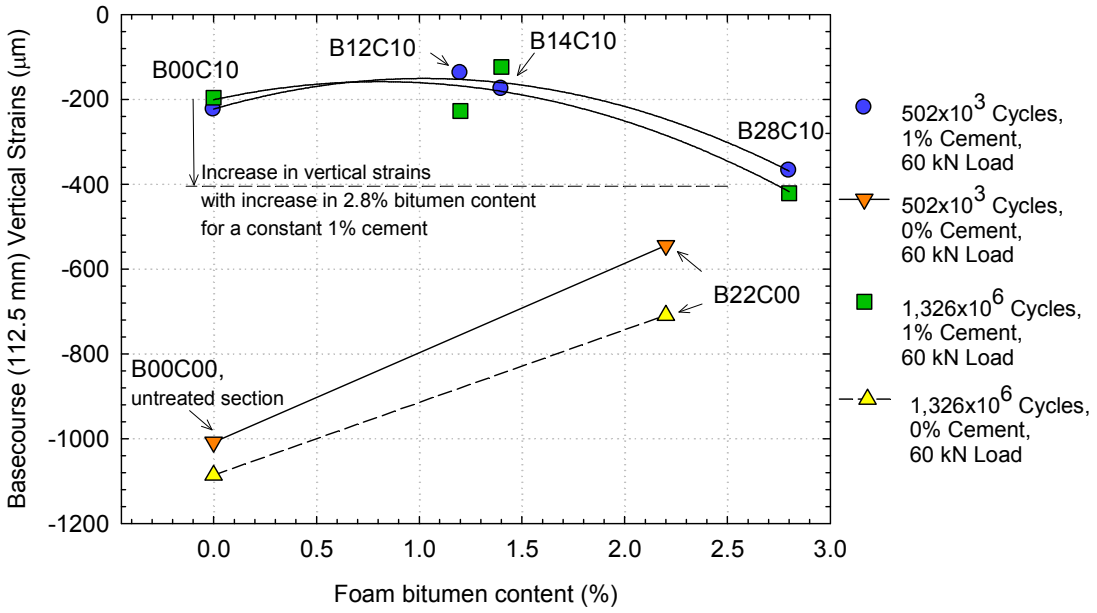

Figure 4.39 Compressive vertical strains in the basecourse (112.5 mm) at 5.02x103 and 1.326x106 load cycles for different bitumen contents

The longitudinal tensile strains at the bottom of the basecourse are presented in Figure 4.40. The highest vertical strains were measured at the untreated section B00C00 (1600 μm), followed by section B22C00 (750 μm). The longitudinal strains measured in the sections stabilised with a common 1% cement were lower than the sections without cement. The longitudinal strains measured in section B00C10 were about 350 μm, in sections B12C10 and B14C10 the strains decreased to 230 and 170 μm, and the lowest were

measured in section B28C10 (120 μm), indicating that, for a constant 1% cement, longitudinal tensile strains decrease with increase in bitumen content.

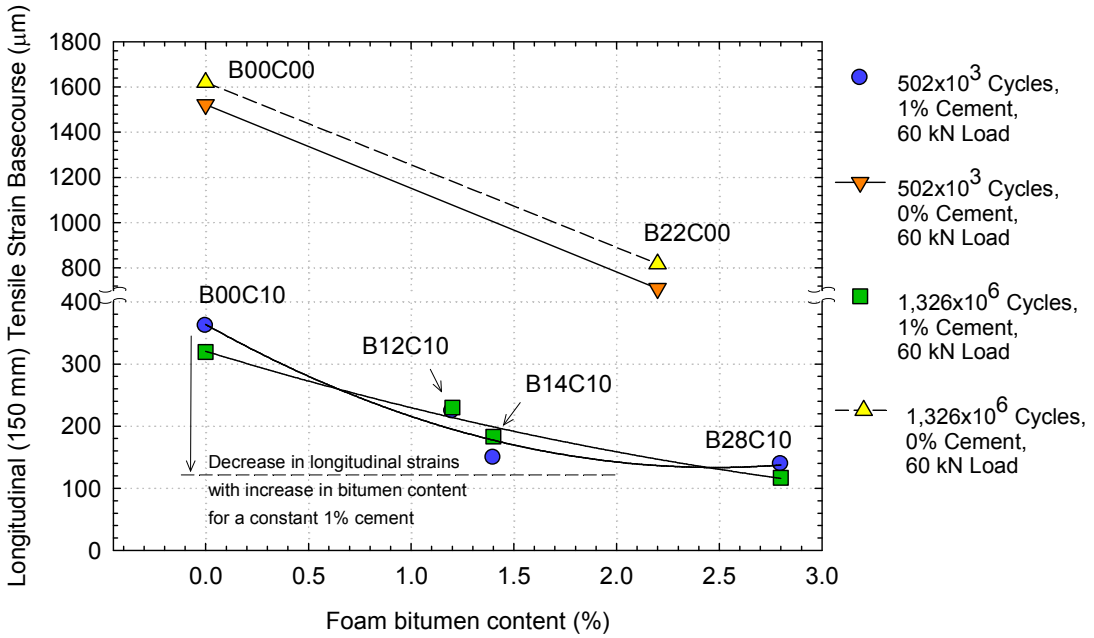

Figure 4.40 Longitudinal tensile strains lower basecourse (150 mm) at 502x103 and 1.326x106 load cycles for different bitumen contents

The compressive vertical strains measured at the top of the subgrade are presented in Figure 4.41. The strains measured at the unbound section (B00C00) were the highest (approximately 3,000 μm). Within the stabilised sections, the highest vertical strains were measured in section B12C10 (2,350 μm). The other stabilised sections follow a trend in which vertical strains decrease with increase in bitumen content. The lowest vertical strain was measured in section B28C10 (1500 μm).

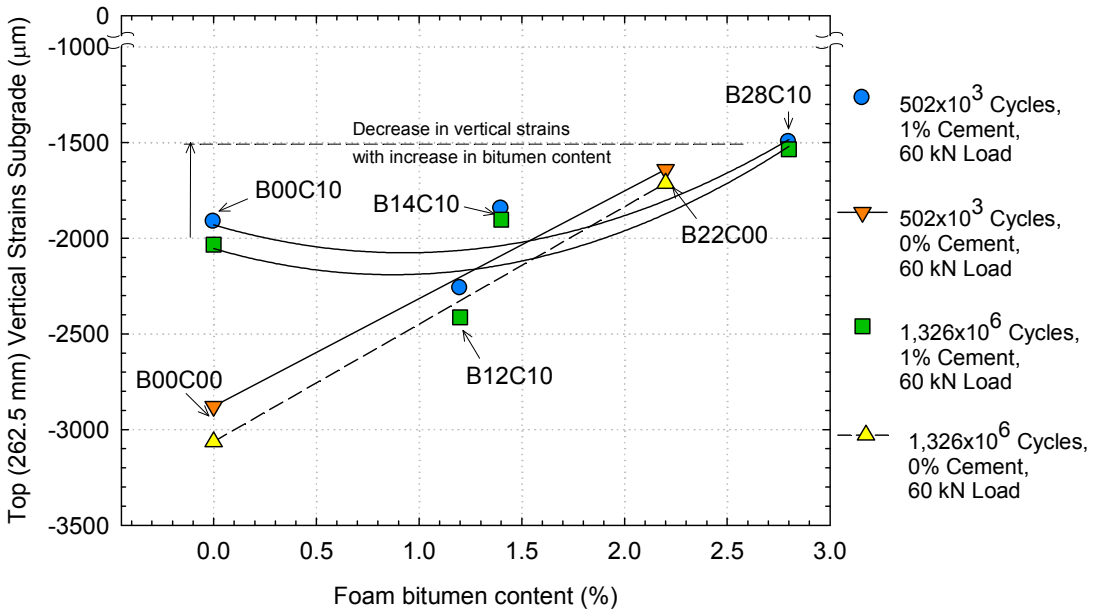

Figure 4.41 Compressive vertical strains at the top of the subgrade (262.5 mm) at 502x103 and 1.326x106 load cycles for different bitumen contents

4.7 Post mortem analysis

4.7.1 **Introduction**

The post-mortem is the last stage of the full-scale pavement experiment, conducted after the end of the accelerated loading. The most important activity in this stage is the excavation of trenches in the pavement sections, in which the plastic deformation of the basecourse and subgrade layers are estimated by measuring the interface transverse profiles (cross sections). In addition, material samples are collected during the excavation of the trenches from both the basecourse and subgrade layers, for bitumen extraction and determination of moisture contents. Another activities normally conducted in the post-mortem are the measurement of the tyre imprints of the SLAVE units and the determination of the coil depth in the basecourse.

4.7.2 **Tyre imprints**

The tyre imprints were taken after the end of the pavement loading, by jacking up one SLAVE unit and spraying black paint over the tyre circumference. Later, a sheet of poster board is positioned on the pavement surface directly under the wheel, and the vehicle is lowered, to create an imprint of both tyres

on the poster board. Finally, the vehicle is jacked up, and the poster board removed. When the tyre imprint was measured, the SLAVE unit was loaded with 40 kN, to jack up the vehicle easier.

Figure 4.42 shows the tyre imprint for one SLAVE unit, loaded with 40 kN, at the end of the foamed bitumen experiment. The limitation of these measurements is that the tyre imprints are taken under static conditions, which could change with the movement of the wheels. The figure shows that the width of the tyres is similar (approximately 250 mm), but the length of the outer tyre imprint is higher (260 mm versus 210 mm), which yields contact areas of 537.5 cm^2 and 475.0 cm^2 for the outer and inner paths, respectively. Pavement/tyre contact stress measurements were not available, but the tyre pressure was recorded in both tyres (690 kPa), suggesting that the contact stress remained similar for both tyres. With these data, the load applied by each tyre was estimated, assuming that the contact stress is similar for both tyres, and that the load is distributed on each tyre proportionally to the respective contact area. The calculated loads were 21.2 and 18.8 kN for the outer and inner wheel loads, respectively (12.7% higher at the outer tyre).

The estimated higher load applied in the outer tyre could explain the higher deterioration observed near the outer wheel path, uniformly observed in all the pavement sections (Table 4.5). Assuming that the damage induced by each tyre is independent, and follows the empirical fourth power law (Eq. 4.2), but a 20-kN instead of 40-kN load reference is used, the relative damage between the tyres could be estimated using the following formula:

$$Damage = \left(\frac{P_{tyre}}{20\_kN} \right)^4 \qquad \text{(Eq. 4.3)}$$

where P_{tyre} is the load of each tyre. Using the previously estimated loads applied by each tyre (21.2 and 18.8 kN), the equation yields a relative damage of 1.26 and 0.78 for the outer and inner wheel loads respectively. In other words, the damage induced by the outer wheel load is approximately 1.6

times higher than the inner wheel load. This relative damage between the outer and inner wheel paths was somewhat observed in the measured surface deformation after the application of 1,000,000 load cycles (Table 4.5), in which the outer-to-inner surface deformation ratio was 1.5 (6:4=1.5, 6 mm at the outer wheel path and 4 mm at the inner wheel path) for sections B00C10, B12C10, B14C10 and B28C10.

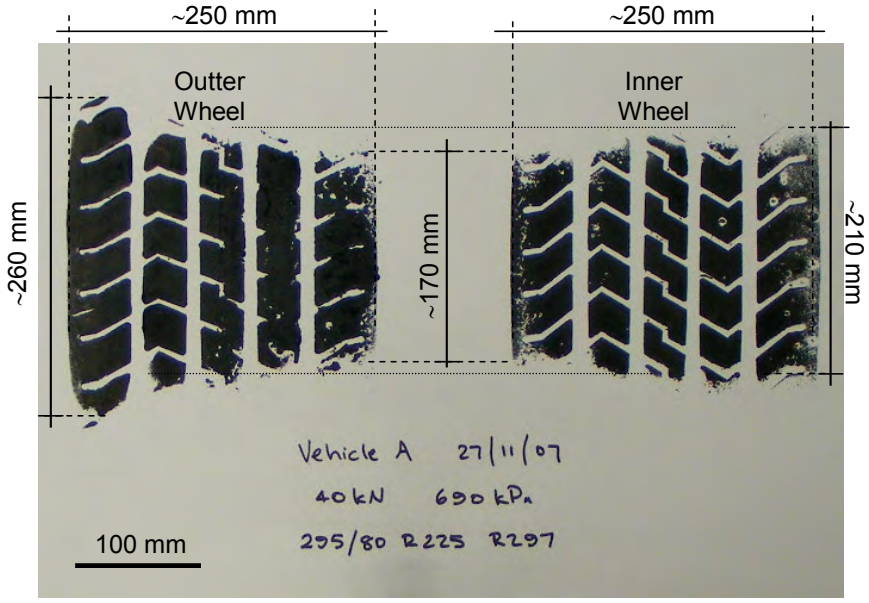

Figure 4.42 Tyre imprint of the SLAVE unit

Although centripetal forces are restrained in CAPTIF, there is a possibility of scuffing caused by the continuous right hand bend of the vehicles. To avoid the scuffing, in previous CAPTIF experiments the test ring was equipped with a slip ring device between the inner and outer wheels on the dual type to allow the tyres to turn at different speeds. The ring was later removed because was not practical and it seemed had no effect. The difference in load between wheels is normally caused by the camber and effective toe-in (or “toe-out”) that must exist.

4.7.3 **Moisture contents of pavements**

Material samples were collected for moisture content tests. Samples were taken at the wheel path from each pavement section, at stations 1 and 4 (B12C10); 11 and 16 (B14C10); 21 and 25 (B28C10); 31 and 33 (B00C10);

40 and 43 (B00C00); and 50 and 54 (B22C00). In each station, four material samples were collected from the basecourse and two from the top of the subgrade. The moisture contents were determined in accordance with NZS 4407:1991 Test 3.1.

The average moisture content results for the basecourse layer are presented in Figure 4.43. The average moisture contents measured before the sealing of the surface during pavement construction (Section 4.4.3), using a nuclear gauge, are included. Results show that moisture contents measured in sections B12C10, B14C10, B28C10 and B00C10 are higher than the original moisture contents, indicating that water was introduced into the pavements during the 'wet' testing of pavements (Section 4.6.2.4). A summary of the moisture contents is presented in Table 4.6, which shows that the pavement section with the highest increase in moisture content is B12C10 (1.5% increase), which is the section with the lowest bitumen content tested in this part of the experiment. Lower increase in the moisture content was measured with increase in the bitumen content (the increase in B14C10 was 0.5% and in B28C10 0.2%), indicating that higher foamed bitumen contents decreases the permeability of the pavement.

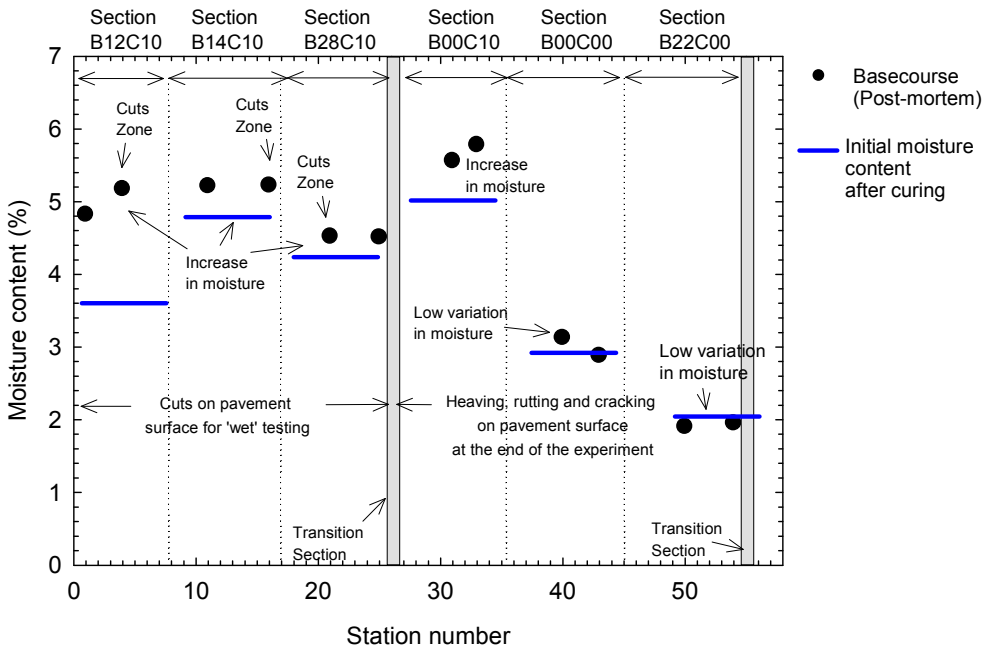

Figure 4.43 Moisture contents measured at the basecourse during construction and post-mortem analysis

Table 4.6 Average of moisture contents measured in the basecourse in post-mortem and construction phase

	B12C10	B14C10	B28C10	B00C10	B00C00	B22C00
Moisture content before sealing (%)	3.6	4.8	4.3	5.0	2.9	2.0
Moisture content in Post-Mortem (%)	5.1	5.3	4.5	5.6	3.0	1.9
Difference (%)	+1.5	+0.5	+0.2	+0.7	+0.1	-0.1

An increase of 0.7% was also found in section B00C10, even though this section was not part of the wet test, and was not sawed on the surface. However, the large heaving and rutting observed in this section before the wet testing, shown in Figure 4.29, induced surface cracking in the outer wheel path (Appendix J, Section J.4). The water was sprayed on sections B12C10, B14C10 and B28C10, however, the circular, clockwise movement of the SLAVE units drifted the water from these sections to section B00C10, introducing water into the basecourse layer (Figure 4.44). The moisture content increase for section B00C00 was 0.1%, lower than the other sections, because this section was located farther from the area where the water was applied (Figure 4.44). The moisture content in section B22C00 decreased for 0.1%.

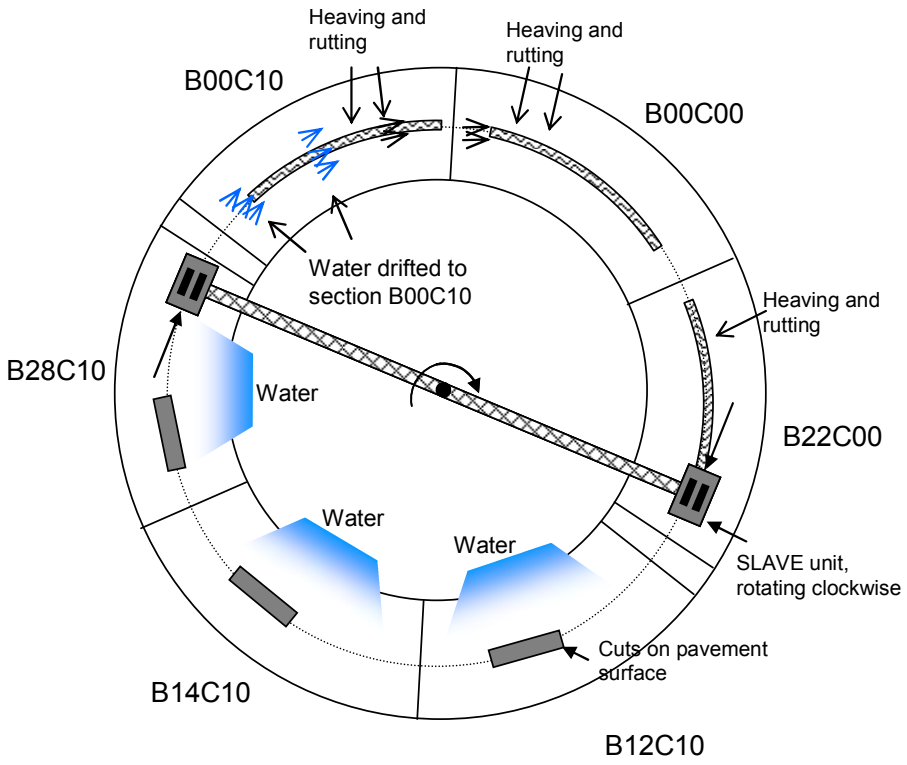

Figure 4.44 Drift of water during wet testing

The moisture contents measured in the subgrade are presented in Figure 4.45. The moisture content measured at the top of the subgrade during the construction of the pavement, before the basecourse was placed, is also included in the figure. In both cases the moissture content was determined drying samples of subgrade in the oven. The results show that moisture contents from sections B12C10, B14C10 and B28C10 increased for approximately 3-4%, with higher increase in the areas where the surface was cut. The increase in moisture contents measured in section B00C00 was about 2%, while only section B22C00 showed decrease in the moisture content of approximately 5%, indicating that water was not introduced into the subgrade in this pavement section during the wet testing of pavements. The moisture measurements in the subgrade show a similar trend to those of the basecourse, the greater amount of water penetrated into the pavement in sections B12C10, B14C10, C28C10 and B00C10, followed by section B00C00 and no water penetrated into section B22C00.

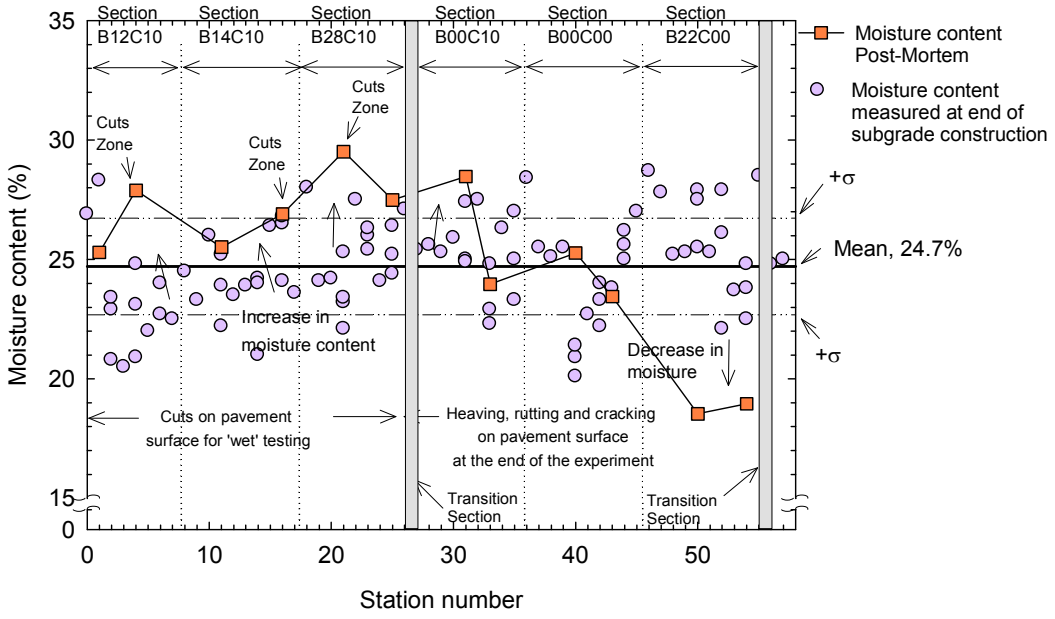

Figure 4.45 Moisture contents measured at the subgrade during construction and post-mortem analysis

4.7.4 **Excavation of trenches and manual surface profile**

Trenches were excavated in each pavement section, at stations 1 and 4 (B12C10); 11 and 16 (B14C10); 21 and 25 (B28C10); 31 and 33 (B00C10); 40 and 43 (B00C00); and 50 (B22C00).

The levels of each pavement layer were recorded to calculate the plastic deformation in each section, using a manual profilometer, which consists of a 4.5 m length aluminium channel section, a machined plastic block which slides along the channel and a 1 m steel ruler which is located in a slot in the plastic block (Figure 4.46). The ruler is lined above the pavement station, approximately 320 mm height above the pavement surface, and lowered down to the surface being measured and the corresponding depth is measured at the edge of the block. The readings are normally taken every 200 mm across the track. Since this is a manual measurement, and usually the interface between the layers is not completely clear, the precision of these readings is about ± 2 mm.

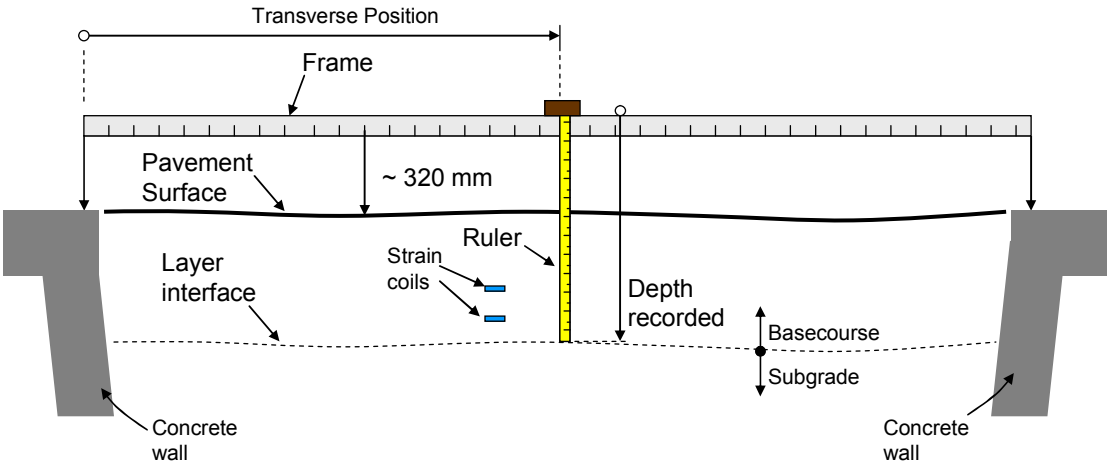

Figure 4.46 Measurements of the manual transverse profiles (cross section)

Two manual profiles, from sections B28C10 and B00C10, are presented in Figure 4.47 and Figure 4.48, respectively. The profiles from the other pavement sections are included in Appendix L. Both profiles depict the swelling of the subgrade layer caused by the introduction of water during the wet testing of pavements, previously described in Section 4.6.2.4. Using the transverse profile measurements, the subgrade swelling was estimated for each section in Table 4.7. No swelling was observed in section B22C00, which showed a vertical displacement of -3 mm, and the lowest swelling (+10 mm) was measured in section B00C00, indicating that a lower water content penetrated into the subgrade in this last section.

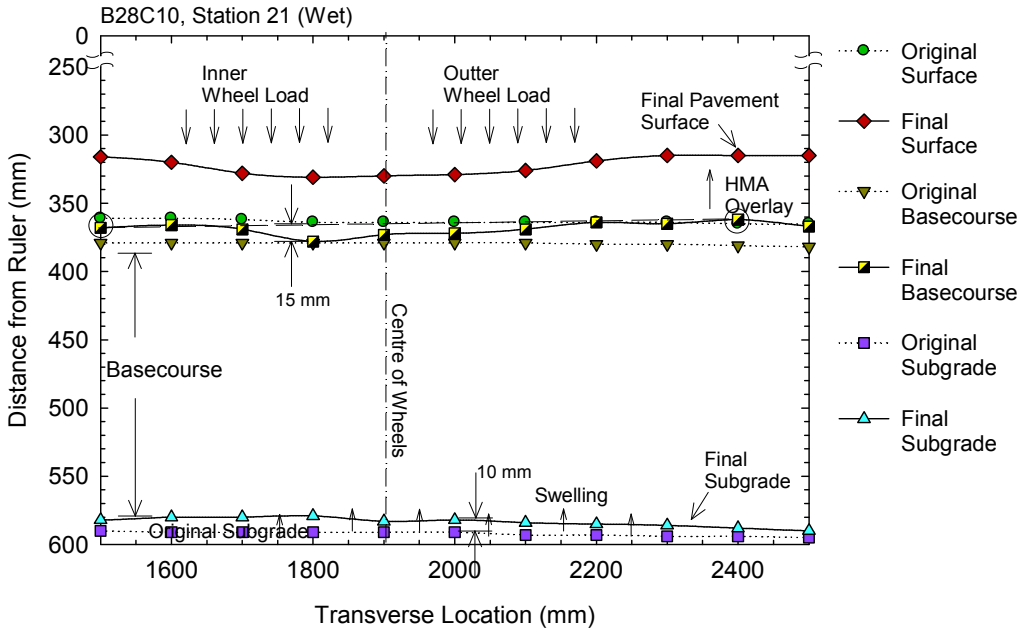

Figure 4.47 Deformation profile at stations 21, Section B28C10

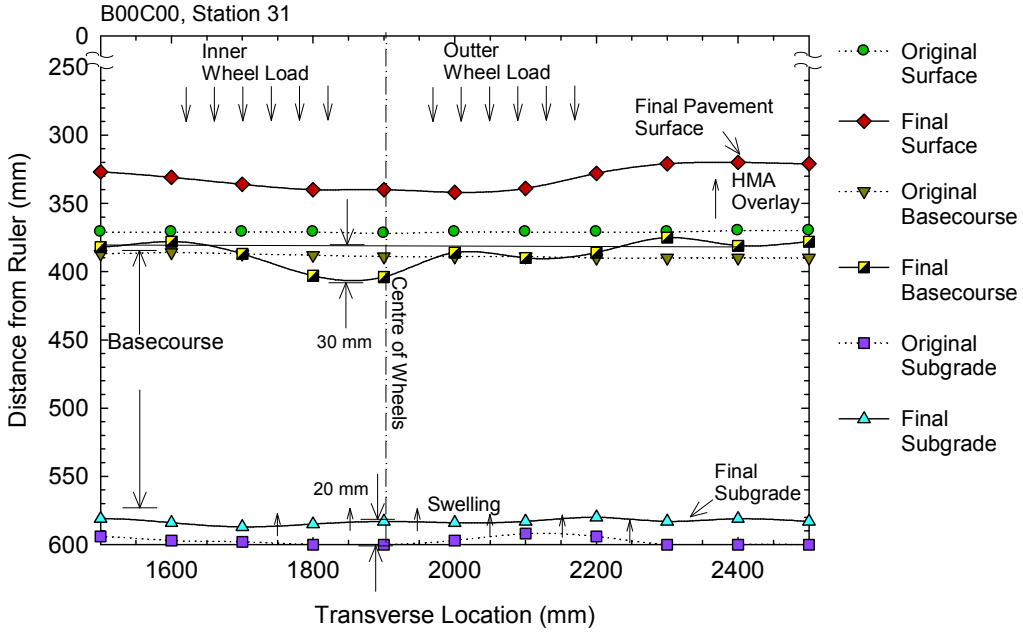

Figure 4.48 Deformation profile at stations 31, Section B00C10

Figure 4.47 and Figure 4.48 also show the as-built and final levels of the basecourse. The final level of the basecourse was displaced upwards by the swollen subgrade, and therefore the initial level could not be used as a reference for the calculation of vertical deformation. Instead, a line was drawn between two points outside the wheel path (at transverse locations of 1500

and 2400 mm, enclosed in circles in both figures), and the deformation in the basecourse calculated as the difference between the level of the line and the lowest level of the basecourse. The calculated deformations in the basecourse are listed in Table 4.7. The greatest basecourse deformation was measured in station 4 (section B12C10, -30 mm), where the surface was cut, and station 40 (B00C00, -30 mm). The other sections with foamed bitumen and cement, showed lower deformation on the cut surface (-12 mm in station 16 for B14C10 and -15 mm in station 21 for B28C10), indicating the lower moisture sensitivity of these last two sections. The deformation in section B22C00 was only -15 mm, because water did not penetrate into this pavement, which stopped further damage during the wet test.

Table 4.7 Approximate deformation of pavement layers observed during the post-mortem analysis (positive = swelling, negative =deformation)

Section	Station	Subgrade (mm)	Basecourse (mm)
B12C10	1	+20	-15
	4 (cut)	+30	-30
B14C10	11	+20	-12
	16 (cut)	+20	-10
B28C10	21 (cut)	+10	-15
	25	+25	-15
B00C10	31	+25	-25
	33	+25	-20
B00C00	40	+10	-30
	43	+10	-25
B22C00	50	-3	-15

4.7.5 **Location of basecourse strain coils and manual profiles**

In the excavation of trenches, the vertical position of the Emu strain coils located in the basecourse was recorded, with the objective of identifying the plastic deformation in the basecourse layers by comparing the original position of the coils during construction with the final position. The original vertical position of the strain coils in the construction of the pavements is

recorded using the ruler shown in Figure 4.46, to assure a 75-mm distance between the coils (Figure 4.17). The vertical position of the coils during the post-mortem analysis is also estimated using this ruler.

During the excavation of the trenches, the coils located in section B12C10 and B22C00 were accidentally displaced, and the coil depth not recorded. The reported position of the recovered coils from the other four sections is presented in Table 4.8. The reported position is the relative vertical distance between the frame that holds the ruler (Figure 4.46), which is approximately 320 mm above the pavement surface, and the strain coil, reported in Table 4.8. The original and final coil positions of the recovered coils are presented in the table.

Table 4.8 shows that the level of the coils measured in the post-mortem phase for sections B14C10, B28C10 and B00C10 is higher than that measured in the construction of the pavement, because the original levels of the basecourse changed by the swelling of the subgrade.

The initial distance between the coils was 75 mm, measured during pavement construction, which remained constant for stations 11 (section B14C10) and 25 (section B28C10), suggesting that the surface deformation observed in the surface profiles occurred mostly in the upper part of the layer. The distance between coils at stations 31 (section B00C10) and 40 (section B00C00) was 71 and 67 mm respectively, which yields a deformation of 4 and 5 mm respectively, indicating that plastic deformation occurred in thse pavements.

Table 4.8 Vertical location of the basecourse strain coils during the post-mortem analysis

Section	B12C10	B14C10	B28C10	B00C10	B00C00	B22C00
Station	2	11	25	31	40	52
Vertical location in construction						
Upper coil (mm)	487	500	486	509	483	470
Bottom coil (mm)	562	575	561	584	558	545
Distance (mm)	75	75	75	75	75	75
Vertical location in post-mortem						
Upper coil (mm)	-	489	475	502	488	-
Bottom coil (mm)	-	564	550	573	558	-
Distance (mm)	-	75	75	71	70	-
Difference (mm)	-	0	0	4	5	-

4.7.6 **Bitumen extraction**

Once the measurement of the levels of the surface profiles was completed, the pavements were demolished using an excavator. During the excavation of the pavements, samples of the basecourse were collected from the sections stabilised with foamed bitumen (B12C10, B14C10, B28C10, B22C00), for bitumen extraction tests. The samples consisted in pavement blocks, with dimensions of approximately 300 mm x 300 mm x 200 mm, which remained unsealed in CAPTIF building at ambient temperature (10-20 °C) for about one month after collection. The blocks were broken in small pieces, to produce between two to four material samples of approximately 15 kg from each section. Later, the bitumen content was determined following the British Standard for extraction of bituminous materials (BSI 2005). The moisture content of the samples was also determined. The results of the bitumen extraction are presented in Figure 4.49, where, the bitumen content was plotted against the station from which the sample was collected.

The moisture contents follow the trend previously discussed in Section 4.7.3, in which the moisture contents measured in sections B12C10 (3.4% and 4.0%) and B14C10 (3.6%, 4.1%, 3.7 and 3.9%) are fairly similar, with lower moisture content measured in section B28C10 (3.0% and 3.1%). The moisture contents measured in the samples recovered from section B22C00 were 1.1% and 1.5%, about one third of those collected from the other sections. The moisture contents determined in this part of the experiment were 1 to 2% lower than those recovered during the excavation of the trenches (see Figure 4.43), because the pavement blocks were aired for one month after the excavation of the pavement sections, reducing their moisture content. The basecourse material samples were collected from the top 100 mm and bottom 100 mm.

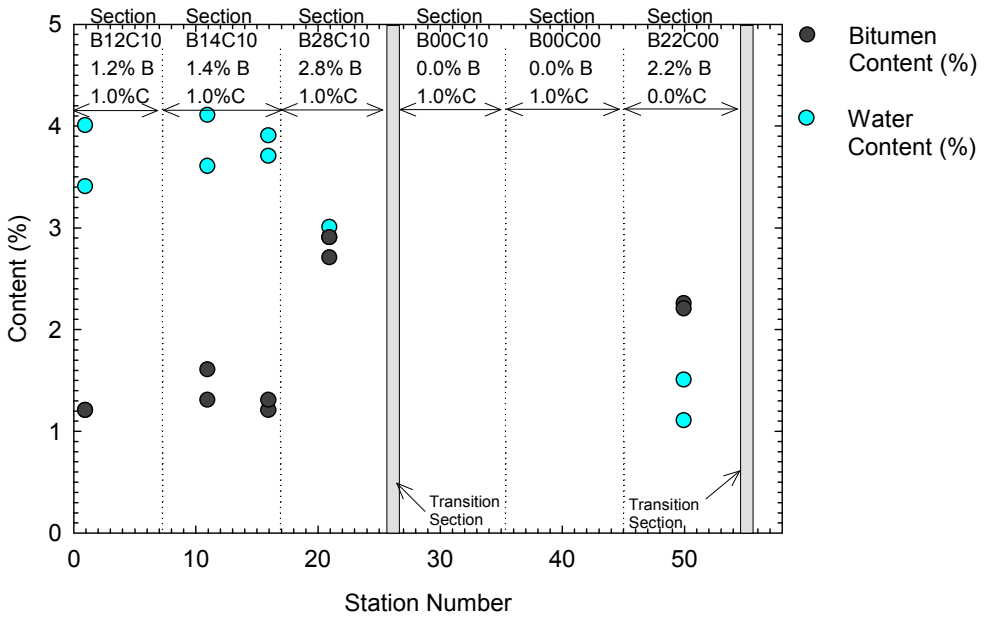

Figure 4.49 Results of the bitumen extraction test

4.8 Discussion of results

4.8.1 Pavement design methods and general performance of foamed bitumen pavements

The pavement design methods used to estimate the thickness of the basecourse layer underestimated the design life of the pavement (Section 4.3.2). After 5.6×10^6 ESAs (Figure 4.30), the surface deformation measured in

the sections with foamed bitumen and cement was 7-8 mm, while both pavement design methods estimated a pavement life, with a final surface deformation of 20 mm, of $1x10^6$ ESAs. In addition, the pavement structural design was conducted for the mix at the optimum foamed bitumen content section (B28C10), and therefore it was expected a poorer behaviour in the other pavements with lower foamed bitumen contents (B12C10 and B14C10). It seems that pavement design methods are overly conservative, however, conditions in CAPTIF are not totally comparable with real roads (e.g. climate conditions are much less severe), and pavements were designed for 95% reliability.

Variation of elastic strains measured in the basecourse, with number of load cycles, was not observed in the foamed bitumen pavements tested in the CAPTIF experiment (see Figure 4.37 and Figure 4.38), indicating that the elastic modulus of these layers remained constant throughout the duration of the experiment (approximately 6 months from initial to final loading), contradicting the results from the two South African accelerated pavement testing presented in Section 2.4, P243/1 and N7. In the P243/1 road South African accelerated testing of pavements (Section 2.4.2), the elastic strains were measured in the foamed bitumen basecourse and the resilient moduli back-calculated. Section 411A4, which was one of the sections tested in the P243/1 experiment, was initially loaded with a 40-kN load, and after 400,000 repetitions, the foamed bitumen layer showed a reduction in the elastic modulus of about 50% (from 2750 MPa at 0 load cycles to 1500 MPa at 400,000 load cycles of 40 kN), as depicted in Figure 2.22. Similar results were obtained in the N7 South African accelerated testing of pavements (Section 2.4.3), in which the initial resilient modulus measured in two pavement sections (415A5 and 416A5) decreased after the initial trafficking of the pavement sections (see Figure 2.24 and Figure 2.25), up to values representative of high quality unbound crushed stone materials (300 – 600 MPa). An opposite trend to these measurements was reported by Loizos and Papavasiliou (2007), who measured a decrease in the pavement deflections after construction of a heavy-trafficked highway in Greece (Section 2.4.5, Figure 2.31). The authors attributed this increase in stiffness to the moisture

loss of the pavements after construction, which is in agreement with the PRIMA light falling weight deflectometer measurements taken during the one-month curing period of the CAPTIF pavements (Figure 4.14).

One possible reason that could explain the constant measurements of vertical strains throughout the CAPTIF experiment is the relatively low surface deformation or pavement deterioration observed below the inner wheel path of the pavement (between 6 and 8 mm, Table 4.5), where the strain coils were installed. However, in the N7 South African pavement section 416A5, after the application of 1,000,000 load cycles of 40 kN, the surface rut depth was about one half than that of CAPTIF (approximately 3-4 mm Figure 2.26), but in 416A5 section a reduction of 50% in the stiffness of the foamed bitumen layer was measured (from 2,000 to 1,000 MPa, Figure 2.25). In other words, there is no evidence to support that the elastic modulus of the foamed bitumen layers tested in the CAPTIF experiment decreased with increase in the number of load repetitions applied to the pavement. This behaviour supports the observations made by the New Zealand Supplement to the Austroads Pavement Design Guide (Section 2.2.5.1), in which is suggested that under New Zealand conditions, foamed bitumen pavements do not show a two-phase behaviour (Figure 2.3), and therefore only the “equivalent granular” phase should be accounted in the design.

4.8.2 **Field and laboratory mixes**

A concern reported during the research was the possible difference in quality (e.g. peak stress) between laboratory mixing and field mixing of materials. The importance of the mixing process was studied by Efrem (2000), who argued that stir-action type mixers, such as the Hobart® mixer used in the laboratory study (Section 3.2.3.3), produces mixes of lower quality than other type of mixers (e.g. pugmill mixers). Efrem reported that producing foamed bitumen mixes with a pugmill mixer yields Unconfined Compressive Strength (UCS) specimens of about 30% higher resistance than specimens prepared using a stir-action mixer.

In the CAPTIF experiment the difference in mixing quality between laboratory and field was compared using the ITS values measured in both group of tests. Both groups of specimens were prepared under nominally identical conditions, using vibratory compaction and cured for 14 days at room temperature (20 °C). Although the bitumen contents used in the laboratory study (0, 1, 2, 3 and 4%) and in the field (1.2, 1.4 and 2.8%) were not the same, the results show consistency between both set of specimens (Figure 4.20). The results show that the laboratory mixing procedure presented in Section 3.2.3.3 yields mixes of similar quality to those prepared in the field using the pavement recycler (Section 4.4.3).

4.8.3 **Pavement performance and laboratory testing**

The pavement test results presented in chapter 4 indicate that stabilization using foamed bitumen and 1% cement improved the performance of the pavements. The rutting of sections B12C10, B14C10 and B28C10 was consistently lower than in the other three sections.

Materials without cement showed comparatively poor behaviour in the laboratory tests, which indicates that cement is an important contributor for developing the indirect tensile strength (Figure 4.20) and the permanent deformation resistance of the materials studied (Figure 4.22). However, sections B00C00 and B22C00, without cement, both performed fairly well in the CAPTIF tests in comparison. This could be explained by the lower moisture contents obtained in sections B00C00 and B22C00 after construction, which were approximately 2% lower (i.e. approximately one half) than those from the other sections (see Figure 4.15, Figure 4.43 and Figure 4.49).

The laboratory tests showed different trends for materials with 1% cement. The ITS results for 1% cement indicate that at higher foamed bitumen contents the strength of the materials increases (Figure 4.20). This is the normal behaviour of foamed bitumen mixes for which strength increases to an optimum bitumen content, after which the ITS value decreases. Conversely, permanent deformation RLT specimens at 1% cement show that the higher

the bitumen content, the lower the permanent deformation resistance (Figure 4.22). In addition, the average Resilient Modulus measured during the RLT tests (Figure 4.23) shows a peak in the specimen with 1.4% bitumen and 1% cement (508 MPa), and decreases in the specimen with 2.8% bitumen and 1% cement (413 MPa), which is only 78 MPa (18%) higher than the average resilient moduli from the other specimens at 1% cement, indicating that the effect of foamed bitumen is low in comparison with the effect of 1% cement, which approximately doubles the average Resilient Modulus from 197 MPa to 432 MPa. The drawback of the RLT testing results obtained for this experiment is that only one specimen was tested after 28 days of curing. However, comparable RLT trends (permanent deformation and resilient modulus) were also observed in the test on laboratory mixes reported in Chapter 3, in which higher foamed bitumen contents yield higher final permanent deformation (Figure 3.17 and Figure 3.18).

4.8.4 **Strain, laboratory and deflection measurements**

The elastic deformations measured in the laboratory in resilient modulus tests are somewhat related with the strains measured in the field using the Emu strain system, at different locations of the pavement as illustrated in Figure 4.50. The compressive vertical strains collected from each pavement section at the basecourse layer (depth=112.5 mm, Figure 4.39), approximately follow the general trend of the strains measured in RLT laboratory tests, presented in Figure 4.24, indicating that in the laboratory and in the field, the foamed bitumen content has a less significant effect on the compressive resilient strains of the mixes in comparison with the effect of 1% cement, as previously discussed in Chapter 3 (Section 3.3.4.2 and Section 3.3.6). The measurements also indicate that compressive resilient strains measured in the laboratory using the RLT test describe the real vertical compressive strains measured in the pavement relatively well (increase in strains with increase in the foamed bitumen content).

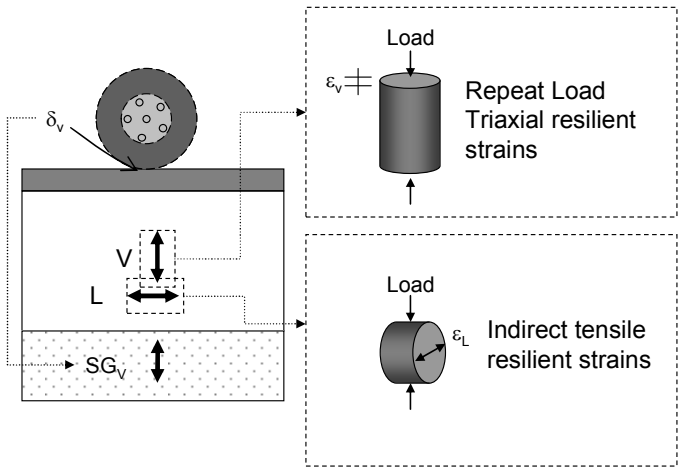

Figure 4.50 Relationship between pavement and laboratory strain measurements

The longitudinal tensile strains measured at 150-mm depth from the top of the basecourse (Figure 4.40) follow the trend of the Indirect Tensile Resilient Modulus Test presented in Chapter 3 (Figure 3.10), and the ITS tests (Figure 4.20). In Figure 3.10, an increase in foamed bitumen content from 0 to 3% yields an increase in the indirect tensile resilient modulus from approximately 2,400 to 6,400 MPa (i.e. a 2.7-times decrease in resilient strains), while the longitudinal tensile strains in the pavement decreased from approximately 340 μm/m to 120 μm/m (i.e. 2.8-times decrease) for an increase in the foamed bitumen content from 0 to 2.8%. These results indicate that indirect tensile resilient modulus tests could describe the trends of the longitudinal strains measured in the pavement.

The vertical strains measured at the top of the subgrade (Figure 4.41) follow a similar trend to those of the FWD deflections (Figure 4.33) and CAPTIF Beam deflections (Figure 4.32) indicating the large effect of the subgrade on the elastic response of the pavements. The decrease in deflections was not captured by the vertical strain measurements in the basecourse at 112.5 mm depth. For instance, the lowest deflection was measured in section B28C10, but this lower deflection was not reflected in the compressive vertical strains in the basecourse (Figure 4.39). In other words, deflections were directly related

(R^2=0.90) to the vertical strains at the top of the subgrade (Figure 4.51) and to the longitudinal strains measured at the lower part of the basecourse (R^2=0.65).

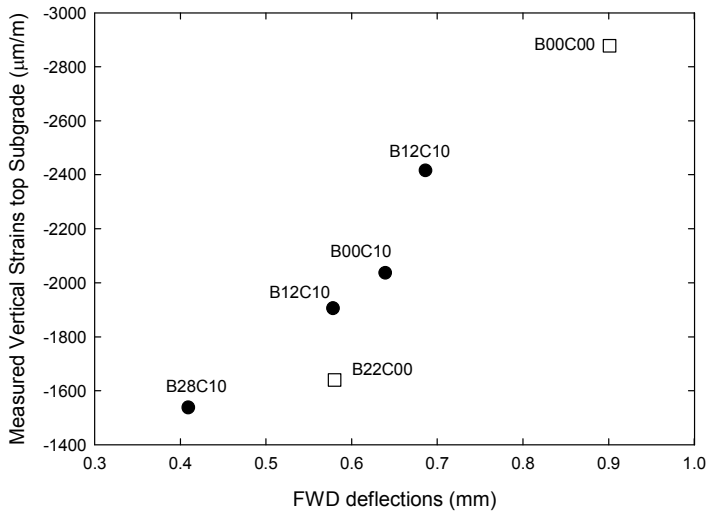

Figure 4.51 Relationship FWD deflections and vertical strains at the top of the subgrade

4.8.5 **Influence of foamed bitumen on the type of failure**

The deflection and performance results indicate that foamed bitumen decreases deflection, horizontal tensile strain at the bottom of the basecourse and vertical strain at the top of the subgrade (Figure 4.41). These effects suggest that foamed bitumen pavements are less likely to fail by fatigue cracking of the asphalt layers on top of the basecourse layer (lower deflection yields lower horizontal strains at the bottom of this layer), and permanent deformation of the subgrade layer (lower elastic strains normally lead to lower plastic strains).

In addition, foamed bitumen increases the elastic compressive vertical strains (Figure 4.39) in the middle of the basecourse, indicating that foamed bitumen decreases the vertical elastic modulus of this layer, and therefore increasing the risk of permanent deformation at the top of the basecourse. The horizontal strains at the bottom of the basecourse layer decreased with increase in the foamed bitumen content, suggesting that tensile fatigue cracking is likely to occur. However, no cracking was observed in the basecourse layers during

the post-mortem phase and permanent deformation at the top of the basecourse was the only distress observed in this layer for the sections with foamed bitumen and cement.

Overall, the results suggest that the optimum foamed bitumen content is 2.8%, because section B28C10 showed the lowest surface deformation, lowest deflection, lower vertical strainat the top of the subgrade and lowest tensile horizontal strain at the bottom of the basecourse. Also, it provides low moisture sensititvity in comparison with section B12C10.

4.8.6 **Stress dependency of the subgrade layer**

The vertical strain profiles show a rapid decrease of the subgrade strains with increase in depth (Figure 4.35 and Figure 4.36). The decrease in measured vertical strains was compared with the calculated vertical strains using a simple pavement model of Section B00C10 created in MePads (CSIR 2006), which is a software for pavement analysis and design based on linear elastic theory. The properties of the model are listed in Table 4.9. For the analysis, a single layer of elastic modulus of 50 MPa was used to model the subgrade layer. The load applied on the pavement model was a dual-wheel load of 60 kN, with a contact pressure of 750 kPa, similar to the load applied in the CAPTIF experiment after 500,000 load cycles.

Table 4.9 Properties of MePads model

Section	Thickness (mm)	Elastic Modulus (MPa)	Poisson Ratio
Asphalt	50	1000	0.40
Basecourse	200	200	0.35
Subgrade	1300	50	0.35

The calculated vertical strains, calculated vertical stress and measured vertical strains of the subgrade are plotted in Figure 4.52. The vertical stresses are depicted on a different scale, plotted at the right axis of the figure.

The results of the analysis show that in comparison, the measured vertical strains decrease at a higher rate with depth than calculated vertical strains. This behaviour is caused by the high stress-dependency of the subgrade layer, shown in the Triaxial Resilient Modulus test conducted on the subgrade specimen, which was part of the laboratory testing of pavement materials in Section 4.5.1.2 (Figure 4.25). Using the calculated vertical stress and the measured vertical strains, the resilient moduli of the subgrade were calculated at 300 mm, 350 mm, 450 mm, 550 mm and 650 mm, listed and plotted in a separate small chart at the bottom part of the figure. For instance, the elastic resilient modulus at 300 mm depth is the quotient between the calculated vertical stress (90 kPa) and the estimated measured vertical strain (2500 mm/m), which yields E=36 MPa. Results show that resilient modulus almost doubles with an increase in depth from 300 to 550 mm, as depicted in the small bar plot. The important stress dependency of the subgrade should be taken into account in the modelling of the pavement.

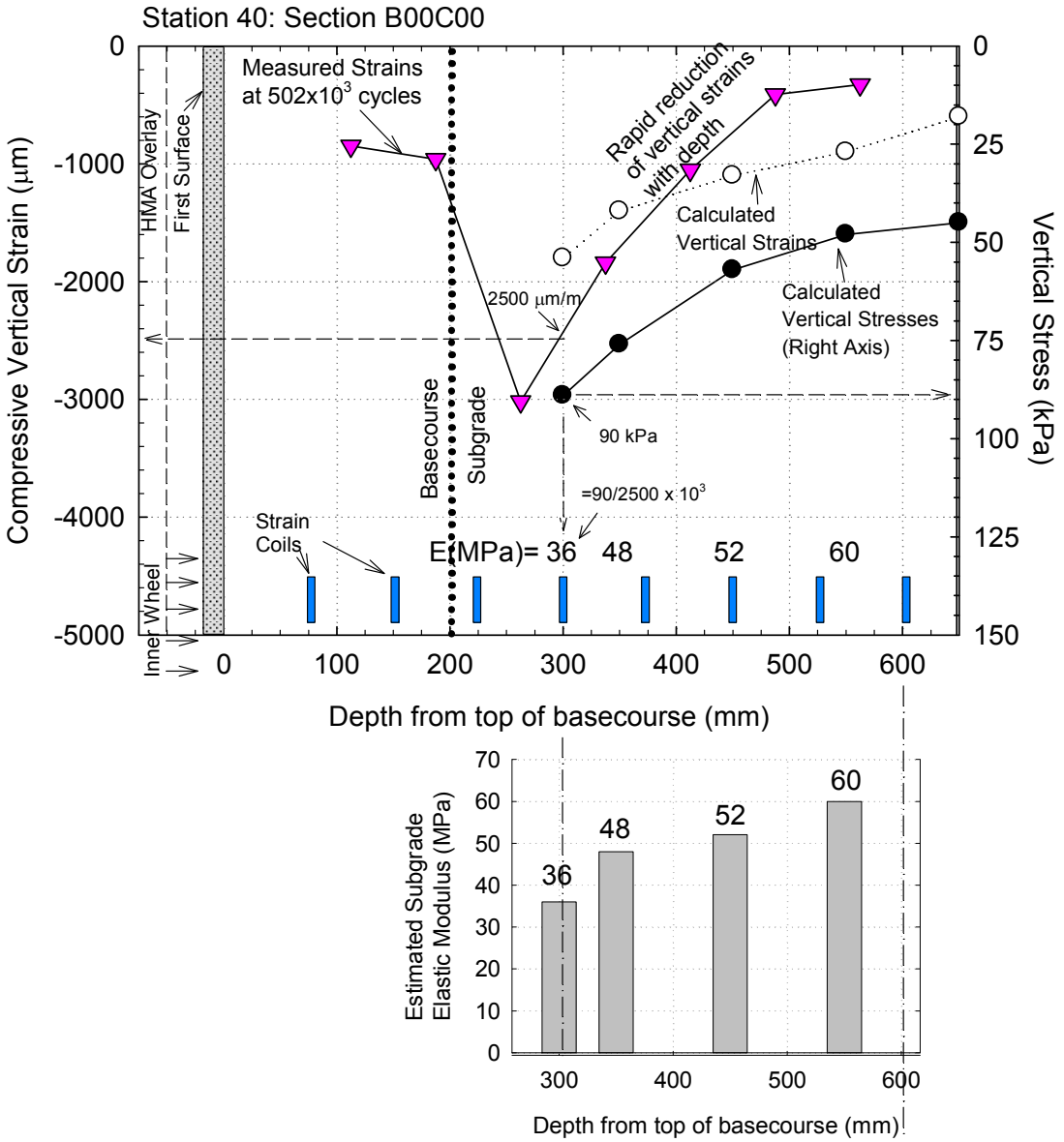

Figure 4.52 Comparison between real vertical strains in the subgrade and predicted vertical strains, and estimated variation in elastic moduli

4.9 Summary and concluding remarks

A full-scale experiment on foamed bitumen pavements with different binding contents has been presented in this chapter. The following conclusions are drawn from the results presented here:

- The rutting depth measured in sections B12C10, B14C10 and B28C10, after the application of 1,326,000 load cycles (5,710,000 ESAs) was the lowest, showing that the addition of foamed bitumen improved the

performance of the materials with 1% cement studied in this research. Sections B00C10, B22C00 and the control untreated section (B00C00) showed larger rutting and heaving by the end of the test. Only 1 mm of difference was observed within the sections stabilised with foamed bitumen and 1% cement.

- Pavement section B28C10 was designed to carry 1,000,000 ESAs of 80 kN with two design methods. However, after the application of 5,710,000 ESAs rutting depths of 7-8 mm were observed, indicating that current design methods for foamed bitumen pavements are over-conservative.

- To differentiate the rutting performance of the sections stabilized with foamed bitumen and cement, water was introduced through surface cuts. After the application of additional accelerated traffic load, section B12C10, the section with the lowest foamed bitumen content, started to show surface cracking, while sections B14C10 and B28C10 performed well, indicating that increase in foamed bitumen content reduces the moisture susceptibility of pavements.

- The deflections of section B28C10 were one half to those of the untreated section (B00C00). Deflections decreased with increase in the bitumen content.

- The ITS values of section B28C10 were double those of sections B12C10 and B14C10, and the ITS values from section B22C00 were the lowest. The results indicate that ITS was a reasonably good predictor of the general performance of the pavements studied (deflections and surface deformation), the highest ITS was measured in the section with the lowest deflection, rutting and moisture susceptibility.

- The triaxial (RLT) testing showed that the addition of 1% cement significantly enhanced the quality of the foamed bitumen mixes. However, the results obtained from the specimens with 1% cement at different bitumen contents showed that an increase in foamed bitumen content increases the permanent deformation in the laboratory triaxial compression tests. The resilient modulus values measured during the triaxial testing could not detect the important improvement in stiffness of section B28C10.

- The basecourse strain measurements follow relatively well the trends observed in most of the laboratory results. The indirect tensile resilient modulus and the ITS results show a relationship with the longitudinal strains measured at the lower part of the basecourse, while the compressive vertical strains are related to the resilient strains measured in the RLT tests. Little difference was observed in compressive vertical strains measurements in sections with 1% cement and different foamed bitumen contents, indicating that foamed bitumen has little effect when the basecourse is loaded in compression. The vertical compressive strains measured at the top of the subgrade followed the surface deflection tests, indicating that surface deflection was controlled by the subgrade elastic response.

This page is intentionally left blank

5 Interpretation of pavement performance and modelling

5.1 Introduction

This Chapter presents the interpretation and modelling of the pavement performance using both laboratory and CAPTIF data. The interpretation was conducted for mixes with 1% cement, at different foamed bitumen contents. The chapter first introduces the I_1-$J_2^{(1/2)}$ stress diagrams used to plot the stress paths induced by the moving wheel loads in CAPTIF pavements, which are compared with the shear stress failure of the mixes estimated from the laboratory testing. The relative damage of the pavements was estimated by the stress ratio, which is the quotient between the actual stress applied and the stress at failure.

The interpretation of results is followed by a three dimensional Finite Element Modelling (FEM) of the CAPTIF pavements, in which the effect of the foamed bitumen content on the total surface deformation was calculated and compared with the trends observed in real CAPTIF pavements. In the FEM, the elastic moduli of the pavement materials were back-calculated using CAPTIF data (beam deflections, pavement strains) and the fundamental shear properties (angle of internal friction and cohesion) of the pavement materials were introduced using the Mohr-Coulomb failure criterion models.

The last part of the chapter presents a simplied two-dimensional FEM analysis of pavements. The analysis consisted of a parametric study, in which the effect of the angle of internal friction and the elastic modulus of the basecourse on the plastic response of the pavement was studied. The parametric study is followed by the modelling of the cyclic loading of the

CAPTIF pavement models, in which instead of one single load, several load repetitions of different magnitudes were applied to simulate the expected wheel load applied in the real pavement. In this last part of the modelling, cracks were introduced into the pavement surface, and the response was compared with no-cracking conditions.

5.2 Interpretation of pavement experimental results by stress ratio analysis in I_1-$\sqrt{J_2}$ diagram

5.2.1 Introduction

The experimental results presented in the previous chapters indicate that 1% cement improves the performance of foamed bitumen mixes in both the laboratory and CAPTIF experiment. Consequently, and also because the addition of 1% cement to foamed bitumen mixes is the common practice in New Zealand (Chapter 1), the interpretation of pavement performance was conducted on three pavements tested in the CAPTIF experiment with a common 1% cement: B00C10 (0% foamed bitumen, 1% cement), B14C10 (1.4% foamed bitumen, 1% cement) and B28C10 (2.8% foamed bitumen, 1% cement).

The foamed bitumen mixes with 1% cement tested in the experimental study have been loaded under a wide range of conditions. In the laboratory, the mixes were cyclically and monotonically loaded, applying relatively simple triaxial and indirect tensile stress conditions. In the CAPTIF, the loading applied by the vehicle wheels induced more complex stress conditions than those applied in the laboratory, imposing varying magnitudes of vertical, horizontal and shear stresses. While horizontal compressive stress conditions are likely to occur at the top of the basecourse layer, horizontal tensile stresses would typically occur at the bottom of the stabilised layers (Figure 5.1).

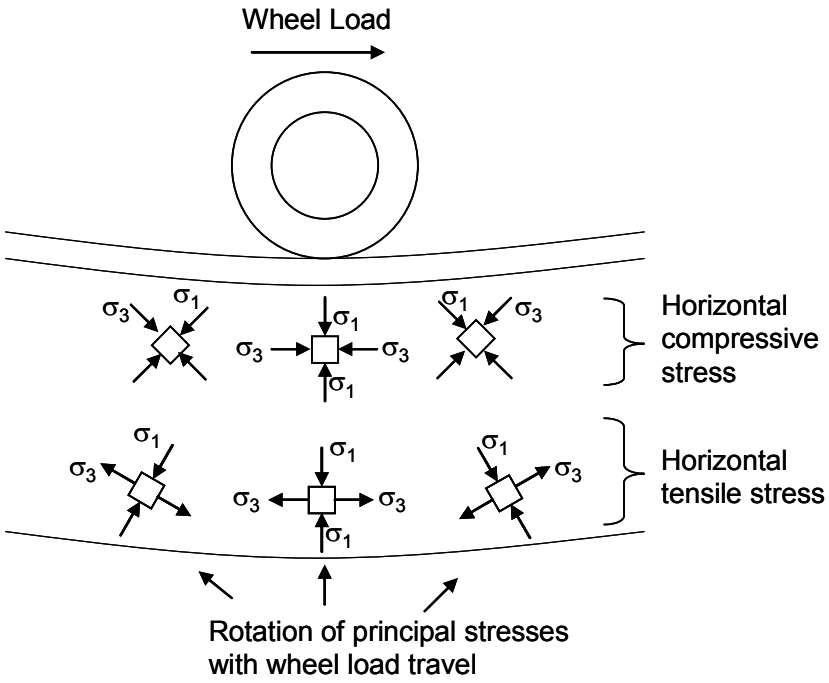

Figure 5.1 Stress state of a pavement under moving wheel load

To understand both laboratory and full-scale experimental results, a stress analysis similar to that previously introduced in Chapter 3 was conducted with CAPTIF pavements. The stress paths induced by the moving wheel load in the basecourse layer were plotted in I_1-$J_2^{(1/2)}$ stress diagrams, and later compared with the shear stress failure of the foamed bitumen mixes at different bitumen contents, by using a stress ratio analysis.

5.2.2 **Stress ratio analysis of basecourse layers**

The stress ratio analysis consisted of the following steps:

- Calculation of principal stresses in the basecourse layer, at different depths (Z) and longitudinal (X) locations of the pavement.
- Calculation of I_1 and J_2 stress invariants, for each of the previously mentioned pavement locations.
- Plotting the stress state of the pavement in a I_1-$J_2^{(1/2)}$ stress diagram.

- Calculation of the stress ratio, by using the peak calculated stress condition of the pavement, at different depths, and the shear failure stress condition of the basecourse.

The first three steps are introduced with an explanatory stress analysis conducted on a hypothetically chosen pavement model, presented in Figure 5.2. The pavement considered for the analysis consisted of a 50-mm asphalt surface (E=1,000 MPa), 200-mm basecourse (E=1,000 MPa) and a 1300-mm subgrade layer (E=30 MPa). The load applied was a 60-kN dual-tyre, with a contact (tyre-pavement) pressure of 750 kPa. The model was created in "mePads" (CSIR 2006), a software for pavement analysis and design based on linear elastic behaviour of layered materials. In the pavement model, the stresses were calculated at four depths (z-axis), measured from the top of the basecourse (37.5 mm, 75.0 mm, 112.5 mm and 150 mm), and at several longitudinal positions (x-axis), ranging from 0 mm (directly under the wheel), where the stress magnitude reaches a peak, to 1000 mm, where the stress is approximately zero. The other longitudinal positions where the stresses were calculated were 50 mm, 100 mm, 150 mm, 200 mm, 250 mm, 300 mm, 400 mm and 500 mm, depicted in Figure 5.2. At each X-Z location the six components of the stress tensor and the three principal stresses, σ_1, σ_2 and σ_3, were calculated and converted to I_1 and J_2 stress invariants of the stress tensor, using formulas 2.11 and 2.15 previously presented in Chapter 2:

$$I_1 = \sigma_1 + \sigma_2 + \sigma_3$$

$$J_2 = \frac{1}{6}\left[(\sigma_1 - \sigma_2)^2 + (\sigma_2 - \sigma_3)^2 + (\sigma_1 - \sigma_3)^2\right]$$

The stress paths induced by the moving wheel loads are presented in Figure 5.2. The peak on principal stresses, together with the calculated stress invariants I_1 and J_2, calculated at X=0, directly under one of the two wheels (Y=0), are summarized in Table 5.1. σ_1, σ_2 and σ_3 are the major, intermediate and minor principal stresses. The soil mechanics sign convention was adopted for the calculations, in which compressive stresses are positive and

tensile stresses are negative. The calculations show decrease of the major (σ_1) principal stress with increase in depth, while the other two principal stresses change from compressive stresses in the upper part of the pavement to tensile stresses at the bottom. The direction of the σ_1 principal stress axis coincides with the vertical axis when calculated directly under the wheel (X=0), while the other two principal directions σ_2 and σ_3 are in the horizontal directions corresponding to X and Y axes respectively.

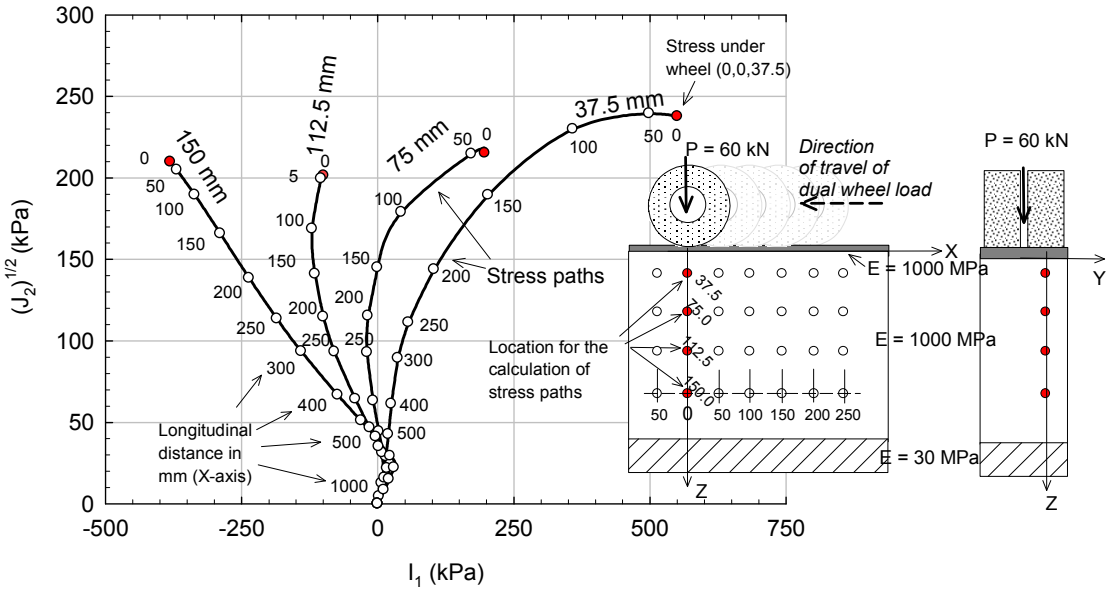

Figure 5.2 Stress path for moving wheel at different pavement depths for a 60 kN load

Table 5.1 Calculated principal stresses and I_1-$J_2^{(1/2)}$ stress invariants for X=0

X (mm)	Z (mm)	σ_1 (kPa)	σ_2 (kPa)	σ_3 (kPa)	I_1 (kPa)	$J_2^{(1/2)}$ (kPa)
0	37.5	474.9	67.73	54.47	597	239
0	75.0	341.84	1.04	-20.51	322	203
0	112.5	237.75	-48.49	-77.54	112	174
0	150.0	161.42	-98.42	-137.57	-75	163

The four curves depicted in Figure 5.2 represent the stress paths at 37.5 mm, 75 mm, 112.5 mm and 150 mm depth (from right to left). The curves were plotted by connecting each of the points that represent the stress condition of the pavement at different longitudinal (X) distances, from 1000 mm up to 0

mm (X=0 is the position directly under the wheel). The calculated stress paths are curved, unlike the simpler straight-line paths applied in the laboratory tests presented in Chapter 3 (Figure 3.31), showing the more complex stress conditions applied in real pavements. Nevertheless, the stress paths presented ignore other effects that could yield even more complex loading conditions, such as the non-uniform contact stress between the tyres and the pavement surface and the dynamic load applied by the wheels. The two curves at the right off the figure (depth = 37.5 and 75 mm respectively) represent a compressive condition ($I_1>0$) while the other curves a tensile condition ($I_1<0$), indicating that about one half of the hypothetical basecourse depth is loaded under tensile stresses, caused by the weak support of the subgrade (E=30 MPa).

For the calculation of the stress ratio, the shear failure of the mixture, obtained from laboratory monotonic compressive triaxial tests, was compared with the stress state of the basecourse. If the stress ratio is low, the mix will develop some plastic deformation for a finite number of load repetitions, but the response will remain essentially resilient after the initial loading. At higher stress ratios, the plastic deformation increases, up to a stress ratio limit, in which permanent deformation will accumulate rapidly. Therefore, the stress ratio has been considered as an approximate measure of the relative damage that will result of repeated load applications at lower stress conditions than the peak stress triaxial monotonic conditions.

The stress ratio was calculated using the stress paths induced by the moving wheel loads and the shear failure of the mixes, plotted in I_1-$J_2^{(1/2)}$ stress diagrams, as follows (Figure 5.3):

- A line was drawn between the origin (0) of the stress diagram and the peak stress of the stress path (A). The length of the 0A line (L) was considered as the magnitude of the actual stress applied.
- The line previously drawn was extended up to the intersection with the estimated shear failure (B). The distance between the origin and the

intersection of both lines (L') was considered as the magnitude of the maximum attainable stress failure.

- The stress ratio was then defined as the quotient L and L'.

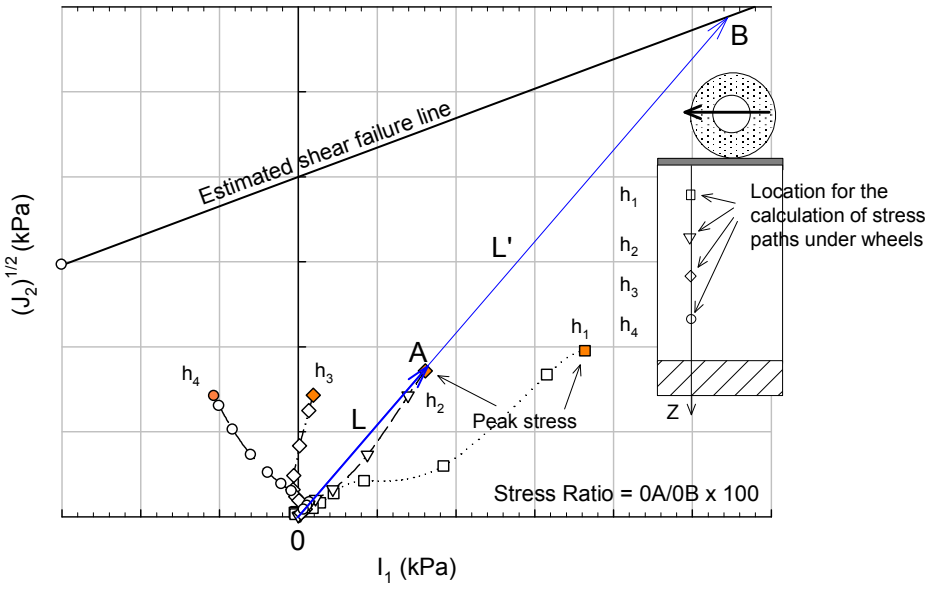

Figure 5.3 Calculation of the stress ratio at different depths

5.2.3 **Calculation of shear failure lines of CAPTIF pavements**

The shear failure of the foamed bitumen mixes was calculated for mixes with 1% cement at 0, 2 and 4% foamed bitumen content, at two compaction efforts, in Chapter 3. The foamed bitumen content of the pavement sections studied in this chapter is 0, 1.4 and 2.8% (B00C10, B14C10 and B28C10), with a common 1% cement, and therefore only the shear properties of the mix without foamed bitumen could be directly used for the analysis. The shear parameters of the other two sections, B14C10 and B28C10, were calculated by interpolating the angle of internal friction and cohesion from the available laboratory data. The shear strength parameters at low compaction effort were used, because the bulk densities obtained in those specimens are more similar to field densities than the bulk densities obtained from high compaction effort specimens (see Figure 4.18 and Figure 3.16).

5.2.4 **Assumptions adopted for the stress ratio analysis**

The stress ratio analysis is conducted for the interpretation of experimental results. Therefore, as in any other interpretation, some simplifications were made in the analysis:

- The shear failure lines were estimated using data from compressive triaxial tests. The failure state in a tensile stress condition (i.e. to the left from the origin in the I_1-$J_2^{(1/2)}$ stress diagram) is an estimation based on a linear extrapolation of the fitted data on the compression side.

- The shear failure lines were determined using laboratory mixed materials, compacted in the laboratory and cured for 28 days in sealed plastic bags. The shear failure line of the actual basecourse materials changes during the curing and loading of the pavements, and therefore is not strictly accurate.

- The pavement software used for the calculation of the stress paths is based on the linear elastic theory. The resilient modulus measured in triaxial tests (Figure 3.24, Figure 3.25 and Figure 4.23) suggests that foamed bitumen mixes are stress dependent, following a similar behaviour to that of unbound granular materials.

The analysis was conducted in the basecourse only, at specific locations (depths), ignoring the effect of loading in the other pavement layers, especially the clay subgrade layer because the purpose of the analysis is to determine the stress ratio of the foamed bitumen layer.

5.2.5 **Stress ratio in CAPTIF pavements**

The stress ratios were calculated at two stages of the CAPTIF experiment:

- Initial stage “20 mm/40kN”: When the surface of the pavement consisted of a 20-mm asphalt layer, and the SLAVE units were loaded with 40 kN.

- Final stage “50mm/60kN”: When the surface of the pavement consisted of a 50-mm asphalt layer, after the 30-mm HMA overlay, when the load of the SLAVE units was increased to 60 kN.

The elastic modulus of the pavement layers were back-calculated using both the vertical strains collected with the Emu strain system at different depths of the pavement, and the deflection bowls collected using the CAPTIF beam deflectometer. The back-calculation of the elastic properties is detailed later in Section 5.3.5.

The stress paths for the stress ratio analysis were calculated at longitudinal distances (in millimetres) of 0, 50, 100, 150, 200, 250, 300, 600 800 and 1000 from the vertical axis directly under one wheel (Y=0), at depths of 40 mm, 80 mm, 120 mm and 160 mm, measured from the top of the basecourse.

The stress paths calculated in pavement B00C10 are presented in Figure 5.4, together with the estimated shear failure line for the mix without foamed bitumen and 1% cement. The back-calculated elastic modulus of the basecourse was 400 MPa. For the 20mm/40kN case, the highest stress ratio was 66%, measured at 160-mm depth, followed by stress ratios of 42% and 20%, at 120 and 80 mm depth. For the case 50mm/60kN, the highest stress ratio was 85%, calculated at 160-mm depth, followed by stress ratios of 54% and 31% at 120 and 80 mm depths respectively. The stress ratios at 40-mm depth were not calculated in both cases, because the direction of the stress paths is almost parallel with the slope of the estimated failure line.

The calculations for pavement B14C10 are presented in Figure 5.5. The back-calculated elastic modulus of the basecourse was 475 MPa. The stress ratios between the induced stress paths and the shear failure lines were calculated and included in Figure 5.5. For the 20mm/40kN case, the highest stress ratio was 61%, measured at 160-mm depth, followed by stress ratios of 40% and 24% at 120 and 80 mm depth. For the case 50mm/60kN, the highest stress ratio was 75%, calculated at 160-mm depth, followed by decreasing stress

ratios of 53% and 33% at 120 and 80 mm depths respectively. The stress ratios at 40-mm depth were not calculated.

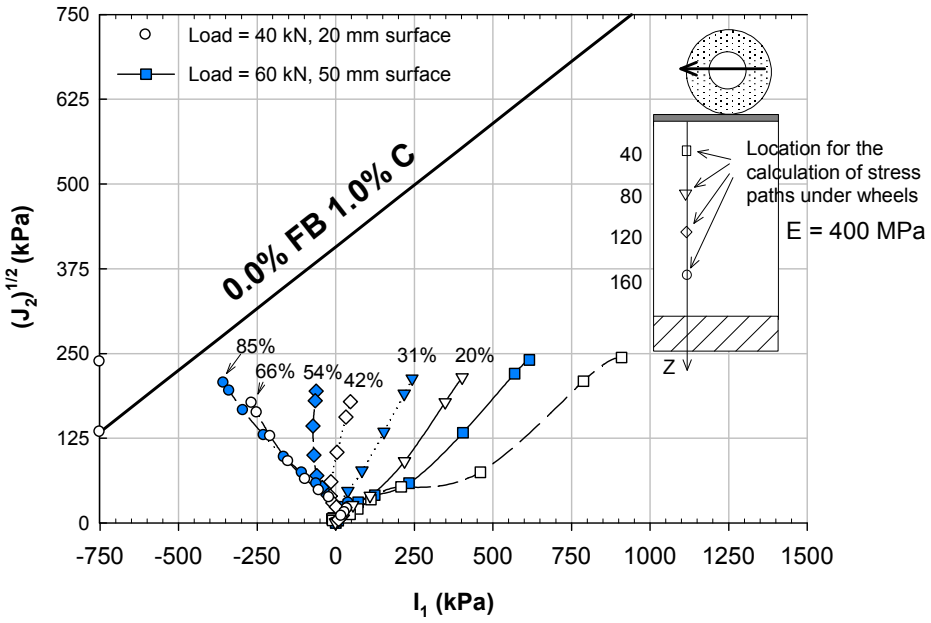

Figure 5.4 Stress paths during first and second phase of CAPTIF experiment at section B00C10 (40 and 60 kN load)

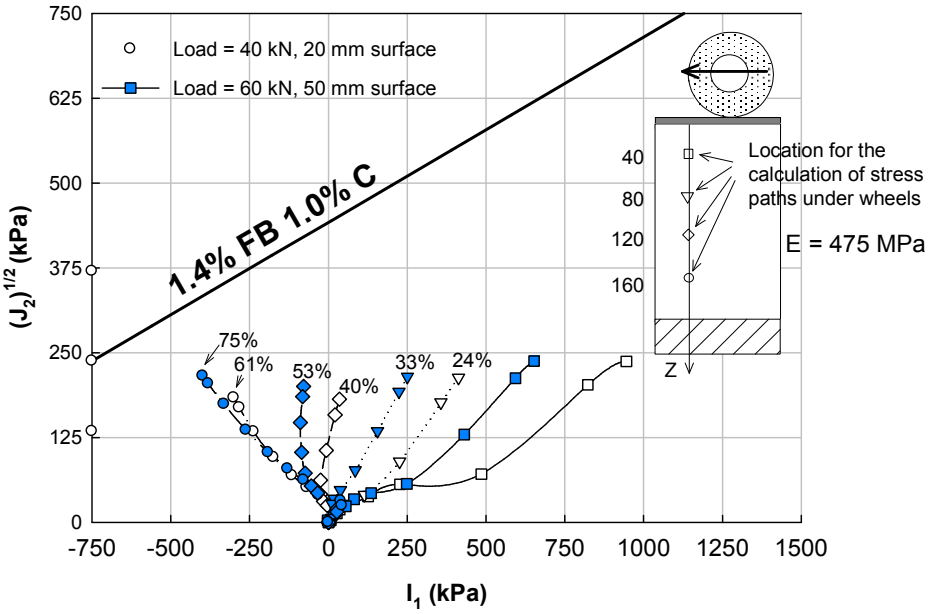

Figure 5.5 Stress paths during first and second phase of CAPTIF experiment at section B14C10 (40 and 60 kN load)

The calculations for pavement B28C10 are presented in Figure 5.6. The back-calculated elastic modulus of the basecourse was 1,000 MPa. For the 20mm/40kN case, the highest stress ratio was 52%, measured at 160-mm depth, followed by stress ratios of 36% and 28% at 120 and 80 mm depth. For the case 50mm/60kN, the highest stress ratio was 72%, calculated at 160-mm depth, followed by decreasing stress ratios of 51% and 34% at 120 and 80 mm depths respectively. A summary of the calculated stress ratios is listed in Table 5.2.

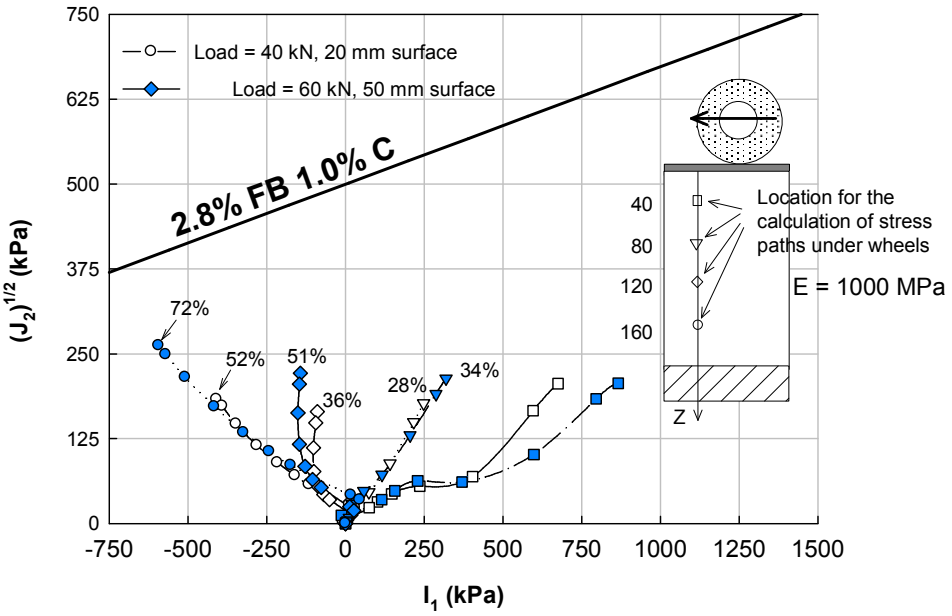

Figure 5.6 Stress paths during first and second phase of CAPTIF experiment at section B28C10 (40 and 60 kN load)

Table 5.2 Summary of estimated stress ratios in percent at different depths for pavements B00C10, B14C10 and B28C10

		Stress Ratio (%) in basecourse:		
Case	Depth (mm)	B00C10	B14C10	B28C10
20mm/40kN	160	66	61	52
	120	42	40	36
	80	20	24	28
50mm/60kN	160	85	75	72
	120	54	53	51
	80	31	33	34

5.2.6 **Damage associated to stress ratio calculations**

During the initial loading of the pavements, when the load was 40 kN and the surface layer was 20-mm thick, the three pavement sections showed low surface deformation in comparison with the unbound control section (B00C00). After 150,000 40-kN load repetitions, the surface deformation in

B00C00 was 6 mm, while in section B00C10 approximately 2.5 mm, and sections B14C10 and B28C10 showed a similar surface deformation of approximately 1.5 mm (Figure 5.7). This trend, in which the surface deformation depths of section B00C10 were higher than those measured in B14C10 and B28C10, remained constant throughout the pavement experiment. At 40 kN the highest stress ratio was calculated at 160-mm depth for the three sections, with a maximum value of 66% in section B00C10.

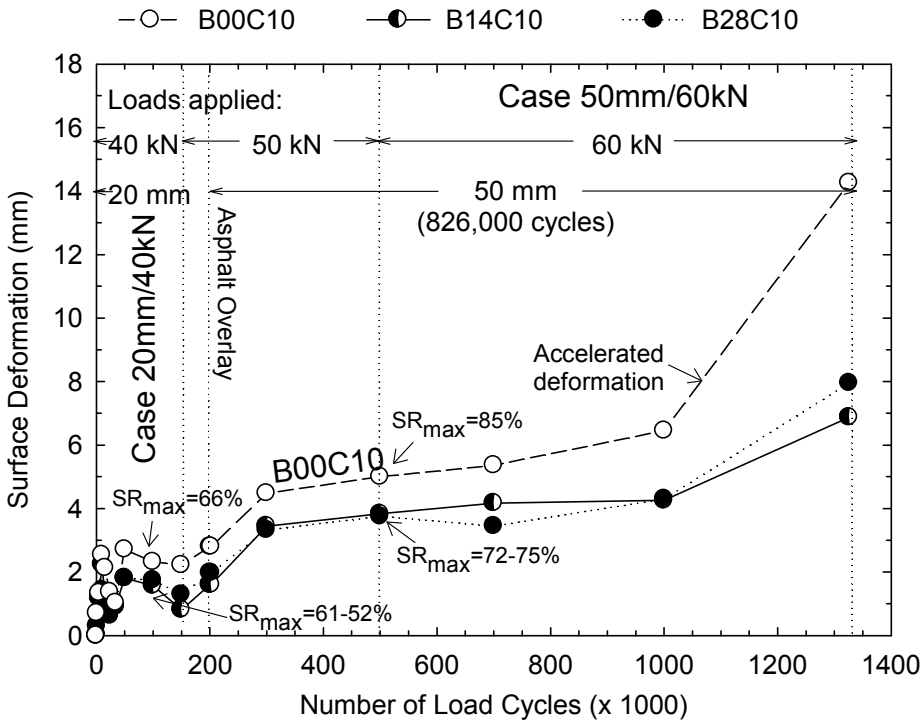

Figure 5.7 Average rut depth measured in sections B00C10, B14C10 and B28C10

When the load was increased to 60 kN (after 500,000 load cycles), and the surface layer was 50-mm thick, the initial surface deformation in B00C10 was approximately 5 mm, while in the other two sections this value was about 3.5 mm. The higher 60 kN load increased the working stress ratio in the three pavements. The most critical stress ratio was calculated at the bottom part of the basecourse, in section B00C10 (85%), while in B14C10 and B28C10 the calculated stress ratios were 72 and 75% respectively.

The performance of the pavements sections remained stable up to 1,000,000 load repetitions, in which B00C10 showed higher surface deformation (6.5 mm, versus 4.2 mm in sections B14C10 and B28C10). After 1,000,000 load repetitions (500,000 repetitions of 60 kN), pavement B00C10 started to show accelerated damage, with 18 mm of heaving and 15 mm of rutting on the surface, measured after 826,000 load repetitions of 60 kN. Conversely, after the same 826,000 repetitions of 60 kN, the rutting measured in sections B14C10 and B28C10 was 7 mm and 8 mm respectively, with a common 3 mm of surface heaving.

The stress ratios presented in Table 5.2 are plotted in Figure 5.8. The analysis shows that increasing the foamed bitumen content decreases the stress ratio in the lower part of the basecourse layer, while increases the stress ratio in the upper part of the layer. The stress ratio at the upper part is below 55% (from 31 to 34%, see Figure 5.8, which has been found a conservative boundary between a stable rate of permanent deformation and accelerated rate of permanent deformation of foamed bitumen mixes under repeated compressive triaxial loading (Jenkins et al. 2007). In other words, although the effect of foamed bitumen is a stress ratio increase at the top part of the pavement, where the predominant stress condition is compression, this value remains within the safe stress ratio range. Even though some plastic deformation will occur after the initial deformation, the response will remain essentially elastic. Conversely, the stress ratio at the bottom part of the pavement is more critical, closer to the estimated shear stress failure line of the mix, and therefore causing a higher relative damage in the basecourse layer. The increase in the foamed bitumen content from 0 to 2.8% reduces the stress ratio of the basecourse from 85% to 72% and consequently the damage applied after each load. In addition, the failure mode in compression is less critical than in extension, because in compression the particles can keep transferring stresses after “failure”, whereas a tensile failure would crack the pavement layer, limiting the transmission of stresses throughout the basecourse layer and transferring the stresses to the bottom layers of the pavements, causing further damage.

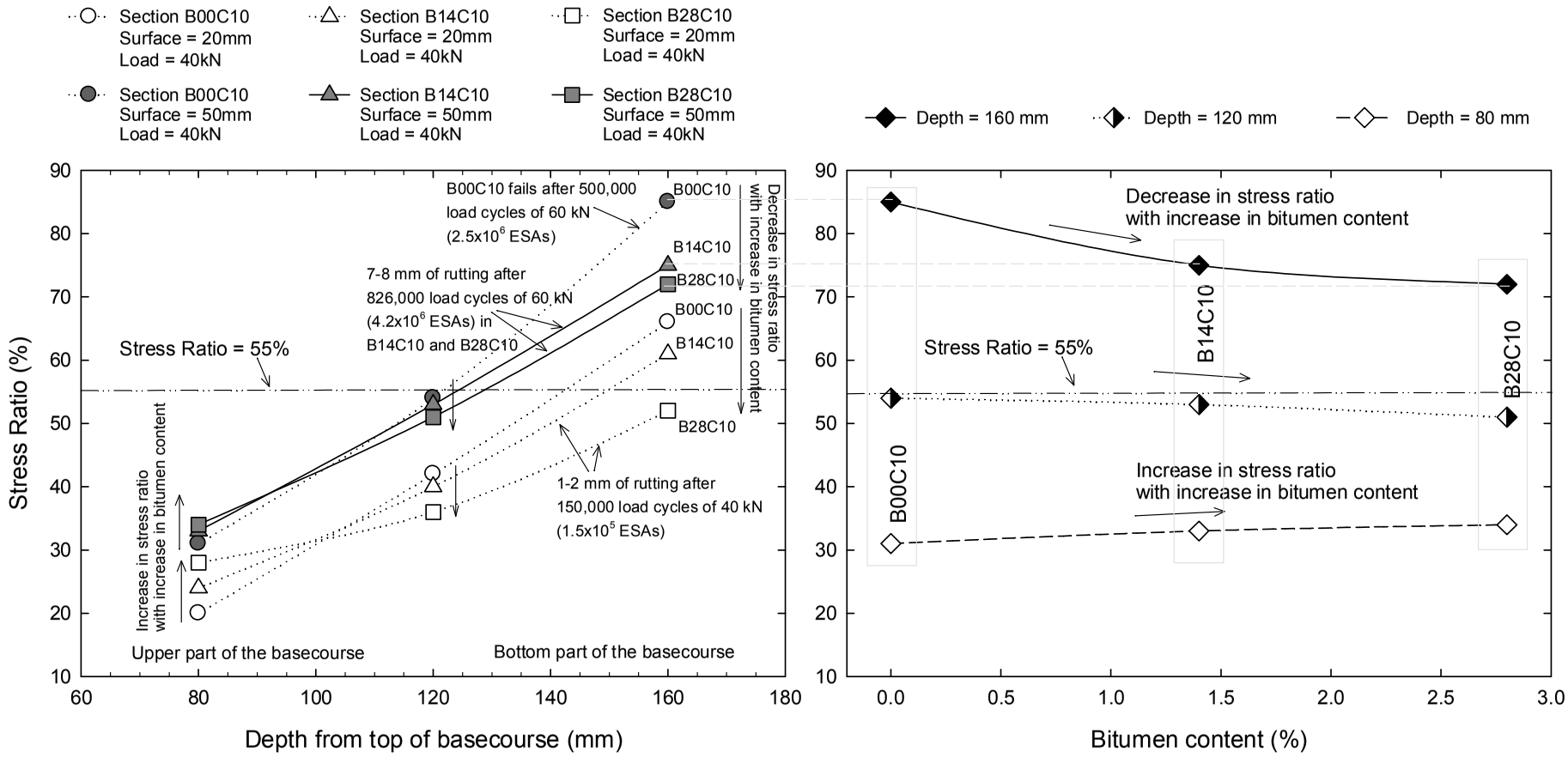

Figure 5.8 Summary of stress ratios at different depths for sections B00C10, B14C10 and B28C10

5.3 Three-dimensional finite element analysis of CAPTIF pavements (monotonic load)

5.3.1 Introduction

Three dimensional finite element analysis of pavements B00C10, B14C10 and B28C10 are presented in this section. The main advantage of using a finite element model over common pavement softwares based on linear elastic analysis, is that plastic models can be incorporated into the pavement layers, and permanent strains can be directly estimated.

The finite element models were created using ABAQUS, a general purpose finite element code, which has been used by other researchers in simulating the response of granular pavements (Section 2.7.4). The plastic material model selected from ABAQUS for the three-dimensional analysis was the Mohr-Coulomb model. The input parameters required by the Mohr-Coulomb model, are the angle of internal friction, dilation angle and cohesion. The plastic parameters for the basecourse layers were estimated using monotonic triaxial test data from the laboratory experimental work (Chapter 3). For the asphalt and subgrade layers, the plastic parameters were estimated using data found in the literature. The elastic moduli were back-calculated using CAPTIF beam deflection bowls and measurements of the elastic vertical strains at different depths.

The finite element modelling, as any other numerical model, is a simplification of the CAPTIF experiment or physical model, and its final purpose is to provide further interpretation of the experimental results. Even though the model tried to simulate CAPTIF conditions as accurately as possible, simplifications were made:

- The simulation considers the application of one load repetition
- The elastic behaviour of materials was modelled as linear
- The dynamic effects were ignored

- The tyre-pavement contact was considered uniform, even though recognized as non-uniform (De Beer 1997)

It is important to notice that isotropic-linear elastic behaviour was assumed in the pavement layers, even though unbound granular and subgrade materials are recognized as non-linear. This simplification was adopted because ABAQUS plasticity material models normally work with isotropic-linear elastic materials only.

5.3.2 **Features of the finite element model**

A three-dimensional (3D) model was created using the ABAQUS/CAE graphical user interface. The 3D formulation was chosen to model the dual tyre assembly in CAPTIF. To reduce the computational effort, a quarter-model was developed using two planes of symmetry. The load, modelled as two squares 200 mm x 200 mm dimensions, had to be reduced to a quarter as presented in Figure 5.9

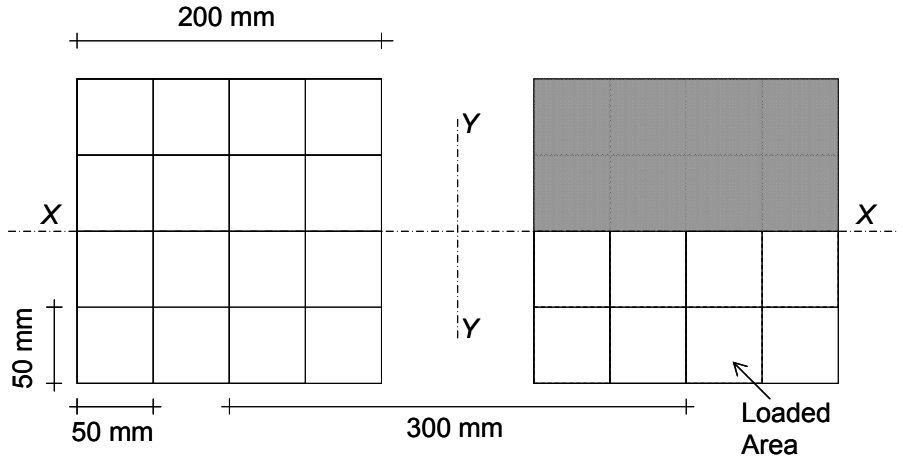

Figure 5.9 Loaded area in the quarter-model finite element model

The thickness of the stabilised basecourse layer was 200 mm, modelled with 4 elements 50-mm high, and the asphalt layer with one element of 50-mm height. The horizontal dimensions were set to be the same as the vertical dimensions. In order to reduce the required computation effort, the element dimensions in the subgrade and in the basecourse that are not close to the loaded area were increased to 100 mm (Figure 5.10).

One of the features of ABAQUS is the ability to tie discrete blocks of elements together. This is achieved by defining two surfaces, one each on the outer faces of two adjacent blocks of elements. One surface is defined as the "slave" surface and the other as the "master" surface. The two surfaces are then tied together by mapping the nodes on the slave surface to phantom nodes on the master surface. The phantom nodes are created by interpolating the degrees of freedom and reaction forces from adjacent nodes to the phantom node. This feature was used in the 3D model to tie the surface layer (Block 1), the area near to the wheels (Block 2) and the rest of the model that includes part of the basecourse and the subgrade (Block 3), presented in Figure 5.10).

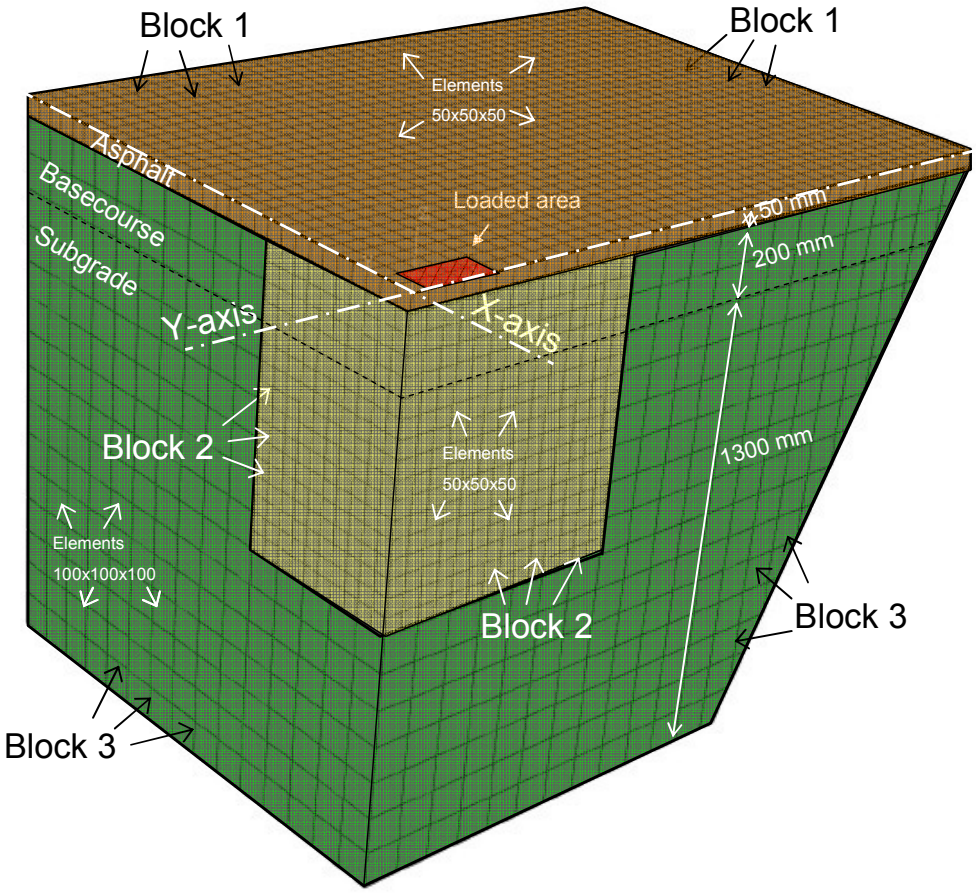

Figure 5.10 Three dimensional view of the quarter finite element model

The models were created with isoparametric solid (hexahedral) elements that have been formulated for the analysis of general displacement/stress problems. Hexahedral cubic elements were selected as these types of elements provide a more accurate solution for straight-forward problems that do involve complex contact conditions, impact, or severe element distortions. Quadratic elements are defined by 20 nodes and solved numerically using Gauss integration over 8 points inside the element (Steven 2005).

For Block 1, 1200 hexahedral cubic elements were used (size 50 mm); for Block 2, 2240 with the same geometry as Block 1; while for Block 3, 3485 hexahedral and wedge elements of average size 100 mm were adopted. The loaded area is composed of 8 elements in each quarter of the model (see Figure 5.9 and Figure 5.10). The area is calculated on the basis of the applied load per dual tyre and the tyre pressure (30kN/750kN) yielding a surface of 0.4 m^2.

5.3.3 **Geometry and boundary conditions**

The size of the 3D model was defined using the pavement tank geometry. Using the dimensions shown in Figure 4.9, the width of the model was set at 2000 mm and the length of the model at 1500 mm. The thickness of the subgrade and basecourse layer was 1,300 mm and 200 mm respectively. The thickness of the asphalt surface was set at 50 mm. The rigid boundaries of the concrete tank were simulated in the finite element model so that the bottom base of the subgrade is prevented from axial movements in three directions. The sides of the model are prevented from any movement perpendicular to the concrete wall.

5.3.4 **Verification of the finite element model with linear elastic software**

Some preliminary checks were conducted to verify the accuracy of the three dimensional finite element model. The elastic vertical strains under one tyre, the surface deflections between the wheels and the vertical stress under one tyre were calculated using the finite element code, and compared with the solutions provided by the linear elastic closed-form solution software MePads (CSIR 2006).

A simple pavement model was constructed for comparison and consisted in a 50 mm asphalt layer (E=1,000 and ν=0.35), 200 mm basecourse (E=300 and ν=0.35) and a 1300 mm subgrade (E=80 and ν=0.40). MePads assumes semi-infinite pavement layers, and to simulate the stiff concrete wall at the bottom of the pavement an additional stiff layer (E=10,000 and ν=0.35) was included.

The vertical strains and stresses were calculated every 100 mm depth under one of the tyres; and the vertical surface deflections each 100 mm in a longitudinal axis parallel to the direction of travel of the wheels. For the vertical strains, the minimum and maximum difference between the finite element model and MePads solutions was -0.2% and +5.4%. For the surface deflections the minimum and maximum difference was -6.4% and +8.3%, while for the vertical stresses the minimum and maximum difference was +2.9% and +10.9%.

The results obtained for the comparison provided a reasonable match and the differences found are mainly caused by the different boundary conditions of the finite element model compared to the layered software. In this last case, the layers are considered infinite in the horizontal direction while the finite element model has constrained boundary conditions. Another factor that affects the results is the shape of the wheel print, which was considered circular (radius=212 mm) for the linear elastic software and rectangular (200 mm x 200 mm) for the finite element analysis (Gonzalez et al. 2007), as illustrated in Figure 5.11.

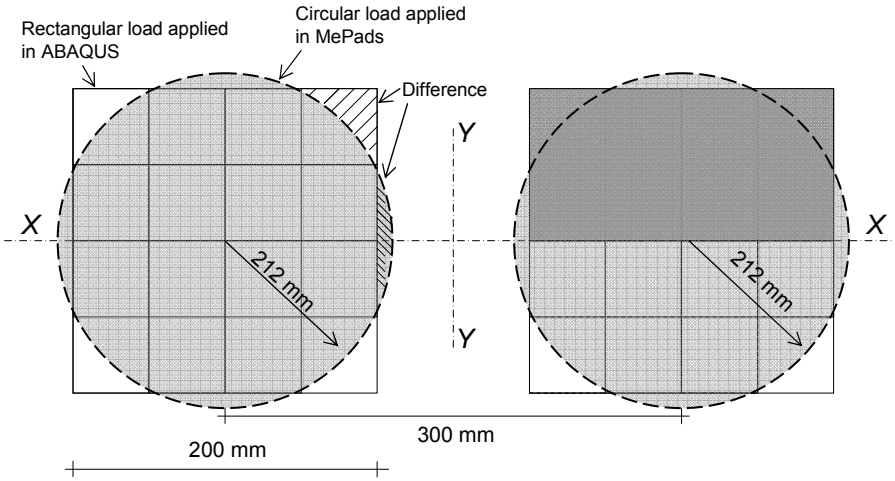

Figure 5.11 Wheel prints adopted for the finite element analysis (rectangular) and the linear elastic analysis (circular)

5.3.5 **Back-calculation of the elastic parameters of the pavement layers**

The modulus of elasticity of the pavement layers was characterised using in-situ measurements taken during the last part of the full-scale experiment (after the application of $1x10^6$ load cycles). Both surface deformation bowls and vertical strain profiles collected using the CAPTIF beam deflectometer and the Emu strain soil system were used for this purpose. For the beam measurements, the wheels were located at the same position in which the vertical strain data were collected (i.e. the maximum vertical deflection was measured between the wheels while one of the wheels was exactly located above the strain coil arrangement, see Figure 5.12).

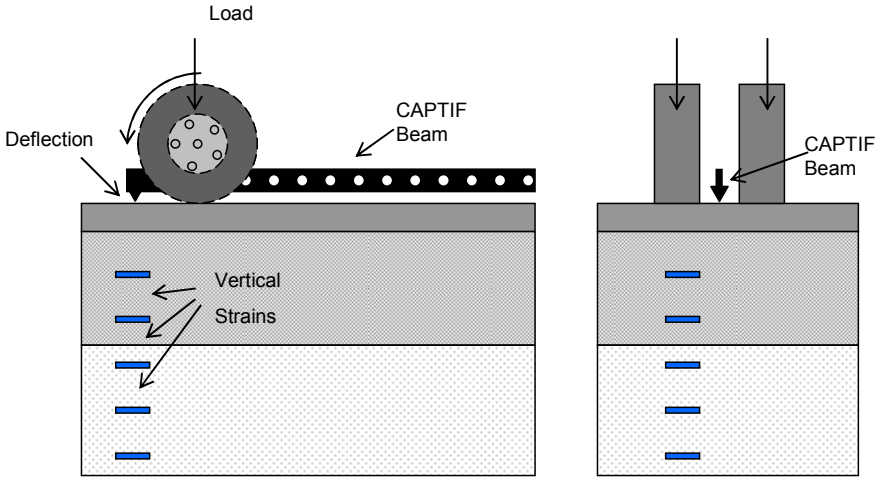

Figure 5.12 CAPTIF Beam and vertical strains measurements used for the back-calculation of the elastic properties of the pavements

By trial and error of the elastic moduli of each pavement layer it was intended to match both the measured vertical strains (with the Emu strain soil system) and surface deflections (using CAPTIF beam) with the finite element model response. The surface response (deflection bowl) calculated from the finite element model was collected each 50 mm, following a longitudinal axis over the direction of displacement of the wheels, from the origin of the pavement model, where the maximum deflection was calculated. The vertical strains were calculated directly below one of the loads, each 50-mm depth from the top of the basecourse.

The elastic modulus that yields the best match between measured and calculated response, or the back-calculated elastic moduli, were 400 MPa, 475 MPa and 1,000 MPa for pavements B00C10, B14C10 and B28C10 respectively, with an assumed Poisson's ratio of 0.35. The elastic modulus of the surface was estimated at 1000 MPa with a Poisson's ratio of 0.35. During the trial and error of the subgrade elastic modulus it was observed a fast decrease in the measured vertical strains with increase in pavement depth. This variation of the subgrade elastic modulus with depth was discussed in Section 4.8.6 (Chapter 4), and it is caused by the increase of resilient modulus of the subgrade with decrease in deviator stress, as was previously observed in the triaxial resilient modulus test (Figure 4.25). To account for the stress dependency of the subgrade, this layer was modelled with a 200-mm thick 24 MPa layer, on a 1100-mm thick 80 MPa layer. These elastic moduli provide a good match with the vertical strain measurements collected using the Emu strain system installed in the subgrade layer. The Poisson's ratio for the subgrade layers was assumed to be 0.40. A summary of the elastic properties of the pavements are listed in Table 5.3.

The collected and calculated deflection bowls, and the collected and measured vertical strains for section B28C10 are presented in Figure 5.13 and Figure 5.14. A cubic polynomial curve was fitted to both the measured and predicted deflections and the R^2 value was included in both figures. The deflection bowls and vertical strains for the other two sections are presented

in Appendix M. A general comparison between measured and predicted surface deflections bowls for the three sections studied is presented in Figure 5.15. A good match between measured and predicted surface deflections was obtained (R^2=0.9984). The same overall comparison to those of the deflections was conducted for the vertical strains and a reasonable R^2 value of 0.8286 (N=16) was encountered (Figure 5.16).

Table 5.3 Elastic and plastic material properties for the FE model

		Section		
		B00C10	B14C10	B28C10
Block	Property	0.0% FB 1.0% Cement	1.4% FB 1.0% Cement	2.8% FB 1.0% Cement
Surface	E (MPa)	1,000	1,000	1,000
	ν	0.35	0.35	0.35
	ϕ (°)	30	30	30
	c (kPa)	210	210	210
	ψ (°)	24	24	24
Basecourse	E (MPa)	400	475	1,000
	ν	0.35	0.35	0.35
	Φ (°)	46	35	23
	c (kPa)	386	390	409
	ψ (°)	36.8	28	18.4
Subgrade 1	E (MPa)	24	24	24
	ν	0.4	0.4	0.4
	Φ (°)	42	42	42
	c (kPa)	17	17	17
	ψ (°)	33.6	33.6	33.6
Subgrade 2	E (MPa)	80	80	80
	ν	0.4	0.4	0.4
	Φ (°)	42	42	42
	c (kPa)	17	17	17
	ψ (°)	33.6	33.6	33.6

ϕ = Angle of internal friction; ψ = dilation angle; E = elastic modulus, c = cohesion, ν = Poisson ratio

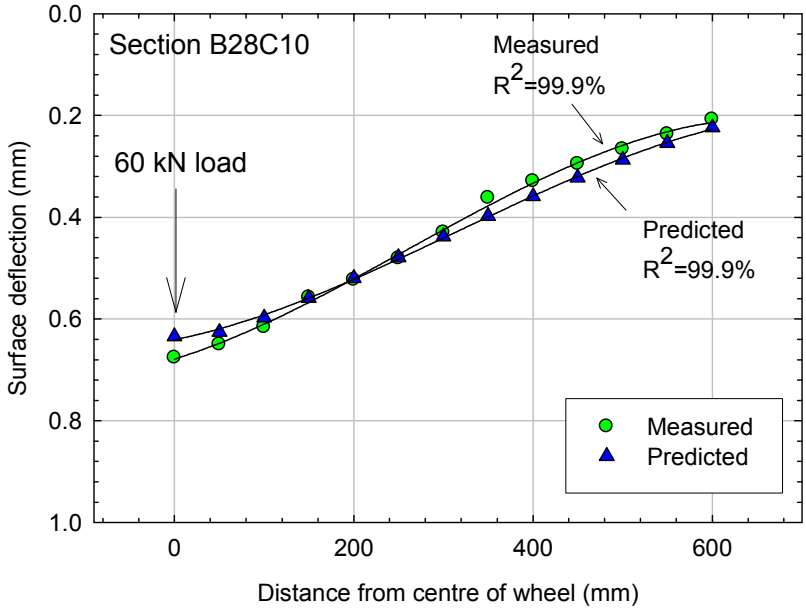

Figure 5.13 Measured and predicted surface deflection bowls for a 60 kN SLAVE load at section B28C10

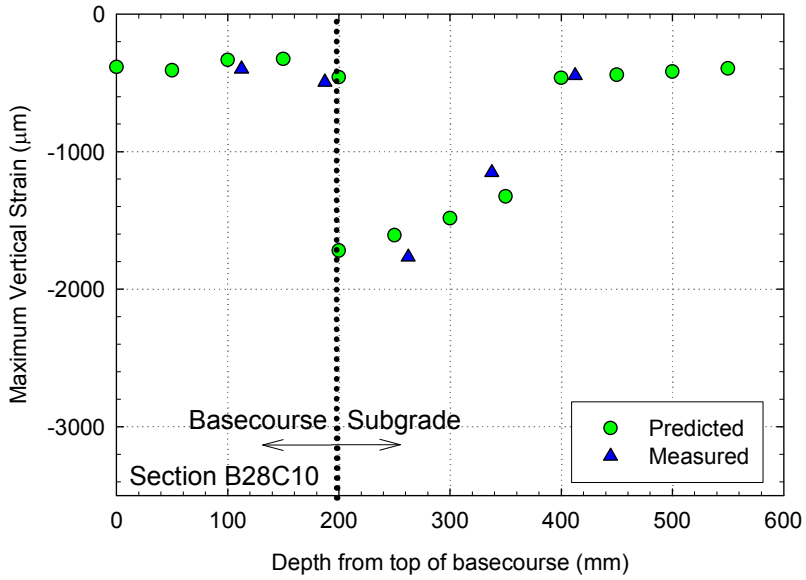

Figure 5.14 Measured and predicted vertical strains for a 60 kN SLAVE load at section B28C10

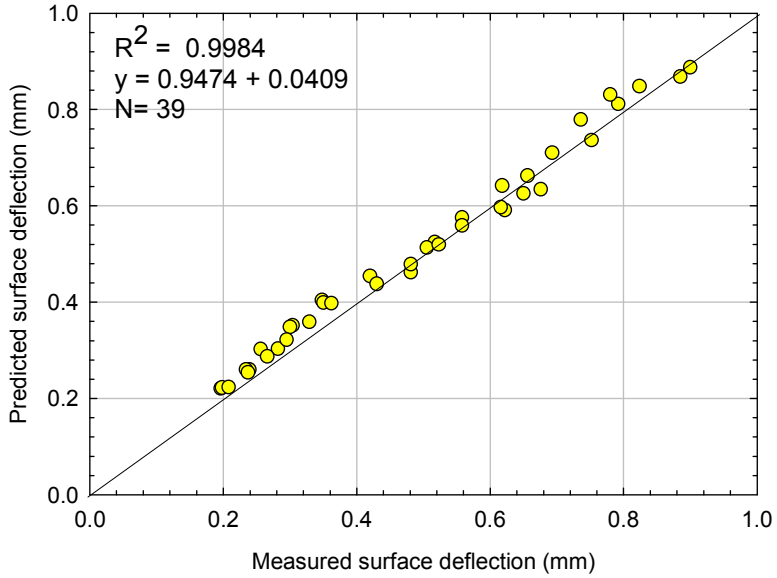

Figure 5.15 Measured versus predicted surface deflections for the three sections studied

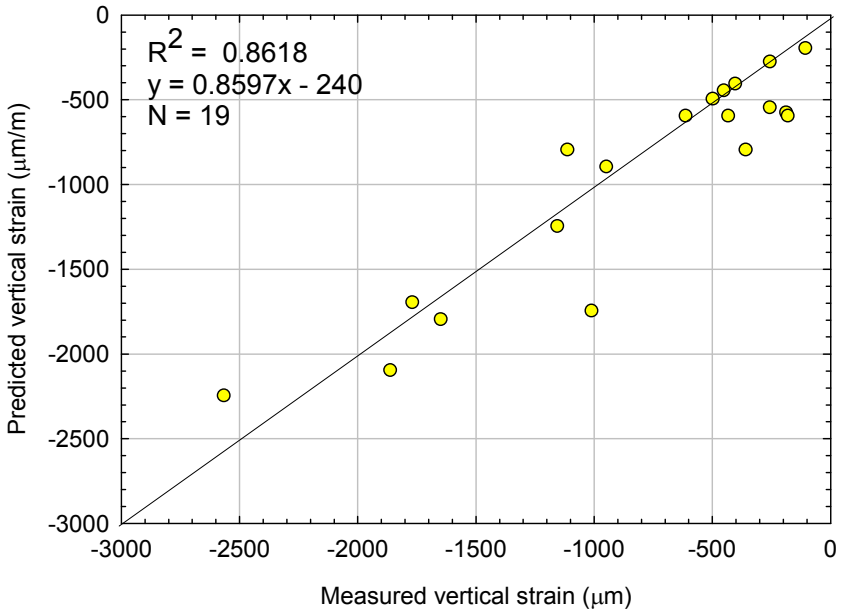

Figure 5.16 Measured versus predicted vertical strains (basecourse and subgrade) for the three sections studied

5.3.6 **Mohr-Coulomb model**

Both the subgrade and basecourse layers were simulated as elastic-plastic materials by using the Mohr-Coulomb model with strain hardening. The Mohr-Coulomb model is available in ABAQUS library materials and has the following properties (Hibbit 2001):

- Is used to model material with the classic Mohr-Coulomb criterion;
- Allows the material to harden and/or soften isotropically;
- Can be used with a linear elastic model only; and
- Can be used for design and applications in the geotechnical area to simulate material response under essentially monotonic loading.

The Mohr-Coulomb assumes that failure occurs when the shear stress at any point in a material reaches a value that depends linearly on the normal stress acting at the same plane. The Mohr-Coulomb model is represented by linear envelope, based on the Mohr's circle for states of stress at failure. The failure line is the best straight line approximation for the envelope of the Mohr's circles as presented in Figure 5.17.

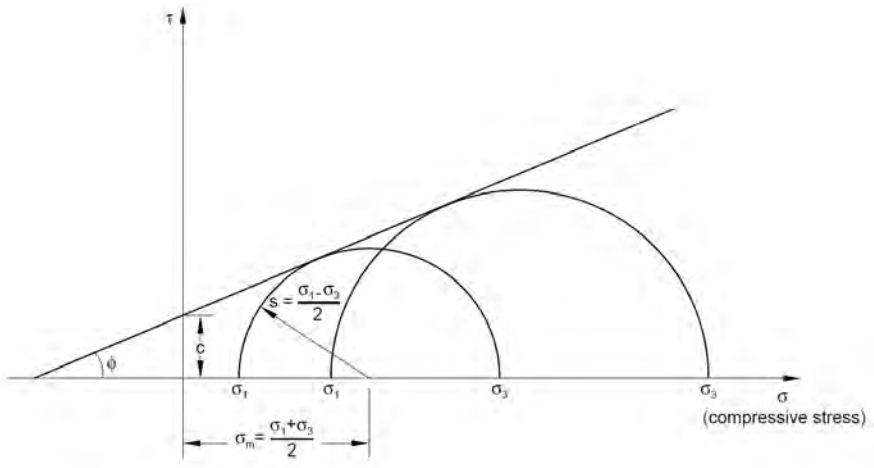

Figure 5.17 Mohr-Coulomb failure model (Hibbit 2001)

5.3.7 **Plastic and elastic parameters**

The angle of internal friction (ϕ) and cohesion (c), or shear strength parameters, were calculated for the basecourse as previously described in Section 5.2.3.

The shear strength parameters (see Table 5.3) for the asphalt surface were estimated using values found in the literature (Fwa and Tan 2005) for Hot Mix Asphalt, while the shear strength parameters of the subgrade were estimated using data available from previous research on granular materials conducted at CAPTIF (Arnold 2004). The same ϕ and c values were assumed for the two subgrade layers (see Table 5.3). The dilation angle (ψ) was estimated using the relationship proposed by Bolton (1986) for sands:

$$\phi = \phi_{crit} + 0.8\psi \qquad \text{(Eq. 5.1)}$$

where ϕ is the angle of internal friction at the peak stress, and ϕ_{crit} is the angle of internal friction at the critical state of the material, the state at which shear deformation can continue in the absence of volume change.

5.3.8 **Surface deformation results**

The computational time required by ABAQUS varied from 15 to 20 minutes for completing the analysis of the 3D pavement model. The permanent deformation in the finite element model was calculated by numerically integrating the vertical permanent strains with depth. The total surface deformation is the integration over the full depth, while the contribution of both the base layer and the subgrade layer can be determined by integrating the permanent strains over the base layer depth and the subgrade layer depth. For the finite element model presented, the calculated permanent deformation does not correspond to the measured plastic deformation in CAPTIF experiment, because the many simplifications made in the model mentioned in Section 5.3.1, in which only one load repetition was applied in the numerical simulation of the pavement. In addition, in the finite element model plastic deformation occurred only when the material attained the plastic state determined by the Mohr-Coulomb failure line, while in real pavements minute plastic strains develop after each load cycle, even though the load applied is well below the failure stress condition of the material. Instead, the objective of the 3D modelling using finite elements was to determine if the predicted plastic deformation behaviour followed the experimental results.

The calculated total permanent deformation is presented in Figure 5.18. The maximum plastic deformation for sections B14C10 and B28C10 was $1.6x10^{-3}$ and $1.3x10^{-3}$ mm respectively, about a fifth of that calculated in B00C10 ($6.7x10^{-3}$ mm). The difference in plastic deformation occurs because the bottom part of the section B00C10 develops larger plastic strains in comparison with the other two sections, and also because the top of the B00C10 subgrade deforms plastically. Figure 5.19 shows the deformed finite element model for each pavement section in the Y-Z plane (refer to Figure 5.10). B00C10 model shows the plastic vertical strain developing in the subgrade layer and at the bottom of the basecourse. The other two models (for B14C10 and B28C10 pavements) do not show plastic vertical strains in the subgrade, but plastic strains developed in the basecourse layer.

The surface deformation in sections B14C10 and B28C10 were similar (Figure 5.18), explained by the 'clockwise' rotation of the shear stress failure line of the B28C10, caused by the addition of foamed bitumen, which increases the tensile strength of the mix, but that at the same time increases the elastic modulus of the basecourse (E=1,000 MPa), which attracts higher stresses to the basecourse layer than pavement section B14C10 (E=475 MPa). As a result, both basecourse layers attain similar plastic vertical strains, or in other words, both basecourse layers were loaded at similar stress ratios and therefore the damage or permanent deformation at the initial loading condition of 60 kN was similar. The similar stress ratio was previously calculated in Table 5.2 for the load case 50mm/60kN.

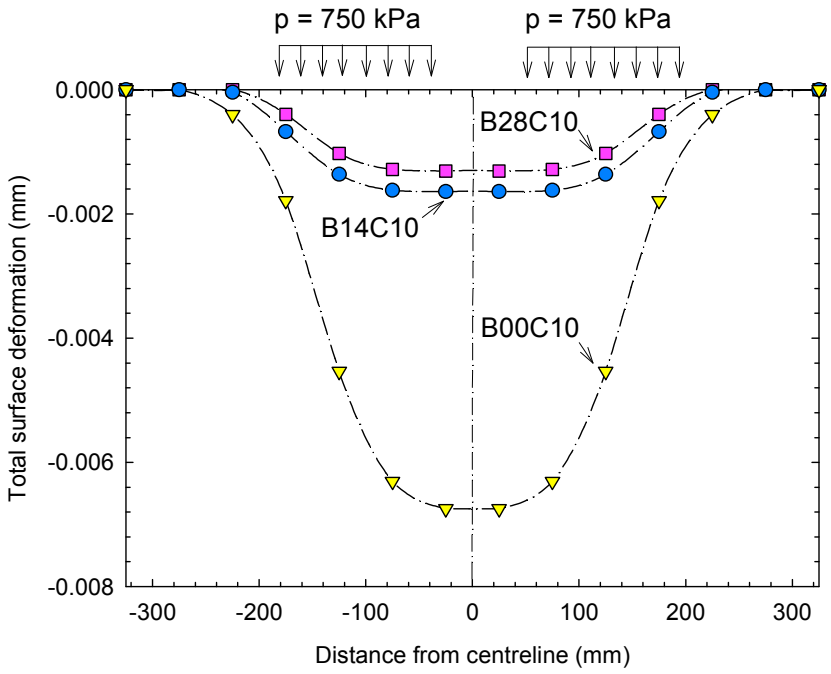

Figure 5.18 Predicted plastic deformation on pavement surface at 60 kN load, contact pressure = 750 kPa

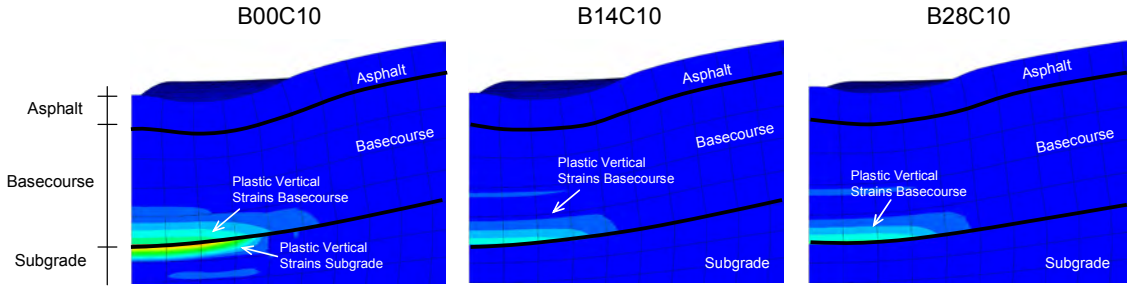

Figure 5.19 Predicted plastic vertical strains from finite element model, near to the loading area

5.3.9 **Increase in loading**

The response of the model to higher loads was studied by increasing the 60 kN load in 10-kN steps. To simulate the increase in load, the contact area between the tyres and the pavement surface was kept constant, but the contact stress was increased from 750 kPa to 1,000 kPa, 1,250 kPa and 1,500 kPa, equating loads of 60 kN (initial load), 80 kN, 100 kN and 120 kN respectively.

The calculated transverse profiles of the surface for each pavement section, at different load magnitudes, are presented in Figure 5.20. The results show that total surface plastic deformation increases with increase in load. The trends calculated at the initial loading of 60 kN remain constant, in which section B28C10 shows lower plastic deformation than the other two sections. At 70 kN, the plastic deformation in B14C10 and B28C10 are similar (maximum plastic deformations of 0.045 and 0.0344 mm), but when the load was increased to 80 kN, B14C10 model predicts a plastic deformation about four times higher than that calculated at B28C10 (maximum of 0.043 mm versus 0.1644 mm). At 90 kN, this difference is greater, with maximum surface plastic deformation in B28C10 of 0.107 mm, while in B14C10 and B00C10 the maximum is 0.347 mm and 0.45 mm respectively.

The lower difference observed in sections B00C10 and B14C10, at 80 and 90 kN is explained by the amount of plastic deformation calculated in the subgrade, that largely exceeds the basecourse deformation (Figure 5.21). At 80 kN, the maximum permanent deformation of the subgrade is 0.202 mm for B00C10 and 0.129 for B14C10, while the deformation in the basecourse is about 0.03 mm for both layers. The distribution of the plastic vertical strains at the three sections, for a load of 90 kN, is presented in Figure 5.21.

This part of the modelling shows the importance of the increase in the elastic modulus of the basecourse observed in B28C10. The higher elastic modulus spreads the stresses applied on the surface over a larger area, reducing the plastic strains in the subgrade. This effect was not evident at 60 kNload, because the amount of plastic deformation in the subgrade was similar to that of the basecourse, but when the load was increased the strains attained in the subgrade were closer to failure and a large amount of plastic deformation was calculated. A comparison between the subgrade and basecourse plastic deformation at different loads is presented in Figure 5.22.

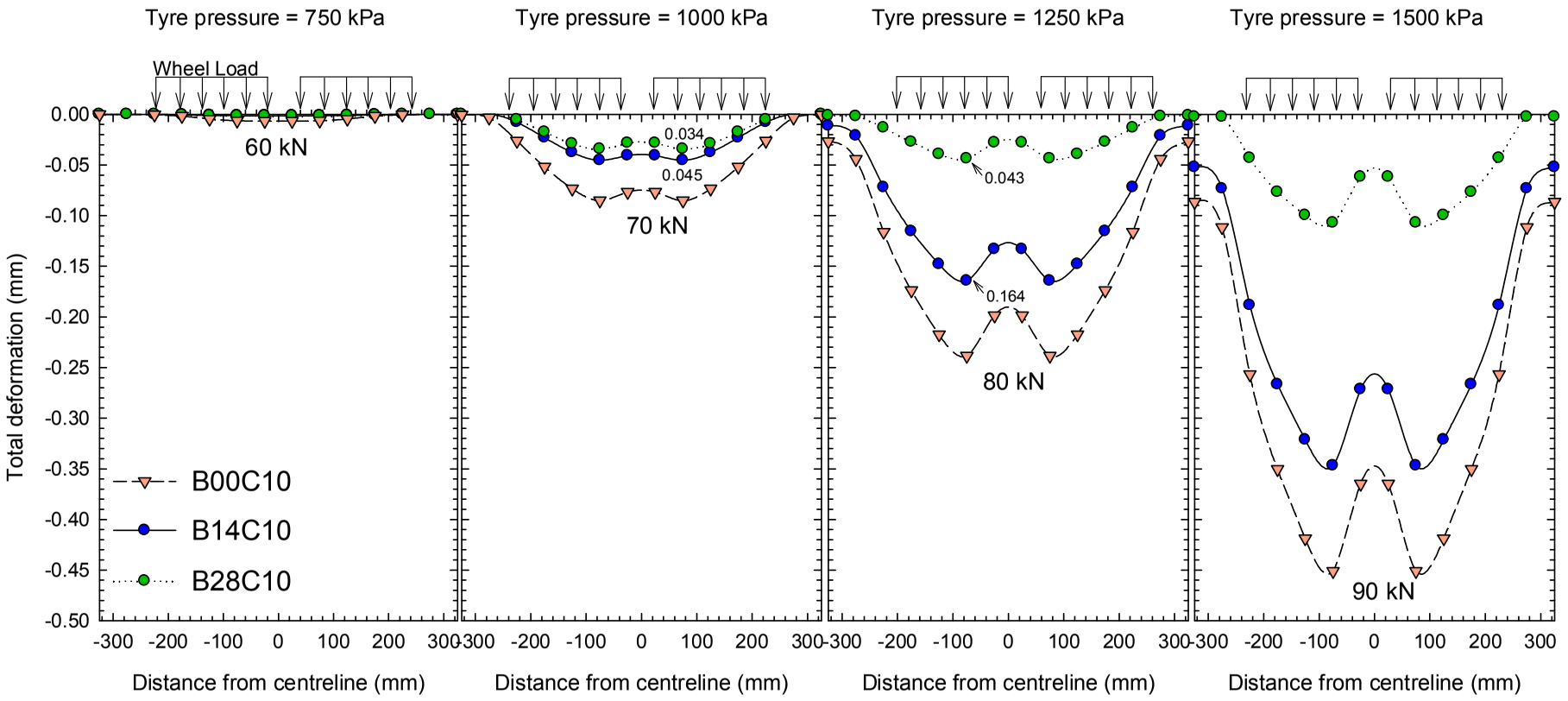

Figure 5.20 Predicted surface profiles at different loads for sections B00C10, B14C10 and B28C10

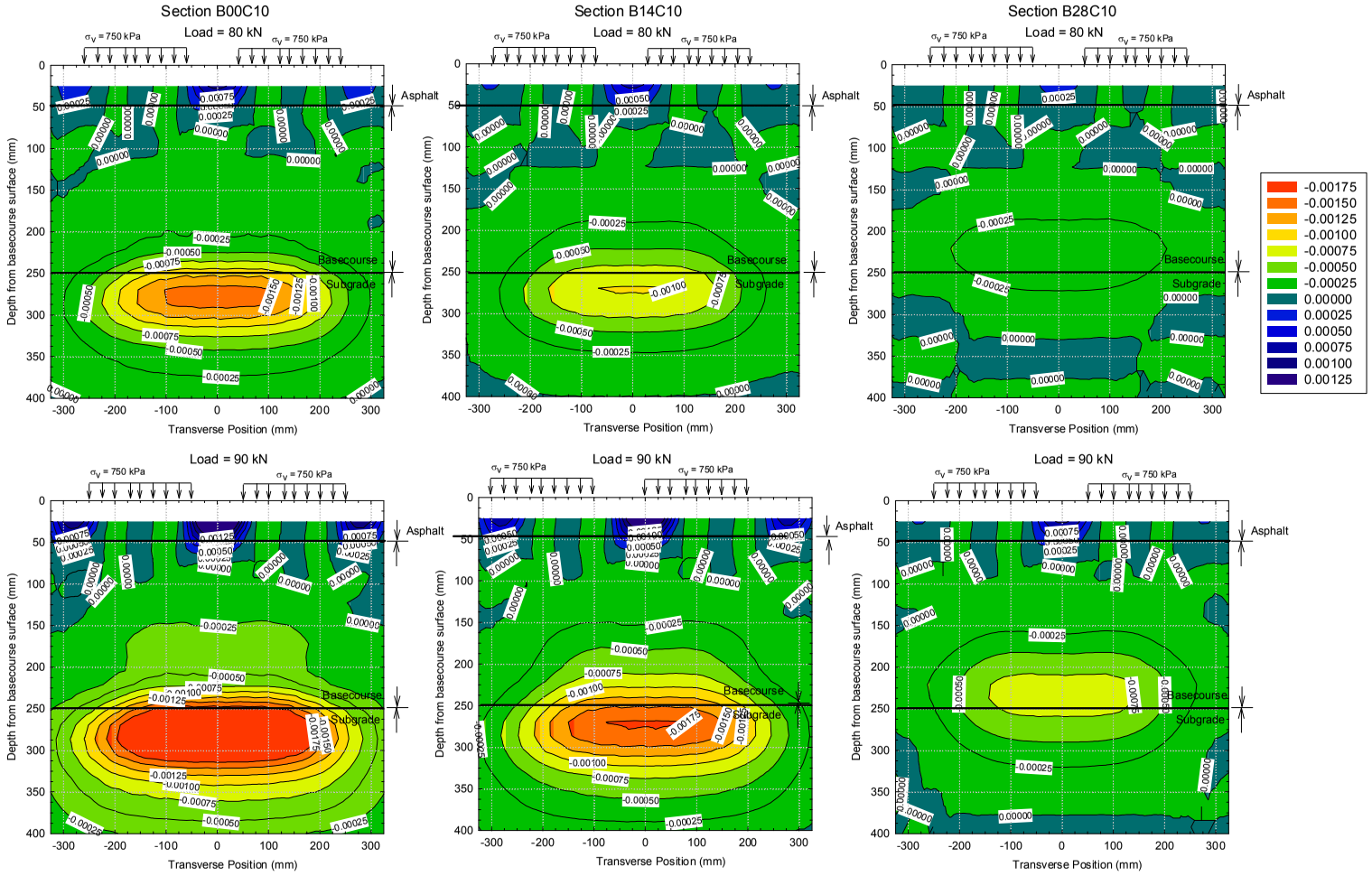

Figure 5.21 Predicted distribution of plastic vertical strain for B00C10, B14C10 and B28C10 (90 kN Load)

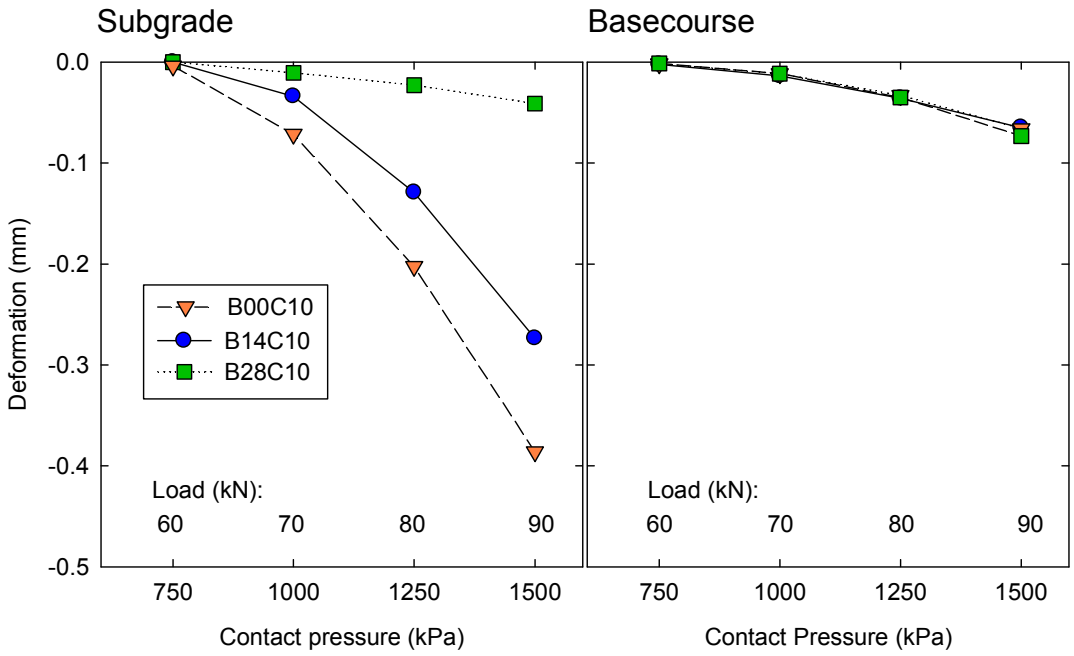

Figure 5.22 Comparison between predicted subgrade and basecourse plastic deformation at different loads

5.4 Two-dimensional finite element analysis for parametric study

5.4.1 Introduction

The three-dimensional finite element model presented in the previous Section was used for the interpretation of CAPTIF results, and provided trends that rank the behaviour of CAPTIF pavements. However, the 3D finite element model was developed for specific CAPTIF materials. Therefore, a parametric study, in which the material properties of the foamed bitumen layer (e.g. angle of internal friction, elastic modulus) are varied was conducted as part of this Chapter. These two variables were chosen because, as observed in the laboratory experimental study, foamed bitumen reduces the angle of internal friction of the mix, and, in the CAPTIF study, it was observed that the elastic modulus of the basecourse increases with increase in foamed bitumen content. Therefore, the objective of the parametric study is to study both effects separately and see how these parameters affect the plastic deformation of the pavement model.

In the previous 3D finite element analysis it was found that the computational time required by ABAQUS was too large to perform the several analyses required by a parametric study. Therefore, the three-dimensional model was simplified, adopting a two-dimensional (2D) finite element model.

The simplified 2D model remained similar to that of the 3D model, but modifications in the geometry, boundary conditions, material model and loads were necessary to create an equivalent model, as detailed in the following Sections.

5.4.2 **Geometry, boundary conditions and element size and type**

The size of the 2D model was defined using the pavement tank geometry. The width of the model was set at 2000 mm and the length of the height at 1500 mm. The thickness of the subgrade and basecourse layer was 1300 mm and 200 mm respectively, with an asphalt thickness of 50 mm. For simplification, the subgrade layer was modelled as one single layer, with an equivalent elastic modulus of E=60 MPa. The elastic properties of the surface asphalt layer was E=1,000 MPa, while the elastic modulus of the basecourse was varied from 250 to 1,000 MPa, every 250 MPa, as part of the parametric study.

The rigid boundaries of the concrete tank were simulated in the finite element model so that the bottom base of the subgrade is prevented from axial movements in all directions, while the movement in the direction of the tank walls is allowed (see Figure 5.23). To reduce the computational effort, a half-model was created using one symmetry axis (Z-axis), as depicted in Figure 5.23. The loaded area is located on the model surface (red vertical arrows at the left of Figure 5.23) simulating one of the two wheels.

A 25-mm element size was adopted for the area near to the loaded area. The model was created with 4-nodes plane stress elements, using reduced integration. The area farther to the load was meshed with larger elements to reduce the number of elements and thus the computational time.

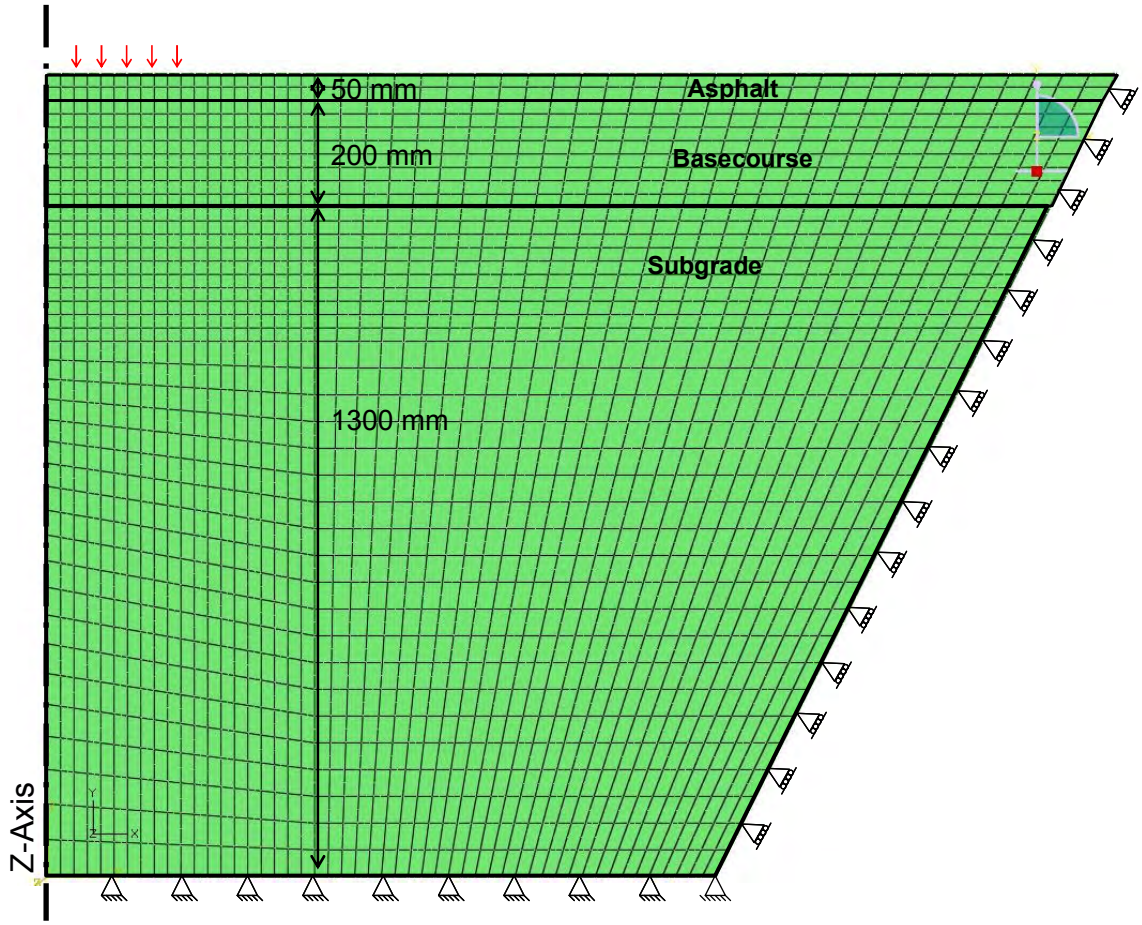

Figure 5.23 View of the two-dimensional finite element model

5.4.3 **Drucker-Prager model**

The Mohr-Coulomb model is not available in two-dimensional problems in ABAQUS. Therefore, the Drucker-Prager material model (Section 2.6.3) with strain hardening was adopted for the 2D modelling of pavements.

The two material parameters required by the Drucker-Prager model, α and k, can also be expressed in terms of the angle of internal friction ϕ and cohesion c, by matching the common intersection points at the vertices of the hexagonal failure envelope (Figure 2.36). The angle of internal friction of the

Mohr-Coulomb model was matched to the Drucker-Prager model, using the following equation:

$$\tan(\alpha) = \frac{1}{\sqrt{3}}\sin(\phi) \qquad \text{(Eq. 5.2)}$$

where α and ϕ is the angle of internal friction expressed for the Drucker-Prager and Mohr-Coulomb models respectively. The k value was matched using the following formula:

$$k = \frac{c}{\sqrt{3}}\cos(\phi) \qquad \text{(Eq. 5.3)}$$

5.4.4 **Load**

The load applied in the finite element model corresponds to a 60-kN load (two loads of 30 kN each). The load was linearly distributed on a length of 175 mm (7 elements off 25 mm). The load was applied in two steps, in the first step the amplitude of the load was increased (from 0 to 60 kN), while in the second step the load was removed. The advantage of loading the model in two steps is that at the end of the second step, when the load has been totally removed, only plastic deformations remain in the model and can be easily read from the software.

5.4.5 **Variables studied**

The variables studied in the parametric study were the angle of internal friction (ϕ) and the elastic modulus of the basecourse layer. The angle of internal friction adopted for the study was 20°, 30°, 40° and 50° (4 values), while the elastic modulus range was 250, 500, 750 and 1000 MPa (4 values). In total, 16 (4 x 4) finite element analyses were performed. The cohesion (c) remained constant for all the models.

5.4.6 **Results**

5.4.6.1 Effect of the angle of internal friction

The effect of the angle of internal friction on the horizontal plastic strains, vertical plastic strains and total surface deformation are presented in this Section.

The effect of decreasing the angle of internal friction in the basecourse (i.e. adding foamed bitumen), for a constant elastic modulus, is a reduction of the horizontal plastic strains of the pavement, and an increase in the vertical plastic strains in the basecourse.

The reduction in the horizontal plastic strains with decrease in the angle of internal friction is explained by the increase of the tensile strength of the basecourse. Figure 5.24 shows the calculated horizontal strains below one of the wheels, at different depths of the pavement, for the case E=1,000 MPa. The figure shows decrease in the horizontal strains of the basecourse with decrease in the angle of internal friction, for instance, the horizontal plastic strain at the bottom of the basecourse (depth = 250 mm) is 4.68×10^{-4} m/m for ϕ=50°, and 3.97×10^{-4} m/m for ϕ=20° (decrease of 15.1%). The decrease in the angle of internal friction in the basecourse also reduces the calculated horizontal strains in the subgrade. At the top of this layer (depth = 250 mm), the calculated horizontal plastic strain is 4.41×10^{-4} m/m for ϕ=50°, and 3.80×10^{-4} m/m for ϕ=20° (increase of 13.8%).

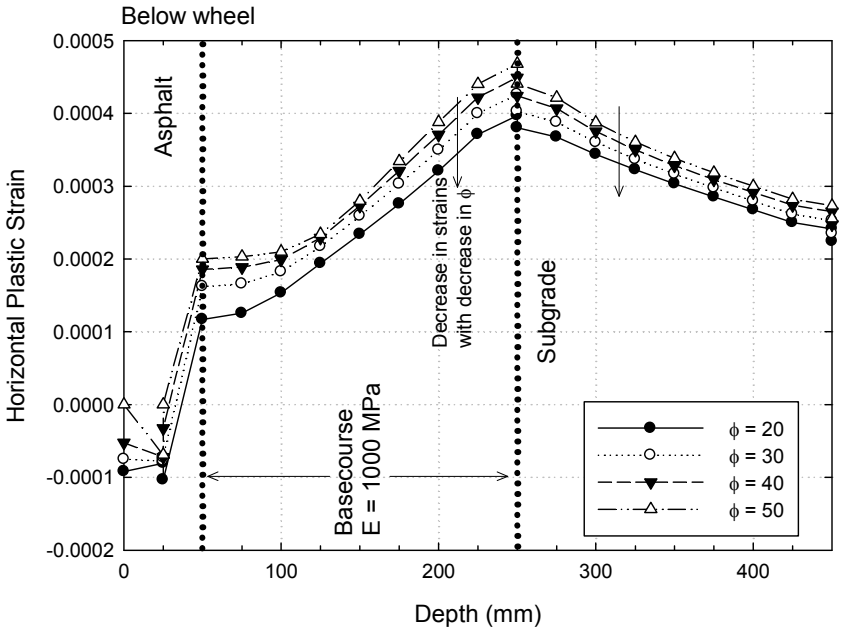

Figure 5.24 Predicted horizontal plastic strains for E=1000 MPa for different ϕ values

Conversely, the plastic vertical strains in the basecourse increase with decrease in the angle of internal friction at the top of this layer, as shown in Figure 5.25, which presents the vertical plastic strains for the case E=1,000 MPa. For instance, at the top of the basecourse (depth = 50 mm) the vertical plastic strain is -1.73×10^{-4} m/m for ϕ=50°, and -2.75×10^{-4} for ϕ=20° (increase in 57.8%), caused by the higher vertical compressive stress condition at this location of the pavement. This increase in the vertical plastic strain decreases with depth, because the decrease in the magnitude of vertical stress with depth. Conversely, in the subgrade layer, the vertical plastic strains decrease with decrease in the angle of internal friction. This is caused by the effect of the higher horizontal plastic strength of the basecourse, which can be loaded at higher horizontal stresses, reducing the horizontal stress in the subgrade.

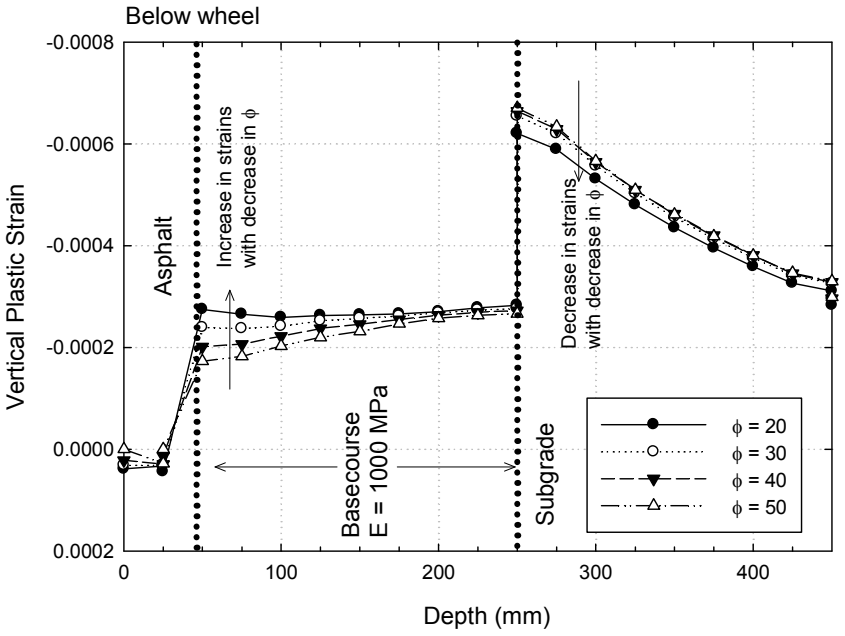

Figure 5.25 Predicted vertical plastic strains for E=250 MPa for various ϕ values

The overall effect of the reduction in the angle of internal friction on the pavement was evaluated by calculating the total plastic deformation for the surface, which accounts for the vertical plastic strains throughout the pavement depth. This effect is presented in Figure 5.26, which shows the reduction in the surface plastic deformation with decrease in the angle of internal friction. At the centre of wheels (transverse position = 0 mm), the plastic deformation is -0.2177 mm for ϕ=50°, while this value decreases to -0.1996 mm for ϕ=20° (reduction of 8.3%).

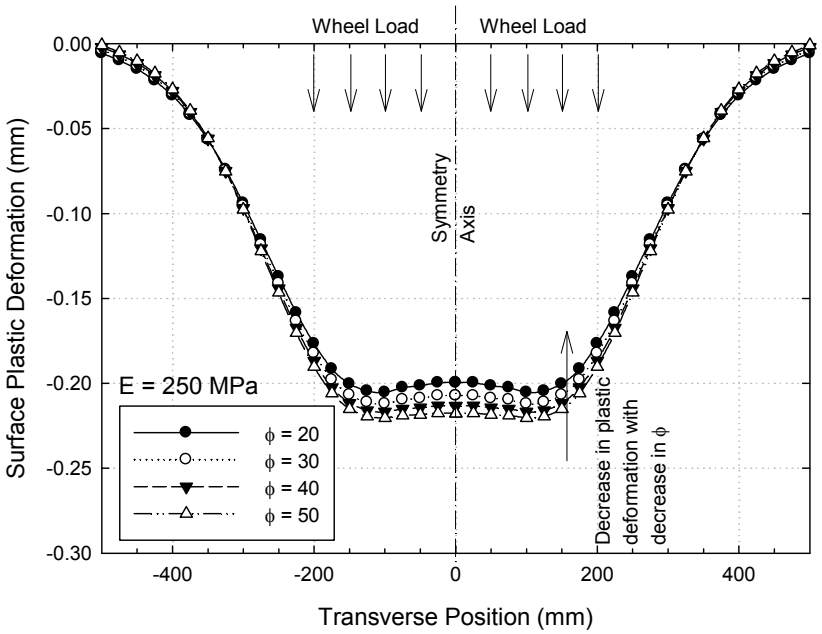

Figure 5.26 Predicted total surface plastic strains for E=250 MPa for various ϕ values

5.4.6.2 Effect of the elastic modulus

The effect of increasing the elastic modulus of the basecourse is a decrease in the vertical plastic strain in the basecourse and the subgrade (see Figure 5.27). Below the wheel (X=150 mm), and at the top of the basecourse (Z=50 mm), the reduction in the plastic vertical strain for an increase in the elastic modulus from 250 MPa to 1,000 MPa is -2.9×10^{-4} to -2.39×10^{-4} (-17.6%), while the same increase in elastic modulus reduced the vertical plastic strain at the top of the subgrade from -8.43×10^{-4} to -6.54×10^{-4} (-22.4%).

The effect of increasing the elastic modulus in the horizontal plastic strains is a combination of decrease in the tensile plastic strains at the top of the basecourse (see Figure 5.28) and an increase at the bottom of this layer.

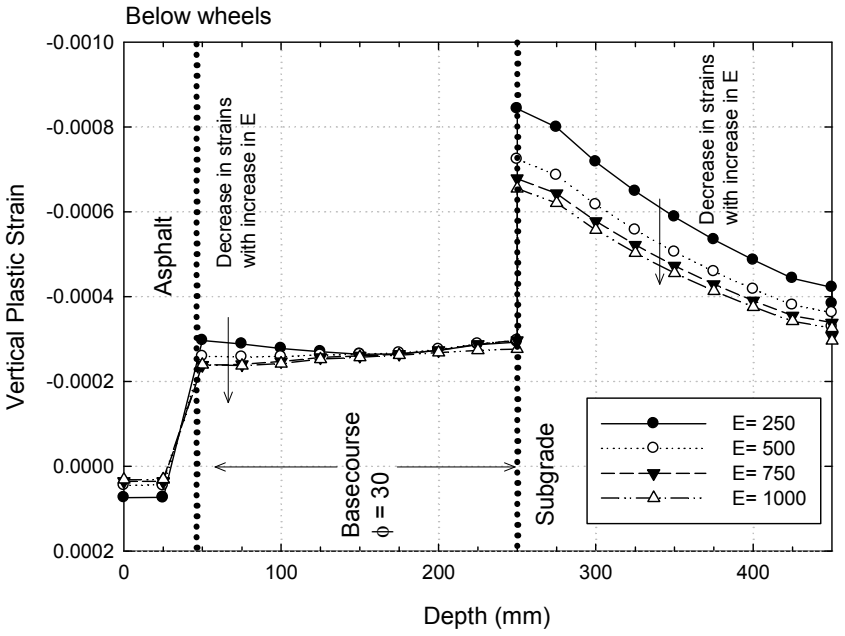

Figure 5.27 Predicted vertical plastic strains for ϕ=30° for various E values

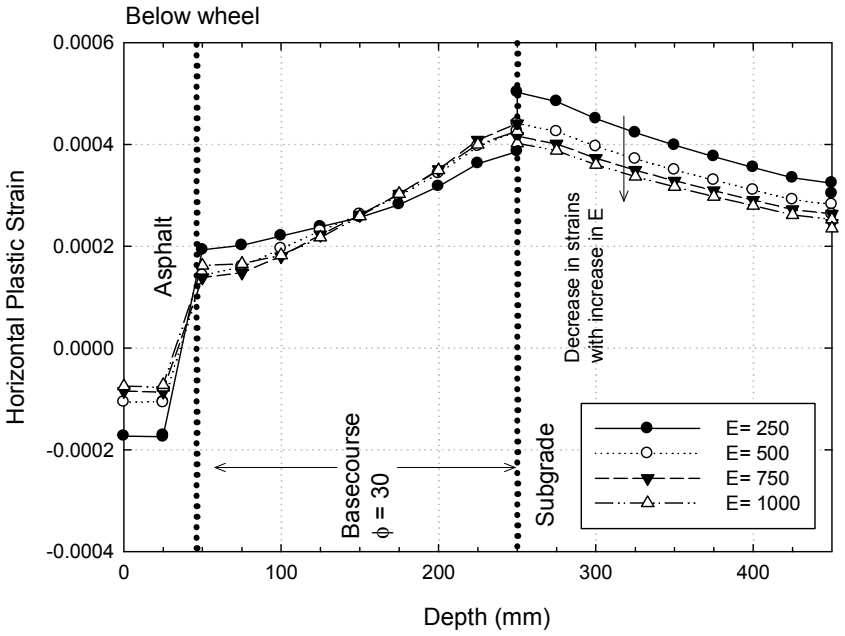

Figure 5.28 Predicted horizontal plastic strains for ϕ=30°

5.5 Two-dimensional finite element analysis for cyclic study

5.5.1 Introduction

The load applied in the finite element models presented in the previous Sections consisted of only one load repetition. Although this type of loading was used for the interpretation of the full-scale experimental results and the parametric study, a more realistic modelling of the CAPTIF pavements should consider cyclic loading.

This Section presents the analysis of CAPTIF pavement models B00C10 and B28C10. In the modelling, cyclic loading was applied instead only one load repetition.

The cyclic analysis consisted in the modelling of the pavement sections (B00C10 and B28C10) without cracking, and with the incorporation of cracking. The cracking was introduced in pavement surface only (hot mix asphalt layer), with the objective of:

- Simulate the last stage of the CAPTIF pavements (after 1,000,000 load cycles), when craking was observed in the pavement surface of section B00C10.
- See the effect of foamed bitumen in the performance of pavements when cracks are present on the surface, which may be representative of poorly maintained pavements.

5.5.2 Cycling loading and steps

The cyclic loading consisted of three different wheel load of 500 cycles each, applied subsequently in three steps (Figure 5.29). The amplitudes were 40, 50 and 60 kN, with a contact pressure between the tyre and the pavement surface of 0.1, 0.11 and 0.12 kN/mm respectively. The length of the uniform load applied in the model was 200 mm (40 kN), 225 mm (50 kN) and 250 mm (60 kN). The shape of the cyclic load was a smooth sinusoidal function created in ABAQUS, with a minimum value of zero at the start and end of each cycle, to simulate when the unloaded condition of the pavement, and a

maximum corresponding to the amplitude of the load (when the load attains its maximum or is located directly above the pavement).

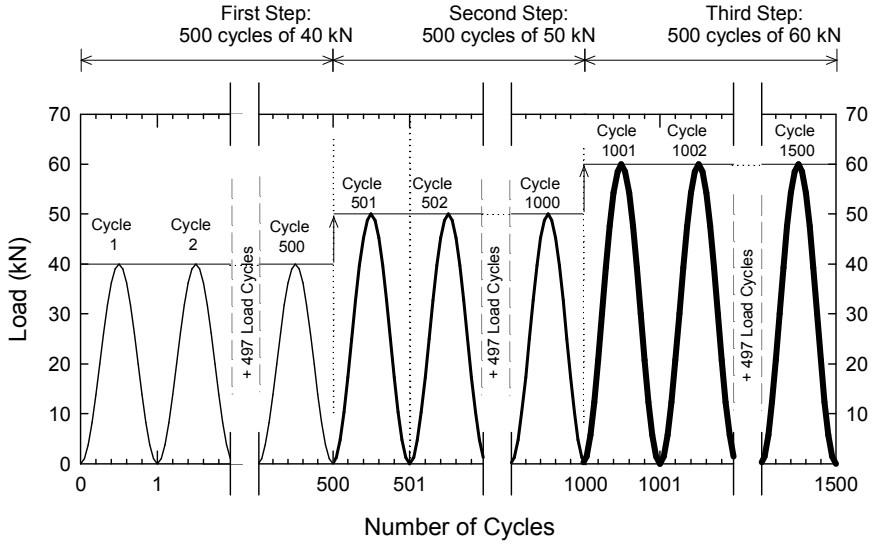

Figure 5.29 Load pulse applied in cyclic loading of pavements

The plastic strain induced by each load cycle was calculated at each finite element, and later internally added to the plastic strain calculated in the previous load cycle by ABAQUS. The vertical and horizontal plastic strains were collected each 50 load cycles, using an internal option of the software. The time required by ABAQUS to complete 500 load cycles was approximately 3 hours (i.e. 9 hours for the completion of the three steps shown in Figure 5.29).

5.5.3 **Modelling the pavement cracking**

Two cracks were introduced to the original 2D pavement model (Figure 5.23) to simulate a distressed condition of the pavement surface. The cracks were modelled by eliminating four finite elements of the asphalt layer, two at the centre of the wheels, close to the symmetry axis (X=0 mm), and the other two near to the outer edge of the wheel path or loading area (X=325 mm), as shown in Figure 5.30. Because the symmetry of the model, the eliminated finite elements create two cracks (at X=+325 mm and X=-325 mm) of dimensions 25 mm width and 50 mm depth, and a wider crack at the centre of wheels (dimensions 50 mm x 50 mm). The position and width of the cracks

were arbitrarly chosen, but the depth (50 mm) intended to simulate a surface severly cracked.

The geometry, boundary conditions, finite element size and type remained identical to the original 2D finite element model.

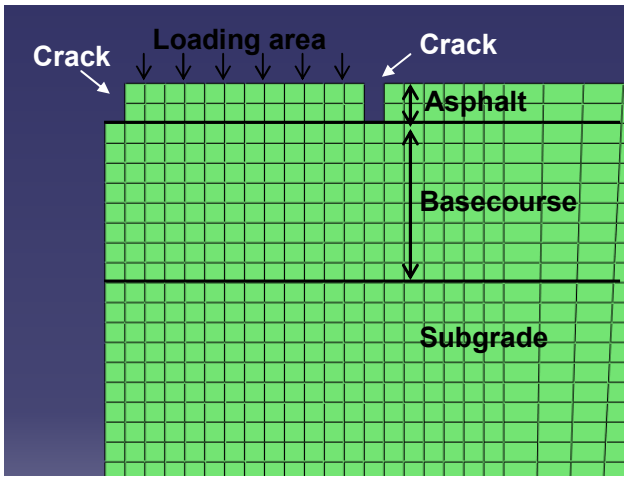

Figure 5.30 Detail of the 2D finite element model in which cracks were introduced into the hot mix asphalt layer

5.5.4 **Results: pavements with no crack**

The total surface deformation for pavements B00C10 and B28C10 with no cracks are presented in Figure 5.31. Both the initial surface deformation and the surface deformation rate (mm per load cycle) were calculated at the centre of the wheels. The shape of the curves show an initial increase in permanent deformation after the initial (first) load cycle, followed by a plateau in which an increasing permanent deformation rate was observed.

The initial surface deformation, when the load was 40 kN, was similar for both pavement models (approximately 0.01 mm), but the surface deformation rate was higher for B00C10 (0.77×10^{-5} mm/cycle, versus 0.2×10^{-5} mm/cycle for B28C10). When the load was increased to 50 kN, after the first 500 load cycles of 40 kN, the surface deformation increased to 0.07 mm and 0.095 mm for B28C10 and B00C10 finite element models, while the surface deformation rates increased to 0.9×10^{-5} mm/cycle and 1.8×10^{-5} mm/cycle respectively. For the final 500 load repetitions of 60 kN the initial surface deformation and the

surface deformation rates increased to a final deformation of 0.1923 mm and 0.2436 mm for sections B28C10 and B00C10 respectively (at 1,500 load cycles), with rates of 1.2×10^{-5} mm/cycle and 2.9×10^{-5} mm/cycle (see Figure 5.31.).

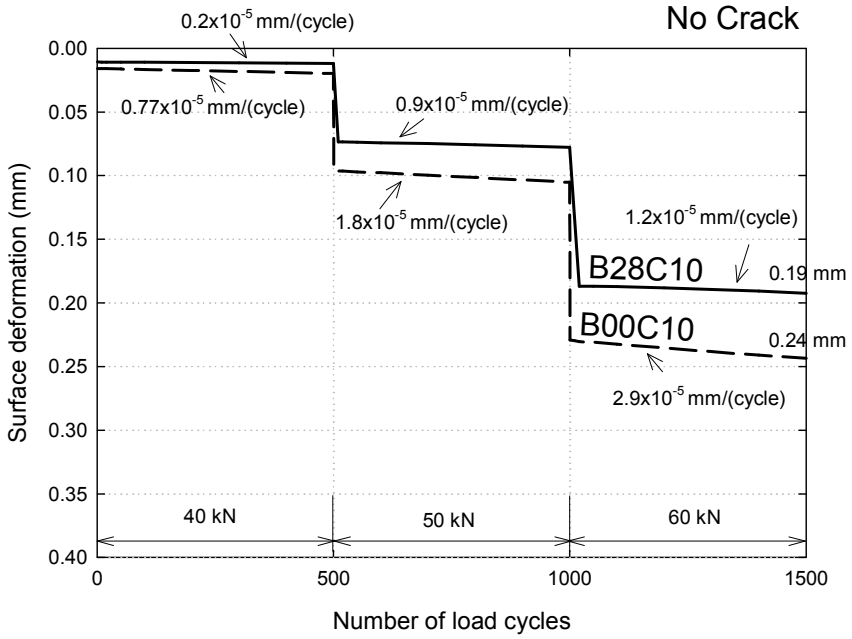

Figure 5.31 Surface deformation calculated at the centre of wheels for pavement without crack

The permanent deformation rates calculated from each pavement model were extrapolated and compared with the real surface deformation measurements from CAPTIF sections B00C10 and B28C10, assuming that the permanent deformation rate calculated in the finite element model remained constant after the calculated 500 load cycles. For instance, the permanent deformation rate calclulated in the pavement model B00C10 is 2.9×10^{-5} mm/cycle, therefore, after 800,000 load cycles the permanent deformation is 23.6 mm (2.9×10^{-5} mm/cycle x 800,000 cycles). The comparison with the real CAPTIF measurements was conducted by sequentially adding the surface deformation induced by the initial 40 kN load (150,000 load cycles), followed by the 50 kN load (350,000 load cycles) and the final load of 60 kN (800,000 load cycles). The results of the extrapolation and the real CAPTIF surface deformation measurements are presented in Figure 5.32. Although the finite element model predicts the trends of the surface deformation, the calculated

deformations were higher than those measured in the CAPTIF. The higher deformation predicted by the model is explained by the material model utilized for the modelling of the cyclic loading, which ignores the effect of the shakedown of the pavement layers (Lekarp et al. 2000; Werkmeister et al. 2004). The shakedown concept refers to the high permanent deformation observed during the initial cyclic loading phase of a pavement, which soon is reduced with increasing number of load cycles, or in other words, the pavement “shakes down”. However, the shakedown material behaviour is not available in ABAQUS for frictional material models (Mohr-Coulomb, Drucker-Prager) and therefore this effect was not considered in the pavement modelling.

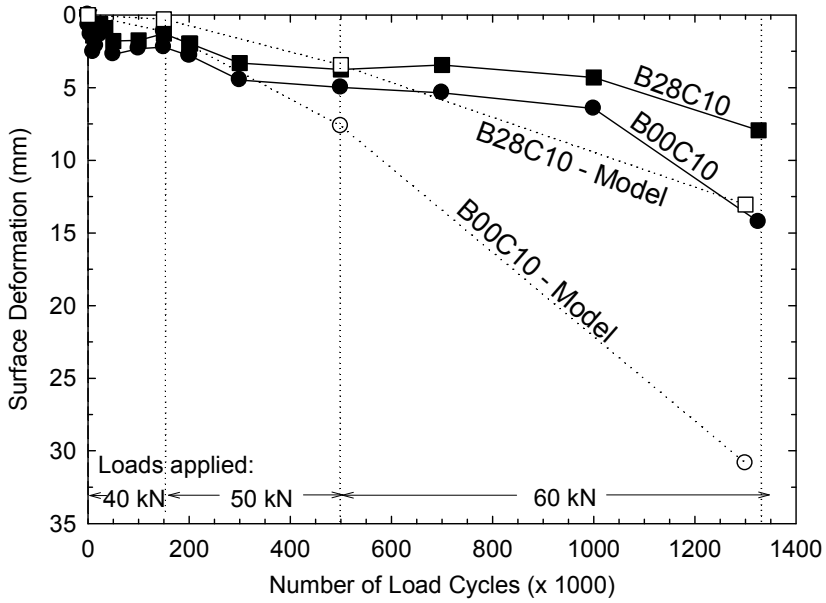

Figure 5.32 Calculated versus predicted surface deformation

5.5.5 **Results: pavements with cracks**

The calculated surface deformation for pavements with cracks is presented in Figure 5.33. The shape of the curves is similar to that of Figure 5.31, but the initial surface deformation and permanent deformation rates are higher than those calculated from the pavement model without cracks. A summary of these values (initial deformation and deformation rate) is listed in

Table 5.4 5.4. The table indicates that the effect of cracking was approximately an increase of 30% in the initial surface deformation and surface deformation rate for both pavement models, while the effect of adding 2.8% foamed bitumen is a reduction of approximately 20-30% of the initial surface deformation and about 50% of the permanent deformation rate.

Overall, pavement model B00C10 was more sensitive to cracking than B28C10, because B00C10 increases the final surface deformation after 1500 load cycles from 0.24 mm to 0.32 mm (33%), while B28C10 increases from 0.19 mm to 0.24 mm (26%) calculated in B28C10.

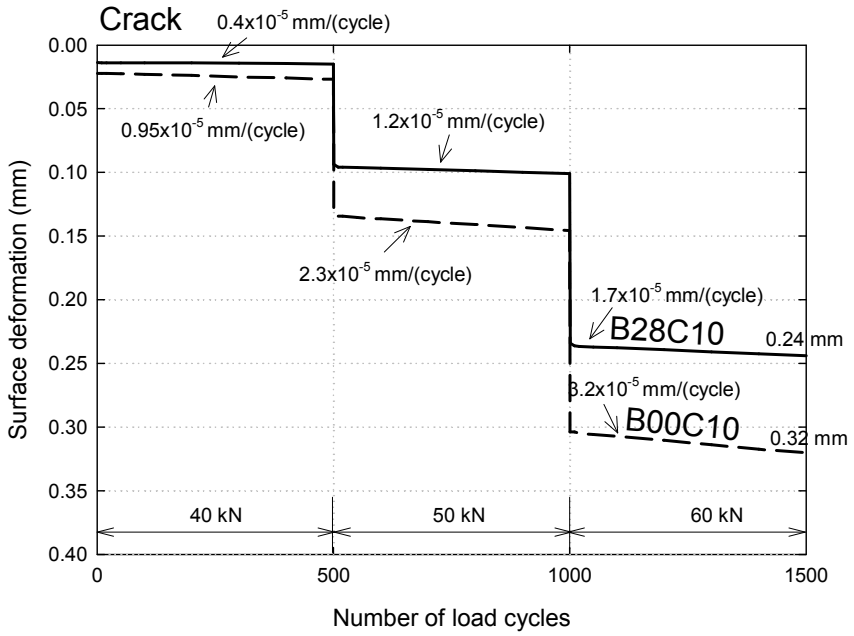

Figure 5.33 Surface deformation calculated at the centre of wheels for pavement with cracks

Table 5.4 Summary of initial and surface deformation rates for pavement models B00C10 and B28C10 with no cracks (N/Crack) and cracks

	Model B00C10				Model B28C10			
	Initial (mm)		Rate (mm/cycle)		Initial (mm)		Rate (mm/cycle)	
	N/Crack	Crack	N/Crack	Crack	N/Crack	Crack	N/Crack	Crack
40	0.016	0.022	0.77	0.95	0.011	0.014	0.2	0.4
50	0.092	0.133	1.8	2.3	0.074	0.094	0.9	1.2
60	0.2292	0.304	2.9	3.2	0.187	0.234	1.2	1.7

5.6 Summary and concluding remarks

The interpretation of the effect of foamed bitumen on pavement performance for pavements with a common 1% cement, has been presented in this chapter. The I_1-$J_2^{(1/2)}$ stress diagrams were used to compare the shear stresses induced in the pavement basecourse by the wheel loads, with the shear failure stress conditions predicted using monotonic triaxial laboratory data. The comparison was conducted by stress ratio analysis, in which the length of the stress paths applied by the moving wheels was compared with the length of the extension of that stress path with the intersection with the shear failure line. The analysis showed that the maximum calculated initial stress ratios of foamed bitumen sections B14C10 and B28C10, when the pavement was loaded with 40 kN, was 61% and 51% calculated at 160-mm depth, and little rutting was observed. When the load was increased to 60 kN, the stress ratio in these sections went up to 75% and 72% respectively, but the foamed bitumen sections remained working in a stable deformation rate with relatively little increase in surface deformation. Conversely, the section stabilised with cement only (B00C10) was initially loaded to a stress ratio of 66% at 40 kN, at a 160-mm depth. When the load was increased to 60 kN this ratio went up to 85%, calculated at 160-mm depth, leading the pavement layer to a higher deterioration rate. The stress analysis explains that a reduction in the angle of internal friction of the basecourse is benefitial for the pavement behaviour, since reduces the stress ratio at the bottom of this layer.

A three-dimensional finite element model was used to analyze the CAPTIF pavements and a Mohr-Coulomb plastic material model was introduced to account for the effects of foamed bitumen into the shear strength of the mixes (i.e. reduction in the angle of internal friction). The elastic parameters of the finite element model were determined back-calculating the elastic modulus of the layers by using data from deflection bowls induced by CAPTIF wheel load, collected using the CAPTIF Beam, plus the strain measurement system installed in the basecourse and subgrade layers. The accuracy of the finite element model was verified by comparing the linear elastic solutions with a widely used computer software used in pavement analysis. The results

provided a reasonable good match between the finite element model and the linear elastic software.

The back-calculation showed that foamed bitumen increases the elastic modulus of the basecourse layer. For section B00C10, the elastic modulus that yields the best match between CAPTIF measurements and the finite element calculations was 400 MPa, while 475 MPa and 1,000 MPa were calculated for B14C10 and B28C10 respectively, showing that the addition of 2.8% of foamed bitumen more than doubles the elastic modulus of the basecourse layer with 1.0% cement.

The three-dimensional finite element results showed that the incorporation of foamed bitumen to a layer with 1.0% cement reduces the total plastic deformation of the surface, following the trends observed in CAPTIF. To simulate the effect of a large number of load cycles, the load and tyre pressure were increased, showing that the minimum rutting occurs at the section with the highest foamed bitumen content. This is a combined effect of lower friction angle (i.e. higher tensile strength) and higher elastic modulus that better protects the subgrade layer of the vertical stress applied.

A simplified two-dimensional (2D) model of pavements was conducted as part of the finite element modelling. The first part of the 2D modelling was a parametric study, in which the effects of decreasing the angle of internal friction of the basecourse, and increasing the elastic modulus of the basecourse on the pavement plastic response were analyzed. In this part of the modelling, the Drucker-Prager material model was used instead of the Mohr-Coulomb model adopted in the three-dimensional finite element analysis. The parameters of this model were estimated by matching the the Mohr-Coulomb parameters (angle of internal friction and cohesion) with the Drucker-Prager model parameters. The results showed that the effects of decreasing the angle of internal friction are:

- A reduction of the horizontal plastic strains of the pavement model

- An increase in the vertical plastic strains at the top of the basecourse
- A decrease in the vertical plastic strains in the subgrade
- A decrease in the total surface vertical plastic strains

In addition, the results also showed that the effects of increasing the elastic modulus of the basecourse are a reduction of the vertical strains of the pavement, and a reduction of the horizontal plastic strains of the sugrade.

In the second part of the 2D finite element modelling three sets of 500 load cycles were applied, at load magnitudes of 40, 50 and 60 kN respectively. The CAPTIF pavement sections analyzed were B00C10 and B28C10, using the same elastic properties determined in the three-dimensional finite element modelling of CAPTIF pavements. The plastic surface deformation was calculated at the centre of the wheels after each load repetition. The results indicated that both the initial plastic deformation and the permanent deformation rate are lower in section B28C10. The results of the finite element modelling were extrapolated from 500 cycles to the real number of load cycles applied in the CAPTIF experiment. The extrapolation showed that the 2D finite element modelling predicts the trends of the real behaviour correctly, however, the plastic deformation is over predicted, because the material models utilized do not account for the ‘shakedown’ of pavements.

In order to simulate a potential pavement cracking in the pavement surface, finite elements of the top hot mix asphalt layer were removed, and the response of the pavements B00C10 and B28C10 calculated. The results showed that the cracking increased the surface deformation for both pavements, but the increase in section B28C10 (26%) was smaller than in section B00C10 (33%), which suggests a better performance of a pavement with foamed bitumen than without foamed bitumen in the field under cracked conditions.

This page is left blank intentionally

6 Conclusions and Recommendations

The research presented in this thesis describes the experimental work on a specific New Zealand granular material mixed with different contents of foamed bitumen and cement. The study involved a comprehensive laboratory testing of mixes loaded under a wide range of load and stress conditions, and an accelerated full-scale experiment on pavement sections of identical mixes to those tested in the laboratory. In addition, numerical analyses were conducted to examine the effect of foamed bitumen on pavement structures. The objective of the research was to investigate the mechanical effects of foamed bitumen in the deformational characteristics and performance of foamed bitumen pavements.

6.1 Deformational behaviour observed in the laboratory

In the laboratory, foamed bitumen mixes were tested under fundamentally two different stress conditions, namely triaxial compressive and indirect tensile stress. Mixes were prepared using a foamed bitumen Wirtgen WLB10 laboratory and a conventional stir-action mixer. Specimens were prepared applying vibratory compaction. Once specimens were compacted, they were left for curing at room temperature (20 °C) for 14 days in double sealed plastic bags. The tests performed on the specimens were: Indirect Tensile Strength (ITS), Indirect Tensile Resilient Modulus (ITM), Repeat Load Triaxial compression (RLT) and Monotonic Load Triaxial compression (MLT).

Preliminary RLT tests were conducted on mixes with 1% cement and 0% cement, at various foamed bitumen contents (0%, 2% and 4%), showed that the material with foamed bitumen only (i.e. with 0% cement) performed poorly in comparison to the specimens with 1% cement (e.g. in the cyclic load triaxial tests, specimens showed high amounts of permanent deformation or failed before the completion of the test). In addition, in the preliminary RLT testing the effect of bitumen on the mixes prepared with 1% cement at various

bitumen contents was not conclusive and the difference in final permanent deformation at the end of the tests was not clear to identify the effect of foamed bitumen. Based on the preliminary results, two actions were taken for the preparation and testing of triaxial specimens: 1) the focus of the research was shifted to the performance of materials with different amounts of foamed bitumen plus an active filler content of 1% cement, which is the commonly adopted cement content in New Zealand and 2) the moisture content of the specimens was increased and the original stress sequence applied in the RLT tests was modified to a more severe sequence, with the objective of attaining a higher permanent deformation at the end of the tests.

For the following cyclic load triaxial tests, specimens were prepared with 0%, 2% and 4% bitumen content, applying two compaction efforts, producing specimens with low bulk density and high bulk density. A total of 350,000 load cycles (4 cycles per second) were applied in seven stress stages (deviator stress of 75 kPa in the first stage, up to 525 KPa in the seventh stage), with a constant confining stress of 50 kPa. Results of the permanent deformation tests at low and high bulk density specimens showed that the addition of foamed bitumen to mixes with 1.0% cement increased permanent deformation, indicating that the deformability of the material measured under cyclic compressive triaxial conditions increases when foamed bitumen is added.

Triaxial specimens for monotonic compressive triaxial tests were prepared with 0%, 2% and 4% foamed bitumen content, applying two compaction efforts, creating specimens with low and high bulk density. A similar trend to that of the cyclic compressive triaxial test was observed in static load triaxial tests under monotonic loading, in which adding foamed bitumen to mixes with 1.0% cement reduced the peak vertical stress, indicating that the triaxial compressive ‘strength’ of the mixes decreases when foamed bitumen is added. The reduction of strength was observed in both low and high bulk density specimens.

Indirect Tensile Strength (ITS) specimens were prepared with bitumen contents of 0%, 1%, 2%, 3% and 4%. Results showed that adding foamed bitumen to the material with 1.0% cement increases the Indirect Tensile Strength (ITS) up to an 'optimum' bitumen content of 2.8%. Similar trends to those of the ITS tests were obtained in Indirect Tensile Modulus tests, in which an optimum foamed bitumen content maximizes the resilient modulus value.

The peak stress data measured in the MLT tests were used to calculate the fundamental shear parameters (angle of internal friction and apparent cohesion) of the mixes, assuming a linear failure envelope. The results indicated that the addition of foamed bitumen reduces the angle of internal friction, while there is no important effect on apparent cohesion. The results of the monotonic triaxial tests (maximum stresses attained) were plotted in stress diagrams. The stresses were expressed in terms of the first invariant of the stress tensor (I_1) and the square root of the second invariant of the deviator stress tensor (J_2). The plotted peak stresses were used to estimate the failure lines of the mixes, at different foamed bitumen contents. The stress diagram showed that increase of bitumen content results in a 'clockwise' rotation of the failure lines. Hence, the incorporation of foamed bitumen reduces the compressive strength of the mix but simultaneously increases the tensile strength, for a constant 1% cement content, which explains why the effect of foamed bitumen on the deformational behaviour of the mixes is different for different tests.

The effect of compaction effort on the permanent deformation RLT tests was unexpected, because higher deformability was observed in specimens with foamed bitumen prepared at high bulk density. It was inferred that the high compaction effort applied to triaxial specimens with foamed bitumen increased bulk density, reducing the air voids and leading to a simultaneous increase in the degree of saturation of the mixes, which could have increased the pore pressure of the mixes during cyclic testing. Additional specimens were prepared for RLT permanent deformation testing and simultaneous pore pressure measurements. Specimens were prepared with 4% foamed bitumen

and 1% cement, compacted at low and high bulk density. Pore pressure measurements showed that, the higher saturation in high bulk density specimens resulted in excess pore pressures about four times greater than those measured in low density specimens, indicating that the higher pore pressure offset the effect of a denser aggregate skeleton, obtaining higher permanent deformation in high bulk density specimens.

6.2 Pavement performance in full-scale experiment

An accelerated full scale experiment on foamed bitumen pavements was conducted at the Canterbury Accelerated Pavement Testing Indoor Facility (CAPTIF). Six pavement sections were tested, three were constructed using foamed bitumen contents of 1.2%, 1.4% and 2.8% respectively, plus a common active filler content of 1.0% cement (named sections B12C10, B14C10 and B28C10). Two pavements were constructed adding cement only (1.0%), and foamed bitumen only (2.2%) to the aggregate, named B00C10 and B22C00 respectively. Finally, one control or reference section with untreated unbound material was constructed (section B00C00). The stabilization process was conducted by machinery normally used in New Zealand, using the same materials (aggregate, bitumen, cement) previously tested in the laboratory. The pavement structure consisted of a clay subgrade (elastic modulus between 60 MPa to 80 MPa), the stabilized layer and a thin asphalt surface. The pavements were left for curing for approximately two months before trafficking. Accelerated loading was applied on the pavement structures and the pavement response, such as surface deformation (rutting), surface deflections and strains were periodically recorded during the execution of the test. The strains were measured at different depths by using an array of Emu strain gauges. Deflections were recorded using both Falling Weight Deflectometer (FWD) and CAPTIF Beam deflectometer, which is a modified Benkelmann beam. Approximately 5.6 million equivalent standard axles were applied on the pavement sections in approximately six months. The speed of the loads during most of the experiment was 30 kph, and the load varied from 40 kN (equivalent to 1 equivalent standard axle) to 60 kN.

The rutting measured in the sections stabilised with foamed bitumen and cement (B12C10, B14C10 and B28C10) was the lowest (between 7 mm to 8 mm), showing that the addition of foamed bitumen significantly improved the performance of materials with 1% cement. The sections stabilised with cement only (B00C10), foamed bitumen only (B22C00), and the control untreated section (B00C00) showed large amounts of rutting (between 14 mm to 17 mm) and heaving (between 14 mm to 18 mm) by the end of the test. Little difference (1 mm) was observed within the sections stabilised with foamed bitumen and 1% cement.

To accelerate the development of permanent deformation and differentiate the rutting performance of sections stabilized with different foamed bitumen content and 1% cement (B12C10, B14C10 and B28C10), water was introduced through surface cuts. After the application of additional accelerated traffic load the section with the lowest bitumen content (B12C10) started to show surface cracking, while the other two sections (B14C10 and B28C10) performed well, indicating that higher foamed bitumen contents reduce the moisture susceptibility and improve the performance of pavements.

The deflections measured during the experiment using the Falling Weight Deflectometer as well as the CAPTIF Beam decreased at higher bitumen contents. The deflections in section B28C10 were the lowest, while the untreated section (B00C00) showed the largest values, doubling deflections measured in B28C10. This indicates that foamed bitumen stabilization has an important effect in the reduction of surface deflections.

The pavement strains measured in the basecourse showed little difference in compressive vertical strains in sections with 1% cement and different foamed bitumen contents, indicating that foamed bitumen has little effect in compression. The vertical compressive strains measured at the top of the subgrade decreased at higher bitumen contents. In the pavements stabilised using 1% cement, tensile longitudinal strains decreased at higher foamed bitumen content. In other words, the observed effect of foamed bitumen is

insignificant under compressive stress conditions, but the effect is relatively significant under tensile stress conditions.

6.3 Deformational behaviour on field mixes observed in the laboratory

Laboratory testing was also conducted as part of the full-scale experiment, using field-mixed material collected during the construction of the pavement sections. The Indirect Tensile Strength (ITS) values for section B28C10 were double those of the sections B12C10 and B14C10. The ITS values from section B22C00 (no cement) were the lowest. The laboratory triaxial tests with field-mixed material showed that the addition of 1% cement significantly enhanced the quality of foamed bitumen mixes (samples without 1% cement failed during the cyclic loading), and the specimens with 1% cement at different bitumen contents showed that an increase in foamed bitumen content increases the permanent deformation in the laboratory tests, corroborating the results from the previous laboratory study. In addition, the resilient modulus values measured in triaxial specimens with 1% cement were relatively similar, showing a peak in the specimen with 1.4% bitumen (collected from section B14C10), instead of the specimens with 2.8% bitumen.

6.4 Stress path analysis and numerical simulations

I_1-$J_2^{(1/2)}$ stress diagrams were used to compare the stress path induced in the stabilised basecourse by wheel loads with the shear failure lines predicted using the static triaxial laboratory data. The mobilized stress ratio (induced stress state / respective failure stress state) was used to calculate the relative damage induced by the wheel loads to the basecourse. The stress ratio analysis showed that foamed bitumen decreases the mobilized stress ratio calculated at the bottom of the basecourse and increases the stress ratio at the top of the basecourse. However, the stress ratios at the bottom of the basecourse were approximately double those calculated at the top, and therefore more critical in the performance of the pavements studied. The effect of foamed bitumen in the stress ratio is explained by the decrease in the

angle of internal friction when foamed bitumen is added, which increases the tensile strength but simultaneously decreases the compressive strength.

A three-dimensional finite element model was used to analyze the pavements with 1% cement tested in the full-scale experiment. The elastic moduli of the model were back-calculated using deflection bowl data and vertical strain measurements, showing that an increase in the foamed bitumen content increases the elastic modulus. A Mohr-Coulomb plastic material model was introduced to account for the effects of foamed bitumen (i.e. reduction in the angle of internal friction, ϕ). The finite element results showed that the incorporation of foamed bitumen reduces the total plastic deformation of the surface, following the trends observed in CAPTIF.

A second, simplified two-dimensional model was created for a parametric study, in which the effect of the angle of internal friction and the elastic modulus of the basecourse were analyzed separately. The results showed that the effects of reducing the angle of internal friction are a reduction of the horizontal plastic strains, an increase in the vertical plastic strains at the top of the basecourse, a decrease in the vertical plastic strains in the subgrade and a decrease in the total surface vertical plastic strains. The effects of increasing the elastic modulus of the basecourse are a reduction of the plastic vertical strains of the pavement and a reduction of the horizontal plastic strains of the subgrade.

The two-dimensional finite element model was also used for modelling of cyclic loading effects, using the elastic properties (elastic modulus) and plastic properties (angle of internal friction and cohesion) of CAPTIF pavements B00C10 and B28C10. The results of the finite element modelling showed that the two-dimensional finite element modelling predicts the trends of the real behaviour correctly, however, the plastic deformation is over-predicted, because the material models utilized do not account for the hardening effects associated with ‘shakedown’. The effect of surface cracking was also modelled in a simplified manner, showing that cracking increased the surface

deformation for both pavements, but the increase in section B28C10 was higher than in section B00C10.

6.5 Recommendations

Based on the conclusions, recommendations for adopting the techniques used in the research for routine design and construction applications are listed.

It is recommended that adding 1% cement has to be considered in the construction of foamed bitumen mixes.

ITS is recommended as a test to measure the strength properties of foam bitumen mixes. It is recommended to adopt foamed bitumen contents that maximize ITS in pavements that have a potential risk of water being introduced into the pavement layers.

RLT testing does not necessarily detect the effect of foamed bitumen in materials with cement. Therefore, it is recommended that complementary tests such as ITS tests should be conducted to assess the properties of foamed bitumen mixes.

It is recommended to use the stress ratio as a potential indicator of pavement performance. In particular, the stress paths from simple routine tests (ITS, UCS) could be used to build approximate shear failure envelopes.

It is recommended to use the minimum moisture content during the construction process (stabilisation), provided maximum density is achieved, to avoid saturation or high pore pressure in the foamed bitumen layers.

It is also recommended to delay the surfacing of the foamed bitumen layer to allow the evaporation of the water (curing).

6.6 Limitations

The study presented in this thesis addressed the deformational behaviour of foamed bitumen pavements and the effect of foamed bitumen in pavement performance. However, as in any other research project, limitations of the study are evident and are summarized below.

Only one type of aggregate and bitumen were used in the research. The effects of foamed bitumen could be different if other materials are used. Only one type of active filler (Portland Cement), and active filler content (1%) was used. This last aspect could have an important effect in pavement performance, since the effect of adding only 1% cement to foamed bitumen mixes lead to a significant improvement in the laboratory performance.

The mixes tested in the laboratory were prepared using one moisture content only. The specimens were prepared applying vibratory compaction, which could not be representative of field compaction. The curing of the specimens was fairly short, because the moisture content remained almost constant before and after curing, which could not be representative of field conditions.

One of the main limitations of the full-scale experiment was that pavements were cured for approximately two months, while in real pavements this is a slow process that could take years. In addition, the traffic (5.6 million equivalent standard axles) was applied in approximately six months only, a traffic volume that could take several years in most New Zealand roads. Therefore, care should be taken when extrapolating the results of this experiment to field pavements.

Another limitation of the full-scale test is that instrumentation to measure pavement permanent strains was not available. Therefore, it was unknown how much plastic deformation developed in each layer during the application of the loads.

In the numerical simulations, several aspects were ignored. The materials were assumed to be linear-elastic, even though resilient modulus measured suggested a stress-dependent behaviour. In addition the shakedown effect was ignored in the modelling.

6.7 Recommendations for further research

More research should be conducted on different types of aggregates, with different bitumen types. The effects of foamed bitumen on the deformational behaviour and performance observed in this research could be different depending on the aggregate type (crushed or natural aggregate), fines content and the properties of the bitumen (e.g. foamability of the bitumen).

Further research is required to relate laboratory performance with in-service pavements. In particular, the effect of long term curing of foamed bitumen mixes was not studied in this research and could have a significant effect on the behaviour of the pavements, especially in the pore pressure measured in triaxial specimens. This is particularly important because the saturation level might be related with curing time in the field.

More research is required to understand the effect of different active fillers in the performance of foamed bitumen mixes. In this research, it was observed that the performance of the mixes increased when only 1% cement was added. Therefore, the effect of adding other amounts of cement and other types of active fillers (e.g. lime, fly ash) should be addressed.

The tensile properties of foamed bitumen mixes should be studied further. In this research, the tensile strength properties were estimated using Indirect Tensile Strength, a test in which the stress conditions within the specimens are not uniform and the horizontal tensile stress is induced by applying vertical compressive stress. In particular, extension tests, in which a uniform tensile stress is applied, should be incorporated as part of a research program to determine stress at failure. This experimental data could be used to calculate more accurately the failure envelopes in stress diagrams.

More versatile constitutive models allowing for combined effects of elastoplastic deformations, cracking, hardening and 3-D stress-strain relationships are needed to simulate more realistically deformational behaviour and performance of pavement structures.

This page is intentionally left blank

7 References

AASHTO (1993). “AASHTO guide for design of pavement structures”. Washington, D.C.

Asphalt Academy (2002). "Interim technical guidelines (TG2): The design and use of foamed bitumen treated materials". Pretoria, South Africa.

AQANZ (2006). "Aggregates". Aggregate and Quarry Association of New Zealand Incorporated. Lower Hutt, New Zealand.

Arnold, G. (2004). "Rutting of granular pavements". PhD Thesis, University of Nottingham, UK.

Arnold, G., Dawson, A., Hughes, D., and Robinson D. (2002). “The application of shakedown approach to granular pavement layers”. International Society for Asphalt Pavements.

Arnold, G., Hughes, D., Dawson, A., and Robinson, D. (2003). “Design of granular pavements”. Transportation Research Record No. 1819, Vol. 2. Eighth International Conference on Low-Volume Roads 2003.

ASTM (2005). ASTM D4318-05. Standard Test Methods for Liquid Limit, Plastic Limit, and Plasticity Index of Soils.

Australia Standards (1995). AS 2891.13.1-1995. "Determination of the resilient modulus of asphalt by the indirect tensile method".

Austroads (2004). "Pavement design: a guide to the structural design of road pavements". Sydney, Australia.

Barksdale, R. D. "Laboratory evaluation of rutting in basecourse materials". Proceedings of the 3rd international conference on the structural design of asphalt pavements, London, UK.

Bishop, A. W. (1960). "The principle of effective stress". Norwegian Geotechnical institute publication (32), pp. 1-5.

Black, P. "Aggregate supply and performance issues, Auckland, New Zealand". 6th International Symposium on Pavements Unbound (UNBAR 6), Nottingham, UK.

Bolton, M. D. (1986). "The strength and dilatancy of sands" Geotechnique, 36(1), pp. 65-78.

Brown, S.F. and Brodrick, B.V. (1981). "Instrumentation for monitoring the response of pavements to wheel loading". Sensors in Highway and Civil Engineering, Institution of Civil Engineers, London, UK, pp. 118-129.

Browne, A. (2008) "Foamed bitumen stabilisation in New Zealand - a performance review and lessons learnt". Recycling and stabilisation conference, Auckland, New Zealand.

Brunton, J. M. and Almeida, J. R. (1992). "Modelling material non-linearity in a pavement backcalculation procedure". Transportation Research Record, No. 1377, pp. 99-106.

BSI (2005). "Bituminous mixtures. Test methods for hot mix asphalt. Soluble binder content". British Standard Institute.

Chazallon, C., Hornych, P., and S. Mouhoubi (2006). “Elastoplastic model for the long-term behaviour modelling of unbound granular materials in flexible pavements”. Journal of Transportation Engineering, American Society of Civil Engineers, Vol. 6, pp. 279-289.

Claesson, J., and Bohloli, B. (2002). "Brazilian test: stress field and tensile strength of anisotropy rocks using analytical solution". International Journal of Rock Mechanics and Mining Sciences, Vol. 39, pp. 991-1004.

Compton, J. (1998). "The dawn of a New Stone Age for Auckland". New Zealand Geotechnical Symposium, Auckland, New Zealand.

Croney, D., and Croney, P. (1998). “The design and performance of road pavements”. McGraw-Hill Professional.

CSIR (2006). "mePADS, Mechanistic Empirical Pavement Analysis and Design Software". Pretoria, South Africa.

Dawson, A. (1994). "The E-mu System, Users Manual”. University of Nottingham, United Kingdom."

De Beer, M. (1997). "Measurement of tire/pavement interface stresses under moving wheel loads". International Journal of Heavy Vehicle Systems, 3(1), pp. 97-115.

Desai, C. S. and Siriwardane, H. J. (1984). “Constitutive laws for engineering materials, with emphasis *on geologic materials”.*

Dodds, A., Logan, T., McLachlan, and J. Patrick (1999). "Dynamic load properties of New Zealand basecourse". Transfund New Zealand, Wellington, New Zealand.

Drucker, D. C., and Prager, W. (1952). "Soil mechanics and plastic analysis or limit design". Quarterly of Applied Mathematics, 10(2), pp. 157-165.

Frobel, T., and Hallet, J. (2008). "Foamed bitumen stabilisation in New Zealand - Projects, do's and dont's, performance". Recycling and stabilisation conference, Auckland, New Zealand.

Fu, P., and Harvey, J. T. (2007). "Temperature sensitivity of foamed asphalt mix stiffness: Field and lab study". International Journal of Pavement Engineering, 8(2), pp. 137-145.

Fwa, T. F., and Tan, S. A. (2005). "C-ϕ; Characterization model for design of asphalt mixtures and asphalt pavements". Journal of ASTM International, 2(3), pp. 121-134.

Efrem, G.E. (2000). "Stabilisation of Cinder with foam bitumen and cement and its use as (sub) base for roads". Master of Science in Engineering Thesis. IHE, Delft, Netherlands.

Gaudefroy, V., Olard, F. o., Cazacliu, B., de La Roche, C., Beduneau, E., and J. P. Antoine (2007). “Laboratory Investigation on the Mechanical Performances of Foamed Bitumen Mixes Using Half-Warm Aggregates”. Transportation Research Board 86th Annual meeting, Washington, D.C.

Gonzalez, A., Saleh, M., and A. Ali (2007). "Evaluating nonlinear elastic models for unbound granular materials in accelerated testing facility". Transportation Research Record, No. 1990, pp. 141-149.

Halles, F. and Thenoux, G. (2009) "Degree of influence of active fillers on the properties of recycled mixes with foam asphalt." Transportation Research Board 88th Annual Meeting, Washington, D.C.

Hayward, B. (2006). "Investigation of road base shear strains using in-situ instrumentation”. Master of Engineering Thesis. University of Canterbury, Christchurch, New Zealand.

Hibbit, Karlsson and Sorensen (2001). "Getting started with ABAQUS Standard".

Holubec, I. (1969). "Cyclic creep of granular materials". RR147, Department of Highways, Ontario, Canada.

Huang, Y. H. (2004). “Pavement Analysis and Design”. Prentice Hall.

Jenkins, K., Collings, D., and Jooste, F. (2008). "TG2: "The Design and Use of Foamed Bitumen Treated Materials. Shortcomings and Imminent Revisions". Recycling and Stabilisation Conference, Auckland, New Zealand.

Jenkins, K., Long, F., and Ebels L. J. (2007). “Foamed Bitumen Mixes = Shear Performance?”. Vol. 8, pp. 85-98. Taylor & Francis Limited.

Jenkins, K. J. (1999). "Mix design considerations for cold and half-warm bituminous mixes with emphasis on foamed bitumen". PhD Thesis. University of Stellenbosch, Stellenbosch, South Africa.

Jones J, & Ramanujam, 2004, Rehabilitation of unbound granular pavements using foamed bitumen stabilisation. International symposium on unbound granular aggregates in roads, Nottingham, United Kingdom.

Kekwick, S. (2005). "Best practice: bitumen-emulsion and foamed bitumen materials laboratory processing". SATC 2005: The 24th Annual Southern African Transport Conference and Exhibition, Pretoria, South Africa.

Kim, Y., Lee, D. Y., and Heitzman, M. (2008). "Laboratory evaluation of cold-in place recycling mixtures using foamed asphalt based on dynamic modulus and repeated dynamic load tests". Transportation Research Board 87th Annual Meeting, Washington, DC.

Kim, Y., Lee, H. D., and Heitzman, M. (2007). "Validation of New Mix Design Procedure for Cold In-Place Recycling with Foamed Asphalt". Journal of Materials in Civil Engineering, 19(11), pp. 1000-1010.

Lee, H. D., and Kim, Y. (2006). “Influences of Binder and RAP Temperatures and Foaming Water Content on Cold-In-Place Recycling Mix Design Process using Foamed Asphalt”. Proceedings of the 2006 Airfield and Highway Pavement Specialty Conference. American Society of Civil Engineers (ASCE).

Leek C, 2009, Review of the performance properties of in-situ foamed bitumen stabilised pavements. City of Canning, Australia.

Lekarp, F., and Dawson, A. (1998). "Modelling permanent deformation behaviour of unbound granular materials". Construction and Building Materials, 12(1), pp. 9-18.

Lekarp, F., and Isacsson, U. (2001). “The effect of grading scale in repeated load triaxial test results”. Gordon and Breach Science Publication. Taylor & Francis Limited.

Lekarp, F., Isacsson, U., and Dawson, A. (2000). "State of the art. II: permanent strain response of unbound aggregates". Journal of Transportation Engineering (ASCE), 126(1), pp. 76-83.

Lekarp, F., Richardson, I. R., and Dawson, A. (1996). "Influences on permanent deformation behaviour of unbound granular materials". Transportation Research Record, No. 1547, pp. 68-75.

Loizos, A., and Papavasiliou, V. (2007). "Evaluation of foamed asphalt cold in-place pavement recycling using nondestructive techniques". Journal of Transportation Engineering (ASCE), 132(12), pp. 970-978.

Long, F. (2001). "The development of structural design models for foamed bitumen treated pavement layers". CSIR Transportek, South Africa.

Long, F., and Theyse, H. (2002). "Second Level Analysis of HVS Data from Road P243/1". CSIR Trasportek, South Africa.

Long, F., Theyse, H. L., Robroch, S. and Liebenberg, J. (2002). “Performance models for deep in situ recycled, bitumen stabilised pavements under accelerated traffic”. International Society for Asphalt Pavements.

Long, F., and Ventura, D. G. C. (2004). "Laboratory testing for the HVS Test Sections on the N7 (TR11/1)".

Merril, D, Nunn, M & Carswell I, 2004, A guide to the use and specification of cold recycled materials for the maintenance of road pavements. Transportation Research Laboratory, Berkshire, United Kingdom.

Nunn, D, Development of a more versatile approach to flexible and flexible composite pavement design, Transportation Research Laboratory, Berkshire, United Kingdom.

MINCAD (2004). "CIRCLY software for pavement design”.

Mitchell, J. (1993). Fundamentals of soil behaviour, John Wiley & Sons, Berkeley, California.

Muthen, K. M. (1999). "Foamed asphalt mixes - Mix Design Procedure." CSIR Transportek, South Africa.

Nataatmadja, A. (2001). "Some characteristics of foamed bitumen mixes". Transportation Research Record, No. 1767, pp. 120-125.

Nataatmadja, A. (2002). “Foamed bitumen mix: soil or asphalt?”. International Society for Asphalt Pavements.

Transit (2007). "New Zealand Supplement to the Document, Pavement Design - A Guide to the Structural Design of Road Pavements (AUSTROADS, 2004)". Wellington, New Zealand.

NZS (1986). "NZS 4402.4.1.3:1986: Determination of the dry density/water content relationship - Test 4.1.3 New Zealand vibrating hammer compaction test." Standards New Zealand, Wellington.

Otte, E. (1972). "Die spannings - varvomingseienskappe van sementgestabiliseerde matreiale". University of Pretoria, Pretoria, South Africa.

Pidwerbesky, B. (1996). "Fundamental behaviour of unbound granular pavements subjected to various loading conditions and accelerated trafficking". PhD thesis, University of Canterbury, Christchurch, New Zealand.

Romanoschi, S. A., and Metcalf, J. B. (2001). "Effects of interface condition and horizontal wheel loads on the life of flexible pavement structures". Transportation Research Record, No. 1778, pp. 123-131.

Ruckel, P. J., Acott, S. M., and Bowering, R. H. (1983). “Foamed-asphalt paving mixtures: preparation of design mixes and treatment of test specimens”. Transportation Research Board Annual Meeting, Washington, DC.

Saleh, M. F. (2004a). "Detailed experimental investigation for foamed bitumen stabilisation". Transfund New Zealand Research Report No. 258, University of Canterbury, Christchurch, New Zealand.

Saleh, M. F. (2004b). "New Zealand experience with foam bitumen stabilization". Transportation Research Record, No. 1868, pp. 40-49.

Saleh, M. F., Steven, B., and Alabaster, D. (2003). "Three-dimensional nonlinear finite element model for simulating pavement response: study at Canterbury Accelerated Pavement Testing Indoor Facility, New Zealand". Transportation Research Record, No. 1823, pp. 153-162.

Saleh, M. and Harrington, P. (2003). "Foamed bitumen stabilisation for New Zealand roads". Transfund New Zealand Research Report No. 250. University of Canterbury, Christchurch, New Zealand.

SHRP (1992). "SHRP Protocol P46: Resilient Modulus of Unbound Granular Base/Subbase materials and subgrade soils."

Snaith, M. S., McMullen, D., Freer-Hewish, R.J. and Shein, A. (1980). "Flexible pavement analysis". Contracted report to Sponsors, European Research Office of the U.S. Army.

Standarization, European Commission (2003). "Unbound and hydraulically bound mixes - Test methods - Part 7: Cyclic load triaxial test for unbound mixtures". European Standard, EC for Standarization"

Station, New Zealand Weather (2006). "Weather Station - ZL3GP, Burwood". Christchurch, New Zealand.

Steven, B. (2005). "The development and verification of a pavement response and performance model for unbound granular pavements". PhD thesis. University of Canterbury, Christchurch, New Zealand.

Sweere, G. T. H. (1993). "Unbound granular bases for roads". Delft University of Technology, Road and Railroad Research Laboratory.

Theyse, H. L. (2004). "First-level analysis report: HVS testing of the foamed-bitumen-treated crushed stone base on the slow lane of the southbound carriageway of the N7 near Cape Town". CSIR Transportek, Pretoria, South Africa.

Theyse, H. L., De Beer, M., and Rust, F. C. (1996). "Overview of South African mechanistic pavement design method." Transportation Research Record, No. 1539, pp. 6-17.

Thom, N. H., Brown, S.F. (1988). "The effect of grading and density on the mechanical properties of a crushed dolomitic limestone". Australia Road Research Board (ARRB) conference, Vol. 7, pp. 94-100.

Thompson, M., Gomez-Ramirez, F., Bejarano, M. (2002). "ILLI-PAVE based flexible pavement design concepts for multiple wheel heavy gear load aircraft." Ninth International Conference on Asphalt Pavements.

TNZ (2006). "Transit New Zealand M/4 2006 Specification for basecourse aggregate", Wellington, New Zealand.

Transit (2007) "Transit New Zealand Specification TNZ T/15, draft, 2007", Wellington, New Zealand.

Van De Ven, M. F. C., Jenkins, K. J., Voskuilen, J. L. M., and Van Den Beemt, R. (2007). "Development of (half-) warm foamed bitumen mixes: State of the art". International Journal of Pavement Engineering, 8(2), pp. 163-175.

Vorobieff, G. (2005). "Design of foamed bitumen layers for roads". AustStab workshop on road stabilisation in Queensland, Australia.

Vuong, B. T. (2004). Incorporation of laboratory performance tests into performance-based specifications for unbound granular materials. ARRB Transport Research Limited.

Werkmeister, S. (2004). "Permanent deformation behaviour of unbound granular materials in pavement constructions". PhD Thesis, Technical University of Dresden, Germany.

Werkmeister, S. (2006). “Shakedown Analysis of Unbound Granular Materials using Accelerated Pavement Test Results from New Zealand CAPTIF Facility”. Pavement Mechanics and Performance – Geo Shanghai International Conference American Society of Civil Engineers, pp. 220-228.

Werkmeister, S., Dawson, A. R., and Wellner, F. (2004). “Pavement design model for unbound granular materials”. Journal of Transportation Engineering, American Society of Civil Engineers (ASCE), Vol. 5, pp. 665-674.

Wirtgen (2004). "Wirtgen Cold Recycling Manual".

Witczak, M., and Uzan, J. (1988). "The universal airport pavement design system, Report I". Department of Civil Engineering, University of Maryland College Park, United States.

A Fundamentals of foam bitumen mixes

A.1 Introduction

Foam bitumen is a hot bituminous binder that has been temporarily converted from a liquid state to a foamed state by addition of a small amount of water. The pioneering research on foamed bitumen was conducted by Dr. Ladis Csanyi, who more than forty years ago injected steam into bitumen at the Bituminous Research Laboratory of the Engineering Experiment Station at Iowa State University (Csanyi 1962). The main motivation of Csanyi's research was the lack of acceptable quality aggregates for road construction and the large quantity of marginal materials in the state of Iowa. The main outcomes of Csanyi's research were the development of a spray nozzle for foamed bitumen production, where the binder is foamed before it makes contact with the mineral aggregate, and to demonstrate that during its stable life, the foam bitumen could be mixed with soils to improve their properties and produce a road building material.

The spray nozzle developed by Csanyi used steam instead of water. He suggested that the use of steam was the simplest, most effective and efficient for producing the foam, and also was available in asphalt plants at that time since a steam jetty was used to keep the jacketing on the piping system and the pugmills warm (Figure A.1).

The Csanyi's spray nozzle was modified in 1970 by Mobil Australia by using small amounts of water (1% to 2%) instead of steam. Hot bitumen and water were mixed in a specially designed expansion chamber to produce the foam. In 1971, the patent for the expansion chamber and nozzle system was granted to Mobil Australia and was extended to more than 14 countries. Since then, trials of foamed bitumen pavements were carried out in several countries, including New Zealand. In a decade, Australia placed more than 400 kilometres of foamed bitumen mixtures, followed by United States, South Africa, New Zealand, Japan and Germany.

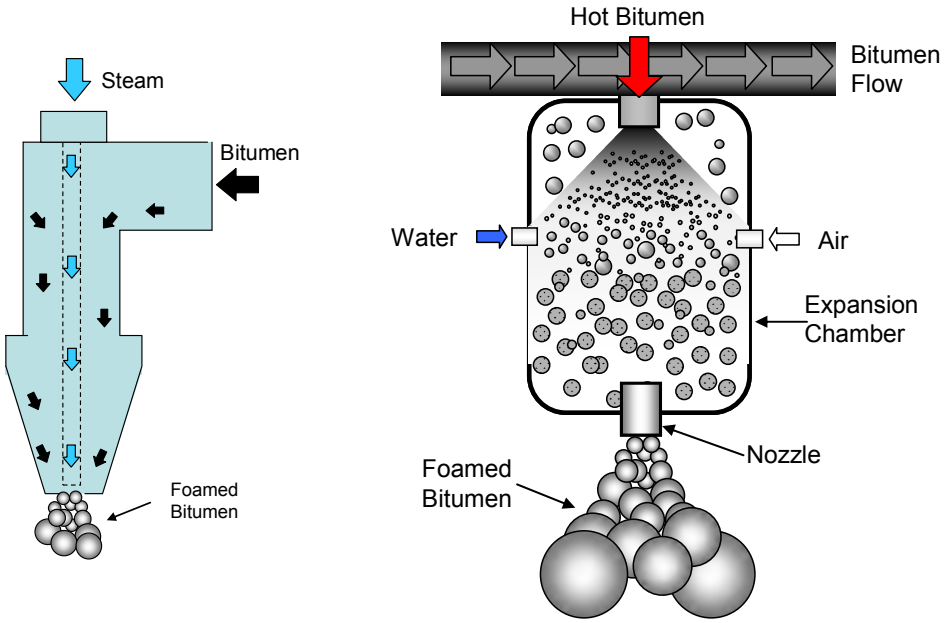

Figure A.1 Diagram of the original spray nozzle developed by Csanyi (1957) (left) and modern expansion chamber for foam bitumen production (right)

In 1990 Mobil Australia's patent rights expired and the interest on foamed bitumen technology grew rapidly since its several advantages in comparison with traditional pavement construction techniques (Jenkins 1994; Thenoux et al. 2006). At the same time, various foamed bitumen plants were developed and introduced into the machinery market, which leaded to upgraded machinery models (Figure A.2) during this decade, that have improved the mixing quality of foamed bitumen mixes.

Only during the last years some formal technical guidelines have been developed in South Africa (Asphalt Academy 2002) and by machinery companies (Wirtgen 2004) that have tried to encourage the technology.

Figure A.2 A modern foam bitumen recycling machine

A.2 Characterization of foamed bitumen and bitumen properties

Generally, foamed bitumen is physically characterized by two empirical indices: expansion ratio and half-life time. The expansion ratio of the foam is defined as the ratio between the maximum volume achieved during expansion and the final bitumen volume once the foam has dissipated (see Figure A.3). The half-life is the time, in seconds, between the moment the foamed bitumen achieves its maximum volume and the time it dissipates to half of the maximum volume.

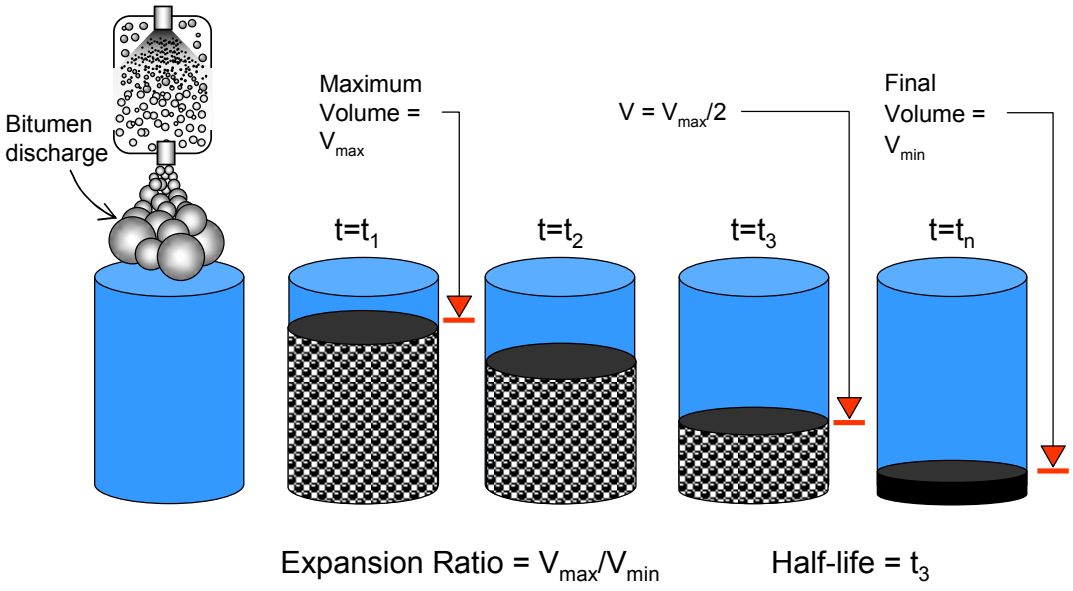

Figure A.3 Decay of foam bitumen with time after discharge

Bowering and Martin (1976) showed that expansion ratio influences the mechanical properties of foam bitumen mixes. They prepared two foam bitumen mixes, using sand as aggregate material. The first mix was prepared using foam bitumen with expansion ratio 3:1, and the second with a bitumen with expansion ratio 15:1. They measured increase in cohesion, Marshall stability and unconfined compressive strength in the mix with increase in expansion ratio. Ruckel et al. (1983) and Acott and Myburgh (1983) recommended limits of 8 to 15 for the expansion ratio and a minimum of 20 seconds for half-life to assure a good quality of the mix. Lee (1981) studied the effect of half-life and expansion ratio on the Marshall properties of foam mixes. The ranges used varied from 5 to 20 for expansion ratio and 11 to 136 seconds for half-life. The study did not show clear trends relative to the foam characteristics and stability. More recently, the South African interim guidelines for the design and use of foam bitumen treated materials (Asphalt Academy 2002) recommended a minimum expansion ratio of 10, and a minimum half-life time of 12 seconds to ensure that adequate coating of aggregate can occur.

Brennen et al (1983) identified the main factors that affect the foaming properties: the amount of foam produced; the amount of water in the foam; and the foaming temperature of the bitumen. The outlines of this study showed that generally an increase in bitumen temperature resulted in an increase in expansion ratio but a decrease in half-life. The same trend was noted for an increase in foaming water application, which is schematically presented in Figure A.4.

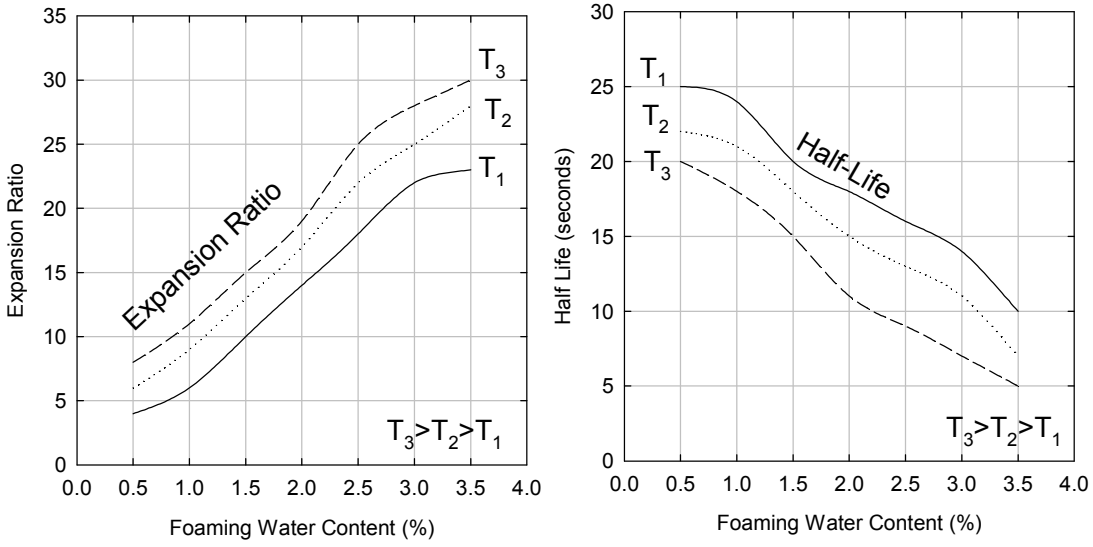

Figure A.4 Typical expansion ratio and half-life measurements on foam bitumen

Jenkins et al. (2000) found that a problem with the normal method for measuring half-life time and expansion ratio in the laboratory is that the process of spraying foam into the receiving vessel takes a considerable time compared to the half life time itself (about 5 seconds). Therefore, performed an extensive study of bitumen foam characterization and found out that an important amount of foam collapses by the time the maximum expansion ratio is recorded. This could not be so relevant for bitumen with good foaming properties, but there is an important effect in short half-life bitumen foams.

A.3 Aggregate properties

Foamed bitumen is usually used as a pavement recycling technique in which a machine reclaims the aggregates (with or without reclaimed asphalt pavements, RAP) from the aged, distressed pavement. Therefore, there is no total control on the input aggregate and a wide range of materials has been treated for use in road construction.

Mobil Oil proposed guidelines for suitable gradations of aggregates that may be utilized for foamed bitumen stabilisation (Akeroyd and Hicks 1988), as summarized in Figure A.5. This chart depicts three different zones, where:

- Zone A is ideal for heavily trafficked roads.
- Zone B is suitable for light traffic, but could be adjusted to zone A by the addition of more coarse material.
- Zone C is unsuitable for foamed bitumen stabilisation unless adjustments to the fine fraction are made to bring it into zone A.

The fine (particles passing the 0.075 mm) content is fundamental in the foamed bitumen stabilisation, and should ideally exceed 5.0%. Ruckel et al. (1983) and Akeroyd and Hicks (1988) suggested amounts of fines between 5% and 20%. The South African Interim Technical Guidelines (Asphalt Academy 2002) recommend determining the type of skeletal structure in the mix. They stated that mixes that are mainly stone skeleton (> 4.75 mm) or filler skeleton (< 0.075 mm) are not suitable for foamed bitumen mixes and their gradations must be adjusted if foamed bitumen is to be used.

Other important property of aggregates that influences foamed bitumen mixes is plasticity. Bowering and Martin (1976) had problems adding foam to clayey gravels unless modified before the addition of bitumen. Lee (1981) suggested that a lime pre-treatment is recommended if plasticity index exceeds 8.0%. Wirtgen (2004) recommends the usage of lime instead of cement when plasticity index exceeds 10%.

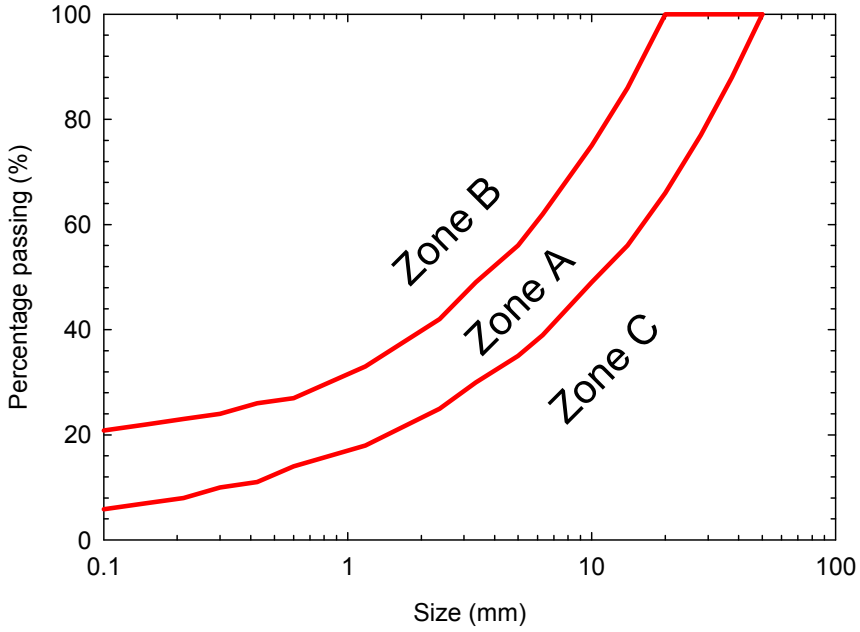

Figure A.5 Recommended particle aggregate size distribution for foam bitumen stabilisation

A.4 Moisture content during mixing

Csanyi (1957) noticed that the water content of the aggregate was important since was a dispersion medium for the foam. Later, Bowering and Martin (1976) and Brennen et al (1983) investigated the effects of varying moisture content in the aggregate before mixing with the foam bitumen and proposed the 'fluff' point, defined as the ideal moisture content of a material for blending with foam bitumen. This point is the moisture content at which the material occupies the maximum loose volume. Brennen et al. (1983) concluded that the amount of moisture is critical, because a lack of it impedes dispersion of the foam, workability and compaction of the mix, and an excess of moisture increases the curing time and reduces the density and strength of the compacted mix. Lee (1981) proposed that the optimum moisture content varies with the gradation of the aggregate, especially with the fraction under 75 μm. Lee concluded that the addition of moisture to a foamed mix after stabilization with foamed bitumen is of no benefit and recommends a moisture content of 65% to 85% of the optimum moisture content according to the AASHTO standard compaction of the aggregate. Ruckel et al. (1983) suggests that a sensitivity analysis should be performed for the mixing

moisture content during the mix design using different optimum moisture contents for the virgin material.

Castedo Franco and Wood (1983) and Wood et al. (1984) stated that the optimum moisture content of the foamed mixes also depends on the total fluid content. The total fluid content is defined as the total content of water and bitumen. More recently, Jenkins (1999) established a relationship that correlates the moisture content before and after mixing, the aggregate temperature and the bitumen content. This relationship is valid for aggregate temperatures between 40 °C and 98 °C. Conversely, Long and Ventura (2004) suggested that for a good quality stabilised material, the foamed bitumen does not contribute to the compaction fluid.

A.5 Compaction

There is not a general agreement on the most suitable compaction technique for foam bitumen mixes. Several methods have been used in laboratory mix design (kneading, Marshall, gyratory compactor). The effect of compaction level and the technique utilized is important as was shown by Brennen et al (1983). They tested recycled materials obtaining double Marshall Stability from samples compacted using gyratory compactor (20 gyrations, 1380 kPa) instead of Marshall.

Nataatmadja (2002) also investigated the effect of the compaction method on the properties of foamed bitumen mixes performing a comparison between Marshall compaction at two levels (50 and 75 blows per face) and gyratory compaction at 85 cycles and 3°. Results showed that gyratory compaction provided higher bulk densities and lower resilient moduli than those obtained using Marshall Compactor. At low bitumen levels the increase in resilient modulus from 50 to 75 blows was less important than that at higher bitumen contents.

For the preparation of large triaxial specimens (300mm x 150mm) vibratory (Long and Ventura 2004) as well as gyratory (Fu and Harvey 2007) compaction has been utilized varying the number of compaction layers.

A.6 Curing conditions

Curing of foam bitumen mixes is the process whereby the mixed and compacted material discharges water through evaporation or pore-pressure induced flow paths (Jenkins 1999). Various accelerated curing methods have been adopted by different researchers and agencies. The strength of foamed bitumen mixes initially improves with time, traffic and temperature, leading to a reduction of moisture of the stabilised pavement layer. Accot and Myburgh (1983) found that the time required for the mix to develop strength in the field ranged from 23 to 200 days. This varies according to road temperature, precipitation and evaporation. Ruckel et. al (1983) state that foamed mix pavements exhibit premature distress in days rather than in weeks or months after construction. In other words, the strength after an early or intermediate cure represents the most critical time period. Nataatmadja (2002) investigated the effect of curing method on the indirect tensile resilient modulus of 100 mm specimens for dry and soaked specimens. Three methods were studied: 28 days air curing temperature (25 °C), 3 days curing at 40 °C and 3 days at 60 °C. The 60 °C provides the highest modulus (dry and soaked), followed by the 40 °C dry, air cured dry, 40 °C soaked and air soaked.

Other curing periods have been adopted by other researchers. Long and Ventura (2004) used 28 days at 20 °C (room temperature) on double sealed triaxial specimens.

A.7 Temperature during mixing

Bowering and Martin (1976) and Castedo and Wood (1983) shown that depending on the aggregate type, the minimum mixing temperature of the aggregate is 13 °C to 23 °C. Below this point poor quality mixes will result. The influence of the aggregate temperature at the time of mixing is significant. Jenkins (1999) showed that the addition of bitumen at 180 °C in the foamed form will only increase the temperature of the mix by some 7 °C to 10 °C and that the original temperature of the aggregate has the dominant effect. He also concluded that at higher mixing temperatures the coating of the aggregate particles increases. Jenkins also shown that the temperature

gradient between the aggregate and the foamed bitumen affects the rate of collapse of the foam.

B History of H40 Aggregate production

B.1 Data History

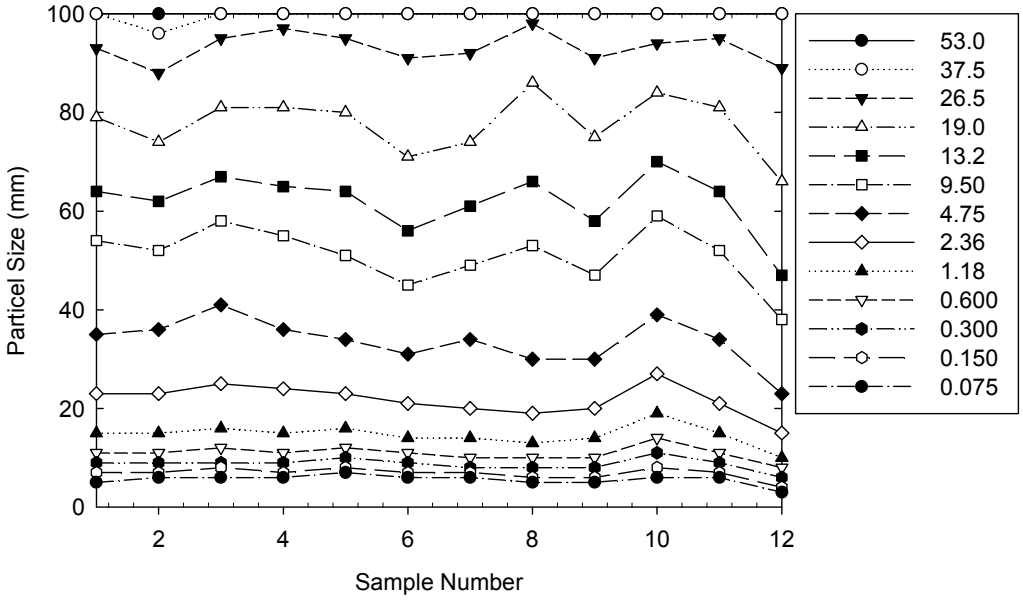

Figure B.1 Production of the H40 quarry in the North Island of New Zealand

C Compaction of Triaxial Specimens

C.1 Preliminary study specimens

Specimen Description	Hunua 0.0% Asphalt 0.0% Cement
Date and Test Number	1-Sep-06 Pr_B0C0_50
Testing date from-to	
Mould Diameter (mm)	150
Optimum Moisture (%)	6.0
Percentage of OMC (%)	70.0
Water Content (%)	4.2
Target Dry Density	
Area of Mould (cm2)	176.7

Mass Dry Material	11960.5
Required Water (ml)	502

Lift #	Ruler 1	Ruler 2	Ruler 3	Ruler 4	Average	Mass (g)	Depth/Lift	Total
Initial	377.0	377.0	377.0	377.0	377.0			0.0
1	326.0	327.0	328.0	328.0	327.3	1914.6	49.8	49.8
2	280.0	280.0	281.0	282.0	282.0	1944.9	45.3	95.0
3	231.0	228.0	231.0	231.0	230.3	1975.6	51.8	146.8
4	185.0	186.0	185.0	185.0	185.3	1924	45.0	191.8
5	135.0	135.0	135.0	133.0	134.5	2000.6	50.8	242.5
6	89.0	87.0	87.0	89.0	88.0	1930	46.5	289.0
6'	87.0	85.0	86.0	86.0	86.0	150	2.0	291.0
-								
-								

Specimen Height	291.0
Speciment Mass	11839.7
Bulk Density	2.302
Dry Density	2.210

Moisture Content Check	
Sample (Wet) + Tray	
Sample Dry + Tray	
Tray Weight	
Sample Wet	0.0
Sample Dry	0.0
MC	#DIV/0!

4

Specimen Description	Hunua 2.0% Asphalt 0.0% Cement
Date and Test Number	14-Sep-06 Pr_B2C0_50
Testing date from-to	
Mould Diameter (mm)	150
Optimum Moisture (%)	6.0
Percentage of OMC (%)	70.0
Water Content (%)	4.2
Target Dry Density	
Area of Mould (cm2)	176.7

Mass Dry Material	11960.5
Required Water (ml)	502

Lift #	Ruler 1	Ruler 2	Ruler 3	Ruler 4	Average	Mass (g)	Depth/Lift	Total
Initial	377.0	377.0	377.0	377.0	377.0			0.0
1	330.0	329.0	328.0	329.0	329.0	1924.8	48.0	48.0
2	281.0	282.0	283.0	282.0	282.0	1962.5	47.0	95.0
3	233.0	234.0	235.0	233.0	233.8	1972.3	48.3	143.3
4	188.0	186.0	187.0	188.0	187.3	1994.3	46.5	189.8
5	141.0	138.0	138.0	140.0	139.3	1991.6	48.0	237.8
6	90.0	90.0	88.0	88.0	89.0	1973.8	50.3	288.0
6'	88.0	88.0	87.0	88.0	87.8	150.0	1.3	289.3
-								
-								

Specimen Height	289.3
Speciment Mass	11969.3
Bulk Density	2.342
Dry Density	2.247

Moisture Content Check	
Sample (Wet) + Tray	14256.4
Sample Dry + Tray	13787.4
Tray Weight	2335.1
Sample Wet	11921.3
Sample Dry	11452.3
MC	4.10%

11

Specimen Description	Hunua 4.0% Asphalt 0.0% Cement
Date and Test Number	12-Oct-06 Pr_B4C0_50
Testing date from-to	
Mould Diameter (mm)	150
Optimum Moisture (%)	6.0
Percentage of OMC (%)	70.0
Water Content (%)	4.2
Target Dry Density	
Area of Mould (cm2)	176.7

Mass Dry Material	11960.5
Required Water (ml)	502

Lift #	Ruler 1	Ruler 2	Ruler 3	Ruler 4	Average	Mass (g)	Depth/Lift	Total
Initial	376.0	377.0	376.0	377.0	376.5			0.0
1	326.0	328.0	329.0	327.0	327.5	1904.5	49.0	49.0
2	282.0	281.0	283.0	282.0	282.0	1870.0	45.5	94.5
3	235.0	234.0	233.0	234.0	234.0	1953.2	48.0	142.5
4	184.0	185.0	185.0	185.0	184.8	1981.0	49.3	191.8
5	135.0	136.0	135.0	135.0	135.3	1976.8	49.5	241.3
6	88.0	88.0	90.0	89.0	88.8	1900.2	46.5	287.8
6'	87.0	86.0	86.0	86.0	86.3	150.0	2.5	290.3
-								
-								

Specimen Height	290.3
Speciment Mass	11735.7
Bulk Density	2.288
Dry Density	2.196

Moisture Content Check	
Sample (Wet) + Tray	14689.4
Sample Dry + Tray	14319.0
Tray Weight	3316.7
Sample Wet	11372.7
Sample Dry	11002.3
MC	3.37%

18

Specimen Description	Hunua 0.0% Asphalt 1.0% Cement	
Preparation date	28-Aug-06	Pr_B0C0_50
Testing date from-to	10/09/2006	12/09/2006
Mould Diameter (mm)	150	
Optimum Moisture (%)	6.0	
Percentage of OMC (%)	70.0	
Water Content (%)	4.2	
Target Dry Density		
Area of Mould (cm2)	176.7	

Mass Dry Material	11960.5
Required Water (ml)	502

Lift #	Ruler 1	Ruler 2	Ruler 3	Ruler 4	Average	Mass (g)	Depth/Lift	Total
Initial	377.0	377.0	377.0	377.0	377.0			0.0
1	328.0	328.0	330.0	329.0	328.8	1820.7	48.3	48.3
2	283.0	284.0	284.0	285.0	284.0	1834	44.8	93.0
3	233.0	233.0	235.0	235.0	234.0	1944	50.0	143.0
4	186.0	186.0	187.0	187.0	186.5	1838.8	47.5	190.5
5	139.0	137.0	138.0	139.0	138.3	1864.6	48.3	238.8
6	88.0	88.0	87.0	89.0	88.0	1981.9	50.3	289.0
6'	86.0	86.0	87.0	87.0	86.5	150	1.5	290.5
-								
-								

Specimen Height	290.5
Speciment Mass	11434
Bulk Density	2.227
Dry Density	2.138

Moisture Content Check	
Sample (Wet) + Tray	12320.4
Sample Dry + Tray	11916.1
Tray Weight	1000.0
Sample Wet	11320.4
Sample Dry	10916.1
MC	3.70%

1

Specimen Description	Hunua 2.0% Asphalt 1.0% Cement	
Date and Test Number	8-Sep-06	Pr_B2C1_50
Testing date from-to		
Mould Diameter (mm)	150	
Optimum Moisture (%)	6.0	
Percentage of OMC (%)	70.0	
Water Content (%)	4.2	
Target Dry Density		
Area of Mould (cm2)	176.7	

Mass Dry Material	11960.5
Required Water (ml)	502

Lift #	Ruler 1	Ruler 2	Ruler 3	Ruler 4	Average	Mass (g)	Depth/Lift	Total
Initial	377.0	377.0	377.0	377.0	377.0			0.0
1	327.0	327.0	328.0	329.0	327.8	1937.6	49.3	49.3
2	280.0	279.0	280.0	279.0	279.5	1967.3	48.3	97.5
3	232.0	232.0	232.0	231.0	231.8	1928.9	47.8	145.3
4	184.0	185.0	186.0	184.0	184.8	1923.4	47.0	192.3
5	135.0	135.0	135.0	136.0	135.3	1969.9	49.5	241.8
6	89.0	89.0	88.0	90.0	89.0	1931	46.3	288.0
6'	86.0	85.0	85.0	86.0	85.5	150	3.5	291.5
-								
-								

Specimen Height	291.5
Speciment Mass	11808.1
Bulk Density	2.292
Dry Density	2.200

Moisture Content Check	
Sample (Wet) + Tray	15003.7
Sample Dry + Tray	14585.6
Tray Weight	3254.8
Sample Wet	11748.9
Sample Dry	11330.8
MC	3.69%

8

Specimen Description	Hunua 4.0% Asphalt 1.0% Cement
Date and Test Number	28-Sep-06 Pr_B4C1_50
Testing date from-to	
Mould Diameter (mm)	150
Optimum Moisture (%)	6.0
Percentage of OMC (%)	70.0
Water Content (%)	4.2
Target Dry Density	
Area of Mould (cm2)	176.7

Mass Dry Material	11960.5
Required Water (ml)	502

Lift #	Ruler 1	Ruler 2	Ruler 3	Ruler 4	Average	Mass (g)	Depth/Lift	Total
Initial	376.0	376.0	376.0	376.0	376.0			0.0
1	326.0	325.0	325.0	325.0	325.3	1999.0	50.8	50.8
2	276.0	277.0	277.0	275.0	276.3	1922.8	49.0	99.8
3	226.0	229.0	230.0	227.0	228.0	1866.7	48.3	148.0
4	183.0	184.0	184.0	183.0	183.5	1804.0	44.5	192.5
5	136.0	134.0	135.0	137.0	135.5	1883.6	48.0	240.5
6	87.0	85.0	85.0	87.0	86.0	1888.3	49.5	290.0
6'	84.0	83.0	84.0	84.0	83.8	150.0	2.3	292.3
-								
-								

Specimen Height	292.3
Speciment Mass	11514.4
Bulk Density	2.230
Dry Density	2.140

Moisture Content Check	
Sample (Wet) + Tray	
Sample Dry + Tray	
Tray Weight	
Sample Wet	0.0
Sample Dry	0.0
MC	#DIV/0!

15

Specimen Description	Hunua 0.0% Asphalt 0.0% Cement
Date and Test Number	22-Sep-06 Pr_B0C0_100
Testing date from-to	
Mould Diameter (mm)	150
Optimum Moisture (%)	6.0
Percentage of OMC (%)	70.0
Water Content (%)	4.2
Target Dry Density	
Area of Mould (cm2)	176.7

Mass Dry Material	12661
Required Water (ml)	532

Lift #	Ruler 1	Ruler 2	Ruler 3	Ruler 4	Average	Mass (g)	Depth/Lift	Total
Initial	377.0	377.0	377.0	377.0	377.0			0.0
1	327.0	328.0	328.0	326.0	327.3	1956.5	49.8	49.8
2	282.0	280.0	280.0	280.0	280.5	1939.1	46.8	96.5
3	234.0	232.0	232.0	234.0	233.0	1923.2	47.5	144.0
4	186.0	185.0	186.0	187.0	186.0	1990.0	47.0	191.0
5	136.0	136.0	136.0	135.0	135.8	2021.4	50.3	241.3
6	87.0	87.0	87.0	87.0	87.0	1946.9	48.8	290.0
6'	85.0	85.0	85.0	85.0	85.0	150.0	2.0	292.0
-								
-								

Specimen Height	292.0
Speciment Mass	11927.1
Bulk Density	2.311
Dry Density	2.218

Moisture Content Check	
Sample (Wet) + Tray	14174.0
Sample Dry + Tray	13735.8
Tray Weight	2335.5
Sample Wet	11838.5
Sample Dry	11400.3
MC	3.84%

13

Specimen Description	Hunua 2.0% Asphalt 0.0% Cement
Date and Test Number	14-Sep-06 Pr_B2C0_100
Testing date from-to	
Mould Diameter (mm)	150
Optimum Moisture (%)	6.0
Percentage of OMC (%)	70.0
Water Content (%)	4.2
Target Dry Density	
Area of Mould (cm2)	176.7

Mass Dry Material	11960.5
Required Water (ml)	502

Lift #	Ruler 1	Ruler 2	Ruler 3	Ruler 4	Average	Mass (g)	Depth/Lift	Total
Initial	377.0	377.0	377.0	377.0	377.0			0.0
1	327.0	328.0	331.0	329.0	328.8	1968.6	48.3	48.3
2	283.0	283.0	283.0	283.0	283.0	1952.7	45.8	94.0
3	235.0	236.0	235.0	235.0	235.3	1979.5	47.8	141.8
4	186.0	187.0	187.0	186.0	186.5	1980.4	48.8	190.5
5	138.0	141.0	141.0	139.0	139.8	1948.5	46.8	237.3
6	91.0	93.0	93.0	91.0	92.0	2007.9	47.8	285.0
6'	88.0	90.0	90.0	89.0	89.3	151.2	2.8	287.8
-								
-								

Specimen Height	287.8
Speciment Mass	11988.8
Bulk Density	2.358
Dry Density	2.263

Moisture Content Check	
Sample (Wet) + Tray	15120.6
Sample Dry + Tray	14604.2
Tray Weight	3256.7
Sample Wet	11863.9
Sample Dry	11347.5
MC	4.55%

12

Specimen Description	Hunua 4.0% Asphalt 0.0% Cement
Date and Test Number	12-Oct-06 Pr_B4C0_100
Testing date from-to	
Mould Diameter (mm)	150
Optimum Moisture (%)	6.0
Percentage of OMC (%)	70.0
Water Content (%)	4.2
Target Dry Density	
Area of Mould (cm2)	176.7

Mass Dry Material	11960.5
Required Water (ml)	502

Lift #	Ruler 1	Ruler 2	Ruler 3	Ruler 4	Average	Mass (g)	Depth/Lift	Total
Initial	377.0	376.0	376.0	377.0	376.5			0.0
1	326.0	328.0	326.0	327.0	326.8	1935.7	49.8	49.8
2	277.0	277.0	280.0	279.0	278.3	1902.3	48.5	98.3
3	232.0	231.0	231.0	232.0	231.5	1868.8	46.8	145.0
4	185.0	184.0	185.0	184.0	184.5	1904.1	47.0	192.0
5	135.0	136.0	137.0	136.0	136.0	1961.0	48.5	240.5
6	88.0	88.0	89.0	89.0	88.5	1916.4	47.5	288.0
6'	86.0	86.0	86.0	86.0	86.0	150.0	2.5	290.5
-								
-								

Specimen Height	290.5
Speciment Mass	11638.3
Bulk Density	2.267
Dry Density	2.176

Moisture Content Check	
Sample (Wet) + Tray	14906.8
Sample Dry + Tray	14472.4
Tray Weight	3316.8
Sample Wet	11590.0
Sample Dry	11155.6
MC	3.89%

19

Specimen Description	Hunua 0.0% Asphalt 1.0% Cement		
Date and Test Number	28-Aug-06	Pr_B0C1_100	
Testing date from-to	12-Sep-06	14/09/2006	
Mould Diameter (mm)	150		
Optimum Moisture (%)	6.0		
Percentage of OMC (%)	70.0		
Water Content (%)	4.2		
Target Dry Density			
Area of Mould (cm2)	176.7		

Mass Dry Material	13000
Required Water (ml)	546

Lift #	Ruler 1	Ruler 2	Ruler 3	Ruler 4	Average	Mass (g)	Depth/Lift	Total
Initial	377.0	377.0	377.0	377.0	377.0			0.0
1	329.0	326.0	329.0	330.0	328.5	1877.1	48.5	48.5
2	279.0	280.0	280.0	281.0	282.0	1892.6	46.5	95.0
3	234.0	233.0	234.0	235.0	234.0	1898.8	48.0	143.0
4	182.0	181.0	185.0	186.0	183.5	1934.3	50.5	193.5
5	137.0	136.0	138.0	139.0	137.5	1888.3	46.0	239.5
6	88.0	88.0	90.0	91.0	89.3	1901.1	48.3	287.8
6'	86.0	86.0	88.0	88.0	87.0	150	2.3	290.0
-								
-								

Specimen Height	290.0
Speciment Mass	11542.2
Bulk Density	2.252
Dry Density	2.161

Moisture Content Check	
Sample (Wet) + Tray	
Sample Dry + Tray	
Tray Weight	
Sample Wet	0.0
Sample Dry	0.0
MC	#DIV/0!

2

Specimen Description	Hunua 2.0% Asphalt 1.0% Cement		
Date and Test Number	8-Sep-06	Pr_B2C1_100	
Testing date from-to			
Mould Diameter (mm)	150		
Optimum Moisture (%)	6.0		
Percentage of OMC (%)	70.0		
Water Content (%)	4.2		
Target Dry Density			
Area of Mould (cm2)	176.7		

Mass Dry Material	11960.5
Required Water (ml)	502

Lift #	Ruler 1	Ruler 2	Ruler 3	Ruler 4	Average	Mass (g)	Depth/Lift	Total
Initial	377.0	377.0	377.0	377.0	377.0			0.0
1	327.0	328.0	329.0	327.0	327.8	1928	49.3	49.3
2	276.0	279.0	279.0	276.0	277.5	1930	50.3	99.5
3	227.0	230.0	229.0	228.0	228.5	1940.9	49.0	148.5
4	182.0	184.0	184.0	182.0	183.0	1978.9	45.5	194.0
5	136.0	134.0	135.0	137.0	135.5	1942.5	47.5	241.5
6	87.0	85.0	86.0	88.0	86.5	1937.5	49.0	290.5
6'	85.0	85.0	85.0	84.0	84.8	150	1.8	292.3
-								
-								

Specimen Height	292.3
Speciment Mass	11807.8
Bulk Density	2.286
Dry Density	2.194

Moisture Content Check	
Sample (Wet) + Tray	15056.6
Sample Dry + Tray	14630.4
Tray Weight	3323.4
Sample Wet	11733.2
Sample Dry	11307.0
MC	3.77%

9

Specimen Description	Hunua 4.0% Asphalt 1.0% Cement
Date and Test Number	28-Sep-06 Pr_B4C1_100
Testing date from-to	
Mould Diameter (mm)	150
Optimum Moisture (%)	6.0
Percentage of OMC (%)	70.0
Water Content (%)	4.2
Target Dry Density	
Area of Mould (cm2)	176.7

Mass Dry Material	11960.5
Required Water (ml)	502

Lift #	Ruler 1	Ruler 2	Ruler 3	Ruler 4	Average	Mass (g)	Depth/Lift	Total
Initial	376.0	376.0	376.0	376.0	376.0			0.0
1	329.0	329.0	328.0	329.0	328.8	1906.6	47.3	47.3
2	280.0	280.0	280.0	280.0	280.0	1906.4	48.8	96.0
3	320.0	233.0	231.0	229.0	253.3	1909.9	26.8	122.8
4	184.0	181.0	181.0	184.0	182.5	1889.8	70.8	193.5
5	133.0	133.0	134.0	134.0	133.5	1913.8	49.0	242.5
6	85.0	85.0	85.0	85.0	85.0	1846.7	48.5	291.0
6'	83.0	82.0	82.0	83.0	82.5	150.0	2.5	293.5
-								
-								

Specimen Height	293.5
Speciment Mass	11523.2
Bulk Density	2.222
Dry Density	2.132

Moisture Content Check	
Sample (Wet) + Tray	14786.0
Sample Dry + Tray	14442.8
Tray Weight	3316.7
Sample Wet	11469.3
Sample Dry	11126.1
MC	3.08%

16

C.2 Detail study specimens, low compaction energy

Specimen Description	Hunua 0.0% Asphalt 1.0% Cement
Date and Test Number	23-Jun-07 D_B0C1_LC_1
Testing date from-to	
Mould Diameter (mm)	150
Optimum Moisture (%)	6.0
Percentage of OMC (%)	100.0
Water Content (%)	5.1
Target Dry Density	
Area of Mould (cm2)	176.7

Mass Dry Material	11960.5
Required Water (ml)	610

Lift #	Ruler 1	Ruler 2	Ruler 3	Ruler 4	Average	Mass (g)	Depth/Lift	Total
Initial	377.0	377.0	377.0	377.0	377.00			0.00
1	329.0	329.0	327.0	327.0	328.00	1850.0	49.0	49.00
2	282.0	282.0	283.0	281.0	282.00	1842.6	46.0	95.00
3	236.0	235.0	236.0	235.0	235.50	1856.3	46.5	141.50
4	190.0	191.0	192.0	191.0	191.00	1858.8	44.5	186.00
5	144.0	141.0	142.0	144.0	142.75	1838.9	48.3	234.25
6	96.0	93.0	94.0	96.0	94.75	1845.6	48.0	282.25
6'	94.0	94.0	94.0	94.0	94.0	150.0	0.8	283.00
-								
-						8		

Specimen Height	283.00
Speciment Mass	11242.2
Bulk Density	2.248
Dry Density	2.139

Moisture Content Check	
Sample (Wet) + Tray	
Sample Dry + Tray	
Tray Weight	
Sample Wet	0.0
Sample Dry	0.0
MC	#DIV/0!

65

Specimen Description	Hunua 0.0% Asphalt 1.0% Cement
Date and Test Number	29-Jun-07 **D_B0C1_LC_2**
Testing date from-to	
Mould Diameter (mm)	150
Optimum Moisture (%)	6.0
Percentage of OMC (%)	100.0
Water Content (%)	5.1
Target Dry Density	
Area of Mould (cm2)	176.7

Mass Dry Material	11960.5
Required Water (ml)	610

Lift #	Ruler 1	Ruler 2	Ruler 3	Ruler 4	Average	Mass (g)	Depth/Lift	Total
Initial	376.0	376.0	376.0	376.0	376.00			0.00
1	328.0	329.0	328.0	329.0	328.50	1859.6	47.5	47.50
2	283.0	282.0	282.0	280.0	281.75	1864.8	46.8	94.25
3	235.0	237.0	235.0	234.0	235.25	1855.9	46.5	140.75
4	189.0	188.0	189.0	188.0	188.50	1855.7	46.8	187.50
5	141.0	139.0	141.0	140.0	140.25	1853.7	48.3	235.75
6	95.0	94.0	94.0	96.0	94.75	1838.2	45.5	281.25
6'	91.0	93.0	92.0	94.0	92.5	150.0	2.3	283.50
-								
-						9		

Specimen Height	283.50
Speciment Mass	11277.9
Bulk Density	2.251
Dry Density	2.142

Moisture Content Check	
Sample (Wet) + Tray	
Sample Dry + Tray	
Tray Weight	
Sample Wet	0.0
Sample Dry	0.0
MC	#DIV/0!

69

Specimen Description	Hunua 0.0% Asphalt 1.0% Cement
Date and Test Number	20-Aug-07 **D_B0C1_LC_3**
Testing date from-to	
Mould Diameter (mm)	150
Optimum Moisture (%)	6.0
Percentage of OMC (%)	100.0
Water Content (%)	5.1
Target Dry Density	
Area of Mould (cm2)	176.7

Mass Dry Material	11960.5
Required Water (ml)	610

Lift #	Ruler 1	Ruler 2	Ruler 3	Ruler 4	Average	Mass (g)	Depth/Lift	Total
Initial	377.0	377.0	377.0	377.0	377.00			0.00
1	329.0	331.0	328.0	326.0	328.50	1856.2	48.5	48.50
2	283.0	282.0	282.0	281.0	282.00	1852.1	46.5	95.00
3	238.0	237.0	235.0	234.0	236.00	1856.4	46.0	141.00
4	190.0	188.0	187.0	190.0	188.75	1851.1	47.3	188.25
5	141.0	140.0	141.0	140.0	140.50	1855.4	48.3	236.50
6	96.0	94.0	97.0	95.0	95.50	1849.3	45.0	281.50
6'	96.0	96.0	96.0	96.0	96.0	150.0	-0.5	281.00
-								
-						3		

Specimen Height	281.00
Speciment Mass	11270.5
Bulk Density	2.270
Dry Density	2.160

Moisture Content Check	
Sample (Wet) + Tray	
Sample Dry + Tray	
Tray Weight	
Sample Wet	0.0
Sample Dry	0.0
MC	#DIV/0!

73

Specimen Description	Hunua 2.0% Asphalt 1.0% Cement
Date and Test Number	15-Jun-07 D_B2C1_LC_1
Testing date from-to	
Mould Diameter (mm)	150
Optimum Moisture (%)	6.0
Percentage of OMC (%)	100.0
Water Content (%)	5.1
Target Dry Density	
Area of Mould (cm2)	176.7

Mass Dry Material	11960.5
Required Water (ml)	610

Lift #	Ruler 1	Ruler 2	Ruler 3	Ruler 4	Average	Mass (g)	Depth/Lift	Total
Initial	377.0	377.0	377.0	377.0	377.00			0.00
1	326.0	328.0	327.0	326.0	326.75	1789.8	50.3	50.25
2	277.0	278.0	279.0	277.0	277.75	1791.2	49.0	99.25
3	228.0	230.0	232.0	230.0	230.00	1780.5	47.8	147.00
4	186.0	185.0	185.0	185.0	185.25	1769.3	44.8	191.75
5	134.0	135.0	137.0	136.0	135.50	1818.2	49.8	241.50
6	89.0	89.0	89.0	89.0	89.00	1785.7	46.5	288.00
6'								
-						1789.1		
-						16	2.1	
						0.9%		

Specimen Height	288.00
Speciment Mass	10734.7
Bulk Density	2.109
Dry Density	2.007

Moisture Content Check	
Sample (Wet) + Tray	
Sample Dry + Tray	
Tray Weight	
Sample Wet	0.0
Sample Dry	0.0
MC	#DIV/0!

58

Specimen Description	Hunua 2.0% Asphalt 1.0% Cement
Date and Test Number	15-Jun-07 D_B2C1_LC_2
Testing date from-to	
Mould Diameter (mm)	150
Optimum Moisture (%)	6.0
Percentage of OMC (%)	100.0
Water Content (%)	5.1
Target Dry Density	
Area of Mould (cm2)	176.7

Mass Dry Material	11960.5
Required Water (ml)	610

Lift #	Ruler 1	Ruler 2	Ruler 3	Ruler 4	Average	Mass (g)	Depth/Lift	Total
Initial	377.0	377.0	377.0	377.0	377.00			0.00
1	328.0	330.0	328.0	326.0	328.00	1825.9	49.0	49.00
2	281.0	281.0	278.0	280.0	280.00	1826.8	48.0	97.00
3	235.0	233.0	234.0	235.0	234.25	1817.7	45.8	142.75
4	189.0	188.0	187.0	187.0	187.75	1800.1	46.5	189.25
5	140.0	138.0	138.0	139.0	138.75	1822.1	49.0	238.25
6	91.0	92.0	92.0	91.0	91.50	1835.0	47.3	285.50
6'	91.0	91.0	91.0	91.0	91.0	150.0	0.5	286.00
-								
-						12		

Specimen Height	286.00
Speciment Mass	11077.6
Bulk Density	2.192
Dry Density	2.085

Moisture Content Check	
Sample (Wet) + Tray	
Sample Dry + Tray	
Tray Weight	
Sample Wet	0.0
Sample Dry	0.0
MC	#DIV/0!

59

Specimen Description	Hunua 2.0% Asphalt 1.0% Cement
Date and Test Number	19-Jun-07 **D_B2C1_LC_3**
Testing date from-to	
Mould Diameter (mm)	150
Optimum Moisture (%)	6.0
Percentage of OMC (%)	100.0
Water Content (%)	5.1
Target Dry Density	
Area of Mould (cm2)	176.7

Mass Dry Material	11960.5
Required Water (ml)	610

Lift #	Ruler 1	Ruler 2	Ruler 3	Ruler 4	Average	Mass (g)	Depth/Lift	Total
Initial	377.0	377.0	378.0	378.0	377.50			0.00
1	328.0	330.0	328.0	325.0	327.75	1866.6	49.8	49.75
2	280.0	282.0	280.0	278.0	280.00	1836.1	47.8	97.50
3	231.0	234.0	234.0	231.0	232.50	1851.0	47.5	145.00
4	186.0	185.0	185.0	185.0	185.25	1833.9	47.3	192.25
5	136.0	136.0	138.0	138.0	137.00	1858.5	48.3	240.50
6	88.0	88.0	89.0	88.0	88.25	1862.3	48.8	289.25
6'	88.0	87.0	87.0	88.0	87.5	150.0	0.8	290.00
-								
-						14		

Specimen Height	290.00
Speciment Mass	11258.4
Bulk Density	2.197
Dry Density	2.090

Moisture Content Check	
Sample (Wet) + Tray	
Sample Dry + Tray	
Tray Weight	
Sample Wet	0.0
Sample Dry	0.0
MC	#DIV/0!

62

Specimen Description	Hunua 4.0% Asphalt 1.0% Cement
Date and Test Number	7-Jun-07 **D_B4C1_LC_1**
Testing date from-to	
Mould Diameter (mm)	150
Optimum Moisture (%)	6.0
Percentage of OMC (%)	100.0
Water Content (%)	5.1
Target Dry Density	
Area of Mould (cm2)	176.7

Mass Dry Material	11960.5
Required Water (ml)	610

Lift #	Ruler 1	Ruler 2	Ruler 3	Ruler 4	Average	Mass (g)	Depth/Lift	Total
Initial	377.0	377.0	377.0	377.0	377.00			0.00
1	332.0	331.0	332.0	331.0	331.50	1670.0	45.5	45.50
2	288.0	288.0	288.0	287.0	287.75	1671.8	43.8	89.25
3	242.0	243.0	243.0	242.0	242.50	1721.6	45.3	134.50
4	192.0	191.0	193.0	192.0	192.00	1961.8	50.5	185.00
5	140.0	140.0	138.0	139.0	139.25	1967.0	52.8	237.75
6	85.0	85.0	86.0	85.0	85.25	1952.0	54.0	291.75
6'								
-								
-						150	4.3	

Specimen Height	291.75
Speciment Mass	10944.2
Bulk Density	2.123
Dry Density	2.020

Moisture Content Check	
Sample (Wet) + Tray	
Sample Dry + Tray	
Tray Weight	
Sample Wet	0.0
Sample Dry	0.0
MC	#DIV/0!

54

Specimen Description	Hunua 4.0% Asphalt 1.0% Cement
Date and Test Number	19-Jun-07 **D_B4C1_LC_2**
Testing date from-to	
Mould Diameter (mm)	150
Optimum Moisture (%)	6.0
Percentage of OMC (%)	100.0
Water Content (%)	5.1
Target Dry Density	
Area of Mould (cm2)	176.7

Mass Dry Material	11960.5
Required Water (ml)	610

Lift #	Ruler 1	Ruler 2	Ruler 3	Ruler 4	Average	Mass (g)	Depth/Lift	Total
Initial	377.0	377.0	377.0	377.0	377.00			0.00
1	328.0	328.0	328.0	325.0	327.25	1816.1	49.8	49.75
2	278.0	279.0	278.0	276.0	277.75	1832.2	49.5	99.25
3	229.0	231.0	231.0	230.0	230.25	1812.3	47.5	146.75
4	184.0	184.0	184.0	183.0	183.75	1794.8	46.5	193.25
5	137.0	135.0	137.0	138.0	136.75	1797.0	47.0	240.25
6	89.0	86.0	89.0	89.0	88.25	1840.3	48.5	288.75
6'	86.0	86.0	86.0	86.0	86.0	150.0	2.3	291.00
-								
-						18		

Specimen Height	291.00
Speciment Mass	11042.7
Bulk Density	2.147
Dry Density	2.043

Moisture Content Check	
Sample (Wet) + Tray	
Sample Dry + Tray	
Tray Weight	
Sample Wet	0.0
Sample Dry	0.0
MC	#DIV/0!

63

Specimen Description	Hunua 4.0% Asphalt 1.0% Cement
Date and Test Number	4-Sep-07 **D_B4C1_LC_3**
Testing date from-to	
Mould Diameter (mm)	150
Optimum Moisture (%)	6.0
Percentage of OMC (%)	100.0
Water Content (%)	5.1
Target Dry Density	
Area of Mould (cm2)	176.7

Mass Dry Material	11960.5
Required Water (ml)	610

Lift #	Ruler 1	Ruler 2	Ruler 3	Ruler 4	Average	Mass (g)	Depth/Lift	Total
Initial	377.0	377.0	377.0	377.0	377.00			0.00
1	332.0	328.0	329.0	333.0	330.50	1825.2	46.5	46.50
2	281.0	282.0	283.0	281.0	281.75	1826.0	48.8	95.25
3	235.0	234.0	237.0	236.0	235.50	1819.0	46.3	141.50
4	186.0	186.0	188.0	188.0	187.00	1827.8	48.5	190.00
5	138.0	138.0	139.0	137.0	138.00	1836.2	49.0	239.00
6	88.0	89.0	90.0	90.0	89.25	1828.5	48.8	287.75
6'	88.0	87.0	90.0	89.0	88.5	150.3	0.8	288.50
-								
-						6		

Specimen Height	288.50
Speciment Mass	11113.0
Bulk Density	2.180
Dry Density	2.074

Moisture Content Check	
Sample (Wet) + Tray	
Sample Dry + Tray	
Tray Weight	
Sample Wet	0.0
Sample Dry	0.0
MC	#DIV/0!

79

C.3 Detail study specimens, high compaction energy

Specimen Description	Hunua 0.0% Asphalt 1.0% Cement
Date and Test Number	5-Apr-07 D_B0C1_HC_1
Testing date from-to	
Mould Diameter (mm)	150
Optimum Moisture (%)	6.0
Percentage of OMC (%)	100.0
Water Content (%)	5.1
Target Dry Density	
Area of Mould (cm2)	176.7

Mass Dry Material	11960.5
Required Water (ml)	610

Lift #	Ruler 1	Ruler 2	Ruler 3	Ruler 4	Average	Mass (g)	Depth/Lift	Total
Initial	377.0	377.0	377.0	377.0	377.0			0.0
1	327.0	326.0	326.0	326.0	326.3	1981.0	50.8	50.8
2	276.0	281.0	280.0	279.0	279.0	1980.0	47.3	98.0
3	232.0	238.0	232.0	230.0	233.0	1933.0	46.0	144.0
4	184.0	190.0	190.0	186.0	187.5	1957.6	45.5	189.5
5	136.0	142.0	142.0	137.0	139.3	1975.6	48.3	237.8
6	93.0	92.0	94.0	92.0	92.8	1980.0	46.5	284.3
6'	92.0	94.0	94.0	91.0	92.8	150	0.0	284.3
-								
-								

Specimen Height	284.3
Speciment Mass	11957.2
Bulk Density	2.380
Dry Density	2.265

Moisture Content Check	
Sample (Wet) + Tray	
Sample Dry + Tray	
Tray Weight	
Sample Wet	0.0
Sample Dry	0.0
MC	#DIV/0!

44

Specimen Description	Hunua 0.0% Asphalt 1.0% Cement
Date and Test Number	12-Apr-07 D_B0C1_HC_2
Testing date from-to	
Mould Diameter (mm)	150
Optimum Moisture (%)	6.0
Percentage of OMC (%)	100.0
Water Content (%)	5.1
Target Dry Density	
Area of Mould (cm2)	176.7

Mass Dry Material	11960.5
Required Water (ml)	610

Lift #	Ruler 1	Ruler 2	Ruler 3	Ruler 4	Average	Mass (g)	Depth/Lift	Total
Initial	376.0	377.0	377.0	377.0	376.8			0.0
1	326.0	330.0	329.0	325.0	327.5	1970.6	49.3	49.3
2	281.0	283.0	282.0	282.0	282.0	1970.7	45.5	94.8
3	236.0	234.0	234.0	236.0	235.0	2010.2	47.0	141.8
4	186.0	185.0	186.0	187.0	186.0	2049.9	49.0	190.8
5	139.0	140.0	141.0	138.0	139.5	2039.2	46.5	237.3
6	90.0	90.0	91.0	91.0	90.5	2067.7	49.0	286.3
6'	88.0	88.0	90.0	89.0	88.8	150.5	1.8	288.0
-								
-								

Specimen Height	288.0
Speciment Mass	12258.8
Bulk Density	2.409
Dry Density	2.292

Moisture Content Check	
Sample (Wet) + Tray	
Sample Dry + Tray	
Tray Weight	
Sample Wet	0.0
Sample Dry	0.0
MC	#DIV/0!

45

Specimen Description	Hunua 0.0% Asphalt 1.0% Cement
Date and Test Number	12-Apr-07 D_B0C1_HC_3
Testing date from-to	
Mould Diameter (mm)	150
Optimum Moisture (%)	6.0
Percentage of OMC (%)	100.0
Water Content (%)	5.1
Target Dry Density	
Area of Mould (cm2)	176.7

Mass Dry Material	11960.5
Required Water (ml)	610

Lift #	Ruler 1	Ruler 2	Ruler 3	Ruler 4	Average	Mass (g)	Depth/Lift	Total
Initial	377.0	376.0	377.0	377.0	376.8			0.0
1	327.0	331.0	328.0	327.0	328.3	2009.5	48.5	48.5
2	283.0	282.0	280.0	281.0	281.5	2010.4	46.8	95.3
3	234.0	232.0	234.0	234.0	233.5	2018.4	48.0	143.3
4	184.0	187.0	186.0	185.0	185.5	2010.5	48.0	191.3
5	137.0	140.0	139.0	136.0	138.0	2029.5	47.5	238.8
6	90.0	91.0	91.0	90.0	90.5	2019.7	47.5	286.3
6'	87.0	86.0	87.0	87.0	86.8	150.2	3.8	290.0
-								
-								

Specimen Height	290.0
Speciment Mass	12248.2
Bulk Density	2.390
Dry Density	2.274

Moisture Content Check	
Sample (Wet) + Tray	
Sample Dry + Tray	
Tray Weight	
Sample Wet	0.0
Sample Dry	0.0
MC	#DIV/0!

46

Specimen Description	Hunua 0.0% Asphalt 1.0% Cement
Date and Test Number	19-Apr-07 D_B0C1_HC_4
Testing date from-to	
Mould Diameter (mm)	150
Optimum Moisture (%)	6.0
Percentage of OMC (%)	100.0
Water Content (%)	5.1
Target Dry Density	
Area of Mould (cm2)	176.7

Mass Dry Material	11960.5
Required Water (ml)	610

Lift #	Ruler 1	Ruler 2	Ruler 3	Ruler 4	Average	Mass (g)	Depth/Lift	Total
Initial	376.0	377.0	377.0	376.0	376.5			0.0
1	326.0	327.0	326.0	326.0	326.3	2003.9	50.3	50.3
2	281.0	282.0	281.0	282.0	281.5	2013.2	44.8	95.0
3	232.0	234.0	234.0	233.0	233.3	2008.1	48.3	143.3
4	185.0	186.0	189.0	187.0	186.8	2016.6	46.5	189.8
5	136.0	138.0	137.0	138.0	137.3	2146.8	49.5	239.3
6	87.0	86.0	89.0	90.0	88.0	2088.5	49.3	288.5
6'	87.0	86.0	86.0	87.0	86.5	113.2	1.5	290.0
-								
-								

Specimen Height	290.0
Speciment Mass	12390.3
Bulk Density	2.418
Dry Density	2.300

Moisture Content Check	
Sample (Wet) + Tray	
Sample Dry + Tray	
Tray Weight	
Sample Wet	0.0
Sample Dry	0.0
MC	#DIV/0!

47

Specimen Description	Hunua 2.0% Asphalt 1.0% Cement
Date and Test Number	21-Feb-07 D_B2C1_HC_1
Testing date from-to	
Mould Diameter (mm)	150
Optimum Moisture (%)	6.0
Percentage of OMC (%)	100.0
Water Content (%)	5.1
Target Dry Density	
Area of Mould (cm2)	176.7

Mass Dry Material	11960.5
Required Water (ml)	610

Lift #	Ruler 1	Ruler 2	Ruler 3	Ruler 4	Average	Mass (g)	Depth/Lift	Total
Initial	376.0	377.0	376.0	376.0	376.3			0.0
1	329.0	327.0	326.0	329.0	327.8	2005.0	48.5	48.5
2	278.0	281.0	282.0	279.0	280.0	2000.7	47.8	96.3
3	228.0	232.0	233.0	230.0	230.8	2004.1	49.3	145.5
4	185.0	184.0	184.0	184.0	184.3	1950.1	46.5	192.0
5	135.0	134.0	134.0	136.0	134.8	2010.2	49.5	241.5
6	84.0	87.0	88.0	88.0	86.8	1951.9	48.0	289.5
6'	82.0	84.0	84.0	82.0	83.0	150.0	3.8	293.3
-								
-								

Specimen Height	293.3
Speciment Mass	12072
Bulk Density	2.330
Dry Density	2.216

Moisture Content Check	
Sample (Wet) + Tray	
Sample Dry + Tray	
Tray Weight	
Sample Wet	0.0
Sample Dry	0.0
MC	#DIV/0!

36

Specimen Description	Hunua 2.0% Asphalt 1.0% Cement
Date and Test Number	21-Feb-07 D_B2C1_HC_2
Testing date from-to	
Mould Diameter (mm)	150
Optimum Moisture (%)	6.0
Percentage of OMC (%)	100.0
Water Content (%)	5.1
Target Dry Density	
Area of Mould (cm2)	176.7

Mass Dry Material	11960.5
Required Water (ml)	610

Lift #	Ruler 1	Ruler 2	Ruler 3	Ruler 4	Average	Mass (g)	Depth/Lift	Total
Initial	376.0	377.0	376.0	376.0	376.3			0.0
1	328.0	330.0	331.0	330.0	329.8	1999.8	46.5	46.5
2	280.0	283.0	283.0	281.0	281.8	2051.3	48.0	94.5
3	233.0	231.0	234.0	231.0	232.3	2052.0	49.5	144.0
4	184.0	187.0	189.0	185.0	186.3	2002.4	46.0	190.0
5	135.0	140.0	141.0	145.0	140.3	2051.3	46.0	236.0
6	85.0	88.0	87.0	86.0	86.5	2141.8	53.8	289.8
6'	83.0	85.0	85.0	84.0	84.3	150.1	2.3	292.0
-								
-								

Specimen Height	292.0
Speciment Mass	12448.7
Bulk Density	2.413
Dry Density	2.295

Moisture Content Check	
Sample (Wet) + Tray	
Sample Dry + Tray	
Tray Weight	
Sample Wet	0.0
Sample Dry	0.0
MC	#DIV/0!

37

Specimen Description	Hunua 2.0% Asphalt 1.0% Cement
Date and Test Number	21-Feb-07 D_B2C1_HC_3
Testing date from-to	
Mould Diameter (mm)	150
Optimum Moisture (%)	6.0
Percentage of OMC (%)	100.0
Water Content (%)	5.1
Target Dry Density	
Area of Mould (cm2)	176.7

Mass Dry Material	11960.5
Required Water (ml)	610

Lift #	Ruler 1	Ruler 2	Ruler 3	Ruler 4	Average	Mass (g)	Depth/Lift	Total
Initial	376.0	376.0	376.0	376.0	376.0			0.0
1	329.0	331.0	330.0	329.0	329.8	2004.4	46.3	46.3
2	279.0	281.0	281.0	280.0	280.3	2081.1	49.5	95.8
3	231.0	233.0	232.0	231.0	231.8	2046.1	48.5	144.3
4	185.0	184.0	184.0	184.0	184.3	2044.4	47.5	191.8
5	135.0	136.0	136.0	134.0	135.3	2043.5	49.0	240.8
6	85.0	86.0	88.0	87.0	86.5	2041.8	48.8	289.5
6'	83.0	83.0	83.0	84.0	83.3	150.3	3.3	292.75
-								
-								

Specimen Height	292.8
Speciment Mass	12411.6
Bulk Density	2.399
Dry Density	2.283

Moisture Content Check	
Sample (Wet) + Tray	
Sample Dry + Tray	
Tray Weight	
Sample Wet	0.0
Sample Dry	0.0
MC	#DIV/0!

38

Specimen Description	Hunua 2.0% Asphalt 1.0% Cement
Date and Test Number	21-Feb-07 D_B2C1_HC_4
Testing date from-to	
Mould Diameter (mm)	150
Optimum Moisture (%)	6.0
Percentage of OMC (%)	100.0
Water Content (%)	5.1
Target Dry Density	
Area of Mould (cm2)	176.7

Mass Dry Material	11960.5
Required Water (ml)	610

Lift #	Ruler 1	Ruler 2	Ruler 3	Ruler 4	Average	Mass (g)	Depth/Lift	Total
Initial	376.0	376.0	376.0	376.0	376.0			0.0
1	326.0	326.0	329.0	327.0	327.0	2046.4	49.0	49.0
2	279.0	281.0	282.0	279.0	280.3	2044.7	46.8	95.8
3	239.0	237.0	239.0	242.0	239.3	2050.8	41.0	136.8
4	181.0	183.0	184.0	182.0	182.5	2054.1	56.8	193.5
5	134.0	133.0	134.0	135.0	134.0	2058.7	48.5	242.0
6	86.0	87.0	87.0	86.0	86.5	2038.0	47.5	289.5
6'	82.0	82.0	83.0	82.0	82.3	150.1	4.3	293.75
-								
-								

Specimen Height	293.8
Speciment Mass	12442.8
Bulk Density	2.397
Dry Density	2.281

Moisture Content Check	
Sample (Wet) + Tray	
Sample Dry + Tray	
Tray Weight	
Sample Wet	0.0
Sample Dry	0.0
MC	#DIV/0!

39

Specimen Description	Hunua 4.0% Asphalt 1.0% Cement
Date and Test Number	2-Mar-07 D_B4C1_HC_1
Testing date from-to	
Mould Diameter (mm)	150
Optimum Moisture (%)	6.0
Percentage of OMC (%)	100.0
Water Content (%)	5.1
Target Dry Density	
Area of Mould (cm2)	176.7

Mass Dry Material	11960.5
Required Water (ml)	610

Lift #	Ruler 1	Ruler 2	Ruler 3	Ruler 4	Average	Mass (g)	Depth/Lift	Total
Initial	377.0	377.0	377.0	376.0	376.8			0.0
1	327.0	327.0	328.0	328.0	327.5	2004.6	49.3	49.3
2	278.0	280.0	279.0	277.0	278.5	1995.4	49.0	98.3
3	232.0	231.0	230.0	232.0	231.3	1923.4	47.3	145.5
4	185.0	183.0	183.0	185.0	184.0	1992.8	47.3	192.8
5	137.0	135.0	135.0	136.0	135.8	1975.3	48.3	241.0
6	88.0	88.0	87.0	88.0	87.8	1925.8	48.0	289.0
6'	84.0	83.0	85.0	85.0	84.3	150.0	3.5	292.5
-								
-								

Specimen Height	292.5
Speciment Mass	11967.3
Bulk Density	2.315
Dry Density	2.203

Moisture Content Check	
Sample (Wet) + Tray	
Sample Dry + Tray	
Tray Weight	
Sample Wet	0.0
Sample Dry	0.0
MC	#DIV/0!

40

Specimen Description	Hunua 4.0% Asphalt 1.0% Cement
Date and Test Number	2-Mar-07 D_B4C1_HC_2
Testing date from-to	
Mould Diameter (mm)	150
Optimum Moisture (%)	6.0
Percentage of OMC (%)	100.0
Water Content (%)	5.1
Target Dry Density	
Area of Mould (cm2)	176.7

Mass Dry Material	11960.5
Required Water (ml)	610

Lift #	Ruler 1	Ruler 2	Ruler 3	Ruler 4	Average	Mass (g)	Depth/Lift	Total
Initial	377.0	377.0	377.0	376.0	376.8			0.0
1	325.0	330.0	328.0	324.0	326.8	1981.0	50.0	50.0
2	276.0	280.0	280.0	277.0	278.3	1973.8	48.5	98.5
3	232.0	231.0	230.0	230.0	230.8	1988.0	47.5	146.0
4	185.0	184.0	182.0	181.0	183.0	1948.7	47.8	193.8
5	134.0	134.0	135.0	134.0	134.3	1976.5	48.8	242.5
6	84.0	86.0	85.0	83.0	84.5	1948.4	49.8	292.3
6'	83.0	84.0	83.0	81.0	82.8	151.3	1.8	294.0
-								
-								

Specimen Height	294.0
Speciment Mass	11967.7
Bulk Density	2.304
Dry Density	2.192

Moisture Content Check	
Sample (Wet) + Tray	
Sample Dry + Tray	
Tray Weight	
Sample Wet	0.0
Sample Dry	0.0
MC	#DIV/0!

41

Specimen Description	Hunua 4.0% Asphalt 1.0% Cement
Date and Test Number	2-Mar-07 D_B4C1_HC_3
Testing date from-to	
Mould Diameter (mm)	150
Optimum Moisture (%)	6.0
Percentage of OMC (%)	100.0
Water Content (%)	5.1
Target Dry Density	
Area of Mould (cm2)	176.7

Mass Dry Material	11960.5
Required Water (ml)	610

Lift #	Ruler 1	Ruler 2	Ruler 3	Ruler 4	Average	Mass (g)	Depth/Lift	Total
Initial	376.0	376.0	376.0	376.0	376.0			0.0
1	327.0	328.0	328.0	327.0	327.5	1969.8	48.5	48.5
2	277.0	279.0	279.0	276.0	277.8	1956.2	49.8	98.3
3	229.0	231.0	231.0	228.0	229.8	1959.0	48.0	146.3
4	193.0	180.0	181.0	183.0	184.3	1957.7	45.5	191.8
5	131.0	131.0	133.0	132.0	131.8	1953.5	52.5	244.3
6	84.0	86.0	87.0	85.0	85.5	1913.7	46.3	290.5
6'	83.0	82.0	83.0	83.0	82.8	150.0	2.8	293.3
-								
-								

Specimen Height	293.3
Speciment Mass	11859.9
Bulk Density	2.289
Dry Density	2.178

Moisture Content Check	
Sample (Wet) + Tray	
Sample Dry + Tray	
Tray Weight	
Sample Wet	0.0
Sample Dry	0.0
MC	#DIV/0!

42

Specimen Description	Hunua 4.0% Asphalt 1.0% Cement
Date and Test Number	2-Mar-07 D_B4C1_HC_4
Testing date from-to	
Mould Diameter (mm)	150
Optimum Moisture (%)	6.0
Percentage of OMC (%)	100.0
Water Content (%)	5.1
Target Dry Density	
Area of Mould (cm2)	176.7

Mass Dry Material	11960.5
Required Water (ml)	610

Lift #	Ruler 1	Ruler 2	Ruler 3	Ruler 4	Average	Mass (g)	Depth/Lift	Total
Initial	376.0	376.0	377.0	376.0	376.3			0.0
1	325.0	329.0	329.0	326.0	327.3	1949.9	49.0	49.0
2	282.0	278.0	278.0	281.0	279.8	1950.7	47.5	96.5
3	229.0	232.0	230.0	227.0	229.5	1952.5	50.3	146.8
4	184.0	184.0	183.0	183.0	183.5	1950.0	46.0	192.8
5	134.0	135.0	136.0	135.0	135.0	1949.6	48.5	241.3
6	86.0	85.0	88.0	88.0	86.8	1949.5	48.3	289.5
6'	85.0	84.0	84.0	86.0	84.8	150.5	2.0	291.5
-								
-								

Specimen Height	291.5
Speciment Mass	11852.7
Bulk Density	2.301
Dry Density	2.189

Moisture Content Check	
Sample (Wet) + Tray	
Sample Dry + Tray	
Tray Weight	
Sample Wet	0.0
Sample Dry	0.0
MC	#DIV/0!

43

C.4 Monotonic specimens, low compaction energy

Specimen Description	Hunua 0.0% Asphalt 1.0% Cement
Date and Test Number	29-Jun-07 **M_0C1_LC_1**
Testing date from-to	
Mould Diameter (mm)	150
Optimum Moisture (%)	6.0
Percentage of OMC (%)	100.0
Water Content (%)	5.1
Target Dry Density	
Area of Mould (cm2)	176.7

Mass Dry Material	11960.5
Required Water (ml)	610

Lift #	Ruler 1	Ruler 2	Ruler 3	Ruler 4	Average	Mass (g)	Depth/Lift	Total
Initial	377.0	377.0	377.0	377.0	377.00			0.00
1	329.0	332.0	331.0	327.0	329.75	1860.6	47.3	47.25
2	280.0	282.0	282.0	280.0	281.00	1840.9	48.8	96.00
3	236.0	236.0	235.0	235.0	235.50	1869.4	45.5	141.50
4	186.0	186.0	185.0	186.0	185.75	1863.8	49.8	191.25
5	139.0	140.0	141.0	140.0	140.00	1855.7	45.8	237.00
6	92.0	92.0	91.0	92.0	91.75	1864.3	48.3	285.25
6'	90.0	89.0	90.0	89.0	89.5	150.0	2.3	287.50
-								
-						10		

Specimen Height	287.50
Speciment Mass	11304.7
Bulk Density	2.225
Dry Density	2.117

Moisture Content Check	
Sample (Wet) + Tray	13586.6
Sample Dry + Tray	13085.8
Tray Weight	2355.4
Sample Wet	11231.2
Sample Dry	10730.4
MC	4.67%

67

Specimen Description	Hunua 0.0% Asphalt 1.0% Cement
Date and Test Number	29-Jun-07 M_0C1_LC_2
Testing date from-to	
Mould Diameter (mm)	150
Optimum Moisture (%)	6.0
Percentage of OMC (%)	100.0
Water Content (%)	5.1
Target Dry Density	
Area of Mould (cm2)	176.7

Mass Dry Material	11960.5
Required Water (ml)	610

Lift #	Ruler 1	Ruler 2	Ruler 3	Ruler 4	Average	Mass (g)	Depth/Lift	Total
Initial	377.0	377.0	377.0	377.0	377.00			0.00
1	327.0	329.0	330.0	326.0	328.00	1846.7	49.0	49.00
2	282.0	280.0	280.0	280.0	280.50	1834.0	47.5	96.50
3	233.0	232.0	233.0	234.0	233.00	1840.2	47.5	144.00
4	184.0	183.0	185.0	185.0	184.25	1866.5	48.8	192.75
5	135.0	137.0	134.0	135.0	135.25	1876.1	49.0	241.75
6	89.0	88.0	88.0	89.0	88.50	1836.4	46.8	288.50
6'	87.0	87.0	87.0	86.0	86.8	150.0	1.8	290.25
-								
-						17		

Specimen Height	290.25
Speciment Mass	11249.9
Bulk Density	2.193
Dry Density	2.087

Moisture Content Check	
Sample (Wet) + Tray	13508.8
Sample Dry + Tray	13019.8
Tray Weight	2336.8
Sample Wet	11172.0
Sample Dry	10683.0
MC	4.58%

68

Specimen Description	Hunua 0.0% Asphalt 1.0% Cement
Date and Test Number	5-Jul-08 M_0C1_LC_3
Testing date from-to	
Mould Diameter (mm)	150
Optimum Moisture (%)	6.0
Percentage of OMC (%)	100.0
Water Content (%)	5.1
Target Dry Density	
Area of Mould (cm2)	176.7

Mass Dry Material	11960.5
Required Water (ml)	610

Lift #	Ruler 1	Ruler 2	Ruler 3	Ruler 4	Average	Mass (g)	Depth/Lift	Total
Initial	377.0	377.0	377.0	377.0	377.00			0.00
1	328.0	327.0	328.0	328.0	327.75	1932.0	49.3	49.25
2	281.0	279.0	280.0	278.0	279.50	1891.0	48.3	97.50
3	234.0	234.0	232.0	232.0	233.00	1808.0	46.5	144.00
4	189.0	186.0	185.0	187.0	186.75	1870.0	46.3	190.25
5	141.0	142.0	138.0	138.0	139.75	1901.0	47.0	237.25
6	95.0	90.0	88.0	88.0	90.25	1998.0	49.5	286.75
6'	91.0	91.0	88.0	88.0	89.5	150.0	0.8	287.50
-								
-						664		

Specimen Height	287.50
Speciment Mass	11550.0
Bulk Density	2.273
Dry Density	2.163

Moisture Content Check	
Sample (Wet) + Tray	
Sample Dry + Tray	
Tray Weight	
Sample Wet	0.0
Sample Dry	0.0
MC	#DIV/0!

80

Specimen Description	Hunua 0.0% Asphalt 1.0% Cement
Date and Test Number	5-Jul-08 M_0C1_LC_4
Testing date from-to	
Mould Diameter (mm)	150
Optimum Moisture (%)	6.0
Percentage of OMC (%)	100.0
Water Content (%)	5.1
Target Dry Density	
Area of Mould (cm2)	176.7

Mass Dry Material	11960.5
Required Water (ml)	610

Lift #	Ruler 1	Ruler 2	Ruler 3	Ruler 4	Average	Mass (g)	Depth/Lift	Total
Initial	377.0	377.0	377.0	377.0	377.00			0.00
1	329.0	328.0	327.0	326.0	327.50	1923.0	49.5	49.50
2	258.5	257.0	256.5	257.0	257.25	1900.0	70.3	119.75
3	227.0	229.0	230.0	227.0	228.25	1900.0	29.0	148.75
4	188.0	186.0	186.0	188.0	187.00	1881.0	41.3	190.00
5	139.0	138.0	138.0	139.0	138.50	1915.0	48.5	238.50
6	91.0	92.0	93.0	90.0	91.50	1908.0	47.0	285.50
6'	90.0	90.0	90.0	90.0	90.0	150.0	1.5	287.00
-								
-						663		

Specimen Height	287.00
Speciment Mass	11577.0
Bulk Density	2.283
Dry Density	2.172

Moisture Content Check	
Sample (Wet) + Tray	
Sample Dry + Tray	
Tray Weight	
Sample Wet	0.0
Sample Dry	0.0
MC	#DIV/0!

81

Specimen Description	Hunua 2.0% Asphalt 1.0% Cement
Date and Test Number	15-Jun-07 M_2C1_LC_1
Testing date from-to	
Mould Diameter (mm)	150
Optimum Moisture (%)	6.0
Percentage of OMC (%)	100.0
Water Content (%)	5.1
Target Dry Density	
Area of Mould (cm2)	176.7

Mass Dry Material	11960.5
Required Water (ml)	610

Lift #	Ruler 1	Ruler 2	Ruler 3	Ruler 4	Average	Mass (g)	Depth/Lift	Total
Initial	377.0	377.0	377.0	377.0	377.00			0.00
1	326.0	328.0	327.0	326.0	326.75	1789.8	50.3	50.25
2	277.0	278.0	279.0	277.0	277.75	1791.2	49.0	99.25
3	228.0	230.0	232.0	230.0	230.00	1780.5	47.8	147.00
4	186.0	185.0	185.0	185.0	185.25	1769.3	44.8	191.75
5	134.0	135.0	137.0	136.0	135.50	1818.2	49.8	241.50
6	89.0	89.0	89.0	89.0	89.00	1785.7	46.5	288.00
6'								
-								
-						16		

Specimen Height	288.00
Speciment Mass	10734.7
Bulk Density	2.109
Dry Density	2.007

Moisture Content Check	
Sample (Wet) + Tray	
Sample Dry + Tray	
Tray Weight	
Sample Wet	0.0
Sample Dry	0.0
MC	#DIV/0!

57

Specimen Description	Hunua 2.0% Asphalt 1.0% Cement
Date and Test Number	19-Jun-07 **M_2C1_LC_2**
Testing date from-to	
Mould Diameter (mm)	150
Optimum Moisture (%)	6.0
Percentage of OMC (%)	100.0
Water Content (%)	5.1
Target Dry Density	
Area of Mould (cm2)	176.7

Mass Dry Material	11960.5
Required Water (ml)	610

Lift #	Ruler 1	Ruler 2	Ruler 3	Ruler 4	Average	Mass (g)	Depth/Lift	Total
Initial	377.0	377.0	377.0	377.0	377.00			0.00
1	327.0	328.0	328.0	327.0	327.50	1868.1	49.5	49.50
2	281.0	282.0	283.0	281.0	281.75	1825.5	45.8	95.25
3	234.0	233.0	234.0	232.0	233.25	1840.9	48.5	143.75
4	184.0	184.0	184.0	183.0	183.75	1856.1	49.5	193.25
5	137.0	136.0	136.0	138.0	136.75	1857.4	47.0	240.25
6	87.0	87.0	88.0	87.0	87.25	1854.0	49.5	289.75
6'	86.0	86.0	87.0	87.0	86.5	150.0	0.8	290.50
-								
-						15		

Specimen Height	290.50
Speciment Mass	11252.0
Bulk Density	2.192
Dry Density	2.085

Moisture Content Check	
Sample (Wet) + Tray	12346.2
Sample Dry + Tray	11857.6
Tray Weight	1198.1
Sample Wet	11148.1
Sample Dry	10659.5
MC	4.58%

60

Specimen Description	Hunua 2.0% Asphalt 1.0% Cement
Date and Test Number	7-Jul-08 **M_2C1_LC_3**
Testing date from-to	
Mould Diameter (mm)	150
Optimum Moisture (%)	6.0
Percentage of OMC (%)	100.0
Water Content (%)	5.1
Target Dry Density	
Area of Mould (cm2)	176.7

Mass Dry Material	11960.5
Required Water (ml)	610

Lift #	Ruler 1	Ruler 2	Ruler 3	Ruler 4	Average	Mass (g)	Depth/Lift	Total
Initial	377.0	377.0	377.0	377.0	377.00			0.00
1	328.0	331.0	328.0	335.0	330.50	1851.0	46.5	46.50
2	283.0	283.0	282.0	280.0	282.00	1853.0	48.5	95.00
3	237.0	237.0	235.0	238.0	236.75	1849.0	45.3	140.25
4	188.0	189.0	190.0	188.0	188.75	1854.0	48.0	188.25
5	141.0	141.0	142.0	141.0	141.25	1845.0	47.5	235.75
6	93.0	95.0	95.0	93.0	94.00	1843.0	47.3	283.00
6'	94.0	93.0	94.0	92.0	93.3	150.0	0.8	283.75
-								
-						642		

Specimen Height	283.75
Speciment Mass	11245.0
Bulk Density	2.243
Dry Density	2.134

Moisture Content Check	
Sample (Wet) + Tray	
Sample Dry + Tray	
Tray Weight	
Sample Wet	0.0
Sample Dry	0.0
MC	#DIV/0!

84

Specimen Description	Hunua 2.0% Asphalt 1.0% Cement
Date and Test Number	7-Jul-08 **M_2C1_LC_4**
Testing date from-to	
Mould Diameter (mm)	150
Optimum Moisture (%)	6.0
Percentage of OMC (%)	100.0
Water Content (%)	5.1
Target Dry Density	
Area of Mould (cm2)	176.7

Mass Dry Material	11960.5
Required Water (ml)	610

Lift #	Ruler 1	Ruler 2	Ruler 3	Ruler 4	Average	Mass (g)	Depth/Lift	Total
Initial	377.0	377.0	377.0	377.0	377.00			0.00
1	328.0	326.0	325.0	327.0	326.50	1850.0	50.5	50.50
2	282.0	280.0	278.0	280.0	280.00	1846.0	46.5	97.00
3	231.0	232.0	230.0	231.0	231.00	1857.0	49.0	146.00
4	185.0	185.0	186.0	186.0	185.50	1848.0	45.5	191.50
5	138.0	139.0	139.0	138.0	138.50	1850.0	47.0	238.50
6	92.0	91.0	92.0	93.0	92.00	1847.0	46.5	285.00
6'	90.0	91.0	91.0	90.0	90.5	150.0	1.5	286.50
-								
-						642		

Specimen Height	286.50
Speciment Mass	11248.0
Bulk Density	2.222
Dry Density	2.114

Moisture Content Check	
Sample (Wet) + Tray	
Sample Dry + Tray	
Tray Weight	
Sample Wet	0.0
Sample Dry	0.0
MC	#DIV/0!

85

Specimen Description	Hunua 4.0% Asphalt 1.0% Cement
Date and Test Number	4-Sep-07 **M_4C1_LC_1**
Testing date from-to	
Mould Diameter (mm)	150
Optimum Moisture (%)	6.0
Percentage of OMC (%)	100.0
Water Content (%)	5.1
Target Dry Density	
Area of Mould (cm2)	176.7

Mass Dry Material	11960.5
Required Water (ml)	610

Lift #	Ruler 1	Ruler 2	Ruler 3	Ruler 4	Average	Mass (g)	Depth/Lift	Total
Initial	377.0	377.0	377.0	377.0	377.00			0.00
1	326.0	329.0	329.0	327.0	327.75	1819.6	49.3	49.25
2	278.0	280.0	279.0	277.0	278.50	1829.6	49.3	98.50
3	231.0	233.0	230.0	227.0	230.25	1819.3	48.3	146.75
4	185.0	184.0	182.0	182.0	183.25	1824.6	47.0	193.75
5	138.0	138.0	134.0	136.0	136.50	1828.8	46.8	240.50
6	89.0	87.0	87.0	89.0	88.00	1819.3	48.5	289.00
6'	88.0	87.0	86.0	86.0	86.8	150.0	1.3	290.25
-								
-						5		

Specimen Height	290.25
Speciment Mass	11091.2
Bulk Density	2.162
Dry Density	2.057

Moisture Content Check	
Sample (Wet) + Tray	
Sample Dry + Tray	
Tray Weight	
Sample Wet	0.0
Sample Dry	0.0
MC	#DIV/0!

77

Specimen Description	Hunua 4.0% Asphalt 1.0% Cement
Date and Test Number	4-Sep-07 M_4C1_LC_2
Testing date from-to	
Mould Diameter (mm)	150
Optimum Moisture (%)	6.0
Percentage of OMC (%)	100.0
Water Content (%)	5.1
Target Dry Density	
Area of Mould (cm2)	176.7

Mass Dry Material	11960.5
Required Water (ml)	610

Lift #	Ruler 1	Ruler 2	Ruler 3	Ruler 4	Average	Mass (g)	Depth/Lift	Total
Initial	377.0	377.0	377.0	377.0	377.00			0.00
1	329.0	329.0	327.0	326.0	327.75	1825.3	49.3	49.25
2	284.0	284.0	281.0	280.0	282.25	1826.2	45.5	94.75
3	236.0	236.0	234.0	236.0	235.50	1820.6	46.8	141.50
4	188.0	187.0	186.0	186.0	186.75	1827.9	48.8	190.25
5	140.0	141.0	138.0	136.0	138.75	1828.3	48.0	238.25
6	91.0	90.0	89.0	90.0	90.00	1827.6	48.8	287.00
6'	89.0	88.0	88.0	88.0	88.3	150.0	1.8	288.75
-								
-						3		

Specimen Height	288.75
Speciment Mass	11105.9
Bulk Density	2.177
Dry Density	2.071

Moisture Content Check	
Sample (Wet) + Tray	
Sample Dry + Tray	
Tray Weight	
Sample Wet	0.0
Sample Dry	0.0
MC	#DIV/0!

78

Specimen Description	Hunua 4.0% Asphalt 1.0% Cement
Date and Test Number	7-Jul-08 M_4C1_LC_3
Testing date from-to	
Mould Diameter (mm)	150
Optimum Moisture (%)	6.0
Percentage of OMC (%)	100.0
Water Content (%)	5.1
Target Dry Density	
Area of Mould (cm2)	176.7

Mass Dry Material	11960.5
Required Water (ml)	610

Lift #	Ruler 1	Ruler 2	Ruler 3	Ruler 4	Average	Mass (g)	Depth/Lift	Total
Initial	377.0	377.0	377.0	377.0	377.00			0.00
1	329.0	327.0	328.0	328.0	328.00	1831.0	49.0	49.00
2	278.0	278.0	282.0	280.0	279.50	1814.0	48.5	97.50
3	234.0	236.0	235.0	234.0	234.75	1725.0	44.8	142.25
4	188.0	189.0	190.0	189.0	189.00	1808.0	45.8	188.00
5	142.0	143.0	143.0	143.0	142.75	1832.0	46.3	234.25
6	91.0	91.0	91.0	91.0	91.00	1890.0	51.8	286.00
6'	89.0	89.0	89.0	89.0	89.0	150.0	2.0	288.00
-								
-						632		

Specimen Height	288.00
Speciment Mass	11050.0
Bulk Density	2.171
Dry Density	2.066

Moisture Content Check	
Sample (Wet) + Tray	
Sample Dry + Tray	
Tray Weight	
Sample Wet	0.0
Sample Dry	0.0
MC	#DIV/0!

82

Specimen Description	Hunua 4.0% Asphalt 1.0% Cement
Date and Test Number	7-Jul-08 **M_4C1_LC_4**
Testing date from-to	
Mould Diameter (mm)	150
Optimum Moisture (%)	6.0
Percentage of OMC (%)	100.0
Water Content (%)	5.1
Target Dry Density	
Area of Mould (cm2)	176.7

Mass Dry Material	11960.5
Required Water (ml)	610

Lift #	Ruler 1	Ruler 2	Ruler 3	Ruler 4	Average	Mass (g)	Depth/Lift	Total
Initial	377.0	377.0	377.0	377.0	377.00			0.00
1	329.0	328.0	329.0	326.0	328.00	1800.0	49.0	49.00
2	281.0	283.0	281.0	278.0	280.75	1844.0	47.3	96.25
3	235.0	234.0	236.0	234.0	234.75	1828.0	46.0	142.25
4	186.0	187.0	187.0	186.0	186.50	1821.0	48.3	190.50
5	140.0	141.0	140.0	140.0	140.25	1821.0	46.3	236.75
6	91.0	90.0	90.0	91.0	90.50	1835.0	49.8	286.50
6'	90.0	91.0	90.0	88.0	89.8	150.0	0.8	287.25
-								
-						633		

Specimen Height	287.25
Speciment Mass	11099.0
Bulk Density	2.187
Dry Density	2.080

Moisture Content Check	
Sample (Wet) + Tray	
Sample Dry + Tray	
Tray Weight	
Sample Wet	0.0
Sample Dry	0.0
MC	#DIV/0!

83

C.5 Specimen for random stress sequence, 2% foam bitumen and 1% cement, low compaction energy

Specimen Description	Hunua 4.0% Asphalt 1.0% Cement
Date and Test Number	7-Jun-07 D_B2C1_LC_R
Testing date from-to	
Mould Diameter (mm)	150
Optimum Moisture (%)	6.0
Percentage of OMC (%)	100.0
Water Content (%)	5.1
Target Dry Density	
Area of Mould (cm2)	176.7

Mass Dry Material	11960.5
Required Water (ml)	610

Lift #	Ruler 1	Ruler 2	Ruler 3	Ruler 4	Average	Mass (g)	Depth/Lift	Total
Initial	377.0	377.0	377.0	377.0	377.0			0.0
1	329.0	330.0	328.0	327.0	328.5	1787.3	48.5	48.5
2	280.0	280.0	281.0	278.0	279.8	1783.3	48.8	97.3
3	232.0	234.0	235.0	232.0	233.3	1759.0	46.5	143.8
4	188.0	188.0	187.0	187.0	187.5	1746.7	45.8	189.5
5	138.0	137.0	137.0	136.0	137.0	1857.0	50.5	240.0
6	87.0	85.0	85.0	85.0	85.5	1850.3	51.5	291.5
6'								
-								
-								

Specimen Height	291.5
Speciment Mass	10783.6
Bulk Density	2.093
Dry Density	1.992

Moisture Content Check	
Sample (Wet) + Tray	
Sample Dry + Tray	
Tray Weight	
Sample Wet	0.0
Sample Dry	0.0
MC	#DIV/0!

55

C.6 Monotonic specimens, high compaction energy

Specimen Description	Hunua 0.0% Asphalt 1.0% Cement
Date and Test Number	5-Jul-07 **M_0C1_HC_1**
Testing date from-to	
Mould Diameter (mm)	150
Optimum Moisture (%)	6.0
Percentage of OMC (%)	100.0
Water Content (%)	5.1
Target Dry Density	
Area of Mould (cm2)	176.7

Mass Dry Material	11960.5
Required Water (ml)	610

Lift #	Ruler 1	Ruler 2	Ruler 3	Ruler 4	Average	Mass (g)	Depth/Lift	Total
Initial	377.0	377.0	377.0	377.0	377.00			0.00
1	330.0	328.0	327.0	330.0	328.75	1958.0	48.3	48.25
2	284.0	284.0	281.0	281.0	282.50	1956.3	46.3	94.50
3	232.0	231.0	232.0	233.0	232.00	2038.6	50.5	145.00
4	187.0	185.0	186.0	189.0	186.75	1951.6	45.3	190.25
5	139.0	140.0	141.0	138.0	139.50	1979.7	47.3	237.50
6	91.0	91.0	92.0	91.0	91.25	1977.9	48.3	285.75
6'	91.0	90.0	90.0	91.0	90.5	75.0	0.8	286.50
-								
-						32		

Specimen Height	286.50
Speciment Mass	11937.1
Bulk Density	2.358
Dry Density	2.243

Moisture Content Check	
Sample (Wet) + Tray	14146.6
Sample Dry + Tray	13652.0
Tray Weight	2337.5
Sample Wet	11809.1
Sample Dry	11314.5
MC	4.37%

70

Specimen Description	Hunua 0.0% Asphalt 1.0% Cement
Date and Test Number	5-Jul-07 **M_0C1_HC_2**
Testing date from-to	
Mould Diameter (mm)	150
Optimum Moisture (%)	6.0
Percentage of OMC (%)	100.0
Water Content (%)	5.1
Target Dry Density	
Area of Mould (cm2)	176.7

Mass Dry Material	11960.5
Required Water (ml)	610

Lift #	Ruler 1	Ruler 2	Ruler 3	Ruler 4	Average	Mass (g)	Depth/Lift	Total
Initial	377.0	377.0	377.0	377.0	377.00			0.00
1	326.0	327.0	326.0	327.0	326.50	1988.1	50.5	50.50
2	281.0	281.0	280.0	279.0	280.25	1971.0	46.3	96.75
3	235.0	234.0	232.0	235.0	234.00	1975.8	46.3	143.00
4	185.5	185.0	185.0	186.5	185.50	2017.9	48.5	191.50
5	136.0	136.0	138.0	138.0	137.00	1971.2	48.5	240.00
6	113.0	113.0	113.5	114.0	113.38	1974.5	23.6	263.63
6'	90.0	90.0	89.0	90.0	89.8	80.0	23.6	287.25
-								
-						18		

Specimen Height	287.25
Speciment Mass	11978.5
Bulk Density	2.360
Dry Density	2.245

Moisture Content Check	
Sample (Wet) + Tray	14138.4
Sample Dry + Tray	13666.6
Tray Weight	2339.4
Sample Wet	11799.0
Sample Dry	11327.2
MC	4.17%

71

Specimen Description	Hunua 0.0% Asphalt 1.0% Cement
Date and Test Number	7-Jul-08 **M_0C1_HC_3**
Testing date from-to	
Mould Diameter (mm)	150
Optimum Moisture (%)	6.0
Percentage of OMC (%)	100.0
Water Content (%)	5.1
Target Dry Density	
Area of Mould (cm2)	176.7

Mass Dry Material	11960.5
Required Water (ml)	610

Lift #	Ruler 1	Ruler 2	Ruler 3	Ruler 4	Average	Mass (g)	Depth/Lift	Total
Initial	377.0	377.0	377.0	377.0	377.00			0.00
1	325.0	326.0	326.0	325.0	325.50	1993.0	51.5	51.50
2	278.0	279.0	280.0	279.0	279.00	1949.0	46.5	98.00
3	227.0	228.0	229.0	227.0	227.75	1997.0	51.3	149.25
4	184.0	182.0	182.0	184.0	183.00	1999.0	44.8	194.00
5	135.0	135.5	134.5	135.0	135.00	1977.0	48.0	242.00
6	86.0	89.0	87.0	86.0	87.00	1955.0	48.0	290.00
6'	84.0	85.0	86.0	84.0	84.8	150.0	2.3	292.25
-								
-						691		

Specimen Height	292.25
Speciment Mass	12020.0
Bulk Density	2.327
Dry Density	2.214

Moisture Content Check	
Sample (Wet) + Tray	
Sample Dry + Tray	
Tray Weight	
Sample Wet	0.0
Sample Dry	0.0
MC	#DIV/0!

86

Specimen Description	Hunua 2.0% Asphalt 1.0% Cement
Date and Test Number	24-May-07 M_2C1_HC_1
Testing date from-to	
Mould Diameter (mm)	150
Optimum Moisture (%)	6.0
Percentage of OMC (%)	100.0
Water Content (%)	5.1
Target Dry Density	
Area of Mould (cm2)	176.7

Mass Dry Material	11960.5
Required Water (ml)	610

Lift #	Ruler 1	Ruler 2	Ruler 3	Ruler 4	Average	Mass (g)	Depth/Lift	Total
Initial	377.0	377.0	377.0	377.0	377.0			0.0
1	327.0	329.0	330.0	328.0	328.5	1992.5	48.5	48.5
2	281.0	280.0	280.0	281.0	280.5	1995.6	48.0	96.5
3	230.0	230.0	233.0	234.0	231.8	2005.2	48.8	145.3
4	182.0	184.0	187.0	184.0	184.3	1989.0	47.5	192.8
5	134.0	134.0	136.0	136.0	135.0	1993.4	49.3	242.0
6	87.0	88.0	90.0	90.0	88.8	2000.1	46.3	288.3
6'	87.0	86.0	86.0	87.0	86.5	150.0	2.3	290.5
-								
-								

Specimen Height	290.5
Speciment Mass	12125.8
Bulk Density	2.362
Dry Density	2.247

Moisture Content Check	
Sample (Wet) + Tray	13166.0
Sample Dry + Tray	12694.7
Tray Weight	1180.1
Sample Wet	11985.9
Sample Dry	11514.6
MC	4.09%

50

Specimen Description	Hunua 2.0% Asphalt 1.0% Cement
Date and Test Number	24-May-07 M_2C1_HC_2
Testing date from-to	
Mould Diameter (mm)	150
Optimum Moisture (%)	6.0
Percentage of OMC (%)	100.0
Water Content (%)	5.1
Target Dry Density	
Area of Mould (cm2)	176.7

Mass Dry Material	11960.5
Required Water (ml)	610

Lift #	Ruler 1	Ruler 2	Ruler 3	Ruler 4	Average	Mass (g)	Depth/Lift	Total
Initial	377.0	377.0	377.0	377.0	377.0			0.0
1	328.0	327.0	328.0	328.0	327.8	1993.6	49.3	49.3
2	281.0	280.0	280.0	281.0	280.5	1997.4	47.3	96.5
3	230.0	228.0	231.0	232.0	230.3	1997.5	50.3	146.8
4	187.0	185.0	184.0	186.0	185.5	1985.7	44.8	191.5
5	138.0	134.0	136.0	138.0	136.5	2008.3	49.0	240.5
6	90.0	87.0	89.0	92.0	89.5	1989.8	47.0	287.5
6'	87.0	85.0	87.0	89.0	87.0	150.0	2.5	290.0
-								
-								

Specimen Height	290.0
Speciment Mass	12122.3
Bulk Density	2.365
Dry Density	2.251

Moisture Content Check	
Sample (Wet) + Tray	
Sample Dry + Tray	
Tray Weight	
Sample Wet	0.0
Sample Dry	0.0
MC	#DIV/0!

Wrong Moisture

51

Specimen Description	Hunua 2.0% Asphalt 1.0% Cement
Date and Test Number	7-Jul-08 **M_2C1_HC_3**
Testing date from-to	
Mould Diameter (mm)	150
Optimum Moisture (%)	6.0
Percentage of OMC (%)	100.0
Water Content (%)	5.1
Target Dry Density	
Area of Mould (cm2)	176.7

Mass Dry Material	11960.5
Required Water (ml)	610

Lift #	Ruler 1	Ruler 2	Ruler 3	Ruler 4	Average	Mass (g)	Depth/Lift	Total
Initial	377.0	377.0	377.0	377.0	377.00			0.00
1	326.0	329.0	325.0	326.0	326.50	1982.0	50.5	50.50
2	281.0	282.0	284.0	281.0	282.00	1917.0	44.5	95.00
3	236.0	37.0	235.0	234.0	185.50	1960.0	96.5	191.50
4	186.0	186.0	187.0	187.0	186.50	2037.0	-1.0	190.50
5	140.0	138.0	136.0	138.0	138.00	2031.0	48.5	239.00
6	92.0	90.0	88.0	89.0	89.75	2023.0	48.3	287.25
6'	87.0	86.0	85.0	88.0	86.5	150.0	3.3	290.50
-								
-						697		

Specimen Height	290.50
Speciment Mass	12100.0
Bulk Density	2.357
Dry Density	2.243

Moisture Content Check	
Sample (Wet) + Tray	
Sample Dry + Tray	
Tray Weight	
Sample Wet	0.0
Sample Dry	0.0
MC	#DIV/0!

89

Specimen Description	Hunua 4.0% Asphalt 1.0% Cement
Date and Test Number	24-May-07 **M_4C1_HC_1**
Testing date from-to	
Mould Diameter (mm)	150
Optimum Moisture (%)	6.0
Percentage of OMC (%)	100.0
Water Content (%)	5.1
Target Dry Density	
Area of Mould (cm2)	176.7

Mass Dry Material	11960.5
Required Water (ml)	610

Lift #	Ruler 1	Ruler 2	Ruler 3	Ruler 4	Average	Mass (g)	Depth/Lift	Total
Initial	377.0	377.0	377.0	377.0	377.0			0.0
1	326.0	326.0	327.5	325.5	326.3	1936.4	50.8	50.8
2	275.0	275.0	278.0	274.0	275.5	1943.9	50.8	101.5
3	230.5	231.0	232.5	229.5	230.9	1829.7	44.6	146.1
4	186.0	187.0	187.0	185.0	186.3	1768.9	44.6	190.8
5	138.5	138.5	139.0	137.5	138.4	1914.4	47.9	238.6
6	91.0	90.0	91.0	90.0	90.5	1954.2	47.9	286.5
6'	87.0	87.0	88.0	89.0	87.8	150.0	2.8	289.3
-								
-								

Specimen Height	289.3
Speciment Mass	11497.5
Bulk Density	2.249
Dry Density	2.140

Moisture Content Check	
Sample (Wet) + Tray	12845.6
Sample Dry + Tray	12405.8
Tray Weight	1182.2
Sample Wet	11663.4
Sample Dry	11223.6
MC	3.92%

52

Specimen Description	Hunua 4.0% Asphalt 1.0% Cement
Date and Test Number	24-May-07 M_4C1_HC_2
Testing date from-to	
Mould Diameter (mm)	150
Optimum Moisture (%)	6.0
Percentage of OMC (%)	100.0
Water Content (%)	5.1
Target Dry Density	
Area of Mould (cm2)	176.7

Mass Dry Material	11960.5
Required Water (ml)	610

Lift #	Ruler 1	Ruler 2	Ruler 3	Ruler 4	Average	Mass (g)	Depth/Lift	Total
Initial	377.0	377.0	377.0	377.0	377.0			0.0
1	329.5	330.5	329.5	330.5	330.0	1905.4	47.0	47.0
2	282.0	284.0	282.0	284.0	283.0	1912.5	47.0	94.0
3	233.5	234.5	234.0	235.0	234.3	1977.2	48.8	142.8
4	185.0	185.0	186.0	186.0	185.5	1922.0	48.8	191.5
5	137.0	137.0	138.0	137.0	137.3	1937.6	48.3	239.8
6	89.0	89.0	90.0	88.0	89.0	1926.3	48.3	288.0
6'	88.0	88.0	88.0	88.0	88.0	150.0	1.0	289.0
-								
-								

Specimen Height	288.0
Speciment Mass	11731
Bulk Density	2.305
Dry Density	2.193

Moisture Content Check	
Sample (Wet) + Tray	12804.0
Sample Dry + Tray	12383.6
Tray Weight	1171.3
Sample Wet	11632.7
Sample Dry	11212.3
MC	3.75%

53

Specimen Description	Hunua 4.0% Asphalt 1.0% Cement
Date and Test Number	7-Jul-08 M_4C1_HC_3
Testing date from-to	
Mould Diameter (mm)	150
Optimum Moisture (%)	6.0
Percentage of OMC (%)	100.0
Water Content (%)	5.1
Target Dry Density	
Area of Mould (cm2)	176.7

Mass Dry Material	11960.5
Required Water (ml)	610

Lift #	Ruler 1	Ruler 2	Ruler 3	Ruler 4	Average	Mass (g)	Depth/Lift	Total
Initial	377.0	377.0	377.0	377.0	377.00			0.00
1	331.0	331.0	328.0	328.0	329.50	1948.0	47.5	47.50
2	281.0	281.0	276.0	282.0	280.00	1954.0	49.5	97.00
3	232.0	231.0	227.0	228.0	229.50	1947.0	50.5	147.50
4	287.0	287.0	286.0	280.0	285.00	1908.0	-55.5	92.00
5	137.0	135.0	134.0	136.0	135.50	1922.0	149.5	241.50
6	90.0	90.0	86.0	89.0	88.75	1920.0	46.8	288.25
6'	84.0	84.0	85.0	88.0	85.3	150.0	3.5	291.75
-								
-						674		

Specimen Height	291.75
Speciment Mass	11749.0
Bulk Density	2.279
Dry Density	2.168

Moisture Content Check	
Sample (Wet) + Tray	
Sample Dry + Tray	
Tray Weight	
Sample Wet	0.0
Sample Dry	0.0
MC	#DIV/0!

89

C.7 Triaxial specimens for pore pressure experiments

Specimen Description	Hunua 4.0% Asphalt 1.0% Cement
Date and Test Number	12-Sep-08 **PP_B4C1_LC_1**
Testing date from-to	
Mould Diameter (mm)	150
Optimum Moisture (%)	6.0
Percentage of OMC (%)	100.0
Water Content (%)	5.1
Target Dry Density	
Area of Mould (cm2)	176.7

Mass Dry Material	11960.5
Required Water (ml)	610

Lift #	Ruler 1	Ruler 2	Ruler 3	Ruler 4	Average	Mass (g)	Depth/Lift	Total
Initial	377.0	377.0	377.0	377.0	377.00			0.00
1	325.0	328.0	328.0	323.0	326.00	1818.0	51.0	51.00
2	274.0	277.0	274.0	272.0	274.25	1815.0	51.8	102.75
3	226.0	228.0	228.0	224.0	226.50	1840.0	47.8	150.50
4	176.0	177.0	178.0	175.0	176.50	1834.0	50.0	200.50
5	126.0	129.0	129.0	126.0	127.50	1845.0	49.0	249.50
6	84.0	83.0	84.0	84.0	83.75	1730.0	43.8	293.25
6'	84.0	83.0	84.0	84.0	83.8	100.0	0.0	293.25
-								
-						649		

Specimen Height	293.25
Speciment Mass	10982.0
Bulk Density	2.119
Dry Density	2.016

Moisture Content Check	
Sample (Wet) + Tray	
Sample Dry + Tray	
Tray Weight	
Sample Wet	0.0
Sample Dry	0.0
MC	#DIV/0!

90

Specimen Description	Hunua 4.0% Asphalt 1.0% Cement
Date and Test Number	12-Sep-08 **PP_B4C1_HC_1**
Testing date from-to	
Mould Diameter (mm)	150
Optimum Moisture (%)	6.0
Percentage of OMC (%)	100.0
Water Content (%)	5.1
Target Dry Density	
Area of Mould (cm2)	176.7

Mass Dry Material	11960.5
Required Water (ml)	610

Lift #	Ruler 1	Ruler 2	Ruler 3	Ruler 4	Average	Mass (g)	Depth/Lift	Total
Initial	377.0	377.0	377.0	377.0	377.00			0.00
1	331.0	330.0	329.0	332.0	330.50	1974.0	46.5	46.50
2	280.0	277.0	278.0	282.0	279.25	2092.0	51.3	97.75
3	231.0	228.0	229.0	232.0	230.00	2010.0	49.3	147.00
4	177.0	176.0	178.0	179.0	177.50	2032.2	52.5	199.50
5	130.0	132.0	133.0	130.0	131.25	1961.0	46.3	245.75
6	84.0	84.0	85.0	84.0	84.25	1972.0	47.0	292.75
6'	84.0	84.0	85.0	84.0	84.3	0.0	0.0	292.75
-								
-						760		

Specimen Height	292.75
Speciment Mass	12041.2
Bulk Density	2.328
Dry Density	2.215

Moisture Content Check	
Sample (Wet) + Tray	
Sample Dry + Tray	
Tray Weight	
Sample Wet	0.0
Sample Dry	0.0
MC	#DIV/0!

91

Specimen Description	Hunua 4.0% Asphalt 1.0% Cement
Date and Test Number	7-Jan-09 PP_B4C1_LC_2
Testing date from-to	
Mould Diameter (mm)	150
Optimum Moisture (%)	6.0
Percentage of OMC (%)	100.0
Water Content (%)	5.1
Target Dry Density	
Area of Mould (cm2)	176.7

Mass Dry Material	11960.5
Required Water (ml)	610

Lift #	Ruler 1	Ruler 2	Ruler 3	Ruler 4	Average	Mass (g)	Depth/Lift	Total
Initial	377.0	377.0	377.0	377.0	377.00			0.00
1	327.0	327.0	325.0	325.0	326.00	1830.0	51.0	51.00
2	278.0	279.0	280.0	280.0	279.25	1821.0	46.8	97.75
3	228.0	229.0	230.0	228.0	228.75	1808.0	50.5	148.25
4	184.0	184.0	183.0	184.0	183.75	1743.0	45.0	193.25
5	136.0	136.0	135.0	136.0	135.75	1800.0	48.0	241.25
6	87.0	88.0	87.0	88.0	87.50	1802.0	48.3	289.50
6'								
-								
-						31		

Specimen Height	289.50
Speciment Mass	10804.0
Bulk Density	2.112
Dry Density	2.009

Moisture Content Check	
Sample (Wet) + Tray	
Sample Dry + Tray	
Tray Weight	
Sample Wet	0.0
Sample Dry	0.0
MC	#DIV/0!

92

Specimen Description	Hunua 4.0% Asphalt 1.0% Cement
Date and Test Number	7-Jan-09 PP_B4C1_HC_2
Testing date from-to	
Mould Diameter (mm)	150
Optimum Moisture (%)	6.0
Percentage of OMC (%)	100.0
Water Content (%)	5.1
Target Dry Density	
Area of Mould (cm2)	176.7

Mass Dry Material	11960.5
Required Water (ml)	610

Lift #	Ruler 1	Ruler 2	Ruler 3	Ruler 4	Average	Mass (g)	Depth/Lift	Total
Initial	377.0	377.0	377.0	377.0	377.00			0.00
1	324.0	326.0	326.0	325.0	325.25	2012.0	51.8	51.75
2	275.0	277.0	279.0	278.0	277.25	1932.0	48.0	99.75
3	226.0	228.0	230.0	228.0	228.00	1935.0	49.3	149.00
4	180.0	180.0	180.0	181.0	180.25	1872.0	47.8	196.75
5	130.0	130.5	131.0	131.5	130.75	1970.0	49.5	246.25
6	80.0	81.0	82.0	82.0	81.25	1900.0	49.5	295.75
6'								
-								
-						50		

Specimen Height	295.75
Speciment Mass	11621.0
Bulk Density	2.224
Dry Density	2.116

Moisture Content Check	
Sample (Wet) + Tray	
Sample Dry + Tray	
Tray Weight	
Sample Wet	0.0
Sample Dry	0.0
MC	#DIV/0!

93

C.8 CAPTIF specimens

Specimen Description	CAPTIF Section B12C10
Preparation date	13-Feb-07 **2**
Testing date from-to	
Mould Diameter (mm)	150
Optimum Moisture (%)	6.0
Percentage of OMC (%)	80.0
Water Content (%)	4.8
Target Dry Density	
Area of Mould (cm2)	176.7

Mass Dry Material	
Required Water (ml)	

Lift #	Ruler 1	Ruler 2	Ruler 3	Ruler 4	Average	Mass (g)	Depth/Lift	Total
Initial	377.0	377.0	377.0	377.0	377.0			0.0
1	329.0	327.0	327.0	326.0	327.3	1911.3	49.8	49.8
2	277.0	280.0	279.0	277.0	278.3	1844.2	49.0	98.8
3	233.0	231.0	230.0	233.0	231.8	1803	46.5	145.3
4	183.0	184.0	186.0	184.0	184.3	1828.5	47.5	192.8
5	137.0	135.0	138.0	140.0	137.5	1807	46.8	239.5
6	89.0	92.0	90.0	88.0	89.8	1814.8	47.8	287.3
6'	86.0	87.0	88.0	87.0	87.0	149.1	2.8	290.0
-								
-								

Specimen Height	290.0
Speciment Mass	11157.9
Bulk Density	2.177
Dry Density	2.078

Moisture Content Check	
Sample (Wet) + Tray	13633.0
Sample Dry + Tray	13173.6
Tray Weight	2335.4
Sample Wet	11297.6
Sample Dry	10838.2
MC	4.24%

Specimen Description	CAPTIF Section B 2.75% Bit1.0% Cem
Preparation date	14-Feb-07 **4**
Testing date from-to	
Mould Diameter (mm)	150
Optimum Moisture (%)	6.0
Percentage of OMC (%)	80.0
Water Content (%)	4.8
Target Dry Density	
Area of Mould (cm2)	176.7

Mass Dry Material	
Required Water (ml)	

Lift #	Ruler 1	Ruler 2	Ruler 3	Ruler 4	Average	Mass (g)	Depth/Lift	Total
Initial	377.0	377.0	377.0	376.0	376.8			0.0
1	327.0	325.0	327.0	328.0	326.8	1851.2	50.0	50.0
2	280.0	280.0	281.0	281.0	280.5	1770.7	46.3	96.3
3	232.0	234.0	233.0	235.0	233.5	1823.7	47.0	143.3
4	183.0	181.0	183.0	184.0	182.8	1850.2	50.8	194.0
5	137.0	135.0	138.0	140.0	137.5	1710.1	45.3	239.3
6	88.0	89.0	92.0	91.0	90.0	1759.1	47.5	286.8
6'								
-								
-								

Specimen Height	286.8
Speciment Mass	10765
Bulk Density	2.124
Dry Density	2.027

Moisture Content Check	
Sample (Wet) + Tray	13501.0
Sample Dry + Tray	12991.4
Tray Weight	2353.0
Sample Wet	11148.0
Sample Dry	10638.4
MC	4.79%

Specimen Description	CAPTIF Section C 4.0% Bit1.0% Cem
Preparation date	14-Feb-07 **6**
Testing date from-to	
Mould Diameter (mm)	150
Optimum Moisture (%)	6.0
Percentage of OMC (%)	80.0
Water Content (%)	4.8
Target Dry Density	
Area of Mould (cm2)	176.7

Mass Dry Material	
Required Water (ml)	

Lift #	Ruler 1	Ruler 2	Ruler 3	Ruler 4	Average	Mass (g)	Depth/Lift	Total
Initial	377.0	376.0	376.0	376.0	376.3			0.0
1	329.0	328.0	328.0	330.0	328.8	1740.8	47.5	47.5
2	278.0	279.0	282.0	278.0	279.3	1758.1	49.5	97.0
3	228.0	234.0	236.0	232.0	232.5	1708.9	46.8	143.8
4	180.0	186.0	186.0	180.0	183.0	1718	49.5	193.3
5	134.0	140.0	144.0	135.0	138.3	1628.6	44.8	238.0
6	91.0	90.0	90.0	90.0	90.3	1749.2	48.0	286.0
6'								
-								
-								

Specimen Height	286.0
Speciment Mass	10303.6
Bulk Density	2.039
Dry Density	1.945

Moisture Content Check	
Sample (Wet) + Tray	13789.0
Sample Dry + Tray	13400.6
Tray Weight	3282.4
Sample Wet	10506.6
Sample Dry	10118.2
MC	3.84%

Specimen Description	CAPTIF Section D 0.0% Bit1.0% Cem
Preparation date	15-Feb-07 **7**
Testing date from-to	
Mould Diameter (mm)	150
Optimum Moisture (%)	6.0
Percentage of OMC (%)	80.0
Water Content (%)	4.8
Target Dry Density	
Area of Mould (cm2)	176.7

Mass Dry Material	
Required Water (ml)	

Lift #	Ruler 1	Ruler 2	Ruler 3	Ruler 4	Average	Mass (g)	Depth/Lift	Total
Initial	376.0	377.0	376.0	376.0	376.3			0.0
1	330.0	327.0	331.0	332.0	330.0	1752.5	46.3	46.3
2	279.0	281.0	281.0	278.0	279.8	1825	50.3	96.5
3	235.0	233.0	233.0	234.0	233.8	1741.9	46.0	142.5
4	186.0	183.0	184.0	187.0	185.0	1818.3	48.8	191.3
5	138.0	135.0	136.0	138.0	136.8	1810.1	48.3	239.5
6	89.0	90.0	90.0	87.0	89.0	1808.2	47.8	287.3
6'								
-								
-								

Specimen Height	287.3
Speciment Mass	10756
Bulk Density	2.119
Dry Density	2.022

Moisture Content Check	
Sample (Wet) + Tray	13063.2
Sample Dry + Tray	12484.0
Tray Weight	2352.1
Sample Wet	10711.1
Sample Dry	10131.9
MC	5.72%

Specimen Description	CAPTIF Section F 2.75% Bit 0.0% Cem
Preparation date	15-Feb-07 **9**
Testing date from-to	
Mould Diameter (mm)	150
Optimum Moisture (%)	6.0
Percentage of OMC (%)	80.0
Water Content (%)	4.8
Target Dry Density	
Area of Mould (cm2)	176.7

Mass Dry Material	
Required Water (ml)	

Lift #	Ruler 1	Ruler 2	Ruler 3	Ruler 4	Average	Mass (g)	Depth/Lift	Total
Initial	377.0	376.0	376.0	376.0	376.3			0.0
1	326.0	330.0	330.0	327.0	328.3	1839.8	48.0	48.0
2	283.0	281.0	282.0	283.0	282.3	1840.9	46.0	94.0
3	230.0	236.0	234.0	230.0	232.5	1910	49.8	143.8
4	188.0	187.0	186.0	188.0	187.3	1843.1	45.3	189.0
5	135.0	139.0	141.0	136.0	137.8	1950.1	49.5	238.5
6	92.0	88.0	91.0	94.0	91.3	1910.5	46.5	285.0
6'	88.0	87.0	89.0	89.0	88.3	150	3.0	288.0
-								
-								

Specimen Height	288.0
Speciment Mass	11444.4
Bulk Density	2.249
Dry Density	2.146

Moisture Content Check	
Sample (Wet) + Tray	
Sample Dry + Tray	
Tray Weight	
Sample Wet	0.0
Sample Dry	0.0
MC	#DIV/0!

Specimen Description	CAPTIF Section E 0.0% Bit 0.0% Cem
Preparation date	7-May-07 **11**
Testing date from-to	
Mould Diameter (mm)	150
Optimum Moisture (%)	6.0
Percentage of OMC (%)	80.0
Water Content (%)	6
Target Dry Density	
Area of Mould (cm2)	176.7

Mass Dry Material	
Required Water (ml)	

Lift #	Ruler 1	Ruler 2	Ruler 3	Ruler 4	Average	Mass (g)	Depth/Lift	Total
Initial	377.0	377.0	377.0	377.0	377.0			0.0
1	325.0	327.0	329.0	328.0	327.3	1922	49.8	49.8
2	278.5	279.5	282.0	280.0	280.0	1901.3	47.3	97.0
3	232.0	232.0	235.0	232.0	232.8	1899.3	47.3	144.3
4	183.0	183.0	183.0	183.0	183.0	1901.1	49.8	194.0
5	135.0	135.0	135.0	135.0	135.0	1931.2	48.0	242.0
6	86.0	86.0	86.0	86.0	86.0	1929.9	49.0	291.0
6'	84.0	84.0	84.0	84.0	84.0	150	2.0	293.0
-								
-								

Specimen Height	293.0
Speciment Mass	11634.8
Bulk Density	2.247
Dry Density	2.120

Moisture Content Check	
Sample (Wet) + Tray	12927.4
Sample Dry + Tray	12390.6
Tray Weight	1458.8
Sample Wet	11468.6
Sample Dry	10931.8
MC	4.91%

Specimen Description	Subgrade
Date and Test Number	23-May-07 **Subgrade**
Testing date from-to	
Mould Diameter (mm)	150
Optimum Moisture (%)	20.0
Percentage of OMC (%)	
Water Content (%)	20.0
Target Dry Density	
Area of Mould (cm2)	176.7

Mass Dry Material	11960.5
Required Water (ml)	2392

Lift #	Ruler 1	Ruler 2	Ruler 3	Ruler 4	Average	Mass (g)	Depth/Lift	Total
Initial	377.0	377.0	377.0	377.0	377.0			0.0
1	324.5	324.0	324.5	324.0	324.3	1570.3	52.8	52.8
2	272.0	271.0	272.0	271.0	271.5	1573.6	52.8	105.5
3	222.0	223.0	222.0	220.0	221.8	1570.3	49.8	155.3
4	171.0	171.0	170.0	170.0	170.5	1570.3	51.3	206.5
5	119.0	121.0	120.0	116.0	119.0	1569.3	51.5	258.0
6	86.0	86.0	86.0	86.0	86.0	967.7	33.0	291.0
6'								
-								
-								

Specimen Height	291.0
Speciment Mass	8821.5
Bulk Density	1.715
Dry Density	1.430

Moisture Content Check	
Sample (Wet) + Tray	
Sample Dry + Tray	
Tray Weight	
Sample Wet	0.0
Sample Dry	0.0
MC	#DIV/0!

D Additional preliminary triaxial tests

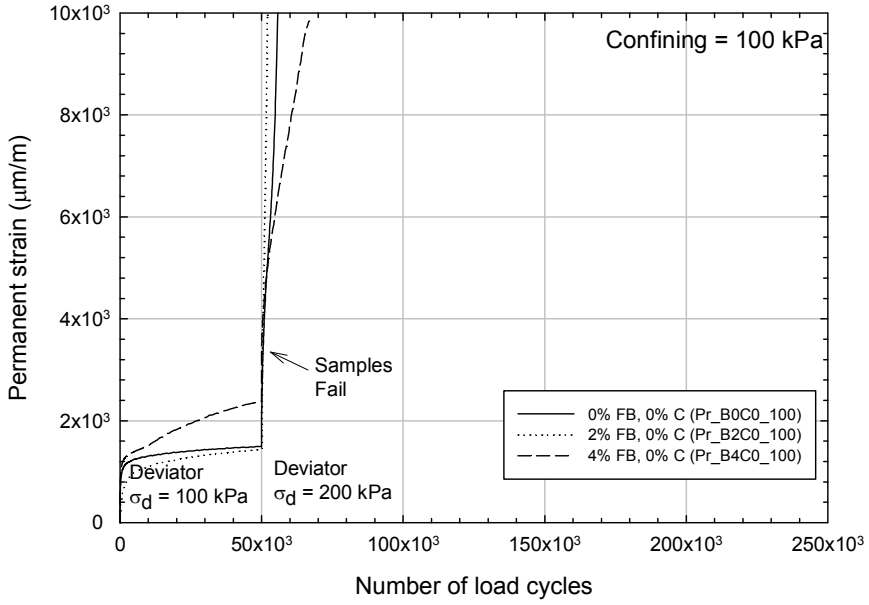

Figure D.1 Results of preliminary permanent deformation study on mixes at 0% foam bitumen (100 kPa confining pressure)

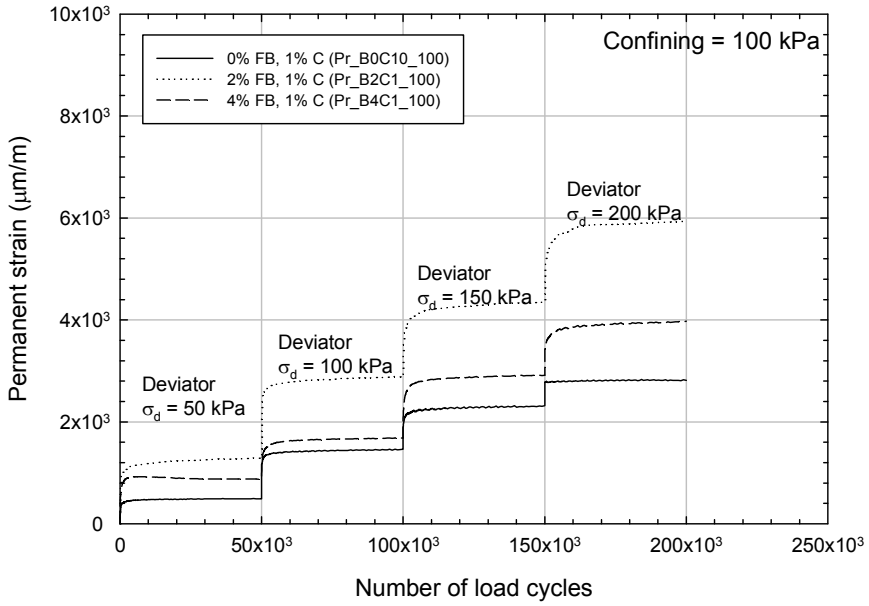

Figure D.2 Results of preliminary permanent deformation study on mixes at 1% foam bitumen (100 kPa confining pressure)

E Scala penetrometer and CBR

CBR (%)	Depth/Blow	CBR (%)	Depth/Blow
1	150	26	7
2	120	27	7
3	90	28	7
4	65	29	6
5	50	30	6
6	45	31	6
7	35	32	6
8	30	33	5
9	25	34	5
10	20	35	5
11	20	36	5
12	18	37	5
13	17	38	4.5
14	15	39	4.5
15	14	40	4.5
16	14	41	4.5
17	13	42	4
18	12	43	4
19	11	44	4
20	10	45	4
21	9	46	3.5
22	9	47	3.5
23	9	48	3.5
24	8	49	3.5
25	8	50	3.5

F Emu strain system

Paterson (1972) and Janoo et. al. (1999) examined the effect of both axial misalignment and axial rotation of the coils relative to each other and they both concluded that as long as the rotation was less than 10° and the misalignment was less than 12 mm, the resultant effect on the static strain was less than 2%.The original Canterbury test track facility used a Bison Model 4101A Soil Strain Gauge (Paterson 1972). This was replaced in 1992 by an automated multi-channel system based on a modified prototype of the Saskatchewan Soil Strain/Displacement measuring system (SSSD) developed by Saskatchewan (Canada) Highways and Transportation (Pidwerbesky 1996).

In 2000 a new soil strain Emu system was purchased from the University of Nottingham to replace the SSSD system. The SSSD system was replaced because of reliability problems with the hardware and commercially manufactured coils could no longer be obtained. The new system still uses the same inductive coil principal as before, but the excitation, reading and decoding hardware is different. An unlimited number of coil pairs can now be read as each coil is connected to a multiplexor upstream of the Emu unit. The supply of coils is also guaranteed as CAPTIF personnel now manufacture them to a specification developed by the University of Nottingham. The multiplexing and computer interface equipment are standard commercial parts and the controlling software is written using the National Instruments LabView computer program.

A typical CAPTIF installation of Emu coils for a project is up to six separate sites, with each site comprising of up to 36 coils arranged in a number of one and three dimensional arrays. Each site comprises of a power supply, an Emu conditioning unit, a 36 channel multiplexor and an industrial computer running Microsoft WindowsXP containing a National Instruments PCI 6025E 16 channel, 12 bit Analog to Digital converter and 8 channels of digital input/output (used to control the multiplexor). This equipment is housed in a

19” rack cabinet located beside the pavement tank. For operational and safety reasons, the trackside computers are operated by remote control software (PC Anywhere) from within the control room. The use of the remote control software allows a single person to simultaneously control all four cabinets. For a one-dimensional array, the coils are arranged in a coaxial stack with the coils spaced at 75 mm centres. This configuration is used to measure vertical strains. The three-dimensional array is an extension of the one-dimensional array, with two co-planar coils being energized from each coil in the central stack. A co-planar coil can be orientated to either measure longitudinal or transverse horizontal strains.

The repeatability of the SLAVE loading on the pavement over a number of laps and the high frequency of loading (one revolution every 4.5 s) was utilized to simplify the electronic systems used to monitor the Emu system. Only one coil pair is energized for each vehicle pass and the output from five vehicle passes is recorded to allow for missed triggers and other events that may influence the system. The 36 coils at each site are typically configured to produce 33 coil pairs, so each set of complete measurements will take 165 vehicle passes. The acquisition software stores the raw voltages in a tab separated array in an ASCII text file. The project, temporal, spatial and collection parameters are also written to the same file to ensure that a complete record of the data is preserved.

G Structural design of pavements

G.1 Design requisites

As was mentioned in Section Chapter 4 the targeted thickness of the basecourse was 200 mm for a targeted traffic of 1 million ESAs and a design reliability of 95%. The following sections detail the design of pavements using the South African TG2 technical guidelines and the New Zealand Supplement to the AUSTROADS design guide.

G.2 Design one: Interim technical guidelines (TG2)

The most widely available document for the structural design of foam bitumen pavements before the execution of CAPTIF foam bitumen experiments were the “Interim Technical Guidelines (TG2): The Design and use of Foamed Bitumen Treated Materials”. The guidelines state that foam bitumen pavements behave in two separate phases. The first phase is when the layer is in an intact, undamaged condition and provides some fatigue resistance. This phase ends when the layer has reached an equivalent granular state, with the time to reach this state defined as the effective fatigue life. The term “equivalent granular state” is used to describe the loss in resilient modulus (stiffness) of the material and is comparable to granular materials only in the stiffness and not in the physical composition of the materials.

The guidelines classify the foam bitumen mixes into four categories (FB1, FB2, FB3 and FB4) depending on their Unconfined Compressive Strength (UCS) and Indirect Tensile Strength (ITS) values (Table G.1). The guidelines provided performance models for materials FB2 and FB3 only.

Two simple pavement design charts are provided in the guidelines for FB2 and FB3 materials and four different project reliabilities. The “Category A” charts (95% reliability) for FB2 and FB3 materials were utilized for design purposes. In these charts the designer has to first choose the expected traffic expressed in Equivalent Standard Axles (ESAs) and then has to select either

thickness of the foam bitumen layer (in millimetres) or subgrade support (in MPa). Only traffic from 10,000 to 1,000,000 ESAs is fully available for materials FB2 and FB2. For CAPTIF test the minimum thickness was 200 mm and therefore the subgrade support was the unknown variable.

Table A.1 Foamed bitumen treated material classification system (Academy 2002)

Material Code		ITS at 25° C (kPa)	
		100 - 300	300 – 500
UCS at 25° C (kPa)	700 – 1400	FB4	FB3*
	1400 – 2000	FB2*	FB1

* Foam bitumen materials where design models are available

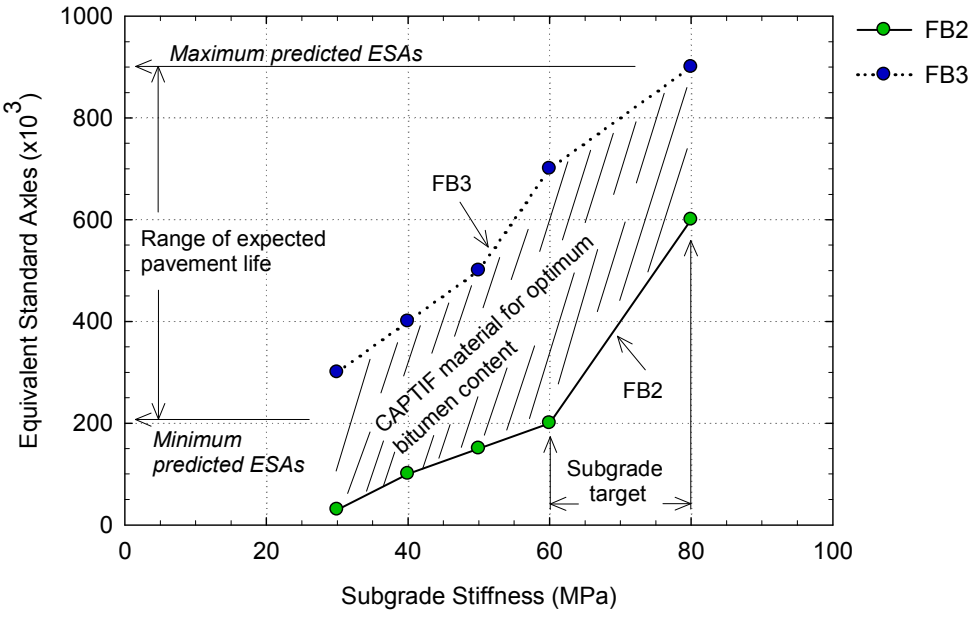

Figure G.1 Pavement design for a 200 mm basecourse of FB2 and FB3 materials at different subgrade stiffness using TG2 guidelines charts

Figure A.4 presents a chart prepared using the solutions provided by the TG2 charts presented above for a 200 mm basecourse of FB2 and FB3 material. The CAPTIF pavement design was carried out for the material at the optimum foam bitumen content (2.8% and 1% cement). This optimum CAPTIF material

was assumed to have properties between a FB2 and FB3 material because its peak ITS at 3.0% was about 300 kPa (Chapter 3). Since the target traffic during CAPTIF experiment was one million ESAs, a subgrade stiffness between 60 to 80 MPa was the target stiffness during the following construction of the subgrade layer. This subgrade stiffness range would provide a minimum and maximum ESAs number of $200x10^3$ and $950x10^3$ respectively. The terminal distress conditions assumed by the TG2 Guidelines method are 20 mm of rutting or shear failure in the subgrade or basecourse, or fatigue cracking on the surface of the pavement.

G.3 **Design two: New Zealand Supplement**

The New Zealand supplement to the AUSTROADS pavement design guide proposes a methodology for the design of foamed bitumen pavements. The method consists on a simple mechanistic analysis of a pavement model using CIRCLY (MINCAD 2004), a linear elastic and multi layered software for pavement analysis and design. The design parameter proposed by this design method is the vertical strain at the top of the subgrade where the allowable standard axles are calculated using the AUSTROADS equation:

$$N = \left[\frac{9300}{\mu\varepsilon}\right]^7$$

where N is the number of the allowable ESAs and $\mu\varepsilon$ is the maximum vertical (compressive) strain at the top of the subgrade calculated from CIRCLY.

The pavement model consisted of a thin asphalt surface, a 200 mm foam bitumen layer and a subgrade layer. The assumed stiffness for the thin-asphalt surface was 3,000 MPa (isotropic) and a Poisson's ratio of 0.40. The foamed bitumen layer was considered anisotropic with no sub-layering and with an elastic modulus of 800 MPa, as recommended by the New Zealand supplement. The subgrade was modelled as anisotropic and sub-layered following the AUSTROADS 2004 recommendations. The Equivalent Standard Axle was modelled in CIRCLY as two pairs of dual tyres with a contact

pressure of 750 kPa. The results of the pavement design for different subgrade supports are presented in Table G.2. A project reliability factor of 95% was adopted for the design. The results indicate that only a very weak subgrade (stiffness of 30 MPa) leads to a pavement structure with a life less than one million ESAs. The terminal distress condition assumed by the New Zealand Supplement method is 20 mm of rutting in the subgrade layer.

Figure G.2 ESAs for different subgrade support using New Zealand supplement design method

Subgrade Stiffness (MPa)	Allowable ESAs
30	574,712
40	1,367,989
50	2,754,482
60	4,975,124
80	13,210,039
100	29,411,117

G.4 Discussion and design adopted

The pavement design from both TG2 Guidelines and New Zealand Supplement design methods provide considerable different results. These differences in part reflect the limited data available to develop these models. However, it was considered that TG2 guidelines provide a more reliable solution than the New Zealand Supplement because they were developed using experimental data. As was mentioned in Chapter 2, these experimental data were collected from laboratory and full-scale testing on foam bitumen materials in South Africa. The drawback is that data were taken from a project where foam bitumen pavements were stabilised with higher cement content (2%) than foam bitumen contents (1.8%) and therefore these are not completely representative of the performance of foam bitumen pavements. Conversely, the main weaknesses of the New Zealand Supplement method is that ignores the deformation of the basecourse and considers the life of the subgrade layer only.

As a result, and considering all the limitations of the design methods presented here, a subgrade support within a range of 60-80 MPa was considered a reasonable value for CAPTIF experiment (Figure G.3).

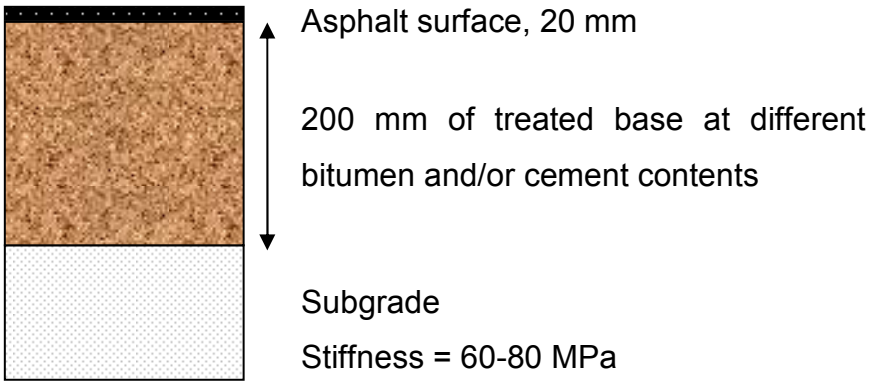

Figure G.3 Final pavement design adopted for CAPTIF project

H Pictures of CAPTIF construction

Figure H.1 Levelling of subgrade layers

Figure H.2 Compaction of subgrade layers

Figure H.3 Installation of Emu strain coils in subgrade layers

Figure H.4 Falling Weight Deflectometer (FWD) measurements on final subgrade layer

Figure H.5 Trucks arriving from the North Island with the untreated unbound H40 aggregate

Figure H.6 Excavation of trenches for stabilisation

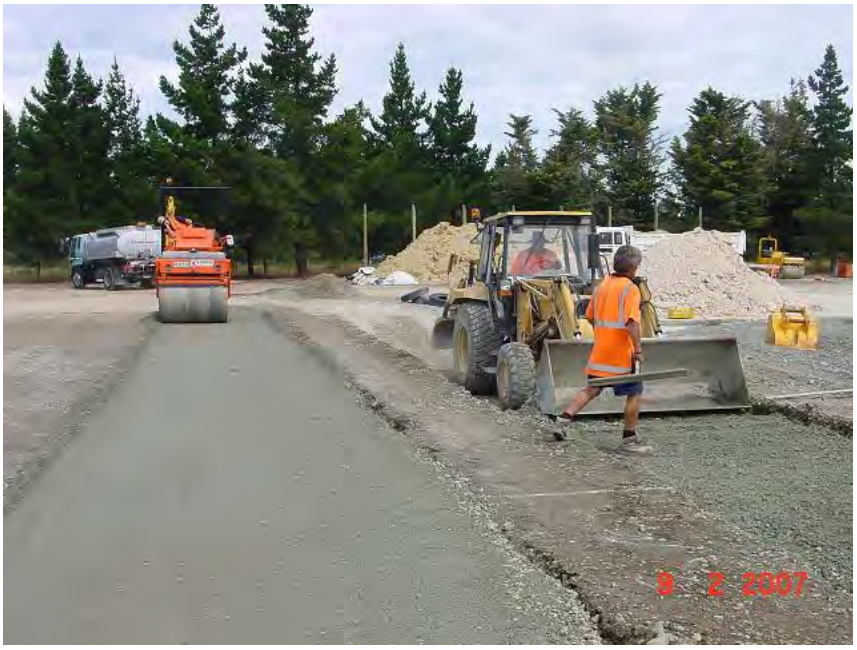

Figure H.7 Laying and compaction of the basecourse material for stabilisation

Figure H.8 Taking samples for laboratory testing immediately after stabilisation

Figure H.9 Excavation of trenches with the stabilised material

Figure H.10 Transportation and laying of the basecourse layer using a paver machine

Figure H.11 Compaction of the basecourse layer

Figure H.12 Installation of Emu soil strain system in the basecourse layer

Figure H.13 Primer over basecourse layer

Figure H.14 Laying of the skim asphalt layer

Figure H.15 Falling Weight Deflectometer testing over asphalt layer, before trafficking

Figure H.16 Falling Weight Deflectometer testing after 1 million load cycles

I Surface profiles

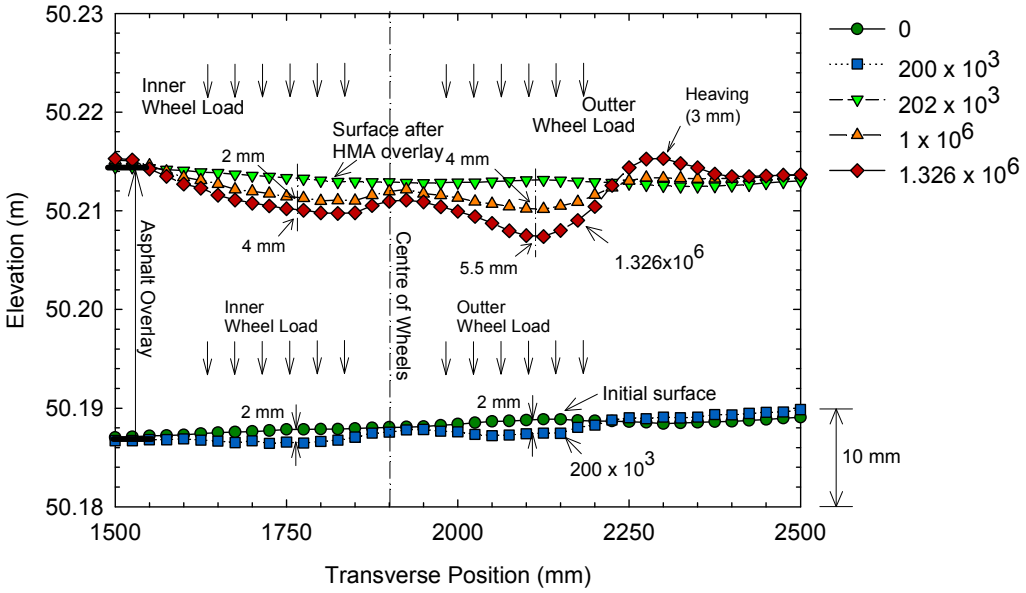

Figure I.1 Surface profile section B12C10

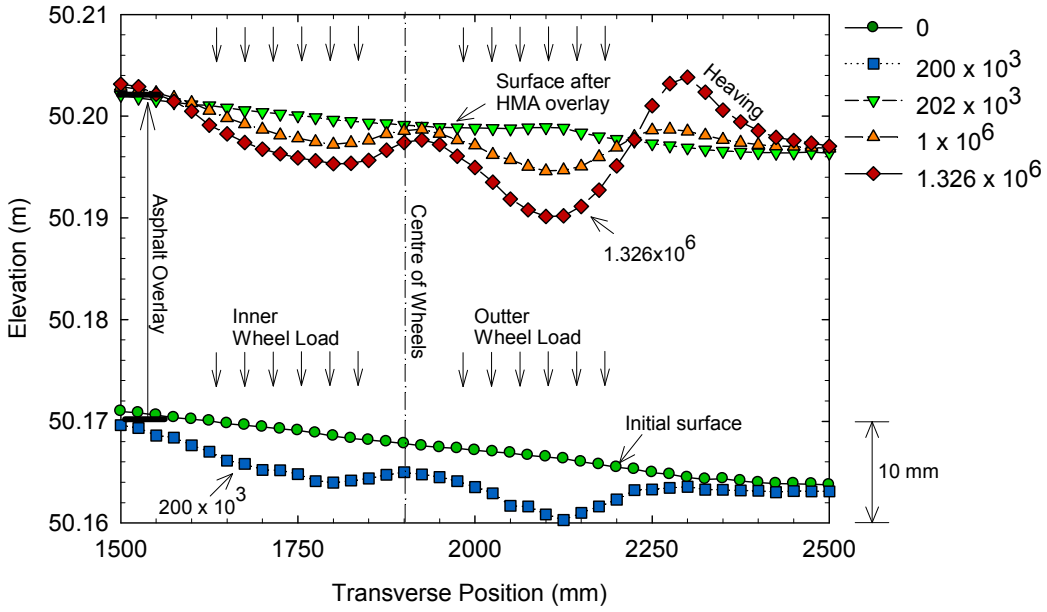

Figure I.2 Surface profile section B00C00

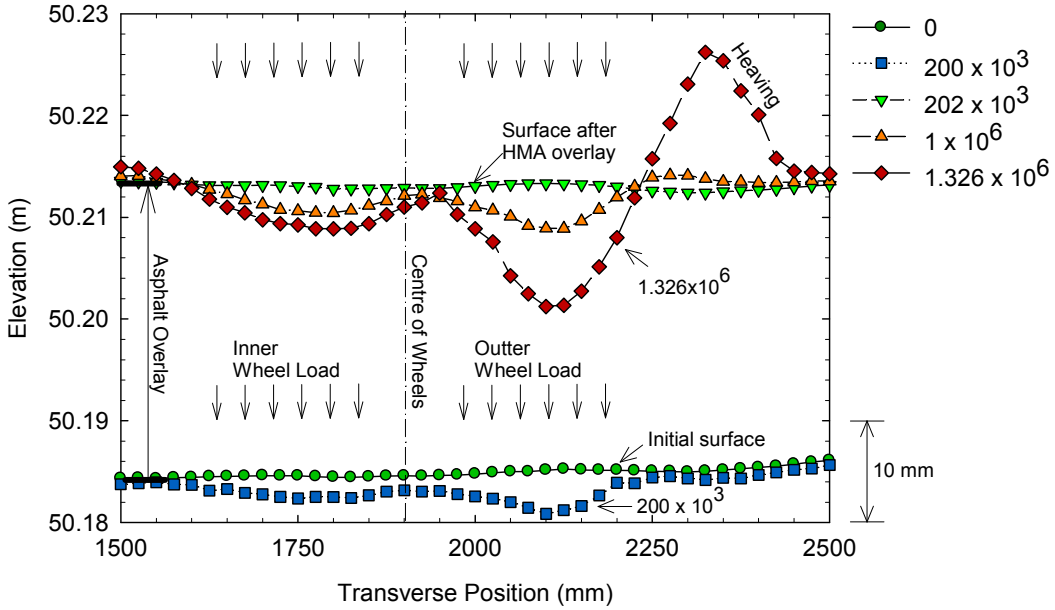

Figure I.3 Surface deformation section B22C00

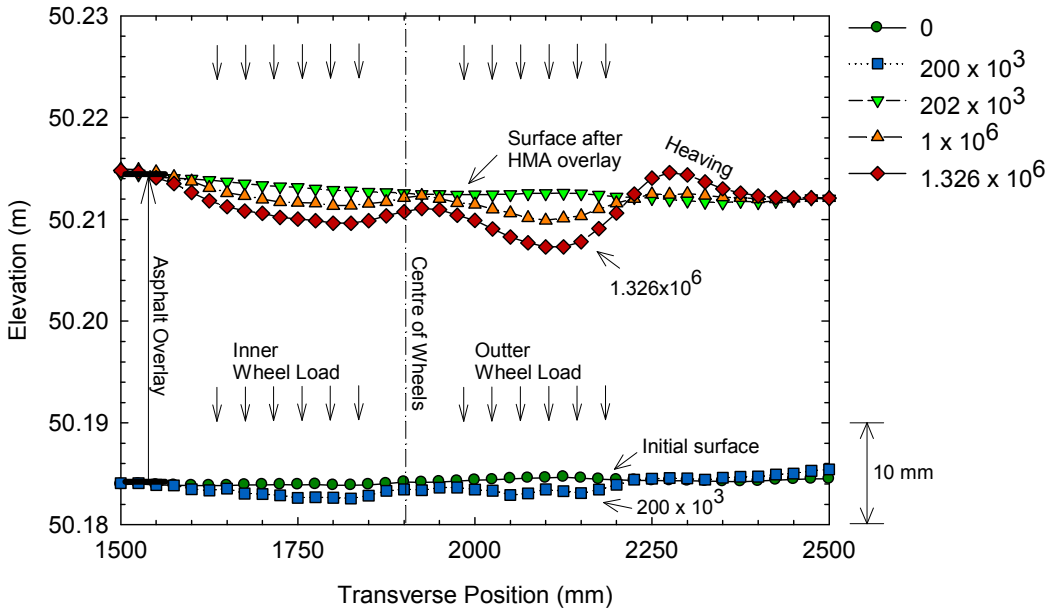

Figure I.4 Surface deformation section B14C10

J Surface pictures

J.1 Section B12C10 (after introduction of water)

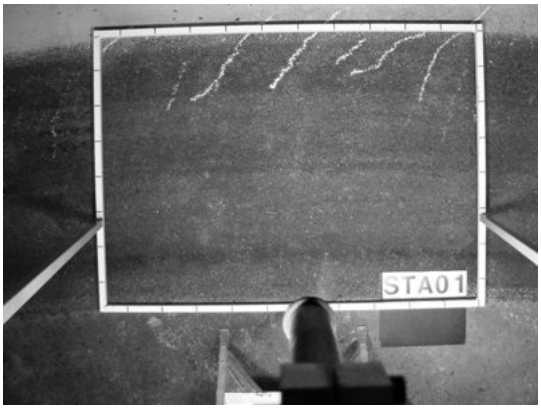

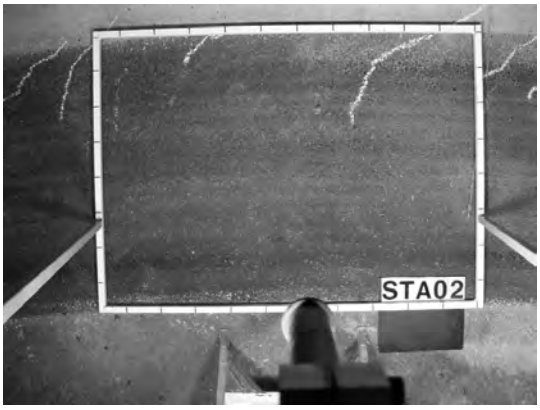

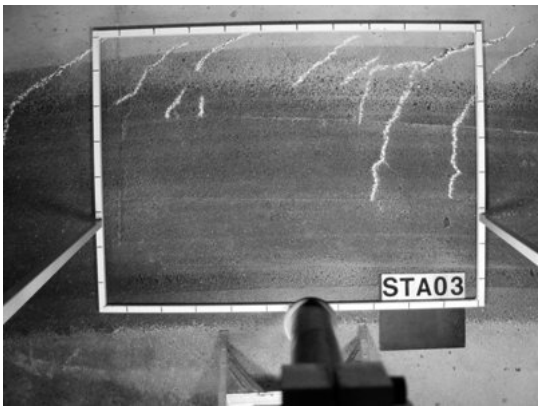

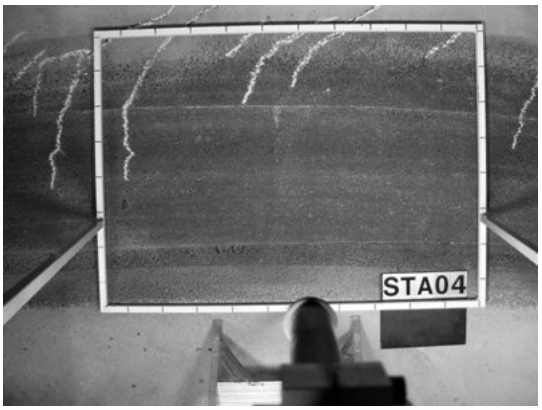

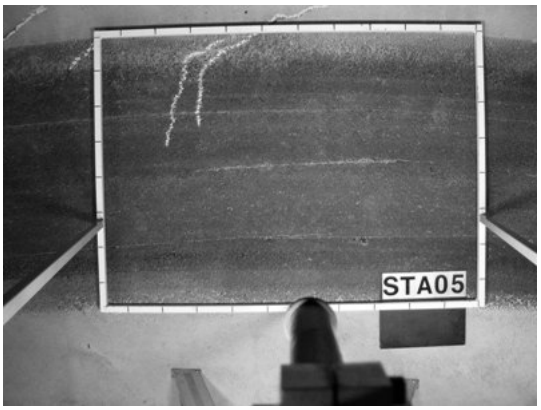

J.2 Section B14C10 (after introduction of water)

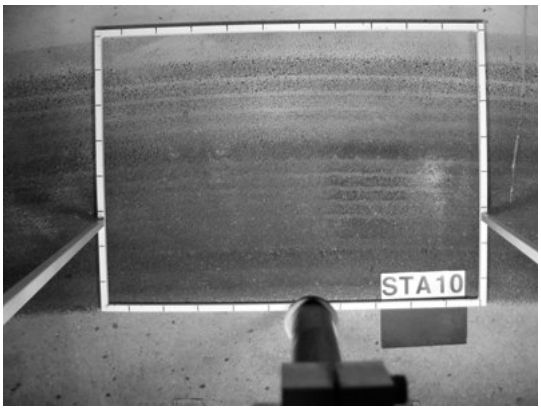

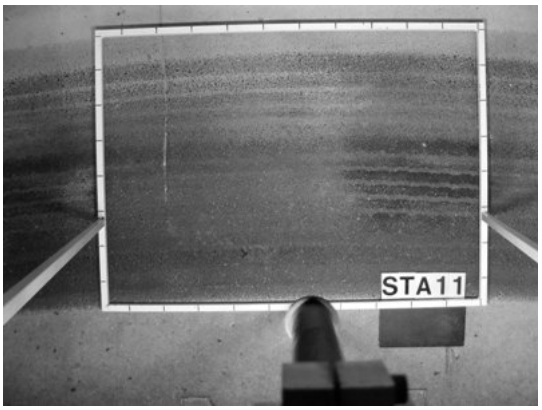

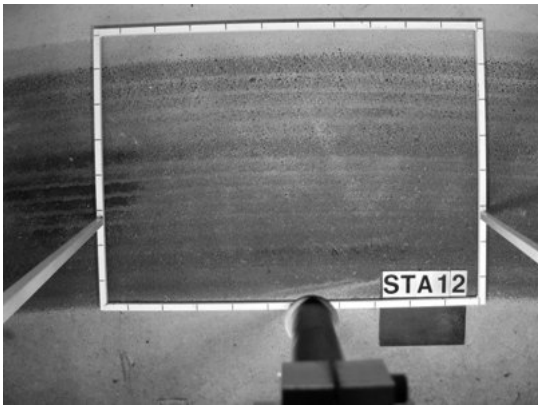

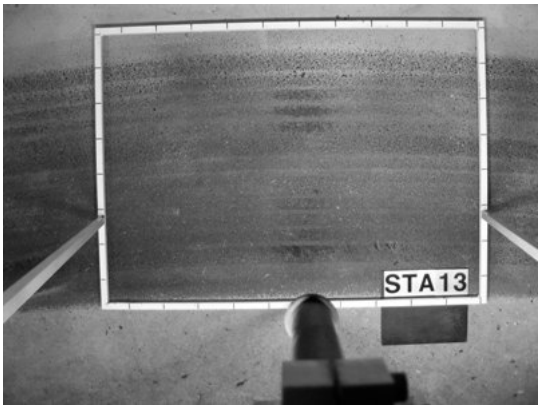

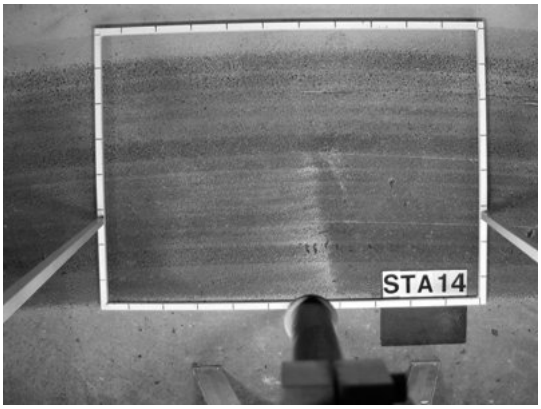

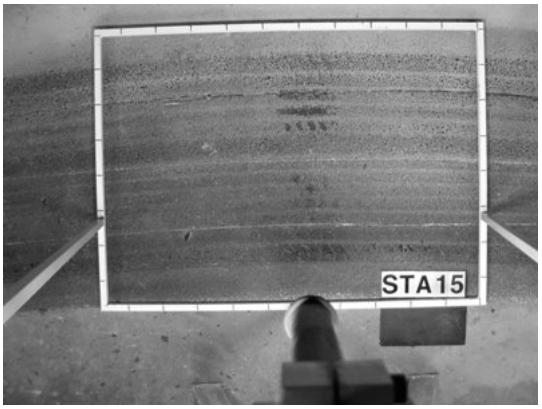

J.3 Section B28C10 (after introduction of water)

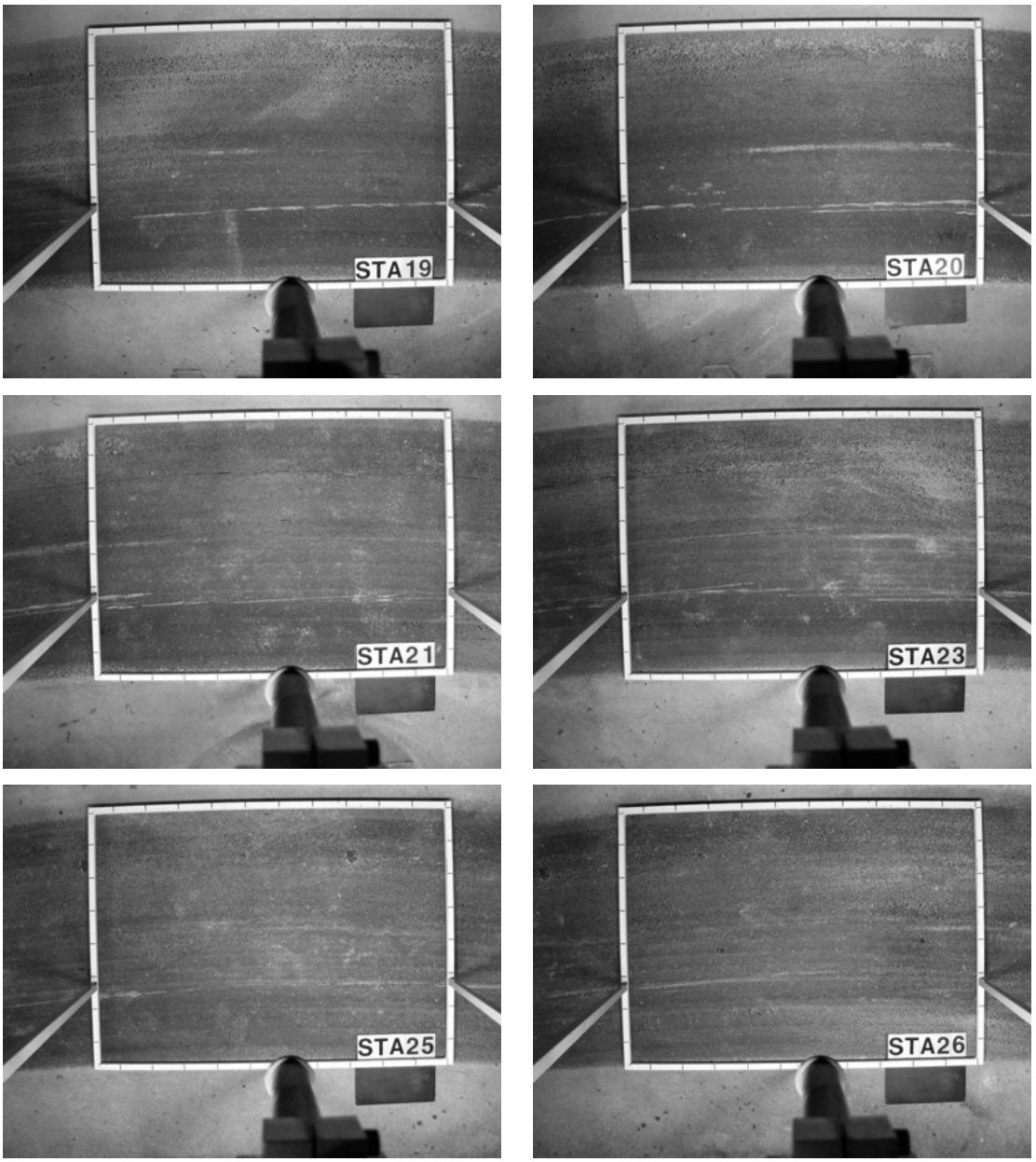

J.4 Section B00C10 (no water was directly introduced)

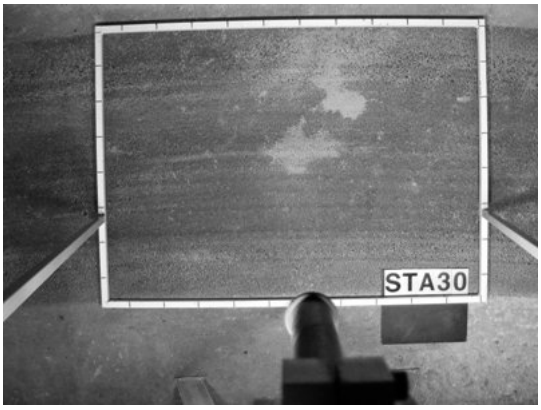

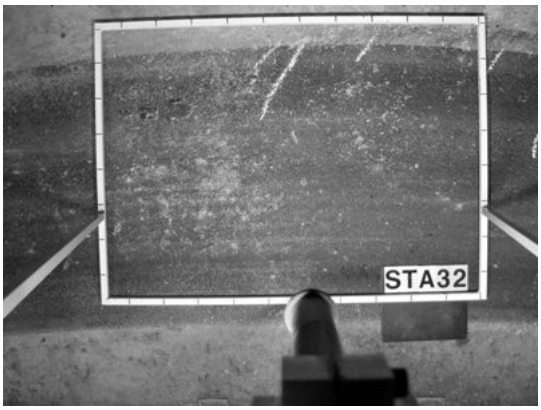

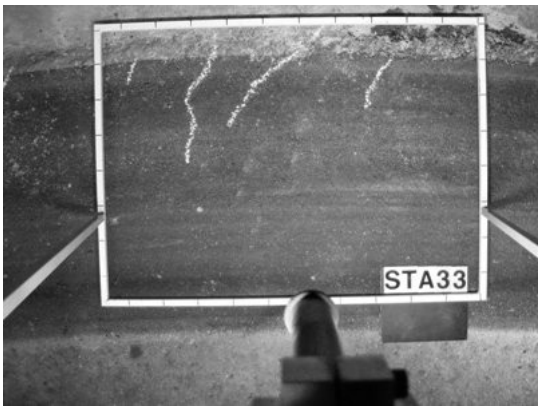

J.5 Section B00C00 (no water was directly introduced)

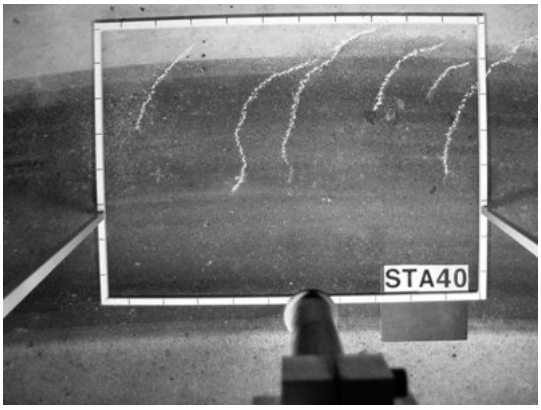

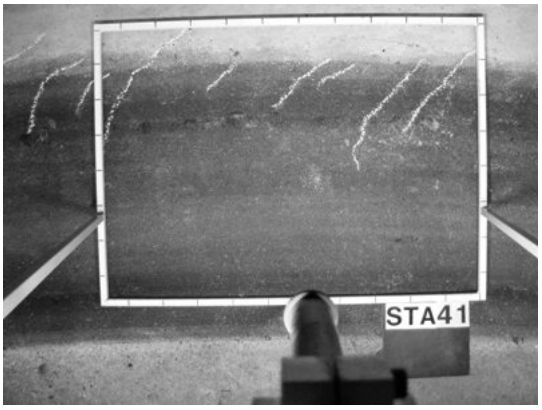

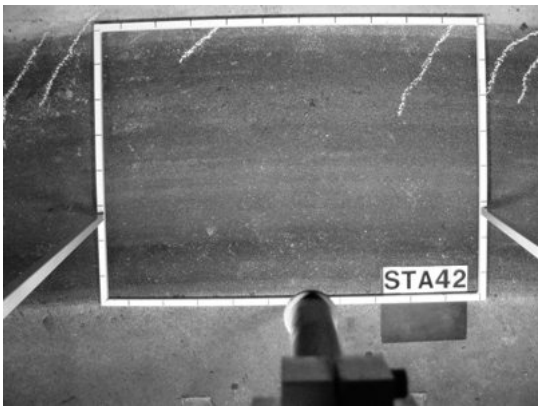

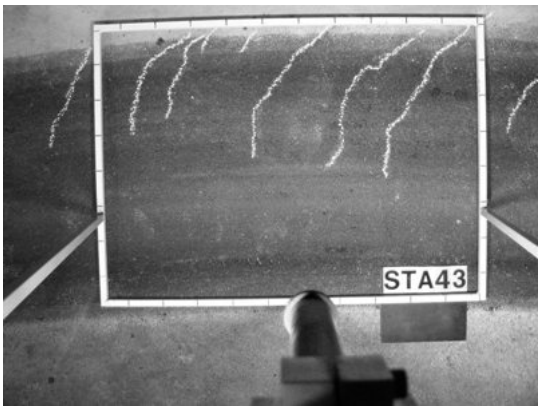

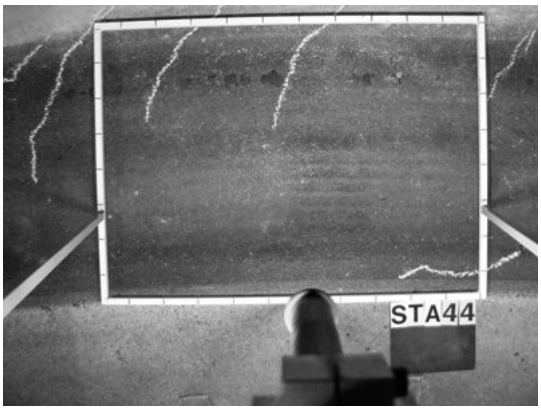

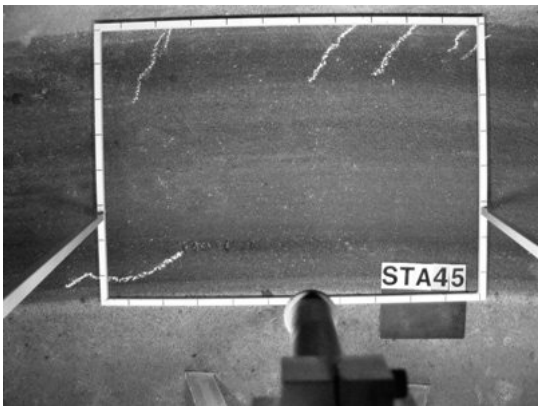

J.6 Section B22C00 (no water was directly introduced)

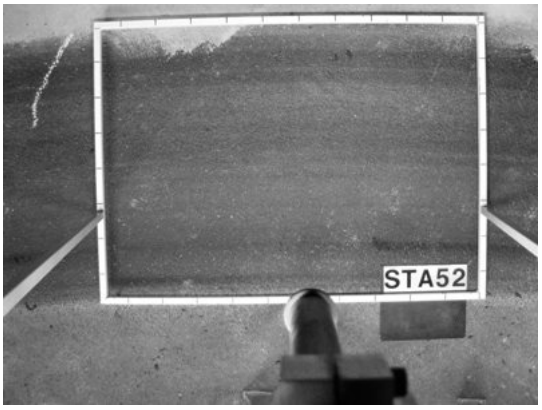

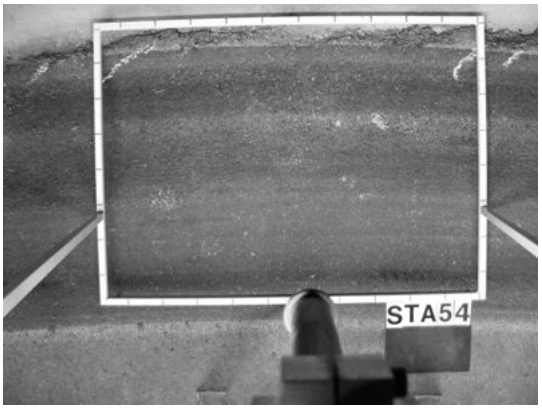

K Vertical strain profiles

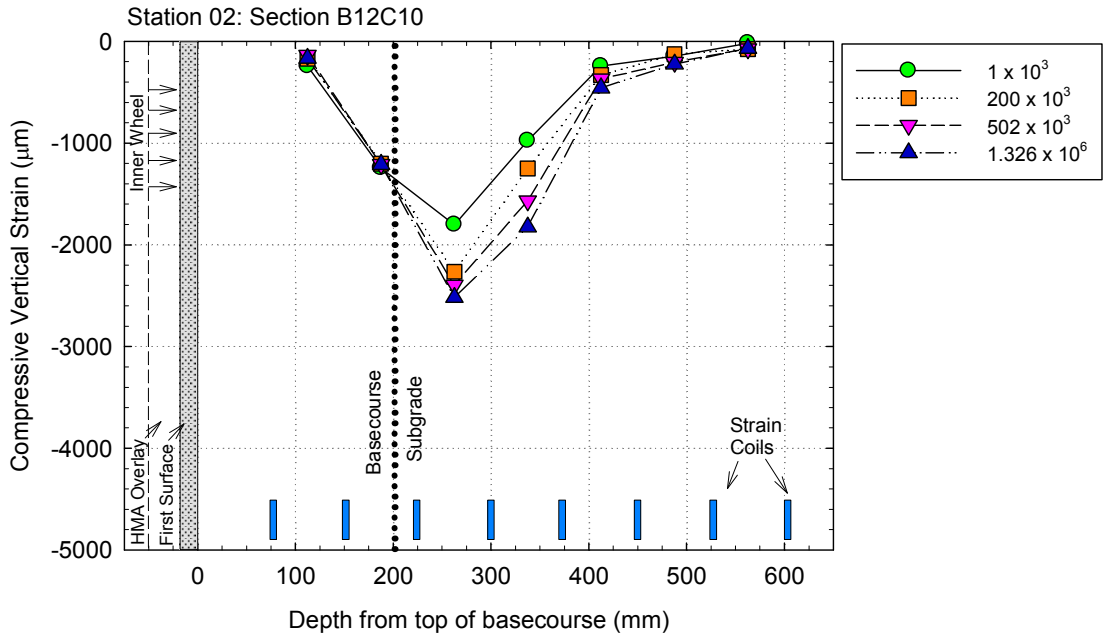

Figure K.1 Vertical strain profile station 02, section B12C10

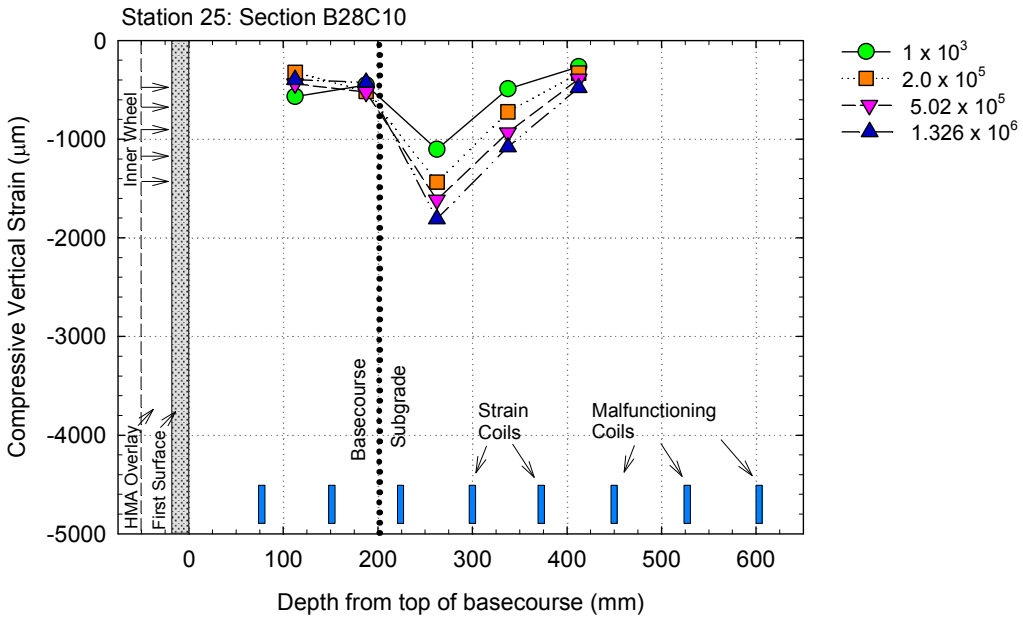

Figure K.2 Vertical strain profile, station 25, section B28C10

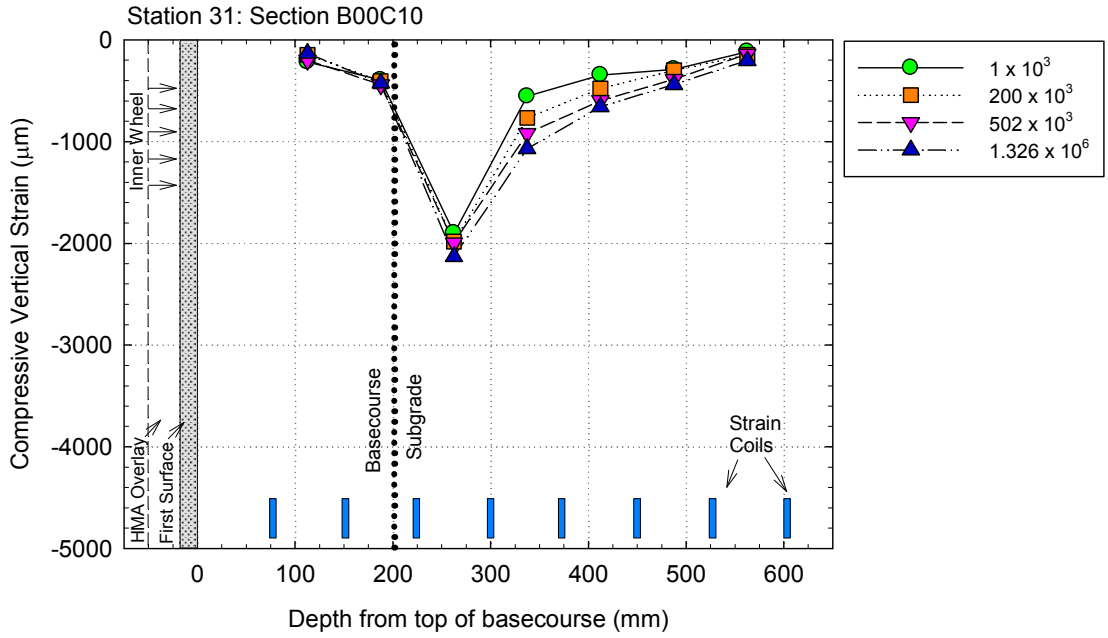

Figure K.3 Vertical strain profile, station 40, section B00C10

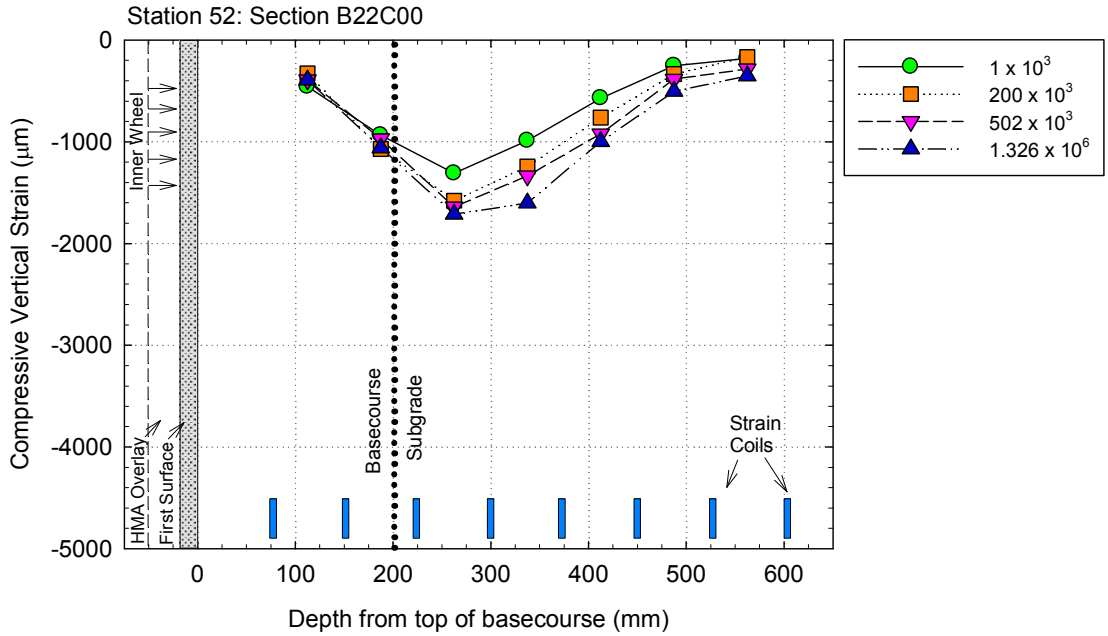

Figure K.4 Vertical strain profile, station 52, section B22C00

L Post-mortem profiles

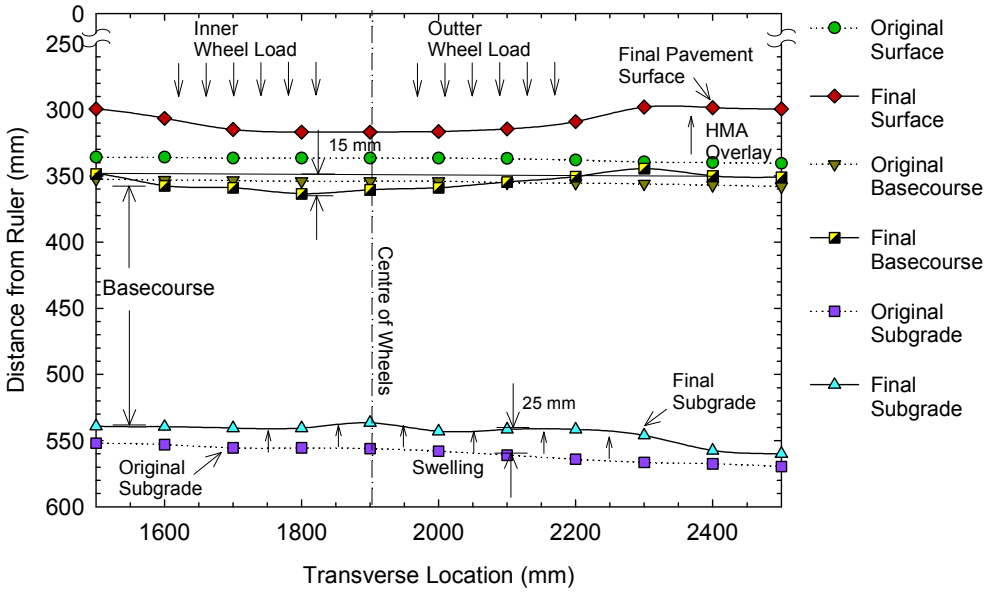

Figure L.1 Transverse post-mortem profile section B12C10

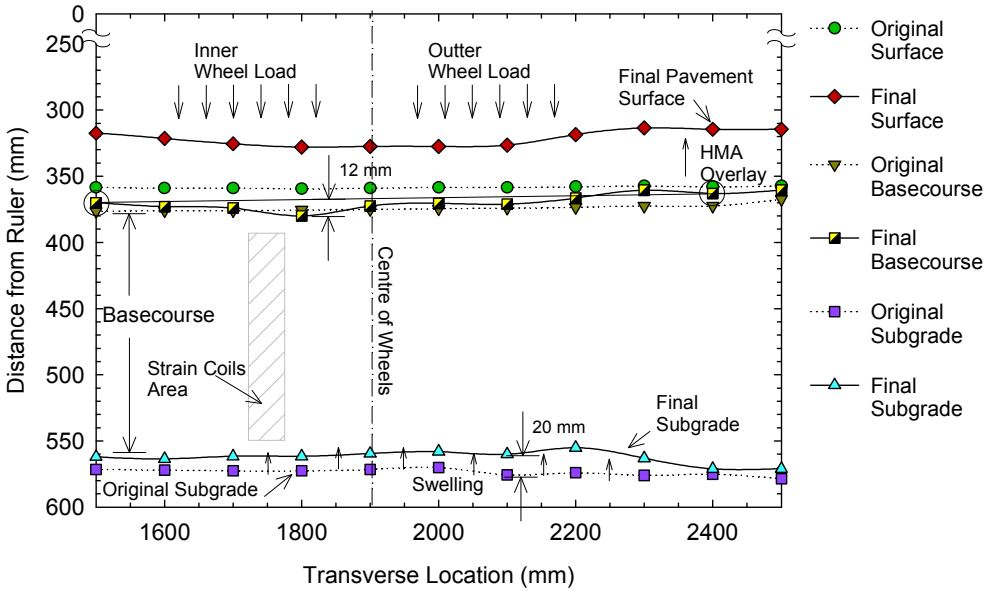

Figure L.2 Transverse post-mortem profile section B14C10

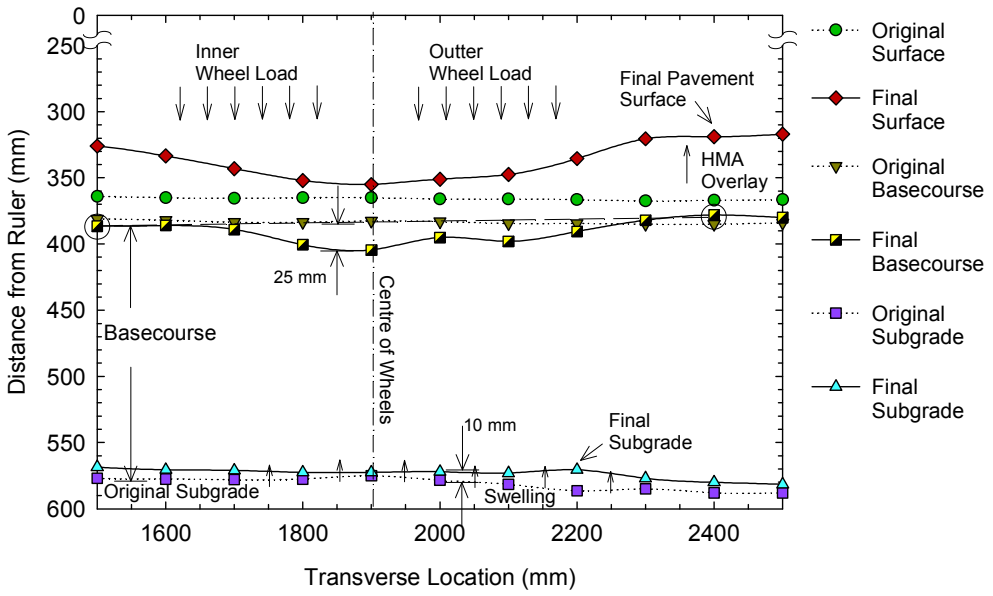

Figure L.3 Transverse post-mortem profile section B00C00

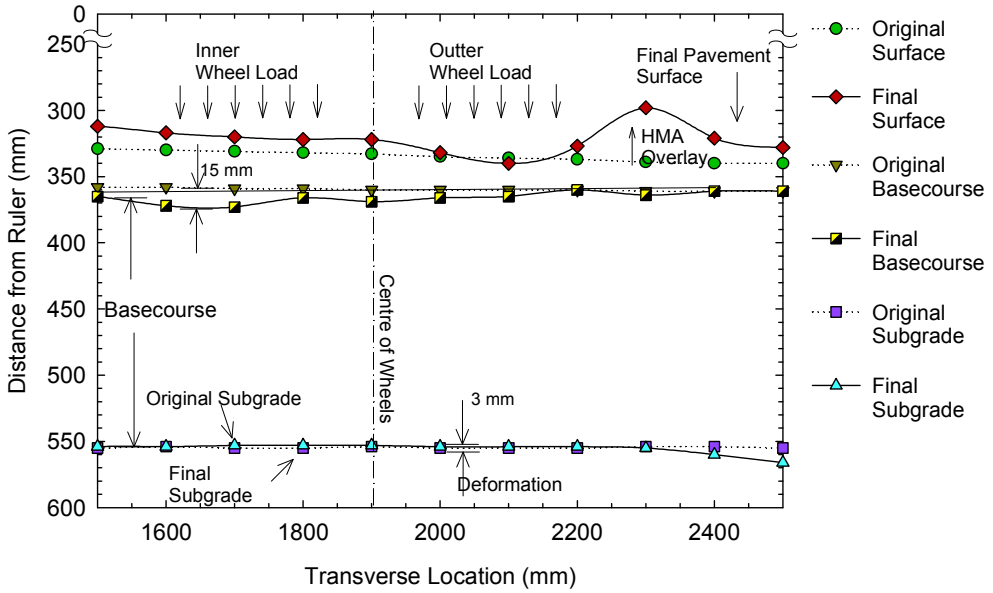

Figure L.4 Transverse post-mortem profile section B22C00

M Deflection bowls and vertical strain measurements

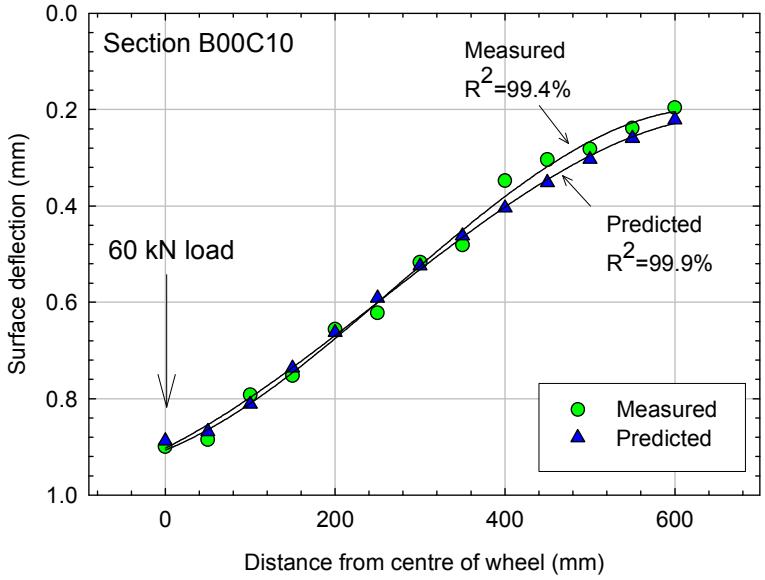

Figure M.1 Measured and predicted surface deflection bowls for a 60 kN SLAVE load at section B00C10

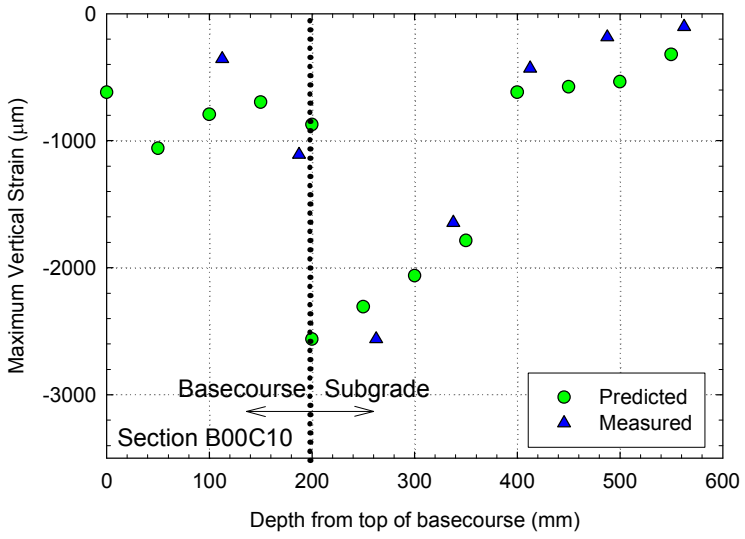

Figure M.2 Measured and predicted vertical strains for a 60 kN SLAVE load at section B00C10

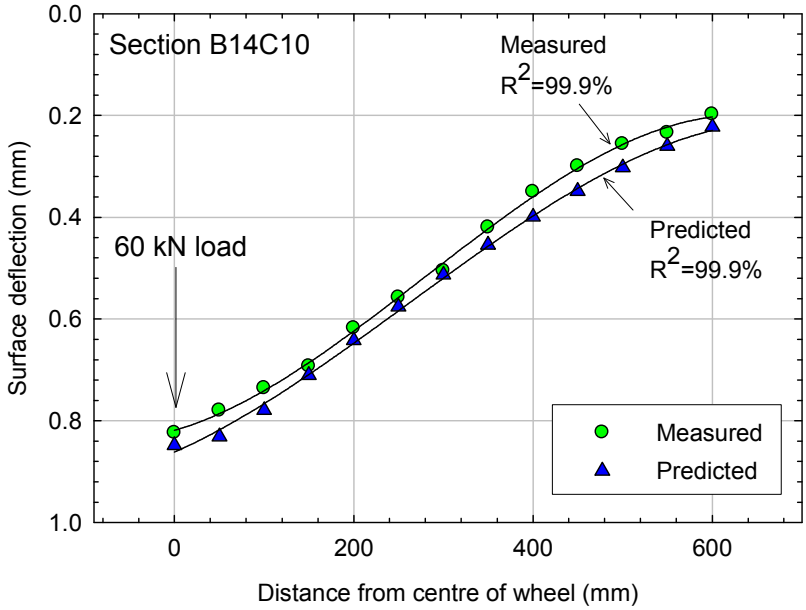

Figure M.3 Measured and predicted surface deflection bowls for a 60 kN SLAVE load at section B14C10

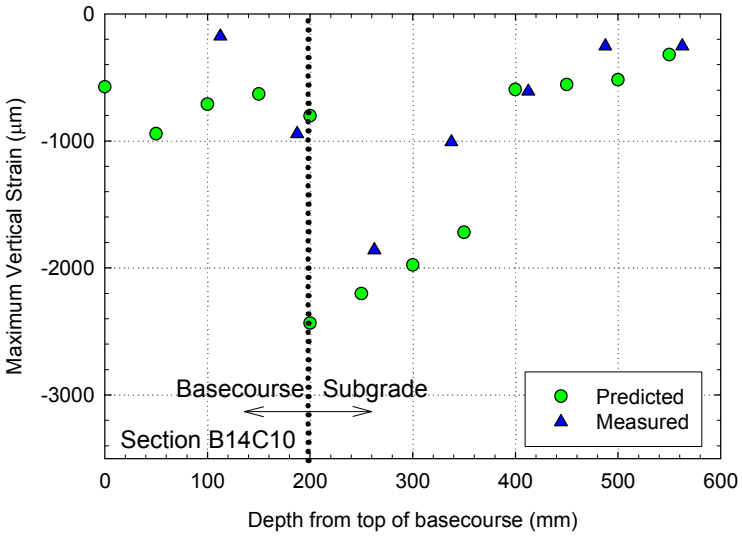

Figure M.4 Measured and predicted vertical strains for a 60 kN SLAVE load at section B14C10

Appendix References

Asphalt Academy (2002). "Interim technical guidelines (TG2): The Design and Use of Foamed Bitumen Treated Materials". Pretoria, South Africa.

Acott, S. M., and Myburgh, P. A. (1983). “Design and performance study of sand bases treated with foamed asphalt”. Transportation Research Record No. 898, pp. 290-296.

Akeroyd, F. M. L., and Hicks, B. J. (1988). "Foamed bitumen road recycling". Highways (Croydon, England), 56(1933), pp. 42-43.

Bowering, R. H., and Martin, C. L. (1976). “Foamed bitumen production and application of mixtures evaluation and performance of pavements”. Minnesota University, Association of Asphalt Paving Technologists.

Brennen, M., Tia, M., Altschaeffl, A. G., and Wood, L. E. (1983). “Laboratory investigation of the use of foamed asphalt for recycled bituminous pavements”. Transportation Research Record, No. 911, pp. 80-87.

Castedo F, L. H., and Wood, L. E. (1983). “Stabilization with foamed asphalt of aggregates commonly used in low-volume roads”. Transportation Research Record, No. 898, pp. 297-302.

Csanyi, L. H. (1957). “Foamed asphalt in bituminous paving mixtures”. Highway Research Board Bulletin, No. 160, pp. 108-122.

Csanyi, L. H. (1962). "Foamed asphalt for economical road construction". Civil Engineering (New York), 32(6), pp. 66-68.

Fu, P., and Harvey, J. T. (2007). "Temperature sensitivity of foamed asphalt mix stiffness: Field and lab study". International Journal of Pavement Engineering, 8(2), pp. 137-145.

Jenkins, K. (1994). "Analysis of a pavement layer which has been treated by single pass in situ stabilisation". Masters Degree, University of Natal, South Africa.

Jenkins, K. J. (1999). "Mix design considerations for cold and half-warm bituminous mixes with emphasis on foamed bitumen". PhD thesis, University of Stellenbosch, Stellenbosch, South Africa.

Jenkins, K. J., Molenaar, A. A. A., de Groot, J. L. A., and van de Ven, M. F. C. (2000). "Developments in the uses of foamed bitumen in road pavements." Heron, 45(3), pp. 167-176.

Lee, D. Y. (1981). :Treating marginal aggregates and soils with foamed asphalt (with discussion and closure)". Association of Asphalt Paving Technologists, pp. 211-250.

Long, F., and Ventura, D. G. C. (2004). "Laboratory testing for the HVS Test Sections on the N7 (TR11/1)."

MINCAD. (2004). "Circly."

Nataatmadja, A. (2002). Foamed bitumen mix: soil or asphalt?, International Society for Asphalt Pavements.

Ruckel, P. J., Acott, S. M., and Bowering, R. H. (1983). Foamed-asphalt paving mixtures: preparation of design mixes and treatment of test specimens, Transportation Research Record, No. 911, pp. 88-95.

Thenoux, G., Gonzalez, A., and Dowling, R. (2006). "Energy consumption comparison for different asphalt pavements rehabilitation techniques used in Chile". Resources, Conservation and Recycling, Netherlands.

Wirtgen. (2004). "Wirtgen Cold Recycling Manual".

Wood, L. E., Altschaeffl, A. G., Cravens Beaudoin, C. M., and Castedo, L. H. (1984). “The use of foamed asphalt in bituminous stabilization of base and subbase materials and recycled pavement layers”. Purdue and Indiana State Highway Commission and Federal Highway Administration.